Investigation and Improvement in Reliability of Asphalt Concrete

Fatigue Modeling using Fine Aggregate Matrix Phase

by

Padmini Priyadarsini Gudipudi

A Dissertation Presented in Partial Fulfillment
of the Requirements for the Degree
Doctor of Philosophy

Approved February 2016 by the
Graduate Supervisory Committee:

Benjamin Shane Underwood, Chair
Kamil Kaloush
Michael Mamlouk
Narayanan Neithalath

ARIZONA STATE UNIVERSITY

May 2016

ABSTRACT

The fatigue resistance of asphalt concrete (AC) plays an important role in the service life of a pavement. For predicting the fatigue life of AC, there are several existing empirical and mechanistic models. However, the assessment and quantification of the 'reliability' of the predictions from these models is a substantial knowledge gap. The importance of reliability in AC material performance predictions becomes all the more important in light of limited monetary and material resources. The goal of this dissertation research is to address these shortcomings by developing a framework for incorporating reliability into the prediction of mechanical models for AC and to improve the reliability of AC material performance prediction by using Fine Aggregate Matrix (FAM) phase data. The goal of the study is divided into four objectives; 1) development of a reliability framework for fatigue life prediction of AC materials using the simplified viscoelastic continuum damage (S-VECD) model, 2) development of test protocols for FAM in similar loading conditions as AC, 3) evaluation of the mechanical linkages between the AC and FAM mix through upscaling analysis, and 4) investigation of the hypothesis that the reliability of fatigue life prediction of AC can be improved with FAM data modeling.

In this research effort, a reliability framework is developed using Monte Carlo simulation for predicting the fatigue life of AC material using the S-VECD model. The reliability analysis reveals that the fatigue life prediction is very sensitive to the uncertainty in the input variables. FAM testing in similar loading conditions as AC, and upscaling of AC modulus and damage response using FAM properties from a relatively simple homogenized continuum approach shows promising results. The FAM phase fatigue life

prediction and upscaling of FAM results to AC show more reliable fatigue life prediction than the fatigue life prediction of AC material using its experimental data. To assess the sensitivity of fatigue life prediction model to uncertainty in the input variables, a parametric sensitivity study is conducted on the S-VECD model. Overall, the findings from this research show promising results both in terms of upscaling FAM to AC properties and the reliability of fatigue prediction in AC using experimental data on FAM.

DEDICATION

To my husband, Venu Madhav Garikapati, for his unconditional support, love, and most importantly being there for me in difficult as well as happy times. This dissertation would not have been possible without his support.

ACKNOWLEDGMENTS

First and foremost, I would like to acknowledge my advisor and mentor Dr. Shane Underwood for providing me the opportunity to pursue my doctoral research under his guidance. His passion and commitment for research has inspired me greatly. He has provided me every opportunity that a graduate student can possibly ask for, right from learning the fundamentals in viscoelastic properties of materials to publishing journal papers from my doctoral research work. The discussions and meetings related to research that we had over the past few years not only helped me in my dissertation research work but also helped me in developing and discussing new ideas with our research group. I admire his conviction to the extra mile to help students. I can undoubtedly say that he is the most dedicated researcher I have ever met.

I would also like to extend my sincere gratitude to Dr. Kamil Kaloush, Dr. Michael Mamlouk, and Dr. Narayanan Neithalath for agreeing to serve on my PhD supervisory committee and for their scholarly advice through the years.

A special thanks to Dr. Waleed Zeiada and Dr. Jeffrey Stempihar for teaching me the basic experimental protocols of asphalt concrete materials and also for their help in designing various instrumentations needed for my research. I would also like to thank lab managers Peter Goguen, Kenneth Witczak, and Jeffrey Ahlstrom for always being available and quickly resolving any issues I faced in the laboratory. I would like to thank BOSE Electroforce systems service engineers Tim Burnet and Jason Rombalski for their help with equipment issues.

TABLE OF CONTENTS

LIST OF TABLES

LIST OF FIGURES

CHAPTER 1 INTRODUCTION

Asphalt concrete (AC) is a composite material consisting of aggregate particles of varying, but controlled sizes, and asphalt binder. The asphalt binder behaves as a thixotropic viscous liquid or a viscoelastoplastic semisolid depending on the temperature. As a result of these behaviors the AC composite exhibits substantially more temperature and time dependence than many other infrastructure materials. The aggregate particles generally occupy 86% of the total volume and form a skeleton that when bound together with the asphalt binder becomes a stable material ideally suited for paving applications. AC pavements play an important role in transportation infrastructure and thus the economic growth of the nation (*1*). Demand for transportation (roadway) infrastructure is growing rapidly owing to recent technological developments (*2*). Over the past fifty years, aggregate and asphalt binder were abundant and low cost resources, but the environmental impacts of stone mining and escalating gas prices are making these resources scarce and expensive (*3*). In addition to the cost of the materials themselves, the AC construction process is very demanding in terms of time, energy, and capital. While the supply side of the infrastructure spectrum is becoming increasingly limited, travel demand and the need for new infrastructure continue to increase. Further complicating this future vision are the emergence of automated electric buses and autonomous vehicles that are not constrained by traditional travel supply issues such as congestion/delays, which could generate greater amounts of traffic in the future than are currently considered by designers (*4*). Autonomous vehicle technology is not limited to passenger vehicles, but is also extending to the truck industry, which might propel an unprecedented increase of truck traffic (*5*). This technology is at least partially

responsible for projections from the United States Department of Transportation (USDOT), which conclude that in the next 30 years the vehicle miles travelled by trucks will grow at a rate of 2.55% annually which is equivalent to a 43% increase in terms of freight movement (*2, 5*). In addition, the federal gas tax has not been increased in the past, 20 years and the highway trust fund is projected to have an annual shortfall of $12 billion (*2*). Together these issues raise some important questions;

- How will the asphalt pavement industry be impacted?

- Even if these trends can be accurately predicted, how reliable are the existing AC material performance prediction models and thus how accurate will any assessment analyses to answer the first question really be?

- Is there a better approach to study and improve fundamental properties of AC so that these accuracies are known and properly accounted for and/or these accuracies are improved?

These are important questions that have far reaching consequences and need to be addressed in engineering to cater the future needs of transportation. As will be presented in substantial detail in Chapter 2, much of the research on these topics have focused on developing more complex models that either consider factors ignored in current generation models or focus on developing performance models that better characterize and relate key material properties to performance. While such models are important and address certain parts of the aforementioned questions, they have given rise to a considerable knowledge gap with respect to the accuracy and reliability of more advanced (and complex) model forms. The work presented in this dissertation seeks to bridge these knowledge gaps and establish a mathematically sound method to assess the reliability of these advanced models.

It is the belief that such a method can result in substantial improvements and a new paradigm to develop and advance the performance modeling of asphalt concrete mixtures and pavements and ultimately the engineering of a more sustainable roadway infrastructure.

1.1 Background

AC pavements deteriorate over time due to traffic, environmental and climatic conditions. The deterioration of a pavement is observed in various forms of distress including rutting, fatigue cracking, thermal cracking, raveling, potholes and bleeding etc. Of these, fatigue cracking is the distress that has recently received the greatest attention from engineers in recent years due to its significant impact on the service life of flexible pavements, a general lack of a reliable material evaluation methodology, and other factors occurring in the asphalt technology field that have collectively contributed to materials that are inherently more prone to fatigue cracking. Since the construction of asphalt pavements involve significant time and monetary constraints, care should be taken in the selection, design and performance prediction of the materials used for construction. Historically, performance prediction of pavement materials has been done using empirical methods while the current state of practice in pavement design procedures involves either empirical or mechanistic-empirical techniques. These tools are primarily used for pavement design and analysis, but not very useful in selection of optimal mix design and/or accurate prediction of the growth of individual distresses over time. It is vital to accurately measure the individual distresses of AC pavements over time in order to predict the pavement performance measures such as pavement condition index (PCI) and international roughness index (IRI). These

measures are used as a reference to select appropriate pavement maintenance and rehabilitation strategies. The growth of mechanistic-empirical pavement analysis techniques and the resulting increase in interest in developing accurate performance prediction measures of AC pavements has motivated researchers to develop mechanistic and mechanistic-empirical methods for performance prediction and mix design.

It has been more than a century since AC materials were first used in the construction of pavements. In the intervening years, research towards the enhancement of this material helped in understanding the several factors related to the usage of AC materials for various climatic locations and traffic conditions. These understandings have subsequently driven much of the research on this material, which has most recently focused on developing new sustainable materials like recycled AC pavements (RAP), warm mix AC, rubberized AC, fiber reinforced AC, polymer modification, and dense graded mixes. Much of this work has been trial and error and driven by anecdotal studies and/or intuition based knowledge, thus while substantial improvements have occurred, the potential for improvement is inherently limited by a lack of a fundamental understanding of this material. For example, to date there is no clearly established universal procedure that can explain the behavior of AC material for any given aggregate gradation and binder type and content. As a result of these two contributing factors (a desire to better incorporate mechanistic characteristics along with a lack of fundamental understanding of material mechanisms), a lot of time is currently being invested in brute force or semi-brute force testing and performance characterization methodologies.

There are many practical and technical reasons for the current state of this field, but one specific technical hindrance is a lack of research in understanding the complexities of AC across the breadth of relevant material and structural length scales. The majority of the new mechanistic models can be considered as significant improvements to the current engineering practice, but they still lack in adequately addressing the changes in various material compositions or addition of new materials. To fill this gap, recent research efforts focused on investigating AC materials at various length scales. Several of these studies suggest that fine aggregate matrix (FAM), which exists between coarse aggregate particles in the AC structure, is closer in scale to the various phenomena that occur in AC materials and provides an accurate means of assessment.

In addition to the assessment of AC materials at various length scales, several mechanistic models have been developed to address AC material performance using fundamental material properties. These models are able to predict the pavement service life more accurately than the existing empirical models. However, most of the mechanistic models consist of input variables that are measured by performing multiple experiments, each with their own variability. Multiple sources of variability introduces additional and unaccounted for uncertainty in comparison with alternative, non-model empirical based approaches. Thus, the assessment of reliability is an important, but often overlooked component in the development of mechanistic models methods for predicting pavement performance.

In light of limited monetary and material resources, reliable AC material performance models are vital to cater to the roadway infrastructure needs of the future.

Fundamental understanding of AC could not only help in the developing of new sustainable materials such as bioasphalt, but also help in reusing/recycling the existing materials, thereby contributing to the reduction of material cost and greenhouse gases.

1.2   Research Objectives

This research study investigates a hypothesis that fatigue modeling for AC derived from experiments on a material that is a scale closer to the actual phenomenon (FAM) can produce more reliable fatigue assessment than tests on the composite as a whole. This dissertation research focuses on addressing the issue of fatigue performance of AC and FAM using the simplified viscoelastic continuum damage model (S-VECD). Specific objectives used to evaluate this hypothesis are:

1. Development of a reliability framework for fatigue life prediction of AC materials using the S-VECD modeling approach as a case study, considering the uncertainty and variability of input parameters.

    This objective includes two sub tasks:

    ➢ Development of reliability framework.

    ➢ Validation of the framework using additional AC mix data.

2. Evaluation of the mechanical linkages between the FAM and AC mix by applying analytical upscaling methods with gross homogenization principles.

    This objective includes three sub tasks:

    ➢ Establish standard instrumentation and testing protocols for FAM, similar to AC mix.

> ➤ Propose, evaluate and validate an upscaling procedure for FAM to AC mix properties.

> ➤ Evaluate the sensitivity of AC Modulus to binder oxidation with FAM phase experimental data.

3. Testing the hypothesis that reliability of fatigue prediction modeling approach of AC can be improved with FAM phase experimental data as a surrogate measure.

    This objective includes two sub tasks:

    > ➤ Reliability analysis of fatigue life prediction using FAM experimental data.

    > ➤ Use of FAM to AC upscaling data in fatigue life prediction reliability analysis.

4. Perform a parametric sensitivity study on the reliability of fatigue life prediction using S-VECD modeling approach in order to identify vital parameters that need accurate characterization within the S-VECD model.

    This objective includes two sub tasks:

    > ➤ Sensitivity of individual parameter (dynamic modulus, damage characteristic curve and failure point) variations in S-VECD model on the reliability of fatigue life prediction using two different accepted failure criteria.

    > ➤ Report on the reliable measurements comparison between the two different model failure criteria approaches.

This dissertation research is divided into two primary parts. FIGURE 1-1 shows the schematic of tasks and subtasks involved in each part. The first part focuses on the

development of a reliability framework for fatigue life prediction of AC and its validation. The second part deals with the investigation of mechanical properties of FAM material by devising standard testing protocols in similar test conditions as AC. These test methods are used to measure mechanical properties of FAM and eventually upscale the results to AC mix properties. Results from the two parts of the research jointly help in testing the proposed hypothesis.
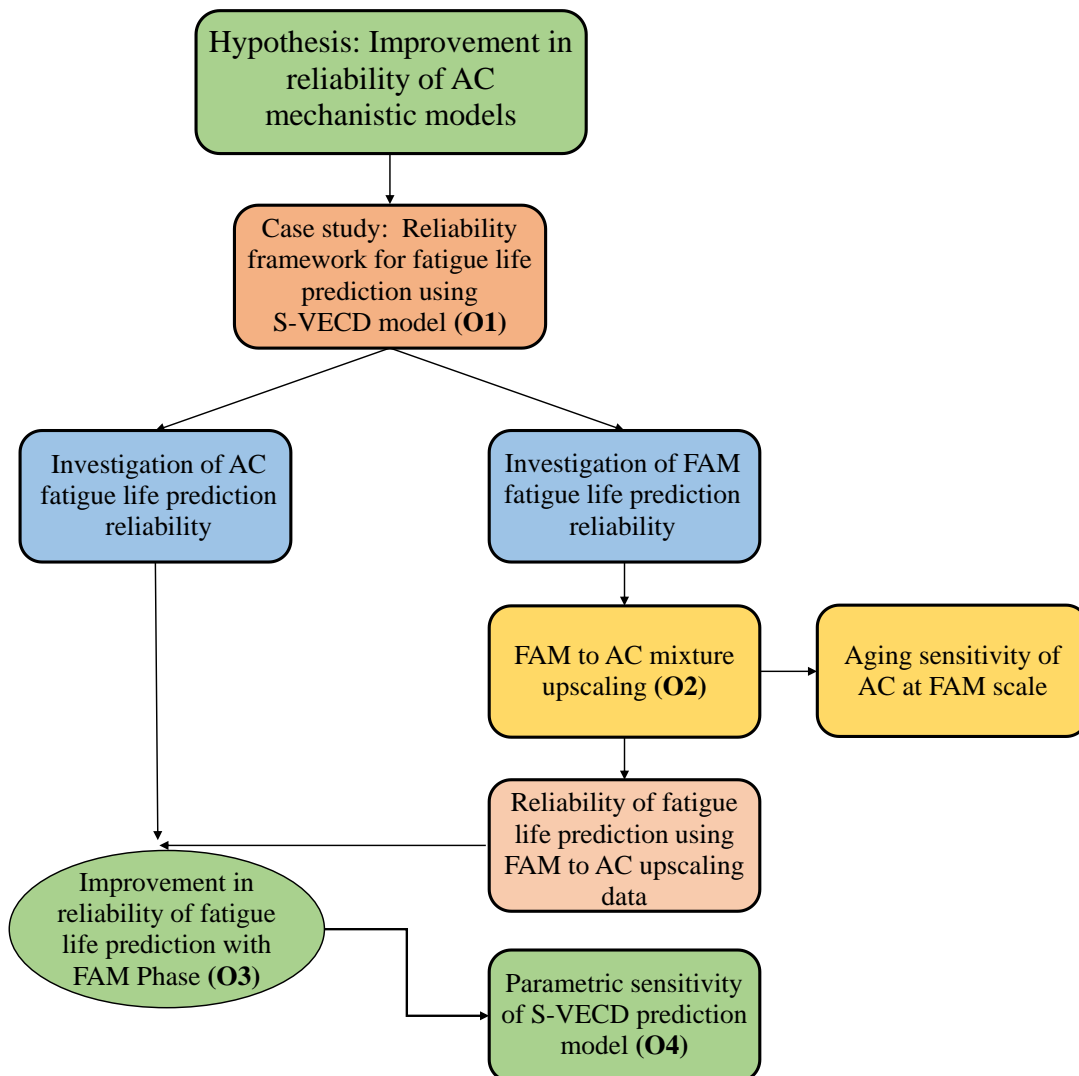
FIGURE 1-1 Schematic of Overall Research Study.

1.3   Dissertation Outline

This dissertation consists of nine chapters. The first eight chapters introduce the research, present the tasks performed towards achieving the research study objectives, and discuss the findings. The ninth chapter details the concluding remarks from the overall research plan and recommendations for future research. A brief summary of each chapter is provided below.

Chapter 1:   *Introduction* – Provides an overall introduction to the research area, background, and need for the research undertaken. It also lists the research objectives and provides an overall outline of the research study.

Chapter 2:   *Literature Review – Reviews* existing literature on various empirical and mechanistic models used for fatigue life performance prediction and explains existing studies on FAM sample gradation and compaction procedures. It also elucidates several failure criteria approaches currently being used for characterizing failure.

Chapter 3: *Material and Test Methods* – Illustrates the type of materials used and the tests conducted on AC samples in the current research study. It also provides details regarding the gradation of AC and FAM materials, fabrication and instrumentation of AC samples for testing.

Chapter 4: *Reliability of Fatigue Life Prediction for AC Materials Using S-VECD Model* – Focuses on development and validation of a reliability framework for fatigue life prediction of AC materials. This framework adopts the S-VECD modeling approach for

fatigue life prediction, and investigates the reliability of fatigue life prediction, given the variability of input parameters (both in the experiment as well as the model).

Chapter 5: *Development of Experimental Protocols for FAM* – Discusses the development of a standardized test procedure for FAM specimens to measure on-specimen displacements for modulus and uniaxial fatigue testing in similar test conditions as AC. It also presents a detailed account of the amount of error observed in measuring mechanical properties of FAM due to machine compliance issues.

Chapter 6: *Modeling of FAM and its Upscaling to AC Mixture* – Presents a comparison between the mechanical properties of FAM and AC mixture in a consistent overall stress state (axial tension–compression) for both modulus and fatigue testing. It also presents an investigation of the mechanical linkages between the FAM and AC mix by applying analytical upscaling methods with gross homogenization principles. In addition, Several FAM materials are tested at different aging levels to address the sensitivity of structural, binder PG grade and source of aggregate on the aging process.

Chapter 7: *Reliability of Fatigue Life Prediction Using Fine aggregate Matrix Test Data* – Reports on the reliability measurements of fatigue life prediction using developed framework at FAM scale. It also shows the comparison of reliability measurements between AC and FAM for various failure criteria approaches.

Chapter 8: *Parametric study on S-VECD Model Fatigue Prediction Reliability* – Provides a detailed analysis on the sensitivity of the S-VECD model to the variability in the model parameters. It also shows the reliability comparison between two modeling failure criteria for the same variation in the input parameters.

<u>Chapter 9:</u> *Conclusions and Recommendations* – Provides a summary of conclusions drawn from the research conducted and the scope of future work.

CHAPTER 2 LITERATURE REVIEW

The recognition and prediction of fatigue for AC was first developed in the empirical studies of the early 1950's. The evolution from empirical to mechanistic models has happened slowly over the course of 60 years. This chapter presents a detailed review of various empirical and mechanical studies in the context of characterizing fatigue cracking in AC materials. It also reviews literature on the application of reliability principles into the AC pavements and studies on the development of FAM mix design and recent studies performed on FAM to study different mechanisms in AC.

2.1 Empirical and Semi-Empirical Fatigue Cracking Studies

Fatigue resistance is defined as the ability of a material to withstand continuous application of traffic load. The service life of an AC pavement against this form of distress is termed as fatigue life. Hveem (*6*) proposed a concept indicating that fatigue cracking is the major form of distress that occurs in AC when pavements are subjected to high traffic loads. This concept motivated the development of laboratory testing protocols to characterize fatigue cracking. Since then, several empirical and semi-empirical fatigue cracking models have been developed. These models were further classified into strain/stress based fatigue models, and energy based fatigue models.

2.1.1 Strain/Stress Based Fatigue Life Prediction Models

Monismith (*7*) and Pell (*8*) developed empirical models to predict fatigue life of AC material using either strain based or stress based approaches (Equation (2.1)).

$$N_f = A\left(\frac{1}{\varepsilon_t}\right)^B$$

$$N_f = C\left(\frac{1}{\sigma_t}\right)^D$$

(2.1)

where;

N_f =   number of cycles to failure,

ε_o =   tensile strain applied,

σ_o =   tensile stress applied, and

A, B, C, D,   =   material constants.

Monismith (*9*) generalized the above strain based equation to account for temperature and frequency dependence by including the AC material stiffness term in the fatigue life prediction model. Several studies adopted these models to predict fatigue life (*10, 11, 12, 13*). In these models, the number of cycles to failure was predicted for various conditions (temperatures, frequencies and different materials) and these predictions were employed to find the coefficients (*K_1, K_2, K_3*) shown in Equation (2.2).

$$N_f = K_1\left(\frac{1}{\varepsilon_0}\right)^{K_2}\left(\frac{1}{S_{mix}}\right)^{K_3}$$

(2.2)

where;

N_f =   Number of cycles to failure,

S_{mix} =   Stiffness of AC mix

ε_o =   Initial strain, and

K_1, K_2, K_3 =   Material constants.

Several researchers used this model form and further developed other fatigue life prediction models such as: i) Shell oil fatigue cracking model for constant stain and constant stress (*10*), ii) Asphalt institute (MS-1) model (*11*) iii) SHRP A-003A- Berkely Fatigue model (*12*) and iv) MEPDG fatigue cracking model (*13*).

2.1.2   *Dissipated Energy Based Fatigue Life Prediction Model*

The dissipated energy concept to understand the fatigue behavior of asphalt concrete materials was first introduced by Van Dijk (*14*). He found that there is a strong relationship between the number of failure cycles and cumulative dissipated energy (shown in Equation (2.3)). Later, this approach was further enhanced by other researchers and lead to the development of dissipated energy based models such as i) Work ratio approach and ii) Dissipated energy ratio approach (*15*, *16*, *17*, *18*).

$$W_N = A\left(N_f\right)^z \tag{2.3}$$

where;

N_f =   number of cycles to failure,

W_N =   cumulative dissipated energy to failure, and

A, z =   experimentally derived mix coefficients.

These fatigue life prediction models were empirical in nature and were developed based on regression analysis of specific mix experimental data. These empirical models are limited to the test mixtures and require significant amounts of experimental data for the regression analysis. In addition, empirical models do not provide any insights to identify

the behavior of a material analytically and thus improve the fatigue resistance of AC material. To overcome the aforementioned problems and better understand the fatigue resistance of AC material, researchers began focusing on accurate characterization of fatigue behavior of AC which eventually led to the development of mechanistic based procedures. The mechanistic approaches are more complex than the empirical models but are applicable to a wide range of materials and loading conditions. The mechanistic models utilize theoretical and fundamental properties of materials that help in characterizing fatigue behavior of AC with simplified laboratory experimental programs (*19*).

2.2   Mechanistic Modeling of Fatigue Cracking

Fatigue cracking is typically a combination of crack initiation and crack propagation. Cracking in AC materials doesn't occur immediately after pavement opens for traffic; it generally appears after millions of load applications. In the process of crack initiation, microcracks grow rapidly and form a Macrocrack. The macrocrack propagates until it reaches to the pavement surface. This forms the basis for two distinct schools of thought in the development of mechanistic models for predicting fatigue life of asphalt pavements.

- *Fracture mechanics based models*: This concept is used in the development of models to characterize crack propagation. This method is founded on the assumption that crack propagation is the dominant phenomenon in fatigue cracking.

- *Continuum Damage based models*: This concept is used in the development of viscoelastic continuum damage (VECD) mechanics based models for AC materials. In VECD theory, crack initiation is assumed to be the dominant phenomenon in fatigue cracking.

15

2.2.1 *Fracture Mechanics Based Approach to Characterize Fatigue Cracking*

Majidzadeh et al. (*20*) pioneered the use of fracture mechanics based approach to predict fatigue cracking in asphalt pavements. This method focuses on the propagation of a single crack in the material, caused by various modes of loading and boundary conditions either individually or in combination. Mode I loading results from the stresses applied perpendicular to the crack plane, Mode II loading occurs due to shear stress along the crack plane and Mode III loading results from out of plane shear loading which causes sliding of crack faces parallel to the crack leading edge (*21*). Mode III loading is rare and generally not considered for simplicity during the modeling of fatigue cracking with the fracture mechanics based approach. Most of the fracture mechanics concepts adopted in the context of AC materials are based on the research carried out by Dugdale (*22*) and Barenblatt (*23*), on solid metals. Their research utilizes the classical linear elastic fracture mechanics theory to develop cohesive crack zone models. Uzan and Levenberg (*24*) developed a simplified cohesive crack model to explain fracture behavior of AC. Molenaar used the fracture mechanics approach to study the reflective cracking of AC materials (*25, 26*). Several studies used laboratory testing protocols to characterize AC fracture properties (*A, n*) (*25, 26, 27, 28, 29, 30*). Some of these test protocols commonly used in practice are briefly described below.

Disk Shaped Compact Tension Test

This test method was developed based on the ASTM E 399 test protocol, which is commonly used for measuring the toughness of metals. Disk shaped compact tension test, DC (T) for AC samples was applied by Wagoner et. al, (*31*) to evaluate the fracture

properties of AC samples. This test is typically used to measure the fracture energy by measuring applied load and corresponding crack mouth opening displacement. One of the advantages of this test procedure is that AC field samples and Superpave gyratory compact samples can be directly tested for testing.

Indirect Tensile Test (IDT)

Indirect tensile test (IDT) is one of the most commonly used test methods in AC industry to measure the tensile strength of AC materials (*32*). In this test procedure, disk shaped AC samples are loaded diametrically at constant rate. The tensile stresses developed due to applied loading cause the sample to crack in the direction of loading. The amount of load and corresponding deformation with respect to time are used to measure the fracture energy and tensile strength of AC specimens. This test procedure was used by several researchers (*32*, *33*) to measure the resistance of AC materials against fatigue cracking performance. This test procedure was enhanced by Roque et. al, (*34*) to investigate the fracture properties of AC materials.

Single Edge Notched Beam Test

Single edge notched beam test was originally used for asphalt binders (*35*, *36*). Mobasher et. al, (*37*) used this test procedure to measure crack propagation properties of AC materials using nonlinear fracture mechanics approach. Following his study, several researchers modified this test method to measure the fracture properties of AC (*38*). Though there is no standard test protocol for this method, the test procedure outlined in ASTM E 399 is generally used. In this test method, AC beams are fabricated and cut to specific dimensions to remove density variations and aggregate segregation. At the center of the beam, a notch

is introduced to simulate a crack. The AC beam is loaded at a constant rate in three point bending conditions. The test is performed until 0.1 inch of crack mouth opening displacement is observed. This test data can be used to measure various material properties such as stress intensity factor (K), crack growth rate, crack length and J-contour

Semicircular Bending Beam Test

Semicircular bending beam (SCB) test was first used to characterize AC mixtures by Krans et. al, (*39*). This test method has been gaining popularity in the recent years to measure the fracture toughness, energy dissipation rate, stress intensity factor, and fracture energy under static loading conditions. These parameters are used to evaluate AC materials and to compare different asphalt mixtures against fracture resistance. Under dynamic loading conditions, the SCB test data can be used to calculate the Paris law coefficients to measure the crack growth as a function of loading cycles (*39*). As this test procedure uses semicircular disk shaped samples, it is possible to reduce the number of cores and it is also easier to obtain field samples. Several researchers used this method to test and characterize fracture behavior of FAM phase as well (*40*, *41*, *42*).

There are several other test procedures in practice to measure the fracture properties of AC materials. Zhou et. al., (*40*) introduced a quick test procedure to predict fracture properties of AC (*A, n*) using the Texas Transportation Institute (TTI) overlay test. From various research studies, it was observed that AC fracture shows plasticity behavior at the crack tip and thus linear elastic fracture mechanics was not considered as an accurate approach to define cracking in AC. To address the plasticity of AC material, time dependent fracture mechanics models were developed (*44*). More recently Stempihar (*45*)

used *C** line integral based approach and developed a *C** fracture test to describe the crack propagation in AC materials. The latest research in this area is being developed by Buttlar et. al, (see fatigue models). Fracture mechanics based approach was also used by researchers to address another form of distress, namely the thermal cracking phenomenon in AC materials. Hiltunen and Roque (*46)* developed TCMODEL as a part of the Strategic Highway Research Program to predict the amount of thermal cracking in asphalt pavements over time.

2.2.2 *Continuum Damage Mechanics Approach to Characterize Fatigue Cracking*

The approach that is recently gaining attention in the asphalt pavement community is the damage based approach, which focuses on the reduction of material stiffness due to repeated loading. The VECD modeling approach was developed based on three important principles 1) elastic-visco elastic principle based on pseudo strain 1) the effect of microcracking on the constitutive behavior using CDM 3) effect of temperature on the constitutive behavior using the time temperature superposition principle using the growing damage. Schapery proposed the elastic-viscoelastic correspondence principle which can be applied to both linear and nonlinear viscoelastic materials (*47*). Several researchers used VECD modeling principles to predict the fatigue behavior of AC materials. Some of those approaches are briefly summarized here.

ENTPE's Approach to Fatigue Damage

In this approach relation between the rate of stiffness change over the number of cycles/ number of load applications was investigated using the fatigue damage analysis approach developed by ENTPE (*48*, *49*). The evolution of damage in the material was divided into

19

three phases in the displacement controlled fatigue test. In phase I which is considered as adaption stage, the reduction in stiffness of material is rapid due to development of microcracks as a fatigue damage and increase of specimen temperature due to dissipated energy and thixotrophy of binder. Phase II is quasi stationary phase, where stiffness decreases gradually mainly due to fatigue damage and effects of dissipated energy and thixotrophy are reduced. Phase III is failure phase where stiffness decrease rapidly because of the macrocrack begin to develop and leads to local crack propagation until complete failure of the specimen (*48*). In the tension-compression fatigue tests macro crack evolution phase can be deducted from the analysis. In this approach for the purpose of simplicity one isotropic damage parameter (D) (*50*) was considered to define the damage in the AC materials. The rate of stiffness change as an index of fatigue was measured using the generic Equation (2.4). Furthur the damage evaluation over the cycles is defined as a function of strain and damage parameter given in Equation (2.5)

$$D_{exp} = \frac{(E_0 - E_N)}{E_0} \qquad (2.4)$$

where;

E_0 =   Initial modulus in the beginning of the test (100th cycle),

E_N =   Stiffness of the sample at cycle N, and

D_{exp} =   experimental Damage parameter.

$$D = f(D)g(\varepsilon_{cycleN}) \qquad (2.5)$$

where;

f is a function of the damage parameter D, and

g is a function of strain evaluation during the cycle.

FHWY & Emin Kutay's Approach

In this approach laboratory experiments were conducted in cyclic tension-compression mode on several accelerated loading facility (ALF) mixtures. The test were conducted in both stress and strain controlled loading modes. The VECD modeling formulations developed by Kim and his associates were used to calculate the pseudo stiffness (Equation 2.8) and pseudo strain (Equation 2.7). For the purpose of calculating continuum damage parameter simplified formulation was derived for cyclic tests at a constant frequency (*51*). Theses formulations were validated using the experiments performed at different temperatures and loading conditions. This study also examines different failure criteria methods to define the point of failure during the cyclic fatigue tests. The summary of simplified formulation developed to calculate the damage parameter is given in equation (2.6)

$$S_{N+\Delta N} = S_N + \left(\frac{\Delta N}{f} \right)^{\frac{1}{\alpha}} \left[-0.5 I \varepsilon_N^R \frac{dC}{dS} \right]^{\alpha}$$

$$\frac{dC}{dS} = \exp(aS_N^b) ab S_N^{b-1}$$

(2.6)

VECD Model Development by Kim and His Associates.

Kim and Little first applied Schapery's viscoelastic constitutive theory in the field of AC pavements (*48*, *53*). Lee and Kim (*54*) later developed the VECD modeling approach and

applied this procedure to the AC materials in both controlled stress and strain cyclic mode of loading. This work was further enhanced by Daniel and Kim (*19*) who showed that damage is a material property and is independent of the mode of loading and can be determined using constant crosshead rate monotonic test (*55*). Chehab et al, (*56*) extended the time-temperature superposition principle from material linear viscoelastic range to the material damage levels. Underwood et al., (*57*) applied these principles to different mixtures and successfully ranked them with respect to their fatigue resistance. VECD modeling approach has also been used to address the moisture damage phenomena in AC materials (*58, 59*). The VECD modeling approach showed positive results in terms of fatigue life prediction of AC materials when they were subjected to simple loading like constant rate tests. For the cyclic loading fatigue test, the regular VECD formulation becomes were found to be more cumbersome, computationally challenging and prone to additional errors in damage calculation. To address this issue, Underwood et al., (*63*), developed a simplified viscoelastic continuum damage model (S-VECD). The S-VECD model comprises of damage calculation in two stages. Damage during the first half loading cycle is calculated using regular VECD formulation (complete pseudo strain calculation), as it is essentially the same as constant rate damage test and significant amount of damage occurs during the first cycle. For the second cycle, S-VECD modeling formulation is used to calculate the damage of material in cyclic loading conditions. This approach was used successfully to characterize the fatigue behavior of modified AC mixtures with RAP and RAS (*60, 61*). Damage growth was modeled using VECD approach by performing indirect tensile strength and semicircular bending beam cyclic tests conducted on polymer modified AC materials (*62*). S-VECD model approach has been successfully used by several

researchers to characterize damage. This approach is adopted in the current research effort to predict fatigue behavior of AC pavements. The model equations and damage curve development procedures corresponding to the S-VECD approach are detailed in later chapters (*63*).

2.3   S-VECD Model Summary

The uniaxial fatigue test of AC mixtures was analyzed using the simplified viscoelastic continuum damage theory (S-VECD). The model and its capabilities are described in detail elsewhere (63), but in short it consists of the following essential components; the pseudo strain (ε^R) function in time and steady-state frequency domains;

$$\varepsilon^R = \frac{1}{E_R} \int_0^t E(t-\tau) \frac{d\varepsilon}{d\tau} d\tau \quad t \leq t_p$$
$$\varepsilon_0^R = \frac{1}{E_R} \left(|E*| \times \varepsilon_0 \right) \quad t > t_p \tag{2.7}$$

the pseudo strain energy density function, W^R,

$$W^R = \frac{1}{2} \left(\varepsilon^R \right)^2 C, \tag{2.8}$$

the stress, σ, to ε^R relationship,

$$\sigma = \frac{dW^R}{d\varepsilon^R} = C \times \varepsilon^R, \text{ and} \tag{2.9}$$

the damage evolution law with respect to time and cycles,

$$\frac{dS}{dt} = \left(-\frac{\partial W^R}{\partial S}\right)^{\alpha} = \left(-\frac{1}{2}\left(\varepsilon^R\right)^2 \frac{dC}{dS}\right)^{\alpha} \qquad\qquad t \le t_p$$

$$\frac{dS}{dN} = \left(-\frac{\partial W^R}{\partial S}\right)^{\alpha} = \left(-\frac{1}{2}\left(\varepsilon_0^R\right)^2 \frac{dC}{dS}\right)^{\alpha} \frac{1}{f} K1 \qquad t > t_p$$

(2.10)

where;

E_R =   reference modulus (taken as 1),

$E(t)$ =   LVE relaxation modulus,

ε =   measured strain,

τ =   integration term,

t =   time,

t_p =   pulse time.

ε_0 =   measured strain amplitude,

C =   pseudo stiffness (material integrity),

S =   damage,

α =   damage evolution rate, and

K_1 =   loading shape factor.

Once the C vs S damage curves plots for each replicate are characterized the replicates were fit to single curve using Equation (2.11).

$$C = 1 - C_{11} S^{C_{12}}$$

(2.11)

Measuring material level properties is not sufficient to accurately predict the fatigue performance of AC pavements. It is equally important to consider structural details of the pavement in the development of performance prediction models. To account for structural

24

details of the pavement, S-VECD model is combined with the results of layered viscoelastic analysis of finite element model in the AC pavement performance prediction (*64*, *65*).

2.4 Failure Criteria

The criteria to define failure in a fatigue test or fatigue prediction is a vital part of any experimental or modeling process regardless of whether it is empirical, fracture mechanics based, or continuum damage based. With most of modeling approaches, an external rule is often applied to relate a characteristic that the model can predict to experimentally observed failure. The failure criteria thus has two important components; i) the method or rule used to identify failure from the model outputs and ii) the method used to identify failure in the experiment. Ideally these two components should be the same. However, in reality these two components can be completely different and results from the experiment are often used to calibrate the model rule. Both these components have been the topic of debate in the context of general issues related to fatigue testing and modeling. The reason for the debate being that individually or in combination with models, different experimental (and model based) failure criteria produce different estimates of the cycle at failure, which directly impact the fatigue life relationship predicted for an AC mixture. Some of the frequently used experimental failure criteria approaches in the literature include; the point at which the phase angle starts to reduce (*66, 67*), the point when the modulus is 50% of the initial value (*68*), and point at the peak of the product of stiffness and corresponding load cycle number (*69, 70*). With respect to model failure criteria, the approaches used by researchers

25

so far include pseudo stiffness at failure point (*19, 54*) and energy release rate approach (*73, 74*).

2.4.1   Experimental Failure Criteria

With respect to defining failure in the experiments, some of frequently used criteria include; the cycle when the phase angle starts to reduce (*66, 67*), the cycle when the modulus is 50% of the initial value (*68*), and peak of the product of stiffness and corresponding load cycle number (N) (*69, 70*). During the fatigue experiment, the phase angle of the specimen increases continuously until a point and then shows a sudden decrease. The sudden decrease in phase angle may in fact not be a real decrease in the time-dependency of the specimen, but rather a serious degradation of the stress-strain response. The cycle at which this apparent decrease occurs is considered the failure cycle (*66, 67*). Failure cycle is also defined as the cycle at which the calculated modulus reduces to 50% of its value at cycle 50 (*68*). This criteria is probably the most used and well-known fatigue failure criteria. Rowe and Bouldin (*69*) used the peak value of the product of cycle number (N) and the stiffness at the corresponding cycle to define failure. Others modified the stiffness term with pseudo stiffness (C) and defined the failure point based on the peak of the product of N and C, which is labeled as the C x N approach (*70*).

2.4.2   Model Failure Criteria Approaches

Rules used to identify failure in the S-VECD model predictions include; the pseudo stiffness at failure (C_f) approach (*19, 54, 71*) and the pseudo energy release rate approach (*72, 73, 74*). The concept of setting failure as a constant value of pseudo stiffness, e.g., C_f, first emerged as an extension of the experiment based 50% initial modulus reduction

approach. In fact both of these approaches are equivalent if the initial modulus is defined based on the linear viscoelastic modulus of the material. Lee and Kim (*54*) analogously proposed a C_f value of 0.5 for cyclic tests. Enhancements were made to this criteria based on experimental observations and the fact that the initial modulus in the 50% reduction rule was based on the modulus at cycle 50 (*19, 56*). Hou et al., (*71*) calibrated a functional relationship between C_f and temperature. He showed that C_f changed at temperatures below the regular S-VECD calibration temperature, but it did not change at the calibration temperature and any higher temperature. This experimental finding suggests that at most temperatures where fatigue is dominant, an appropriate failure criteria can be established by simply averaging the C values at the failure cycle in the S-VECD characterization tests. The failure cycle changes depending on the experimental definition of failure and so does the C_f value.

Another approach in model failure criteria is the dissipated energy approach. The concept behind this approach was to quantify the accumulation of energy during damage (*75*). However, the first iteration of this approach considered both viscoelastic damage and incremental damage to the material due to plastic deformation. Refinements were made to this approach to separate viscoelastic energy by developing dissipated pseudo strain energy principles (*76*). Zhang et al developed a new energy based approach that represents the rate of damage dissipation which can be applied to the S-VECD model to predict fatigue failure (*73*). This approach assumed that the pseudo strain energy release rate had a unique relationship with the N_f. Limitations of this approach were later identified with respect to explaining different modes of loading. It was suggested that the unique relationship

27

actually exists between the average pseudo strain energy release rate, G^R, and N_f (*72*) as shown in Equation (2.12).

$$G^R = \frac{\int_0^{N_f} W_C^R}{N_f^2} \qquad (2.12)$$

$$W_C^R = \frac{1}{2}(1-C) \times (\varepsilon_0^R)^2 \qquad (2.13)$$

In practice, the relationship between G^R and N_f follows the power law function as shown in Equation (2.14). Akin to the C_f approach, since the failure cycle changes from one experimental failure criteria to another, the corresponding relationship (*a* and *b* coefficients) also changes.

$$G^R = aN_f^{\,b} \qquad (2.14)$$

2.5   AC Reliability Studies

Prediction models developed based on the experimental data as input parameters are prone to uncertainties at various levels. Such uncertainties will have an impact on the material characterization and eventually the pavement design process. These uncertainties can be classified into two types: 1) systematic errors associated with variation in input parameters 2) uncertainty of the predictive model and lack of fit (*76*). Uncertainty in either of these forms will ultimately impact the reliability of the model predictions. Reliability analysis in pavement design was first introduced in the AASHTO 1986 pavement design guide in order to better calculate the present serviceability index of pavements. Reliability analysis of prediction models has been a topic of interest for several years in various fields. This

approach is used in semiconductor industries (*79*), Electronic systems (*80*), and failure rate of modeling methodologies (*81*). The Mechanistic Empirical Pavement Design Guide (MEPDG) (AASHTO Pavement ME Design) incorporated reliability by using the standard deviation of measured distress obtained from calibration (*78*). While advanced fatigue life prediction models have shown promise at producing accurate and generally applicable deterministic prediction of material performance than their empirical counterparts (*7, 8, 63, 72, 83 -86*), the reliability of these predictions has not received substantial attention. To the knowledge of the author, no studies were found on the evaluation of reliability of predictions of these advanced models. It is worth noting that the advanced models introduce additional experiments and requisite variables each with its own inherent variability. It can be conjectured that while better deterministic predictions can be made with the help of these models, the overall reliability of these predictions might not be as good. More recently Kahil et.al, (87) developed a probabilistic modeling approach to identify reliable prediction models for dynamic modulus of AC materials. Several other studies used probabilistic distribution approaches to predict the fatigue life of materials (88, 89).

2.6 FAM Studies

Material characterization based on its performance is relatively simple when it deals with one single material. However characterization of a blend of materials as a single product is not that straight forward due to the physical and chemical interactions at different scales. AC characterization and evaluation is complicated by the heterogeneous nature of the material, and the multiple scale manifestation of relevant behavior mechanisms. One

strategy that has been applied in other fields for some time and has recently gained greater attention in the AC community involves scale targeted experiments and modeling. FAM is characteristically one scale smaller than AC and is believed to have a substantial influence on the mechanical properties and evolution of the damage in AC. Researchers are working towards conducting tests on minimal amount of binder or/and mastic, and mechanistically upscale the results to predict the mechanical properties of AC (*87*).

Along these lines, Kim (*91*) first started analyzing the FAM material in order to better understand the healing phenomenon. Several researchers carried out experimental studies on FAM with an intent to characterize the moisture damage and healing phenomenon in the AC material (*91 - 96*). It is believed that microstructure of the FAM has a significant influence on the mechanical properties and evolution of damage in AC, as it exist between the coarse aggregate particles in AC. One important limitation in FAM related studies is the representativeness of FAM material produced in an experimental setting to the actual material that exists between coarse aggregate particles in AC. Kim et al., reflected this phase by testing asphalt mixed with sand in order to characterize AC mixture healing (*96*). In their study, Ottawa sand was mixed with 8% of binder content by weight of sand and compacted to 12 mm x 50 mm (d x h) samples. The binder content of 8% was used to provide an average of 10 microns of film thickness (based on the method proposed by Hveem (91)). Zollinger proposed that the composition of FAM should be based on that of the parent AC mixture (*97*). He further suggested that FAM should wholly consist of aggregates finer than the 1.18 mm sieve size and that the binder content should be calculated based on an effective film thickness. Subsequently, several researchers

carried out studies to predict appropriate gradation and binder content of FAM samples (*97, 98, 99*).

In addition to the mix design, the fabrication procedures also play an important role in accurately understanding the engineering significance of the material. Recently Izadi et al, compared the structure of FAM inside the AC mixture with lab fabricated FAM specimens under different compaction procedures. It was concluded from their study that Gyratory compacted FAM samples have a closer resemblance to the actual FAM structure (*93*). The results of the study further conclude that binder content and percentage air voids have a significant impact on the engineering properties of FAM than gradation (*93*). Another related study by Underwood and Kim (*99*) corroborated this finding and quantified the variation in engineering properties for percentage changes in the binder content and air voids. From their study, it was observed that one percent increase in binder content results in a 20-35% decrease in the modulus and one percentage increase in air voids results in a 5-8% decrease in the strength of FAM a material. The variation in engineering properties of FAM material varies with respect to the maximum aggregate size in AC mix gradation. So, care should be taken while developing FAM mix design for a corresponding AC mixture. To calculate the binder content of the FAM, aggregate film thickness approach developed by Radovskiy for compacted AC mixture was used in the current research effort (*98, 100*). This procedure is very similar to the method developed by Stanton and Hveem, the only difference being that aggregate particles are assumed to be spherical (*101*).

Fatigue life of an AC material plays a critical role in the service life of pavements. This importance is well recognized in the AC pavements research community and lead to development of various empirical, semi empirical and mechanistic models to predict the

31

fatigue life of AC material. Some essential factors missing in fatigue life prediction models developed so far include: i) Placing sufficient emphasis on the reliability (in addition to accuracy) of developed models and ii) Including the actual micro-structure properties of FAM in these models in similar loading conditions as AC. Goal of the current research effort is to fill these critical gaps in the literature.

CHAPTER 3 EXPERIMENTAL PROGRAM

3.1 Overview

In this research effort, two different AC specimens and the corresponding FAM mixes were prepared and tested for linear viscoelastic properties and damage characterization of materials. The AC specimens were fabricated with two different asphalt binders PG 64-22 and PG 76-16. The same mix design was used for both binders with 6.0% binder content and 94% aggregate. The FAM specimens for corresponding AC mix were fabricated with the same asphalt binders (PG 64-22 and PG 76-16) with 12.9% binder content. For simplicity, these mixes are henceforth labeled as either AC_1 or AC_2 respectively. Likewise the corresponding FAM materials are referred to as FAM_1 and FAM_2. The experimental plan for both AC and corresponding FAM is shown in FIGURE 3-1.
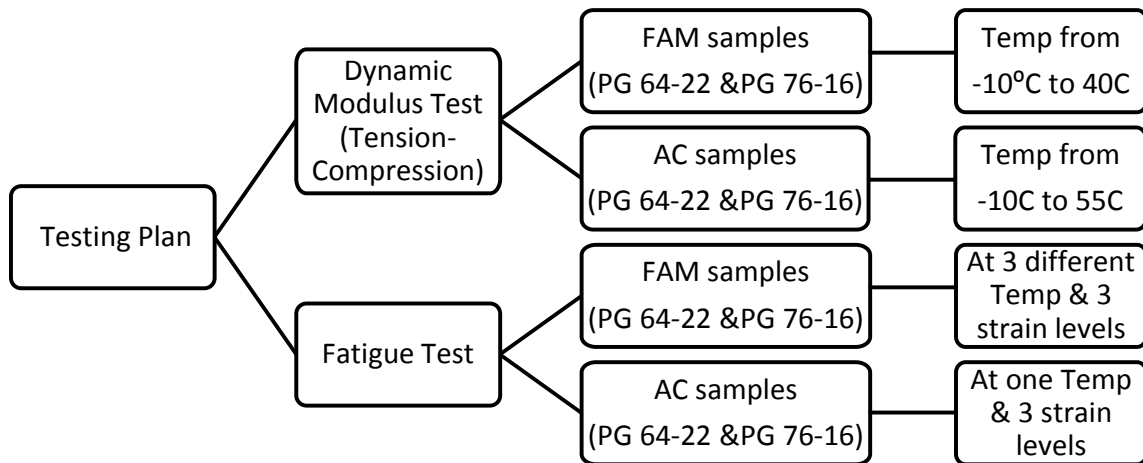
FIGURE 3-1 Experimental Plan

The AC gradation used in this research contains five stockpiles of crushed Salt River gravel of sizes 3/4 in., 1/2 in., 3/8 in., sand, and crushed fines. Superpave 19 mm nominal maximum size of aggregate (NMSA) mixture from the CEMEX Phoenix, Arizona area was used to fabricate AC samples. All the stock piles were oven dried overnight in separate aggregate pans at $110 \pm 5°C$ to dry out moisture present in the aggregates before blending and sieving for the target gradation. The dried aggregate stockpiles of sizes 3/4 in., 1/2 in., 3/8 in., sand, and crushed fines were cooled and blended at proportions of 18%, 12%, 17%, 18%, and 35% respectively to achieve the target gradation of ADOT approved Superpave mix design (*104*). The blended aggregate was sieved using the Gilson Test Master Sieve shaker according to the procedure outlined in AASHTO T-27 and retained aggregate on each size of the sieve was stored separately. Sieved aggregate was used in the batching process for fabrication of AC samples. Specific gravity experiments were conducted on coarse and fine aggregate stockpile samples according to the procedures outlined in AASHTO T85-10, and AASHTO T84-10 respectively. Bulk and apparent specific gravity values of the stockpiles are reported in TABLE 3-1.

TABLE 3-1 Bulk and Apparent Specific Gravity of Aggregate Stockpile

Stockpile	3/4"	1/2"	3/8"	Sand	Crushed fines
Blend percentage	18	12	17	18	35
Bulk specific gravity(Dry)	2.618	2.589	2.599	2.547	2.539
Apparent specific gravity	2.689	2.688	2.696	2.685	2.681

Sieved aggregate was batched at the target gradation shown in TABLE 3-2 and a washed sieve analysis was carried out to account for excess fines from each size of the aggregate. On an average, 2.3% of excess fines were measured from the total batched aggregate. This correction factor was used while batching the aggregate for AC sample preparation to ensure that the amount of fines in the AC mixture confirm to the target gradation. Two AC mixtures were prepared with the same gradation but with different asphalt binders mentioned previously, which were both obtained from HollyFrontier, Phoenix, AZ.

TABLE 3-2 Summary of Asphalt Concrete Gradation

Aggregate Sieve Size (mm)	AC Gradation (% Passing)
25	100
19	91
12.5	83
9.5	76
4.75	60
2.36	46
1.18	32
0.6	22
0.3	13
0.15	8
0.075	4.9
Pan	0
Volumetric Concentration of Filler	27.20%
Binder Content of AC	6%

3.2   Sample Preparation

3.2.1   AC mixture

Sieved aggregate was batched at the target gradation given in TABLE 3-2. Batched aggregate was heated overnight at 160°C. 500 ml Asphalt Binder tins were kept in the oven at 160°C for about 2-3 hours to reach the mixing temperature (160°C). Once asphalt binder reached the mixing temperature, preheated aggregate and 6% of total weight of the binder were blended in the mixing bucket for 90 seconds. The AC mix was transferred into large pans, spread evenly and kept in the oven for 2 hours at compaction temperature to facilitate the short term aging process. Then the AC mixture was cooled and used for conducting theoretical maximum specific gravity (G_{mm}) experiment according to the procedure outlined in AASHTO T209-11. The G_{mm} values of replicates from both the AC mixtures are reported in TABLE 3-3. Average G_{mm} value of each AC mix was used to calculate the percentage air voids of the respective AC sample. Required amount of (short term) aged AC mixture was transferred into Gyratory molds and compacted using the Superpave Gyratory compactor to a diameter (d) of 150 mm and a height (h) of 180 mm. Once the compacted AC samples cooled down, they were cut and cored to a final test specimen geometry of 75 mm (d) x 150 mm (h). After coring and cutting, the air void content of all specimens was measured using the procedure outlined in AASHTO T166-10. The measured air voids of both AC mixture samples were measured to be in the range of 4.0±0.5% as shown in the Appendix A (Table A.3).

TABLE 3-3 Measured Maximum Specific Gravity of Replicates for Both AC mixtures

AC mixture	Sample no.	G_{mm}	Average G_{mm}
PG 64-22	1	2.411	2.411
	2	2.410	
PG 76-16	1	2.427	2.424
	2	2.422	

3.2.2 FAM

As described in the literature review chapter, several researchers started investigating FAM material to explain phenomena such as moisture damage and healing properties of AC mix (*91 - 96*). Though several methods exist in the literature to fabricate FAM material, no standard protocols have been set yet. Careful review of the existing literature was conducted and the FAM material gradation (*102*) and fabrication (*99*) was developed as a part of the current research effort. The gravimetric experiments performed by Underwood and Kim were used as the basis for calculating the percentage binder content and gradation of FAM (*98*). Their study suggests that for a 19 mm nominal maximum aggregate size mixture, the corresponding FAM material maximum aggregate size should be 1.18 mm. Aggregate film thickness approach developed by Radovskiy (for compacted AC mixture) was used to calculate the binder content of FAM (*98, 100*). This procedure is very similar to the method developed by Stanton and Hveem, the only difference being that aggregate particles were assumed to be spherical (*101*). Likewise, as suggested in the literature and based on microstructural investigation, the target air void content of the FAM was established based on the assumption that 52% of total air voids in the mixture existed in the FAM phase (*99*). The binder content of FAM samples in the current study was calculated as 12.9% for a corresponding binder content of 6% in the AC mixture. The

37

engineering properties of FAM material vary depending on the maximum aggregate size in AC mix gradation. So, care should be taken while developing FAM mix design for a corresponding AC mixture. The maximum aggregate size for FAM was established according to the corresponding nominal maximum size aggregate of AC mix. TABLE 3-4 shows the maximum aggregate size of FAM for corresponding AC with varying NMSA (*102*).

TABLE 3-4 Nominal Maximum Aggregate size of FAM for corresponding AC mix

NMSA (mm)	Maximum FAM Particle Size (mm)
37.5	2.36
25	1.18
19	1.18
12.5	0.6
9.5	0.6
4.75	0.3

FAM Mix Design Procedure for Corresponding AC Mix

In the process of calculating FAM binder content and gradation from AC mix design it was assumed that mastic coats all the aggregate particles with uniform film thickness. Volumetric concentration of filler, mastic film thickness, and aggregate gradation of FAM were determined using the procedure outlined below (*102*).

Select maximum size of the aggregate for the corresponding AC mix from TABLE 3-4.

1. Calculate initial gradation of FAM by normalizing the sieve size as 100% passing sieve six for FAM gradation using Equation (3.1).

$$P_{Fi} = \frac{P_i}{P_{FM}} \times 100 \qquad (3.1)$$

38

where;

P_{Fi} =   initial percentage passing sieve size i within the FAM,

P_i =   percentage passing sieve size i from the AC gradation,

P_{FM} =   percentage passing of FAM maximum size sieve from AC

                 gradation

2. Calculate the mass of each sieve size aggregate, M_{Fi} in the FAM, except for the

filler using Equation (3.2)

$$M_{Fi} = \frac{\left(P_{F(i+1)} - P_{Fi} \right)}{\left(G_{sb,i} * \rho_{water} \right)} \tag{3.2}$$

3. Estimate the number of particles of each size using Equation (3.3)

$$N_i = \frac{M_i}{\dfrac{\pi}{6} \left(\dfrac{d_{i+1} + d_i}{2} \right)^3} \tag{3.3}$$

where;

N_i =   total number of particles for the current sieve size,

d_{i+1} =   sieve size opening for the sieve size immediately larger than the

                 current sieve size (cm),

d_i =   sieve size opening for the current sieve size (cm), and

ρ_{water} =   density of water (1 grams/cm^3).

4. Compute the volume of mastic that coats the FAM aggregates using Equations (3.4)

and (3.5). For this calculation, the film thickness is determined by assuming that

the mastic uniformly coats all the aggregate particles.

$$V_{mastic,i} = \frac{\pi}{6} \left[\left(\frac{d_{i+1} + d_i}{2} + 2t \right)^3 - \left(\frac{d_{i+1} + d_i}{2} \right)^3 \right] \qquad (3.4)$$

$$V_{mastic,calc} = \sum_{i=1}^{J} \left[N_i * V_{mastic,i} \right] \qquad (3.5)$$

5. Calculate the amount of absorbed asphalt in each of the FAM particles using Equation (3.6).

$$M_{ba} = \sum_{i=1}^{N} M_{ba,i} = \sum_{i=1}^{N} \left[(P_{i+1} - P_i) \left[\frac{1}{G_{sb,i}} - \frac{1}{G_{se,i}} \right] G_b \right] \qquad (3.6)$$

Where;

M_{ba} =   total mass of absorbed asphalt in mixture (grams),

$M_{ba,i}$ =   mass of absorbed asphalt for aggregate retained on sieve i (grams),

P_{i+1} =   percentage passing the sieve size immediately larger than the current sieve size,

P_i =   percentage passing the current sieve size,

$G_{sb,i}$ =   bulk-specific gravity of aggregate size i,

$G_{se,i}$ =   effective specific gravity of aggregate size i, and

G_b =   specific gravity of binder.

6. Determine the total mass of filler and asphalt in FAM by using the volume of mastic, the volumetrically averaged concentration, %VC (using Equation (3.7)), the absorbed mass of asphalt binder, and the specific gravities of the filler and mastic, using Equations (3.8) and (3.9).

$$\%VC = \frac{V_{075}}{V_{075} + V_{be}} \times 100 \qquad (3.7)$$

where;

$\%VC$ = volumetric concentration of filler within the mastic,

V_{075} = volume of aggregate particles smaller than 75 μm (cm^3), and

V_{be} = effective volume of asphalt binder (cm^3).

$$M_{075} = \frac{\%VC}{100} * V_{mastic,calc} \left(G_{sb,075} * \rho_{water} \right) \qquad (3.8)$$

$$M_b = \left[1 - \frac{\%VC}{100} \right] * V_{mastic,calc} \left(G_b * \rho_{water} \right) + M_{ba} \qquad (3.9)$$

7. Recalculate the gradation based on the masses derived from Step 2 and the filler mass derived from Step 6

8. Calculate the total asphalt content of FAM by equating Equation (3.7) to Equation (3.5).

Using the procedure outlined above, mix design for FAM was developed for corresponding mix design of AC mix as shown in TABLE 3-5. FAM aggregate material was batched according to the gradation shown in the TABLE 3-2 and blended with required quantity of asphalt binder at a mixing temperature of 160^{0}C. Similar to AC, the blended FAM material was also kept in the oven at compaction temperature for two hours to facilitate the short term aging process. The FAM material was cooled and tested for G$_{mm}$. The average G$_{mm}$ value of FAM material was used in the calculation of air voids in the FAM test specimen. Required amount of FAM material at compaction temperature was transferred to Gyratory molds and compacted to a height of 100 mm and diameter of 150

mm using the Superpave Gyratory compactor. Once the sample reached the target height, it was cooled at room temperature for about 30-45 minutes and removed from the gyratory molds. The compacted sample was then cored and cut into FAM samples of 20 mm diameter and 50mm height. Detailed description of sample air void distribution across the height and diameter of compacted FAM sample and information regarding finalizing the test specimen geometry are provided in Chapter 5. Extreme care was taken while preparing the FAM samples as the objective of this effort was to prepare the FAM material as realistically as it exists in the overall AC mixture. Air voids of all FAM test samples measured was given in Appendix A (Table A.2).

TABLE 3-5 Summary of AC and corresponding FAM mix design

Aggregate size (mm)	AC Gradation (% Passing)	FAM Gradation (% Passing)
25	100	100
19	91	100
12.5	83	100
9.5	76	100
4.75	60	100
2.36	46	100
1.18	32	100
0.6	22	67
0.3	13	38
0.15	8	21
0.075	4.9	11
Pan	0	0
Volumetric Concentration of Filler		27.20%
Binder Content of FAM		12.90%
Binder Content of AC		6%
Thickness of Mastic Film		25.14 (μm)

TABLE 3-6 Measured Maximum Specific Gravity of Replicates for Both AC mixtures

FAM mix	Sample no.	Gmm	Average Gmm
FAM_PG 64-22	1	2.214	2.213
	2	2.211	
FAM_PG 76-16	1	2.215	2.215
	2	2.215	

3.3   Test Methods

3.3.1   AC Test Methods

For the purposes of this study AC mixtures were subjected to two different experimental

protocols dynamic modulus and axial fatigue. Both protocols involved tensile loading; so

all specimens were glued to end platens prior to testing. Custom designed gluing jigs that

ensured proper vertical alignment were built and gluing was performed using Devcon 5

minutes epoxy (*105*). For the AC mix specimens, brass buttons were glued onto the sample

surface 90 degrees apart. Brackets were attached to these buttons and used to secure four

sets of linear variable displacement transducers (LVDTs). The LVDTs used for the mixture

tests were MHR100 (± 2.54 mm span) with a gauge length of 100 mm. Dynamic modulus

and fatigue testing was conducted on AC test specimens using the IPC Global UTM 25

servo-hydraulic load frame with environmental chamber (shown in FIGURE 4-2). These

tests were performed by applying repeated sinusoidal loading at a fixed temperature and

frequency.
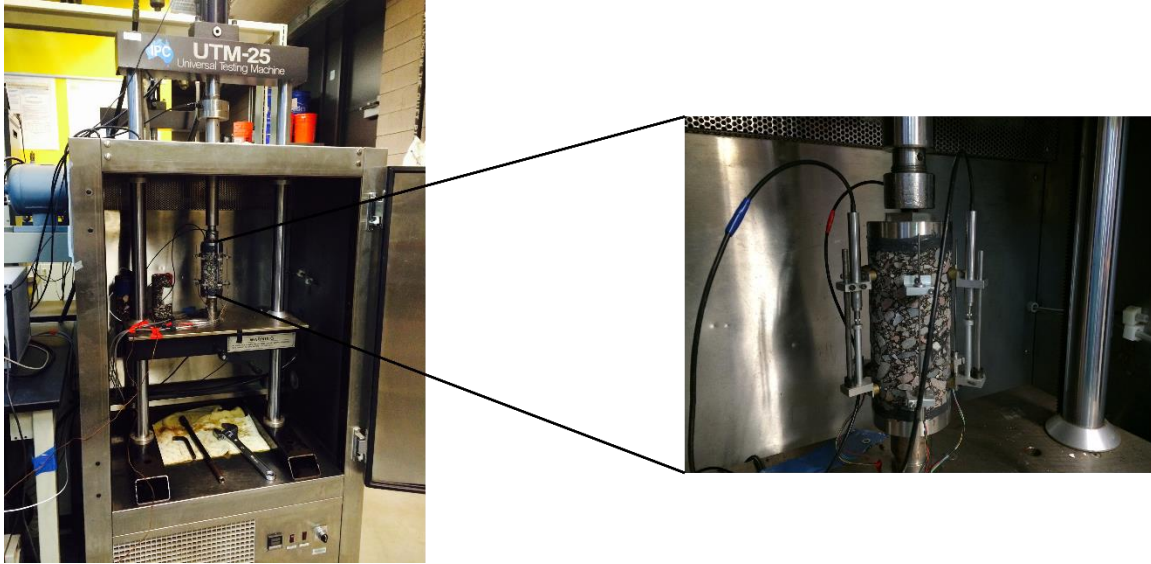
FIGURE 3-2 AC Sample Setup Inside UTM 25 Equipment (Magnified View of Sample Instrumentation in The Right).

Dynamic Modulus Test

The Complex Modulus is a property of a viscoelastic material and it is determined by testing the material under sinusoidal loading conditions. It is a complex number normally denoted as E^* that contains both real and imaginary components, referred to as the Storage Modulus and Loss Modulus respectively. The absolute value or norm of E*, referred to as the dynamic modulus and denoted as $|E^*|$ is more commonly used in the asphalt concrete literature and is determined from experimental data as shown in Equation (3.10) (*103*).

$$| E^* |= \frac{\sigma_0}{\varepsilon_0} \tag{3.10}$$

Where;

σ_0 = peak stress (determined via the method shown in AASHTO T 342) (*106*),

44

ε_0 =   recoverable peak strain (determined via the method shown in AASHTO T

          342) (*106*)

The experiment conducted to characterize the |E*| of the mixture is outlined in AASHTO T-342 with the exception that loading was conducted in tension-compression mode instead of compression only mode. To ensure linear response of the material, tests on AC were conducted at stress levels that yield on-specimen strain values between 50 and 70 µε. The output from this test included temperature ($-10 - 54°C$) and frequency ($25 - 0.1$ Hz) dependent dynamic modulus, |$E*$|, and phase angle, ϕ. IPC Global UTM 25 servo-hydraulic load frame includes a temperature chamber to control and maintain test temperatures within $\pm 0.5°C$. During all the tests, temperature was monitored with an instrumented dummy specimen the same geometry as the test sample. Four replicates from each mix type were tested for modulus.

Fatigue Test

Fatigue tests on AC specimens consist of the repeated and controlled application of sinusoidal loading (either controlled through the load cell or the actuator displacement). In the current research effort, such tests were conducted using tension-compression mode by controlling the actuator. Axial fatigue testing was performed at a frequency of 10 Hz according to AASHTO TP107 (*108*), the diameter of the specimen was 75 mm and the test temperature was 18°C for both PG 64-22 and PG 76-16 AC mixtures. Four tests were performed at different on-specimen strain levels to achieve failure cycles between 1,000 and 100,000. Prior to performing the fatigue test, the |$E*$| value was measured at 18°C and

10 Hz and used to both normalize the results for specimen-to-specimen variation. Fatigue tests were conducted using a controlled sinusoidal actuator displacement tests at 19ºC and 10 Hz, but for 3 different strain levels.

3.3.2   FAM Test Methods

FAM specimens were tested in similar loading conditions as AC for both modulus and fatigue using BOSE Electro Force 3330 series II Axial/Torsional electromechanical load frame with a capacity of ±3 kN and an actuator travel distance of ±12.7 mm (FIGURE 3-3). The load cell in this equipment is positioned on the top and the displacement measurements of the actuator were taken at the top of the loading cell. A torsional load cell (not used in this study) is positioned at the bottom of the loading train of the equipment. To overcome instrument compliance issues, which can occur when deformations are taken via the equipment sensors, FAM samples were instrumented similar to the AC mixture. Since different equipment was used for FAM and AC mixture testing, extreme care was taken to ensure that both machines had the same temperature calibration. Due to the size of the test specimen, only two sets of LVDTs were mounted and these were separated by 180°. The FAM LVDTs were MHR 010 (± 0.254 mm span) with a gauge length of 25 mm. Protocols for FAM sample preparation, instrumentation and testing (similar to test conditions of AC samples) were developed as a part of this research effort. FAM test samples of geometry 20 mm (d) X 50 mm (h) are glued to a set of end platens and instrumented with 010MHR (±0.254 mm) to measure the displacement of the samples during testing. The instrumentation of FAM sample and the test setup is shown in FIGURE 3-3.
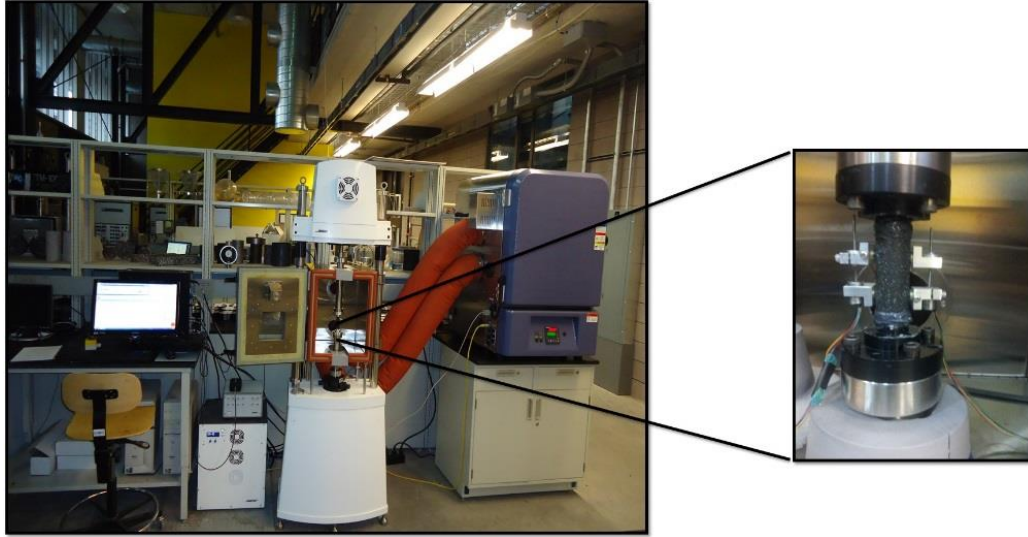
FIGURE 3-3 FAM Sample Setup Inside BOSE Equipment (Magnified View of Sample Instrumentation in The Right).

In all the tests, instrumented FAM specimen was installed inside the BOSE equipment for temperature conditioning. The equipment was kept in the stress control mode with a target load of zero Newtons so that the sample could freely expand and contract during the conditioning phase of the experiments. Thermocouples were installed on the surface and in the middle of the FAM specimen and temperature was closely monitored during conditioning. Testing was performed once this thermally instrumented specimen showed equilibrium (after approximately one hour). In this study, two different tests were performed; temperature and frequency sweep test to determine the dynamic modulus and time-sweep tests to determine the fatigue performance.

Dynamic Modulus Test

The dynamic modulus test was performed by applying repeated sinusoidal loading at a fixed temperature and frequency. In this study the tension-compression mode of loading

was used to test FAM specimens for dynamic modulus measurements at temperatures of -10, 5, 21, 30 and 40°C and frequencies of 20, 10, 5, 1, 0.5, and 0.1 Hz. The number of loading cycles for each frequency were chosen to be same as AC testing method (based on AASHTO T 342 specification) in order to balance the need to reach steady-state loading and the desire to complete the test in a reasonable short period of time(*106*). To ensure linear response of a material, tests on FAM were conducted at stress levels that yielded on-specimen strain values between 60 and 80 $\mu\varepsilon$. For each condition, both on-specimen strain and actuator strain were recorded and analyzed separately to determine $|E^*|$ and assess the impact of machine compliance. The test was performed on four replicates for each FAM type and the results were averaged.

Fatigue Test

Fatigue tests on FAM specimens consist of the repeated and controlled application of sinusoidal loading followed in the AC mixture. Fatigue testing was conducted using tension-compression mode of loading at constant actuator strain levels. Tests were conducted at three different strain levels and at temperatures 10°C, 19°C, and 25°C. The target strain levels at each temperature were set to reach a fatigue life of 1000, 10000 and 100000 cycles. Both on-specimen strain and actuator strain were recorded for analysis purposes. The actuator and on specimens strain comparisons for FAM testing are presented in the Chapter 5.

3.4   Summary

This chapter describes various types of aggregate and binder used in this research effort to fabricate AC and FAM samples. It also provides a summary of AC and FAM materials mix

design, instrumentation, and the test methodologies used in this study. As a part of the study, testing protocols are developed for FAM in similar loading conditions (axial direction) as AC. A brief summary of these test methodologies is given in this chapter. Detailed description of FAM instrumentation and testing protocols are presented in Chapter 5.

CHAPTER 4 RELIABILITY ANALYSIS OF FATIGUE LIFE PREDICTION FROM THE VISCOELASTIC CONTINUUM DAMAGE MODEL

4.1 Introduction

Fatigue cracking is one of the major types of distress observed in AC pavements. This distress initiates due to the repeated application of traffic loads. The ultimate propagation of these cracks allows moisture to enter the AC and supporting layers, which leads to further reduction in the service life of a pavement structure. Hence it is important to predict the fatigue resistance of AC materials before using them in construction. Researchers have used several different modeling techniques as discussed in the literature review chapter for the purposes of pavement fatigue life prediction; 1) Empirical fatigue models (10), 2) artificial neural network models (109), 3) fracture models (46, *110*, 111), and 4) viscoelastic continuum damage models and simplified viscoelastic damage models (S-VECD) (19, 48, *56, 57, 63*). Overall there has been considerable interest in adopting one or the other of the latter two, mechanistic based modeling approaches (112, *79, 83*). The essential goal for each of these models is to predict the performance of a pavement structure. Current practice with pavement analysis results in reliability based predictions of either distresses for a given design (the mechanistic-empirical paradigm) or the allowable number of wheel applications for a given design and serviceability loss (empirical paradigm). The important concept that exists in both approaches is

reliability (83, *84, 78*). Reliability analysis in pavement design was first introduced in the AASHTO 1986 pavement design guide in order to better calculate the present serviceability index of pavements. More recently, the Mechanistic Empirical Pavement Design Guide (MEPDG) (now AASHTO Pavement ME Design) incorporated reliability by using the standard deviation of measured distress obtained from calibration procedure using the existing data (*78*). So while advanced models have shown promise at yielding more accurate and generally applicable deterministic prediction of material performance than their empirical counterparts (*7, 8, 63, 72, 83-86*) the reliability of these predictions has not received substantial attention. In fact during the literature search, no studies were found on the evaluation of reliability of advanced model predictions. However, these models introduce additional experiments and requisite variables that each carry unique and inherent variability. It is therefore plausible that while better deterministic predictions can be made, the overall reliability of these predictions may not be as good.

One potential test case used in this research study for reliability analysis is S-VECD model, which has gained particular interest among the research community and considerable literature has been published on this approach (*19*, 48, *54, 56, 57, 63*). In short, the S-VECD method involves experimental characterization of the inherent fatigue resistance of the asphalt concrete mixture in terms of the damage characteristic curve. This curve is identified from repeated loading axial fatigue experiments with varying strain magnitudes. Each test is individually analyzed and the resultant individual curves are averaged to obtain the one that represents the given mixture. To create a complete fatigue prediction algorithm, this damage curve is coupled with two additional functions; the inherent linear viscoelasticity (separately characterized with temperature and frequency

sweep experiments) and a failure criteria. Thus, there exist three possible sources of variation that contribute to the overall reliability of S-VECD based predictions. In this study, the issue of reliability in advanced models is evaluated by using the S-VECD model as a test case and by considering each of these three sources of variation.

There is considerable body of existing literature on the S-VECD model theory, failure criteria methods, and the effort towards developing accurate failure criteria (*19, 56, 57, 63, 72, 66 - 70*). Deciding which of these criteria is accurate or works best in fatigue life prediction with the S-VECD model is beyond the scope of this study. Rather, the intent is to evaluate the relative merits of each only from the perspective of reliability. By understanding the sources of variability and their impact on ultimate reliability it is believed that the experimental and analytical processes inherent in the model can be improved so as to improve the overall reliability of model predictions.

4.2   Failure Criteria Variation

4.2.1   Experimental Failure Criteria Variation

As mentioned in the literature review chapter some of frequently used criteria with respect to defining failure in the experiment are; the cycle when the phase angle starts to reduce (*66, 67*), the cycle when the modulus is 50% of the initial value (*68*), and peak of the product of stiffness and corresponding load cycle number (N) (*69, 70*). During the fatigue data analysis, failure was defined separately for these methods. Each of these methods have been applied to the experiments and the resultant failure envelopes are shown in TABLE 4-1 where it can be seen that number of failure cycles (N_f) changes from one failure criteria approach to other.

52

TABLE 4-1 AC_1 Variation in Number of Failure Cycles for Different Experimental Failure Criteria

Strain Level	N_f		
($\mu\varepsilon$)	PA drop	$C \times N$	50% reduction of initial modulus
210	86,668	91,587	73,092
245	14,832	13,481	14,709
329	18,579	15,362	12,877
468	3,606	3,019	2,784

4.2.2 *Variation in Model Failure Criteria Approaches*

Rules used in this research two identify failure in the S-VECD model predictions include; the pseudo stiffness at failure (C_f) approach (*19, 54, 56, 71*) and the pseudo energy release rate approach (*72, 73, 74*). The summary of these model failure criteria approaches are explained in detail in the literature review chapter.

First model failure criteria considered is pseudo stiffness at failure approach. Since the failure cycle changes depending on the experimental definition of failure and so too do the values of C_f in the S-VECD characterization tests. For example, in the case of the study mixture C_f is 0.310 when using the phase angle drop method, 0.433 when using the 50% initial modulus method, and 0.412 when using the $C \times N$ method. To demonstrate the effect of different failure criteria consider Equation (4.1), which produces an estimate of the number of cycles to failure given a strain amplitude, damage characteristic relationship, test temperature and frequency, and C_f. Since the average C_f value is different from one definition of failure to another the predicted fatigue life is also different as shown in FIGURE 4-1. Note that these comparisons are all deterministic, meaning they are *correct* in so much as the different experimental definitions of failure are correct.

$$N_f = \frac{\left(f_{red}\right)\left(2^{3\alpha}\right)\left(\dfrac{(1-C_f)}{C_{11}}\right)^{\frac{(\alpha-\alpha C_{12}+1)}{C_{12}}}}{\left(\alpha-\alpha C_{12}+1\right)\left(C_{11}C_{12}\right)^{\alpha}\left[\left(\varepsilon_0\right)\left(|E*|_{LVE}\right)\right]^{2\alpha}K_1} \qquad (4.1)$$
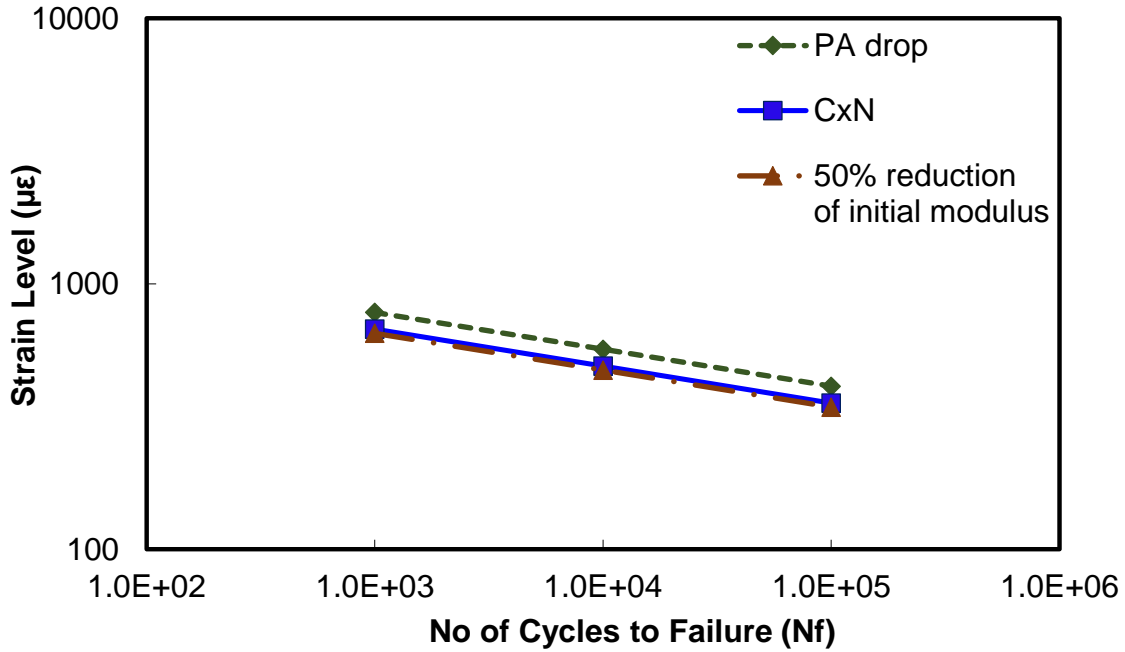
FIGURE 4-1 AC_1 Simulated Fatigue Lives Plot or AC Mixture According C_f Model Failure Criteria Using Three Different Experimental Failure Point Identification Methods.

The second model failure criteria uses pseudo strain energy release rates. Average pseudo strain energy release, G^R rate for each experimental failure criteria was calculated using the, Equation (2.12). The relationship between G^R and N_f follows the power law function shown in Equation (2.14). Like with the C_f approach, since the failure cycle changes from one experimental failure criteria to another the corresponding relationship (a and b coefficients) also changes. The effect of differences in the G^R characteristic equation from one experimental failure criteria to another is shown in FIGURE 4-2.
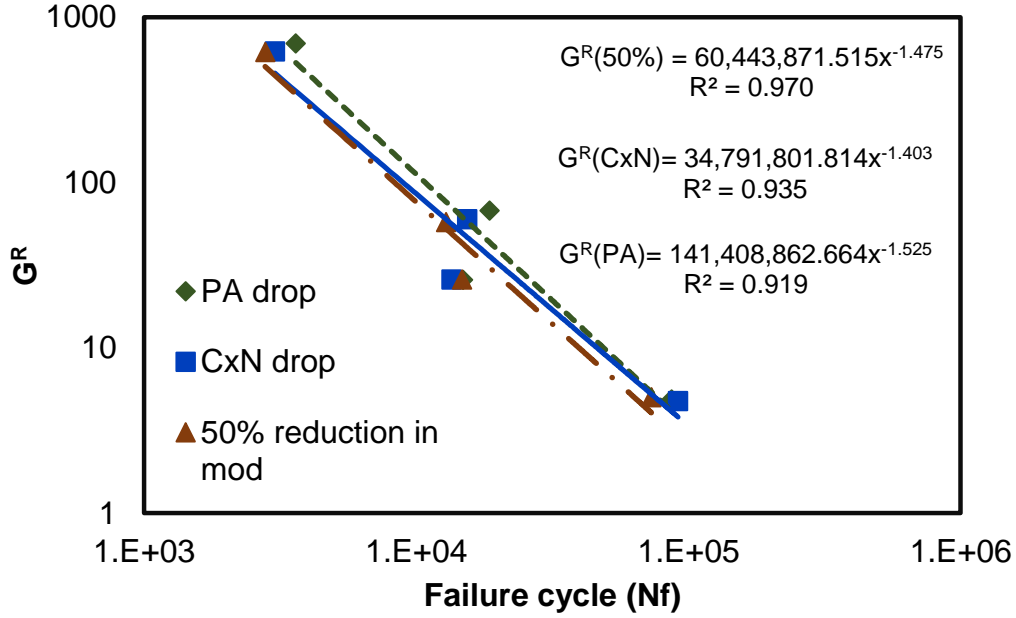
FIGURE 4-2 AC_1 Variation in G^R Characteristic Equation for Different Experimental Failure Criteria.

The effect of the differences in a and b as a function of the experimental failure criteria can be found by examining Equation (4.2). This equation estimates N_f for a given a strain amplitude, damage characteristic relationship, test temperature and frequency, and G^R characteristic relation. The effect of differences in the G^R characteristic equation in predicting number of failure cycles from one experimental failure criteria to another is shown in FIGURE 4-3. As mentioned in previous section these comparisons are deterministic.

$$N_f = \left[\frac{\dfrac{\alpha - C_{12}\alpha + 1}{\alpha - C_{12}\alpha + 1 + C_{12}} \dfrac{C_{11}}{2a} \left[\dfrac{1}{2}(\varepsilon_0)(|E*|_{LVE}) \right]^2 \times}{\left(\dfrac{(\alpha - C_{12}\alpha + 1)(C_{11}C_{12})^\alpha \left[\dfrac{1}{2}(\varepsilon_0)(|E*|_{LVE}) \right]^{2\alpha} K_1}{f_{red} \times 2^\alpha} \right)^{\frac{C_{12}}{\alpha - C_{12}\alpha + 1}}} \right]^{\frac{\alpha - C_{12}\alpha + 1}{(\alpha+1)(b+1) - C_{12}(\alpha + b\alpha + 1)}} \tag{4.2}$$
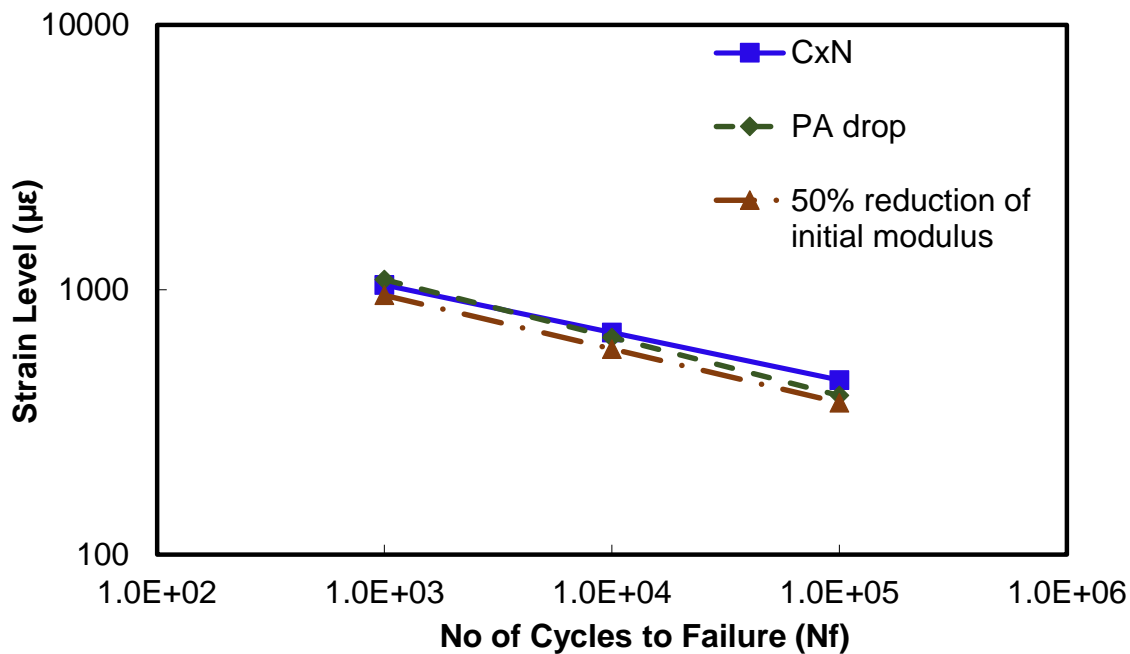
FIGURE 4-3 AC_1 Simulated Fatigue Lives Plot or AC Mixture According G^R Model Failure Criteria Using Three Different Experimental Failure Point Identification Methods.

4.2.3   *Summary of Failure Criteria Comparisons*

It should be noted that the fatigue life predictions for the different experimental and model failure criteria shown in FIGURE 4-1 and FIGURE 4-3 was performed simply to show the differences in prediction values from one approach to another. The intention is not to suggest the particular failure criteria that is accurate. In fact, one could consider all three accurate in so-much that they are consistent with the rules and procedures used to identify failure in the experiments. Instead, the intention is to show that the reference for the accurate prediction of fatigue life of an AC mixture varies is dependent upon the failure criteria adopted. The remaining sections of this chapter evaluate the reliability of these

different predictions given the inherent variability of the linear viscoelastic characterization, the damage characterization, and the failure criteria.

4.3 Reliability Analysis Framework

Reliability is a common practice used for measuring the consistency/precision of prediction measurements. It is not a method that can be used to assess the accuracy, and thus in this study *accurate* varies according to the failure criteria considered. In the reliability analysis considered here, the reference *accurate* fatigue life prediction for each failure criteria approach is considered to be that shown in FIGURE 4-1 & FIGURE 4-3. The reliability analysis was conducted for each failure criteria approach at two fatigue life cycles, 1,000 (low) and 100,000 (high) cycles. The factorial combinations of experimental and model based failure criteria were evaluated for a total of 12 different cases. FIGURE 4-4 shows a flow chart of the different cases considered here.
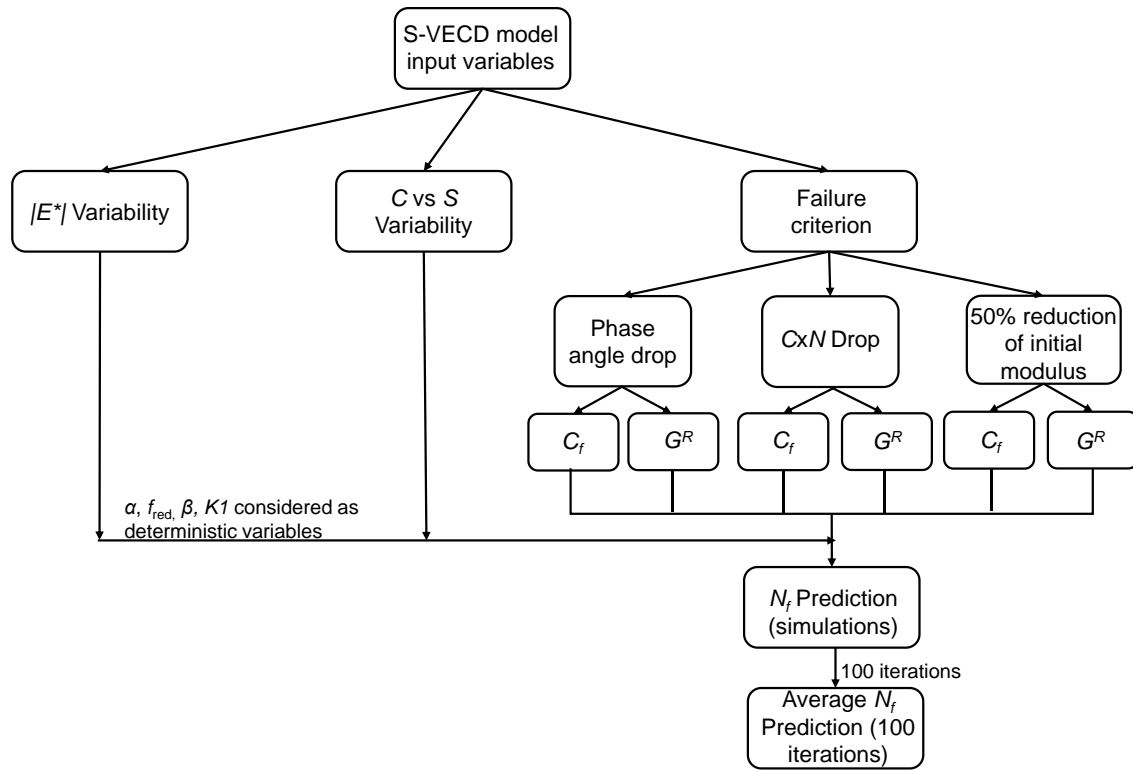
FIGURE 4-4 Monte Carlo Simulation Procedure for Reliability of Fatigue Life
Prediction for Various Failure Criteria Approaches.

The approach adopted to evaluate reliability involved multiple Monte Carlo simulations considering the observed variation in $|E^*|$, damage characteristic curves, and failure criteria. A similar approach has been applied to develop reliability metrics for pavement related applications in the past and affords a robust and proven methodology (*83, 78*). Outside of the pavement and materials community it is also a common procedure for developing reliability analysis of prediction models (*113*). The simulation technique is developed to establish the distribution of output variable according to the input variable probabilistic distributions. The step by step procedure for this Monte Carlo simulation technique used in this study is described below.

Step 1: Identify the strain levels for each of the 12 different evaluation cases that yield 1,000 and 100,000 cycles to failure.

Predicting the number of cycles to failure requires strain input as well as input for the model variables. In this step, the deterministic prediction is performed for each of the 12 different evaluation cases by using the average or representative values for the input variables. This strain value is then used later on in Steps 4 and 5 to perform the Monte Carlo simulations.

Step 2: Identify the input variables that are associated with uncertainties in the response variable.

In the current study the response variable is the predicted cycles to failure and the input variables that include uncertainty are modulus, damage characteristic relationship, and the variation within each model failure criteria. These input variables were modeled using probabilistic distributions established in Step 2. Other inputs, including α, $f_{red,}$ β and K_1 were considered as deterministic variables.

Step 3: Identify the probabilistic distributions of input variables associated with the uncertainty or variability in measurements by using a frequency diagram.

From the available experimental data modulus distribution is considered as normal distribution. Due to limited experimental data on G^R characteristic equation coefficients and C_f, these variables are assumed as normal distributions. The damage characteristic curve slope variable (C_{12}) distribution was assumed as uniform because the variation in slope of the characteristic equation need to be restricted in

59

such a way that the resulting characteristic equation lies within the replicate C vs S damage curves. The normal and uniform distribution formulations are given in the Equation (4.3) and (4.4) respectively.

$$f_x(x) = \frac{1}{\sqrt{2\Pi}\sigma} \exp\left[-\frac{1}{2}\left(\frac{x-\mu}{\sigma}\right)^2\right] \qquad (4.3)$$

$$f_x(x) = \frac{1}{m-n} \qquad (4.4)$$

Where;

μ, σ = mean and standard deviation of population

m, n = maximum and minimum values of a population

Step 4: Generate 10,000 sets of random numbers for the input variables according to their probabilistic distribution.

The number of simulations used was established in such a way that Monte Carlo procedure will reach the convergence criteria with less number of iterations and less computational time.

Step 5: Predict the fatigue life for each randomly generated combination of input variables from Step 4.

The strain level identified in Step 1 is combined with the 10,000 sets of random numbers from Step 4 to produce 10,000 different predictions for the number of cycles to failure. These predictions constitute a single Monte Carlo simulation.

60

Step 6: Run the Monte Carlo simulation for 100 iterations.

The number of iterations selected for this step was chosen that the simulations could be completed in reasonable amount of time and also to reach convergence criteria of 5%.

Step 7: Calculate the reliability of S-VECD model fatigue life prediction from the average of 100 iterations.

The reliability of the fatigue life prediction for different levels of prediction error (*%Error*) was calculated using Equation (4.5) below (*113*). Note that the % *Error* is the difference in the deterministically predicted N_f and the values from Step 6 divided by the deterministic value, e.g., a ±50% error at 100,000 cycles indicates a prediction between 50,000 and 150,000 cycles. It could be argued that since fatigue performance plots are shown in logarithmic space that the fair error definition should be based on error of the logarithm of predicted fatigue life. However, this approach ignores the actual use of these models, which is to predict the failure cycle arithmetically. Even in mechanistic-empirical prediction algorithms where damage is quantified, it is taken as the ratio of applied cycles to N_f. In this, the arithmetic error provides a better match to the true impacts of prediction errors.

$$P((1-X\%)N_f < N_f < (1+X\%)N_f) = \frac{number\ of\ simulations\ where\ N_f\ is\ within\ \%Error}{total\ number\ of\ simulations} \quad (4.5)$$

4.4   Reliability Framework to S-VECD Model

4.4.1   *Reliability of Fatigue Life Prediction for C_f Failure Criteria*

The variations in input variables for the Monte Carlo simulations considering C_f as the model failure criteria are summarized in TABLE 4-2. FIGURE 4-5 shows the reliability of fatigue life predictions for the different failure criteria as a function of prediction percentage error to the accurate value. As mentioned earlier, accurate fatigue life prediction is a matter of the experimental wise definition of failure. In this figure the reference cycles to failure is set based on the deterministic prediction from each respective method. Percentage error calculated for each failure criteria approach is based on the reference accurate fatigue life predicted (shown in FIGURE 4-1) using the deterministic values because the objective of this study is to see the reliability of different methods. From FIGURE 4-5 it can be observed that in order to achieve high reliability the resultant error will also be high, e.g., the error for 90% reliability in all cases is approximately ±50%. In addition to predict fatigue life with 50-60% reliability the error associated with prediction is 30%, but to have 90% reliability of error in prediction quickly increase to 50%. It is also observed that the reliability measurements from the various failure point identification methods are different as the reliability increases. However in both low and high fatigue life prediction cases the 50% modulus reduction approach tends to have higher reliability than the other two methods. The reason for this trend could be the less variation associated with the C_f parameter for 50% modulus reduction approach than other approaches.

TABLE 4-2 AC_1 Variation of Input Parameters for Predicting Fatigue Life Using C_f Approach

Experimental Failure Criteria	Parameter	Mean	Standard Deviation	CV
PA drop	$|E^*|$ (MPa)	8863	524	5.9
	C_{12}	0.504	0.012	2.3
	C_f	0.31	0.081	26.3
	G^R (High cycles) [1]	3.641	1.118	30.7
	G^R (Low cycles) [2]	622.5	130.5	20.9
C x N	$|E^*|$ (MPa)	8863	524	5.9
	C_{12}	0.504	0.012	2.3
	C_f	0.412	0.052	12.6
	GR (High cycles) [1]	3.819	1.319	34.5
	G^R (Low cycles) [2]	372.1	121.9	32.8
50% reduction of initial modulus	$|E^*|$ (MPa)	8863	524	5.9
	C_{12}	0.504	0.012	2.3
	C_f	0.433	0.028	6.3
	G^R (High cycles) [1]	2.932	0.93	31.7
	G^R (Low cycles) [2]	352.1	84.2	23.9

[1]$high$ = 100,000 cycles, [2]Low = 1,000 cycles
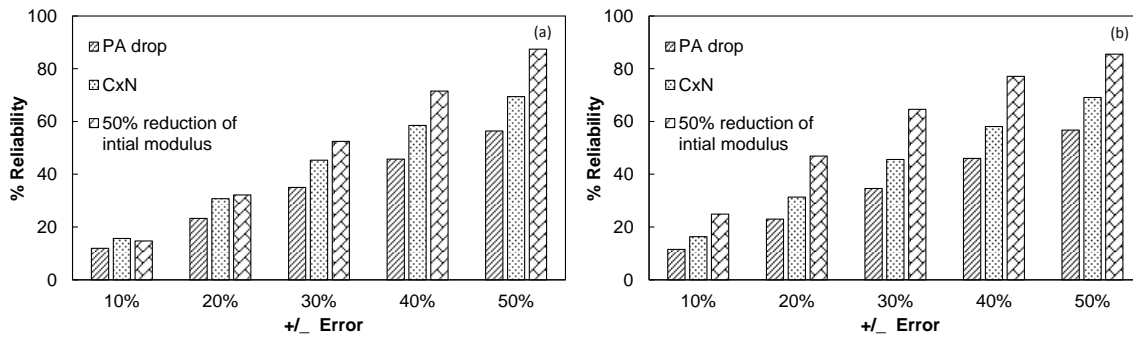
FIGURE 4-5 AC_1 Reliability of Fatigue Life Prediction for Various Experimental Failure Point Identification Methods Using C_f Failure Criteria for; (A) High and (B) Low Number of Failure Cycles.

4.4.2 Reliability of Fatigue Life Prediction for G^R Failure Criteria

The variations in input variables for the Monte Carlo simulations considering G^R as the model failure criteria are given in TABLE 4-2. In this approach characteristic equation coefficients were calculated for every combination of three out of the four tests conducted. The variation in G^R values were calculated using the characteristic equations developed for each of the three test combinations. The G^R values distribution was then randomly generated within the observed experimental G^R range using its point estimates as shown in TABLE 4-2 for low and high fatigue life cycles. This procedure was performed to make sure that the characteristic equation coefficients generating for simulations are representative of within the observed experimental G^R range. FIGURE 4-6shows the reliability of fatigue life prediction measurements for G^R method at low and high number of failure cycles for the different evaluation techniques for target percentage prediction error. Similar to the analysis with the C_f approach, accurate fatigue life prediction is based on experimental definition of failure as shown in FIGURE 4-3. In this approach, the reliability measurements for each experimental criteria are not substantially different. In this case also 50% modulus reduction approach shows more reliability than other two failure criteria approaches for both high and low number of failure cycles. FIGURE 4-6 shows that the reliability variation with the prediction error and that the difference in reliability between the different experimental failure criteria is not that different from low to high number of failure cycle predictions.

FIGURE 4-6 AC_1 Reliability of Fatigue Life Prediction for Various Experimental Failure Point Identification Methods Using G^R Failure Criteria for (A) High and (B) Low Number of Failure Cycles.

4.4.3 Reliability Comparisons between C_f and G^R Failure Criteria

For model failure criteria reliability comparison purpose, reliability analysis for both C_f and G^R failure criteria was conducted at 10,000 cycles. The reason for choosing this fatigue cycle number is to avoid errors that are associated with extrapolation of the G^R failure criteria.

FIGURE 4-7 shows the reliability measurements of different experimental failure criteria approaches for both C_f and G^R model approaches at 10,000 failure cycle prediction. It can be observed that C_f approach is showing more reliable measurements than the G^R approach irrespective of experimental failure criteria. However this statement is only true with respect to reliability predictions only not for accurate fatigue life predictions. In reality the method gives more accurate prediction is still debated.
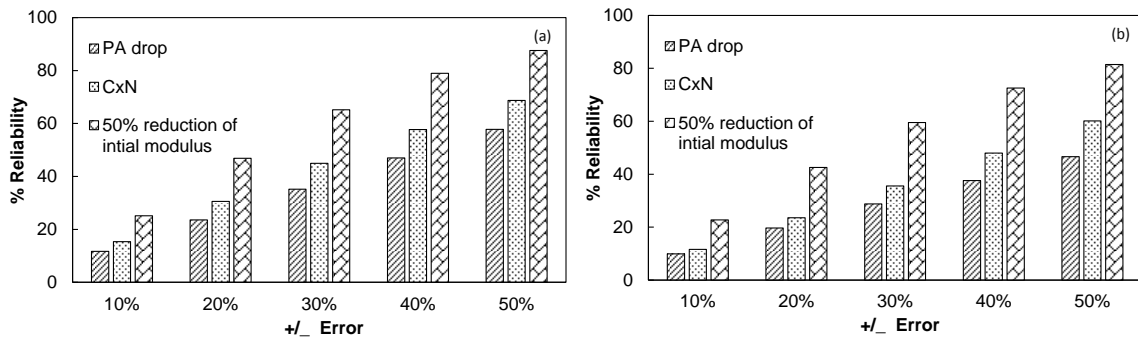
FIGURE 4-7 AC_1 Reliability of Fatigue Life Prediction for Various Experimental Failure Point Identification Methods for 10,000 Cycles (A) C_f Failure Criteria and (B) G^R Failure Criteria.

4.5   Reliability Analysis for AC_2 Mixture Data

Reliability analysis was also conducted for AC_2 mixture data in similar to AC_1 data. The purpose of this analysis on AC_2 is to confirm the trends observed between C_f and G^R failure criteria approaches from AC_1 mix data. In addition, will also shows that developed reliability framework is generalized approach can be used for any other mixtures. Variation observed in G^R characteristic equations, simulated fatigue lives using deterministic method for C_f and G^R approaches for each experimental failure criteria is given in the Appendix B Figure B-18 to B-20.

4.5.1   *Reliability of Fatigue Life Prediction Using C_f and G^R Failure Criteria*

Reliability analysis was conducted for AC_2 data for above mentioned three experimental failure approaches and two model failure criteria approaches in similar to AC_1 mix. The variation in input parameters of S-VECD model used for AC_2 mix reliability simulations are given in TABLE 4-3.

66

TABLE 4-3 AC_2 Variation of Input Parameters for Predicting Fatigue Life

Experimental Failure Criteria	Parameter	Mean	Standard Deviation	CV
PA drop	$|E^*|$ (MPa)	11308	705	6.2
	C_{12}	0.558	0.067	12.064
	C_f	0.481	0.019	3.965
	G^R (High cycles) [1]	3.35	2.29	68.17
	G^R (Low cycles) [2]	43.40	8.39	19.33
C x N	$|E^*|$ (MPa)	11308	705	6.2
	C_{12}	0.558	0.067	12.064
	C_f	0.511	0.066	12.967
	GR (High cycles) [1]	3.24	1.84	56.71
	G^R (Low cycles) [2]	42.33	5.76	13.60
50% reduction of initial modulus	$|E^*|$ (MPa)	11308	705	6.2
	C_{12}	0.558	0.067	12.064
	C_f	0.473	0.023	4.897
	G^R (High cycles) [1]	3.09	2.08	67.29
	G^R (Low cycles) [2]	42.92	8.32	19.39

[1]$high$ = 100,000 cycles, [2] Low = 1,000 cycles

Probabilistic distributions of input parameters were considered in similar to AC_1 mix and reliability simulations were conducted for 100 iterations and averaged. As mentioned earlier, percentage error calculated for each failure criteria approach is based on the reference accurate fatigue life predicted which is shown in Appendix B Figure B-18 &B-20. Reliability analysis results for each experimental criteria for both C_f and G^R approaches are given in FIGURE 4-8 and FIGURE 4-9. Reliability of the fatigue life prediction for C_f model failure criteria is observed to be sensitive with respect to the experimental failure criteria, where as in the case of G^R approach it is not very sensitive. This similar trend was also observed with AC_1 mix reliability results. From FIGURE 4-8 it can be observed that the PA drop approach is showing more reliable results than other two, which is in line with the variation observed from test replicate C_f values from AC_2

data which is shown in TABLE 4-3. Similar trend is also observed in G^R approach reliability results which is shown in FIGURE 4-9.
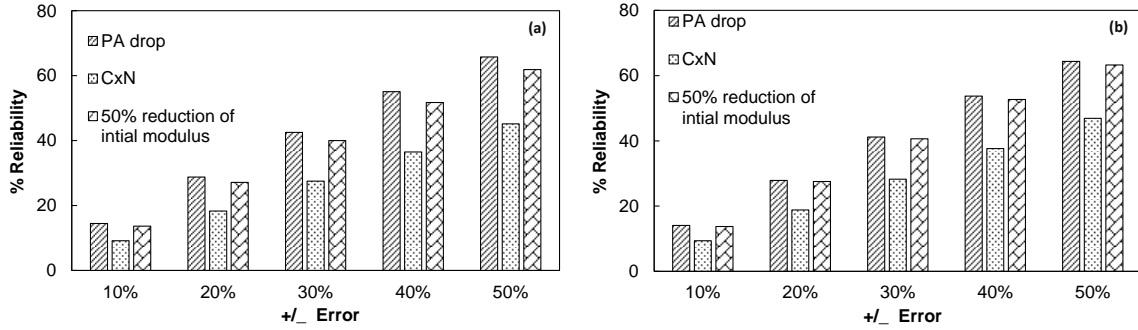
FIGURE 4-8 AC_2 Reliability of Fatigue Life Prediction for Various Experimental Failure Point Identification Methods Using C_f Failure Criteria for; (A) High And (B) Low Number of Failure Cycles.
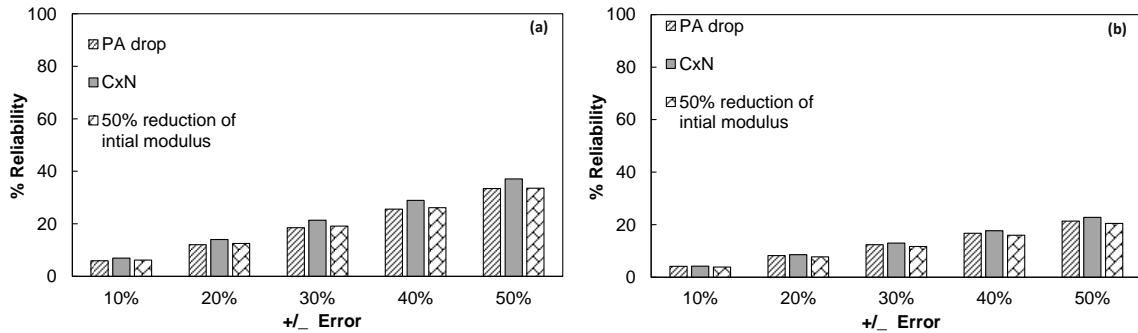
FIGURE 4-9 AC_2 Reliability Of Fatigue Life Prediction for Various Experimental Failure Point Identification Methods Using G^R Failure Criteria For (A) High And (B) Low Number of Failure Cycles.

In similar to AC_1 mixture reliability analysis, for reliability measurements comparison between model failure criteria approaches reliability analysis was conducted at 10,000 cycles for both C_f and G^R failure criteria. FIGURE 4-10 shows the reliability measurements of AC_2 mixture for different experimental failure criteria approaches for

both C_f and G^R model approaches at 10,000 failure cycle prediction. It can be observed that C_f approach is showing more reliable measurements than the G^R approach irrespective of experimental failure criteria. Similar trend was also observed in the AC_1 mixture fatigue prediction reliability results.
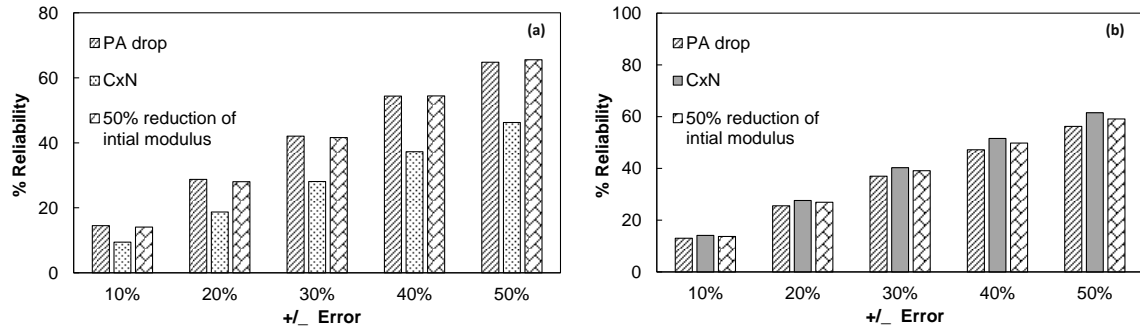
FIGURE 4-10 AC_2 Reliability of Fatigue Life Prediction for Various Experimental Failure Point Identification Methods for 10,000 Cycles (A) C_f Failure Criteria and (B) G^r Failure Criteria.

4.6   Reliability Analysis for Different Gradation Mixtures

Reliability analysis was performed for five AC mixtures with different gradations and volumetric properties. The purpose of conducing this analysis was to assess the adoptability of reliability framework for various AC mixtures. Data obtained as part of the project titled "Selection of Long Lasting Rehabilitation Treatment Using Life Cycle Cost Analysis and Present Serviceability Rating" conducted for the Oklahoma Department of Transportation was used for the analysis. Modulus and fatigue experimental data of each mixture was analyzed to predict the variation of input variables in the S-VECD model formulation. Reliability analysis was conducted at three different experimental failure criteria using C_f as the model failure criteria in the S-VECD model. Since S3 64-22, and S4 64-22 mixtures

69

failed before reaching 50% of the initial modulus, analysis could not be performed for these mixtures using 50% reduction of initial modulus failure criteria. TABLE 4-4 shows the volumetric information of AC mixtures and experimental failure criteria considered for analysis. The replicate modulus data of each mixture is given in Appendix B Table B.13 to B17 and damage characteristic curve plots in Appendix B Figure B-13 to B-17.

TABLE 4-4 Ac Mixtures Volumetric Information and Experimental Failure Criteria Used For Each Mixture Reliability Analysis

Mix type	PA Drop	C x N	50% modulus reduction	Mix type	%AC	% RAP	NMSA
S3 64-22	Y	Y	NA	Base	4.4	15	19.0
S4 64-22	Y	Y	NA	Surface	4.8	25	12.5
S4 70-28	Y	Y	NA	Surface	5.0	15	12.5
S4 76-28	Y	Y	Y	Surface	4.9	15	12.5
S5 76-28	Y	Y	Y	Surface	5.3	15	9.5

NA= Not Available

Reliability analysis was conducted for all five mixtures at 10,000 cycles. As mentioned earlier, the reason for choosing 10,000 failure cycles for the analysis was to avoid any errors associated with extrapolation of results beyond the experimental failure number of cycles. The reliability framework developed in this study was used to predict the fatigue life of all the five AC mixtures. The variation observed in the input variables of S-VECD model formulation for each AC mix is presented in TABLE 4-5 and TABLE 4-6. The reliability analysis of fatigue life prediction for each mix is shown in FIGURE 4-11 and FIGURE 4-12.

TABLE 4-5 Variation of S3 64-22, S4 64-22 AC Mixtures Input Parameters for Predicting Fatigue Life

Experimental Failure Criteria	Parameter	S3 64-22			S4 64-22		
		Mean	SD[1]	CV	Mean	SD[1]	CV
PA drop	$|E*|$ (MPa)	9037	998	11.0	8764	403	4.6
	C_{12}	0.545	0.043	7.9	0.528	0.017	3.2
	C_f	0.551	0.071	13.0	0.505	0.050	9.9
C x N	$|E*|$ (MPa)	9037	998	11.0	8764	403	4.6
	C_{12}	0.545	0.043	7.9	0.528	0.017	3.2
	C_f	0.552	0.074	13.4	0.521	0.062	11.8

[1]SD= Standard Deviation

TABLE 4-6 Variation of S4 70-28, S4 76-28, S5 76-28 AC Mixtures Input Parameters for Predicting Fatigue Life

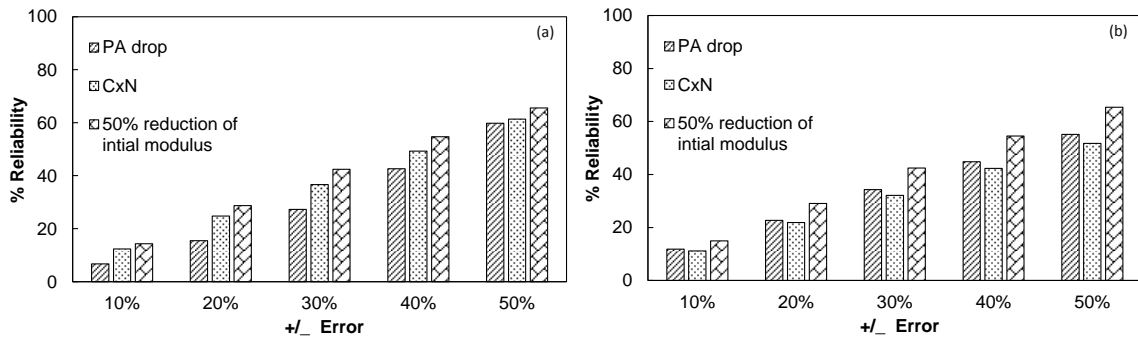| Experimental Failure Criteria	Parameter	S4 70-28			S4 76-28			S5 76-28		
		Mean	SD[1]	CV	Mean	SD[1]	CV	Mean	SD[1]	CV
PA drop	$|E*|$ (MPa)	4031	388	10	4552	93	2	5559	415	7
	C12	0.366	0.026	7	0.298	0.021	7	0.343	0.044	13
	Cf	0.250	0.093	37	0.139	0.092	66	0.162	0.105	65
C x N	$|E*|$ (MPa)	4031	388	10	4552	93	2	5559	415	7
	C12	0.366	0.026	7	0.298	0.021	7	0.343	0.044	13
	Cf	0.285	0.076	27	0.221	0.135	61	0.178	0.094	53
50% reduction of initial modulus	$|E*|$ (MPa)	4031	388	10	4552	93	2	5559	415	7
	C12	0.366	0.026	7	0.298	0.021	7	0.343	0.044	13
	Cf	0.420	0.060	14	0.349	0.036	10	0.372	0.040	11

[1]SD= Standard Deviation
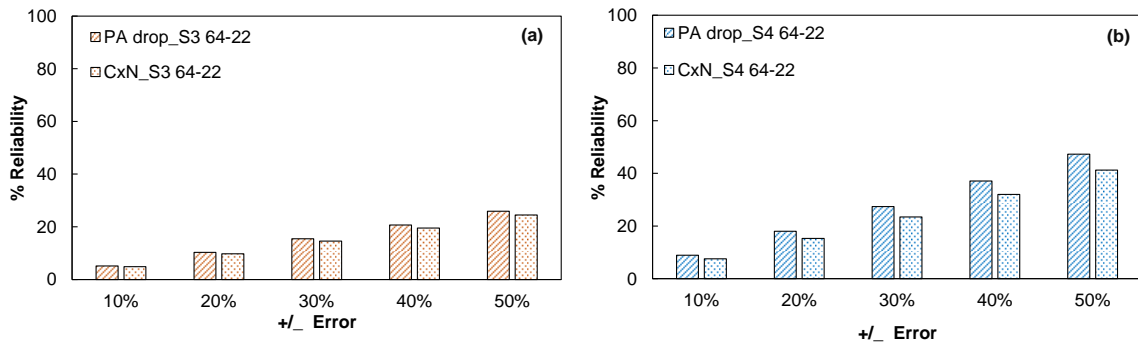
FIGURE 4-11 Reliability of S3 64-22 AC Mix Fatigue Life Prediction for Various Experimental Failure Point Identification Methods Using C_f Failure Criteria
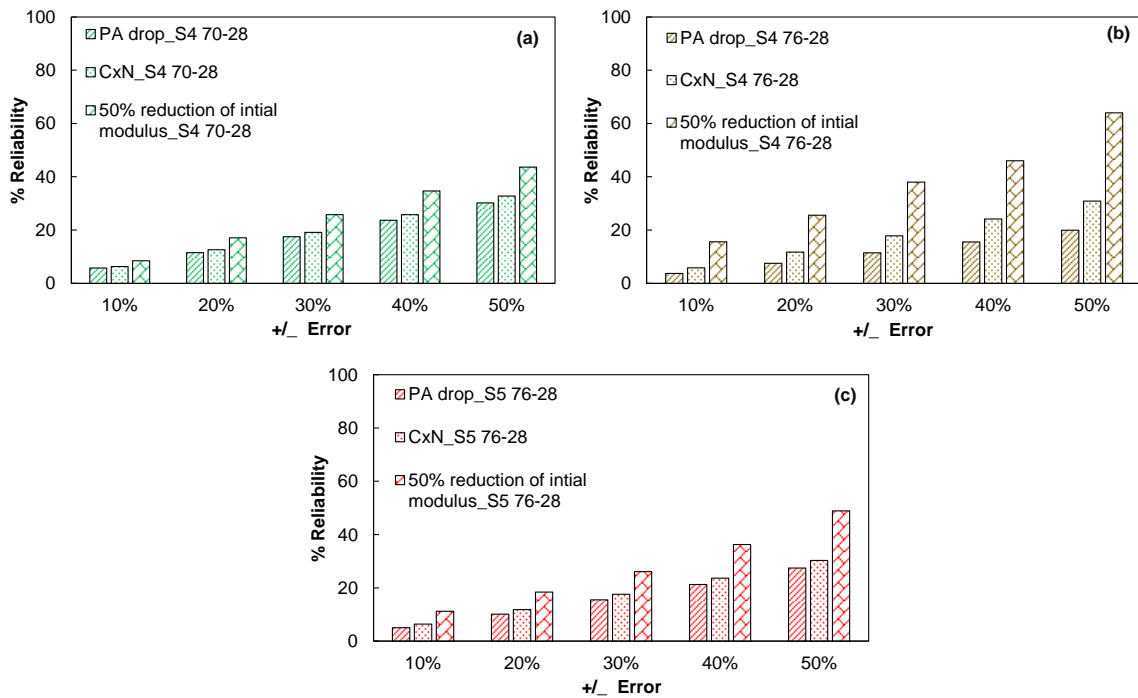
FIGURE 4-12 Reliability of S5 76-28 AC Mix Fatigue Life Prediction for Various Experimental Failure Point Identification Methods Using C_f Failure Criteria.

One important observation that can be made from TABLE 4-4 for the S3 64-22 mix, the mean and coefficient of variation of the two failure criteria are not very different. Even through there is very slight higher variation observed with the C x N method, it was tracked in the reliability analysis. From the FIGURE 4-11(a) it can be observed that the fatigue life prediction using C x N method is slightly less reliable than the PA drop method. This trend is in line with the variation observed in the experimental failure criteria. From FIGURE 4-12 it can be observed that 50% modulus reduction approach is showing higher reliability comparative to other failure methods due to the lesser variation (TABLE 4-6) of the input parameters in 50% modulus reduction failure method. A similar trend can be observed for all the other mixtures as well meaning that the reliability is greater when there is lesser variation in failure criteria. This analysis corroborates that the reliability framework developed in this study is generic and can be adopted for analyzing the reliability of any AC mix. From FIGURE 4-12 (a) and (b) it can be observed that S4 76-28 is showing more reliable results than the S4 70-28 with respect to the 50% modulus reduction failure method but different trend is observed if comparison is made with respect to C x N or PA drop method. Because each input parameter variation is different from one mixture to other it is difficult to comprehend which input parameter is having significant impact on the reliability of fatigue life prediction of AC mixture. To understand the impact of input variables on reliability prediction of failure cycles parametric sensitivity analysis is warranted.

4.7   Summary

Mechanistic models offer the potential to provide better performance prediction of asphalt concrete mixtures. These methods generally involve multiple experiments with their own variability, which introduces additional sources of uncertainty in comparison with alternative, non-model based approaches. Thus, an important component in this process of evaluating these models and subsequently for developing even more accurate methods is the assessment of the predicted reliability. The reliability of the predictions using these models has not received substantial attention, although this factor will contribute considerably to the overall real-world utility of the models. This chapter focused on the development of general reliability framework and adoption of the framework in analyzing the reliability of fatigue predictions using the simplified viscoelastic continuum damage model (S-VECD). Modulus and fatigue tests were conducted on a standard dense graded asphalt mixture to characterize the model and create deterministic fatigue life predictions. Monte Carlo simulations were then used to calculate the reliability of these fatigue predictions given the variation in input parameters. The analysis was conducted for combinations of three different experimental failure criteria and two model failure criteria at two different strain levels for a total of 12 study cases. Differences in reliability amongst the combinations of these failure conditions are identified and discussed. The summary of reliability analysis study is given below.

- Reliability of fatigue life prediction using S-VECD modeling for C_f failure criteria observed to be sensitive to the type of experimental failure criteria used.

- The reliability trends are in line with the variation observed from test replicate C_f values from the chosen experimental failure method. Meaning that if the observed

variation in C_f is high for one experimental failure criteria over another, the experimental failure criteria that produces the lower C_f variation will produce more reliable results.

- Conversely, the reliability of the fatigue life prediction for the G^R approach is not very sensitive to the experimental failure criteria. It was observed that 50% modulus reduction approach yields more reliable results than the other two in AC_1 where as in CxN approach shows more reliable results in AC_2. This trend also agrees with the variation observed in G^R values from one method to other of both mixtures.

- Comparing the two model failure criteria, it was observed that fatigue life predictions using C_f failure criteria approach shows more reliable measurements than G^R when characterization is performed with three tests irrespective of which approach yields more accurate fatigue life prediction.

- Depending upon the selection of failure criteria the prediction errors could range from ±22 to ±52 % at a 50% level of reliability depending on the exact combination of failure criteria and strain level.

- To assess the adoptability of reliability framework for other mixtures, reliability analysis was performed for five mixtures of different gradation and volumetric properties of AC. From this analysis it was observed that reliability framework is tracking the variation of input variable parameter quite well in to the reliability predictions.

CHAPTER 5 DEVELOPMENT OF MODULUS AND FATIGUE TEST PROTOCOL

FOR FINE AGGREGATE MATRIX FOR AXIAL DIRECTION OF LOADING

5.1   Introduction

AC is a viscoelastic material used in the construction of flexible pavements. Accurate

mechanical characterization of this material is complicated by the blend of various size

aggregates and the fact that the binding agent, asphalt binder, has a wide range of modulus

values over typically encountered in-service conditions. Today, routine accurate evaluation

of the material mechanical properties is performed using expensive and time consuming

macro scale characterization experiments. Due to time and monetary constraints necessary

in such experimentation, it is not possible to easily test multiple AC mixtures for the

purposes of optimizing mixture designs and/or choosing a mixture design that will yield

the best performance. To overcome this limitation, researchers have been trying to predict

AC properties with a minimal amount of binder or/and mastic testing and then using these

results to mechanistically upscale the results and predict the mechanical properties of AC

(*87, 114*). One pathway to perform this upscaling analysis is to establish the link between

the AC and the FAM that exists between the coarse aggregate. FAM is a distinct phase in

AC and consists of the combination of asphalt binder, fine aggregate and filler. In the

discrete segregation of length scales, the FAM phase is characteristically one length scale

immediately below AC (*91*). Many of the initial studies with FAM focused on the experimental characterization of relative material performance in the presence of mitigating factors like moisture damage and healing (*93, 95, 97, 115, 116*) . However, some have incorporated the experimental results into computational and analytical upscaling methods in order to estimate the AC properties (*114, 117, 118*).

Most of this existing literature has been developed using experimental results derived from oscillatory shear testing coupled with Dynamic Mechanical Analysis (DMA). In these cases experiments are performed by applying a torsional cyclic loading to a solid cylindrical sample while simultaneously measuring the angle of rotation. Strain is calculated based on the angular displacements of shaft and these calculations are used to determine the resultant mechanical properties of FAM (*92 - 99, 114 - 119*). The degree to which the equipment are accurately calibrated for machine compliance factors during FAM testing is not clear. In addition, every equipment will have a different amount of compliance depending on the stiffness of the sample, which is itself affected by the test temperature and frequency. The overall impact of this compliance on the accuracy of these results is not known. It should be noted that the same process is also applied to the testing of asphalt binder and mastic (*120 - 122*); however, since FAM is much stiffer than binder and mastic the impacts are likely of larger magnitude.

One important question in FAM related studies is whether the material produced in the lab accurately resembles the FAM that exists between coarse aggregate particles in AC. Kim et al., reflected this phase by testing asphalt mixed with sand in order to characterize AC mixture healing (*96*). In their study, Ottawa sand was mixed with 8% of binder content by weight of sand and compacted to 12 mm x 50 mm (d x h) samples. The binder content

of 8% was used to provide an average of 10 microns of film thickness based upon the film thickness calculation method of Hveem. Zollinger proposed that the composition of FAM should be based on that of the parent AC mixture (*97*). He went on to argue that FAM should wholly consist of aggregates finer than the 1.18 mm sieve size and that the binder content should be calculated based on an effective film thickness. Subsequently, several researchers carried out studies to predict the gradation and binder content of FAM samples (*98, 99*). A study by Izadi et al., indicates that binder content and percentage air voids are more influential factors on the engineering properties of FAM than gradation (*93*). Another study corroborates this observation and quantifies the variation in engineering properties for percentage changes in the binder content and air voids (*99*). In addition to the mix design, the fabrication procedures also play an important role in accurately understanding the engineering significance of the material. Recently Izadi et al, compared the internal structure of FAM inside the AC mixture with lab fabricated FAM samples under different compaction procedures. It was concluded that Gyratory compacted FAM samples have a closer resemblance to the actual FAM structure (*93*).

So while much research has been instigated to study the composition of FAM, a critical yet missing link in the literature is measuring mechanical properties of FAM in consistent loading conditions as AC mix (which is generally uniaxial) so that direct comparisons between these scales can be made. The motivation for this research effort is to close that missing link by testing FAM samples in uniaxial loading conditions so that comparative assessment can be made between FAM and AC in continuum damage evaluation approach. This chapter mainly focused on the following objectives,

- Developing a standard test procedure for FAM specimens to measure on-specimen displacements for modulus and uniaxial fatigue testing under similar test conditions as AC.

- Quantifying the error in measuring FAM mechanical properties due to machine compliance issues.

5.2 Pilot Studies on FAM

Before fabricating and testing actual FAM specimens two relevant pilot studies were conducted to first determine the most appropriate sample instrumentation process and sample size and then to identify the appropriate compaction geometry to achieve uniform specimen density.

5.2.1 FAM Sample Instrumentation

The first issue considered in preparing FAM samples was the ability to accurately measure loads and displacements during testing. In this study, testing was to be conducted under both tension and compression modes of loading, which required attaching end platens to specimens as well as mounting any necessary brackets for on-specimen deformation measurements. The end platens were manufactured with aluminum and had a mass of approximately 120 g each. All specimens were glued to these end platens using Devcon 5 minute steel putty epoxy. In AC mixture testing, these end-platens are typically manufactured with steel and are grooved for better adhesion to the glued test specimens (*108*). However, aluminum was found to perform better in FAM testing because the lower mass caused less unintended damage occurring due to creep. In addition, the strength and modulus advantages of steel over aluminum were smaller because less overall force was

needed for testing the FAM specimens. To ensure proper vertical alignment of FAM specimens, a specially prepared gluing jig, shown in FIGURE 5-1 was used.

Experience based on axial testing of AC mixtures suggests that on-specimen deformation measurement is needed for accurate characterization of mechanical properties, and that reliance on machine mounted transducers can lead to errors (termed machine compliance) (*108 - 125*). Most experimental studies with FAM rely on these machine transducers presumably under the belief that machine compliance will not substantially affect the characterization since FAM has a relatively low modulus when compared to AC mixture. One of the primary objectives of this study was to confirm or refute this assumption and thus it was necessary to obtain the on-specimen deformation of samples during loading. Three different options were evaluated; 1) miniature axial extensometers (± 1.00 mm) manufactured by Epsilon Technology Corporation and consisting of full bridge 350 ohm strain gages, 2) miniature linear variable displacement transducers (LVDTs) (± 0.254 mm), with a 9.5 mm body diameter and 3) sub-miniature LVDTS (± 2.54 mm) with a 5 mm body diameter. The gauge length for measurements with all devices was set at 25 mm to ensure 1) that the measurements were taken on a sufficiently large representative volume element (RVE) (*125*) and 2) for the practicality of installing devices with reasonably small noise-to-signal ratio. Initially strain gauges were also considered for this purpose however due to the comparative difficulty in gluing the gauges on the curvature of the FAM specimen, the potential for temperature sensitivities, and the high cost of this option they were eliminated from the pilot study.

The extensometers were configured using a full wheatstone bridge as per the manufacturer's suggestion. The miniature and sub-miniature LVDTs were routed through manufacturer supplied LVDT analog conditioners, which were subsequently calibrated to the proper span. In all cases, on-measurements were taken along the diametrical axis 180° apart. The extensometers accommodated these measurements into a single assembly, whereas both LVDTs required two separate mountings. The mounting assembly consisted of brass studs that were glued to the surface of the sample and brackets that were later affixed to the studs. FIGURE 5-1 shows the brass studs and mounting brackets used for the LVDTs and FIGURE 5-2 shows all three types of displacement transducers setup on the FAM sample.

During the pilot study the specimens were instrumented with the different devices and the resulting output were monitored for accuracy, precision, and signal creep. It was first found that the extensometers yielded very precise results, but that the weight of the extensometers resulted in notable signal creep. After several trials (including some with different methods to affix the extensometers to the surface), it was determined that the measured creep was too substantial for accurate on-specimen deformation measurement. This effect was particularly obvious at temperatures greater than room temperature and thus the extensometers were eliminated from further consideration. The sub-miniature LVDTS overcame this limitation, but showed high signal noise due to the combination of a 25 mm gauge length and the relatively large range of +/- 2.5 mm for the LVDTs. These problems were subsequently overcome by using the miniature LVDTs, which while having a larger diameter also had a lower mass than the sub-miniature LVDTs (3 g versus 4 g) and a smaller span (± 0.254 mm span), which resulted in lower signal noise.
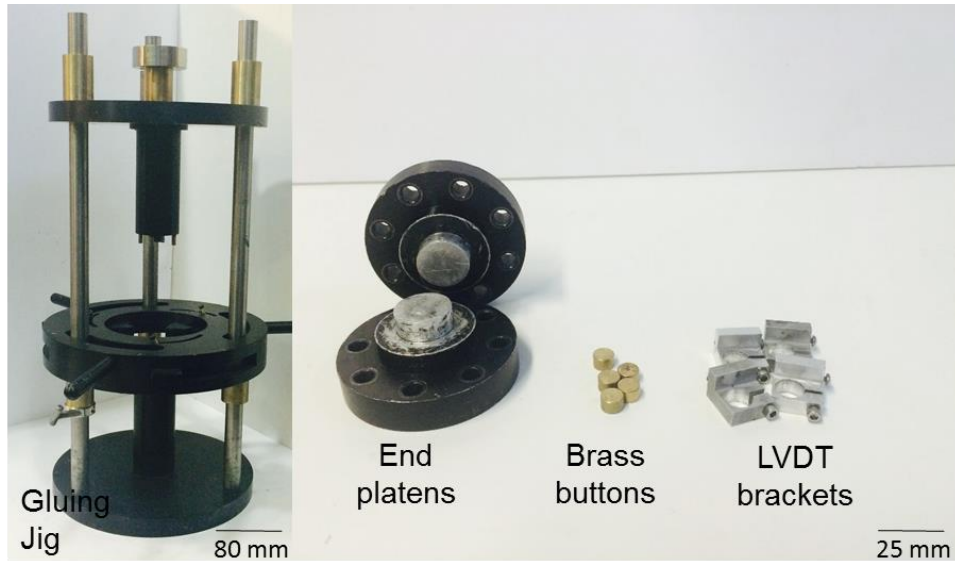
FIGURE 5-1 FAM Instrumentation Tools.
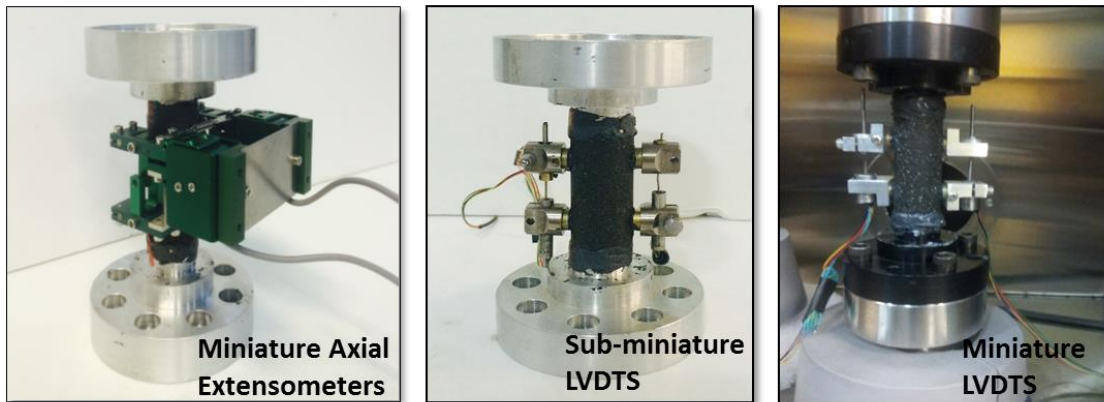
FIGURE 5-2 Various Displacement Transducers Setup on FAM Sample.

5.2.2   *FAM Compaction Geometry*

An important task in the process of fabricating FAM material in a laboratory environment

is to ensure that it accurately resembles the FAM that exists in AC mixture. This replication

includes both the composition as well as the compacted structure. From the literature,

different procedures have been followed to create FAM; 1) repeatedly impacting the

sample until a final testing geometry is achieved, 2) pressing the samples into molds (*94, 116, 126*) Gyratory compaction (*97*). Izadi et al., conducted a systematic study of these methods and determined that the structure created from the gyratory compaction best replicated the FAM structure within asphalt concrete mixtures. Based on this work, the research team decided to create FAM samples using the gyratory compaction procedure. The FAM geometry is optimized to both maximize the number of FAM specimens that can be cored from one compacted sample and to ensure that the specimens that are extracted have uniform air voids (both in terms of the single specimen and between specimens. To determine this uniform compaction geometry, 150 mm diameter gyratory samples were compacted at three different heights 70 mm, 100 mm, and 150 mm.

The basis for judging the different geometries was the spatial distribution of air void contents in the final compacted sample. More uniform distribution of air voids across locations where test specimens were to be extracted would ensure better repeatability in the test results. To evaluate the distribution of air voids 20 mm diameter specimens were cored at various locations points on the sample surface and then cut into smaller pieces 15 mm in length as shown in FIGURE 5-3. The coring locations were taken at the edge, intermediate, and center points of the gyratory sample as well as at different radial angles. The 20 mm diameter was chosen based on the previously discussed instrumentation study.
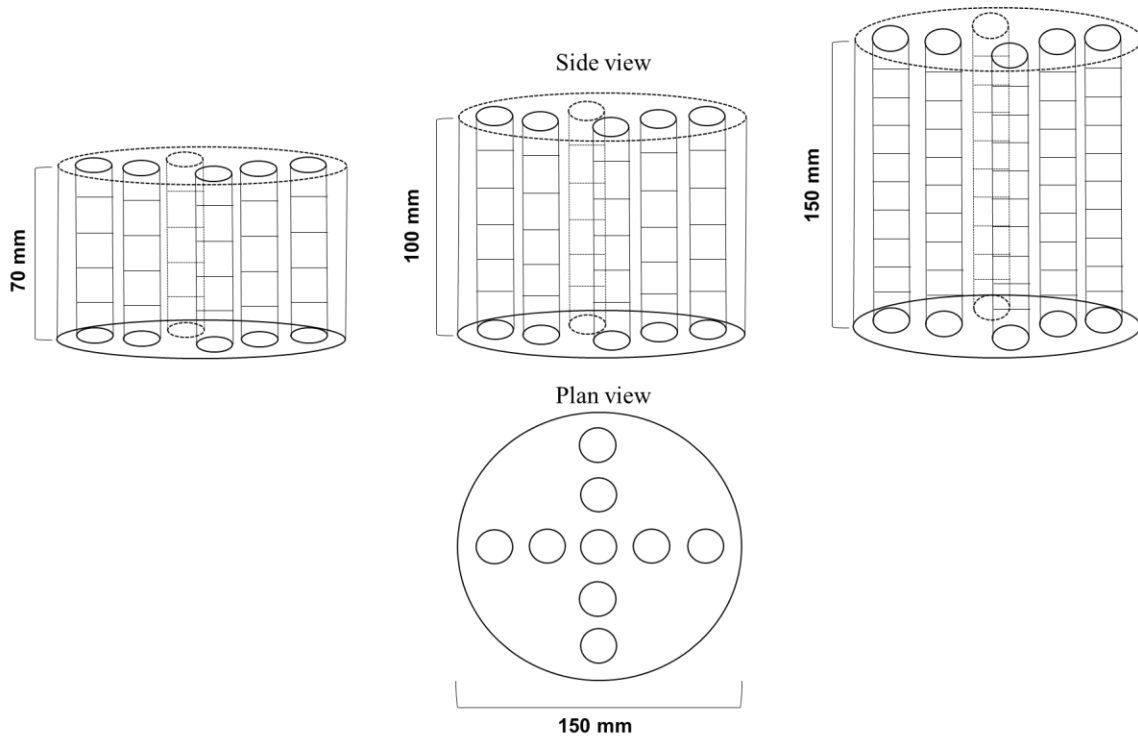
FIGURE 5-3 Side and Plan View Schematic of Compacted FAM Samples Coring and Cutting for Air Void Distribution Study.

After cutting and coring each 15 mm specimen, they were thoroughly dried in front of a fan for 24 hours. Afterwards the bulk specific gravity, G_{mb}, was measured using the procedure outlined in ASTM D 2726 for AC compacted samples. Since the weight of these specimens was much smaller than that considered in ASTM D 2726, a balance with precision to $1/100^{th}$ of a gram was utilized (*127*). In parallel with these measurements, uncompacted samples of the FAM were tested for their maximum theoretical specific gravity, G_{mm}, according to ASTM D 2041. The air void content was then calculated via Equation (5.1) (*128*).

$$AV\left(\%\right)=100\left(1-\frac{G_{mb}}{G_{mm}}\right)$$ (5.1)

The results of the air void distribution study are summarized in FIGURE 5-4 and FIGURE 5-5 below. Of principle interest was the distribution of air void content within ± 25.0 mm of the vertical center since the FAM test specimens would have a total height of 50 mm. The air voids distribution of FAM samples cored at various locations on the outer edge were found to be more homogeneous than the samples cored at the intermediate radius and center of the compacted FAM samples which is shown in FIGURE 5-4. FIGURE 5-5 depicts the standard deviation of air void content in the 50 mm FAM specimens cored from center of FAM compacted sample of different heights. As expected, it is observed that as the gyratory sample height increases that the air void content becomes more consistent. Since the 100 mm gyratory sample yielded very similar results as the 150 mm tall gyratory sample and required only 67% of the material it was selected as the final compaction geometry. Air void distribution of FAM samples compacted at different heights along the length of the sample were shown in Appendix A (Figure A-1).
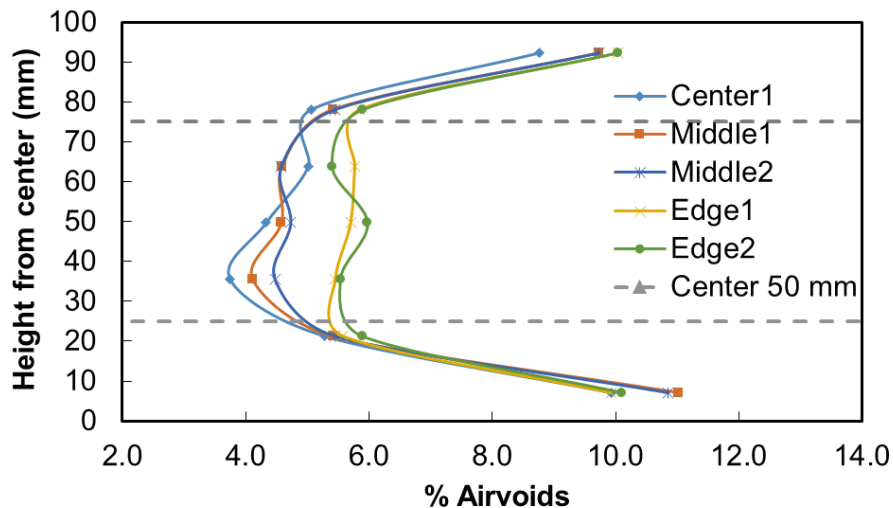
FIGURE 5-4 Air Void Distribution of FAM Specimens Cored at Various Locations from 100 mm Height of Compacted FAM Sample.
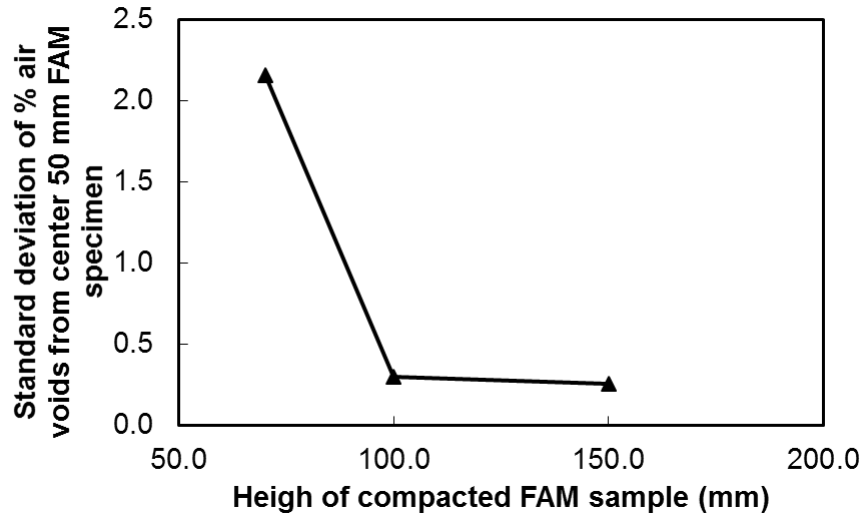
FIGURE 5-5 Air Void Distribution of FAM Specimens Cored From Various Height of Compacted FAM Samples.

5.2.3 Pilot Studies Summary

Based on the observations from the two pilot studies, the final FAM geometry was determined to be 20 mm x 50 mm (d x h). It was also determined that in order to achieve this geometry, gyratory samples would be compacted to a height of 100 mm and that only samples cored from the outer edge would be used for testing. In this case it was possible to extract 12 FAM test specimens from each compacted gyratory sample.

5.3 Experimental Data Analysis and Results

5.3.1 Dynamic Modulus

Dynamic modulus data was analyzed to develop so-called mastercurves, which analytically combine the effects of both temperature and frequency of loading. The process of creating these mastercurves is explained in considerable details in the literature (*129, 130*). The relevant details specific to this study are that the sigmoidal function, Equation (5.2), was

used to model the mastercurve and that the second order polynomial function, Equation (5.3), was used to model the shift factor function .

$$\log|E^*| = a + \frac{b}{1 + \dfrac{1}{e^{d+g\log(f_r)}}} \tag{5.2}$$

$$\log a_T = \alpha_1(T^2 - T_R^{\,2}) + \alpha_2(T - T_R) \tag{5.3}$$

where;

a = minimum value of log $|E^*|$,

$a+b$ = maximum value of log $|E^*|$,

d, g = parameters describing shape of sigmoidal function,

f = applied frequency (Hz),

f_r = reduced frequency (Hz),

a_T = shift factor function (f_r/f),

T = test temperature (°C),

T_R = reference temperature (°C),

α_1, α_2 = coefficients of the second order polynomial equation.

The results from the $|E^*|$ testing and analysis using both the actuator and on-specimen deformations are summarized in FIGURE 5-6 and FIGURE 5-7 for the two study materials. For ease of presentation, hereafter FAM made with PG 64-22 binder is labeled

as FAM1 and the FAM that uses PG 76-16 is labeled as FAM2. Modulus calculated using the actuator measured displacement values are referred as FAM_ACT and those from the on-specimen measured values as FAM_LVDT. FIGURE 5-6 shows that the error in using actuator displacements to calculate modulus is very high at low temperatures (75% and 79% for FAM1 and FAM2 respectively at -10°C and 20 Hz). FIGURE 5-7 shows the error in phase angle measurements and its time dependency variation between actuator and LVDT data. As stated before, machine compliance is highly dependent on the stiffness of the testing material relative to that of the components of the machine along the loading direction. When the specimen modulus is high (such as at low temperatures), the error in measuring modulus of the specimen is also high, but when the specimen modulus is low (such as at high temperatures) the error will also be low. Overall it was observed that by directly using the machine mounted transducers to calculate $|E^*|$ the percentage error with the actual $|E^*|$ could be as large as 79% and as small as 5% depending on the test temperature and frequency of loading. These errors also extend to the determination of phase angle, which are compared for the actuator and on-specimen LVDTs in FIGURE 5-7. Since the actuator displacements are affected by deformation of elastic components along the loading train the phase angle determined from the actuator is smaller (e.g., more elastic) than the on-specimen mounted measurements. Replicate mastercurves for modulus and phase angle of both FAM materials are given in Appendix B (Figure B-7 to B-10) and replicate damage characteristic curves are given in Appendix B (Figure B-11 to B-12).
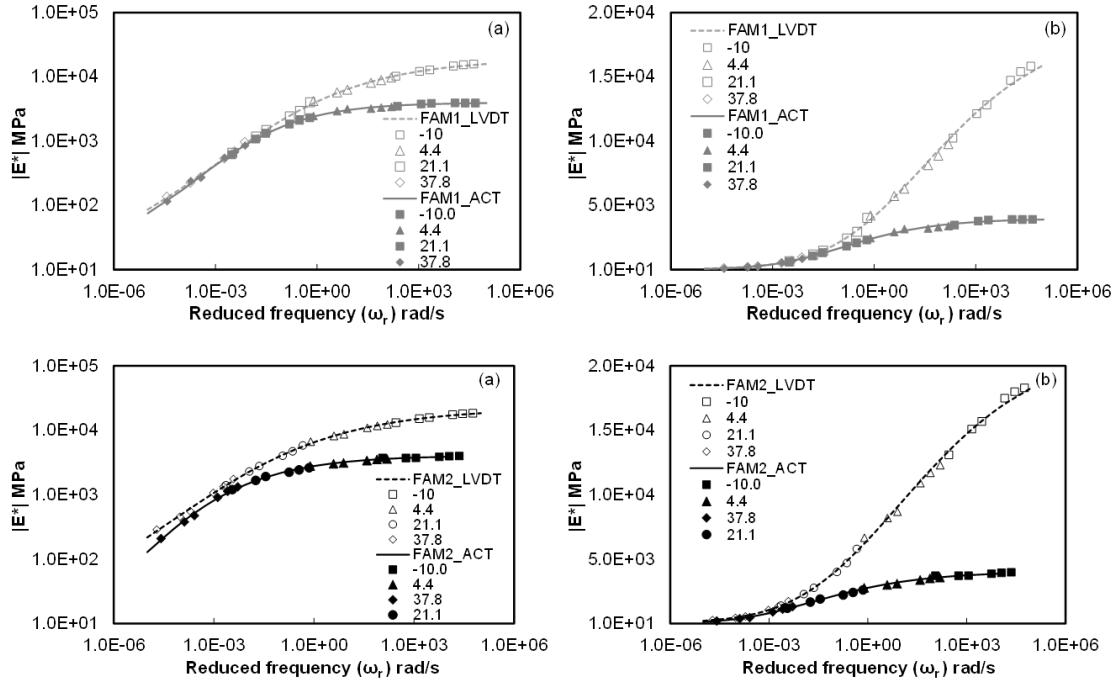
FIGURE 5-6 Master Curve Plots for FAM1 &FAM2 According to LVDT and Actuator Strain Data; Logarithmic Scale & (b) Semi-Logarithmic Scale.
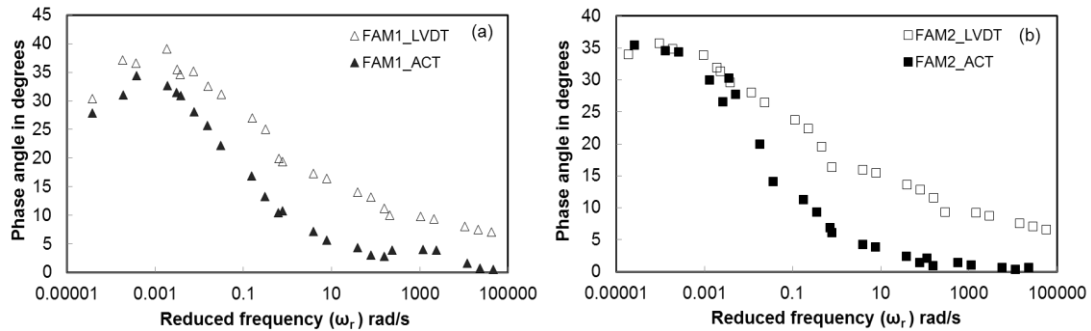
FIGURE 5-7 Phase Angle Plots for (a) FAM1 and (b) FAM2 According to LVDT and Actuator Strain Data.

In most testing devices used to study FAM, the machine compliance is corrected for by using an approximate and constant stiffness that relates the applied load to the deformation of the machine components, Equation (5.4) (*131, 132*).

$$\Delta L_M = P \times MCF \tag{5.4}$$

where;

ΔL_M = deformation of the machine components (μm),

P = applied load at particular (N), and

MCF = machine compliance factor (μm/N).

Since both on-specimen and actuator displacements were measured in this experiment such a methodology could be objectively evaluated. The mathematical process is similar to that adopted in other test equipment. First, the machine only deformation was backcalculated from the known actuator and on-specimen strains, Equations (5.5) through (5.7). This calculation does make the assumption that the on specimen strains were uniform across the entire sample length.

$$\Delta L_M = \Delta L_{Act} - \Delta L_{Sp} \tag{5.5}$$

$$\Delta L_{Act} = \varepsilon_{Act} \times L$$
$$\Delta L_{Sp} = \varepsilon_{Sp} \times L \tag{5.6}$$

$$\Delta L_M = (\varepsilon_{Act} - \varepsilon_{Sp}) \times L \tag{5.7}$$

where;

ΔL_{Act} = change in displacement from actuator reading (μm),

ΔL_{Sp} = change in displacement from LVDT readings (μm),

ε_{Sp} =   on specimen strain measured using LVDTs (με),

ε_{Act} =   strain measured using actuator (με), and

L =   length of the sample (μm)

To calibrate the *MCF*, Equation (5.7) is first used to calculate the change in machine displacement as a function of applied load level. The load level and the corresponding change in displacement machine displacement are then plotted and fitted to a linear function as shown in FIGURE 5-8 The slope of the function is the *MCF*, which is found to be 34 nm/N. The *MCF* is used via Equation (5.8) (with L given in μm) to calculate the actuator corrected strain, ε_{ACS}.

$$\varepsilon_{ACS} = \varepsilon_{Act} - P \times \frac{MCF \times 1000}{L} \qquad (5.8)$$
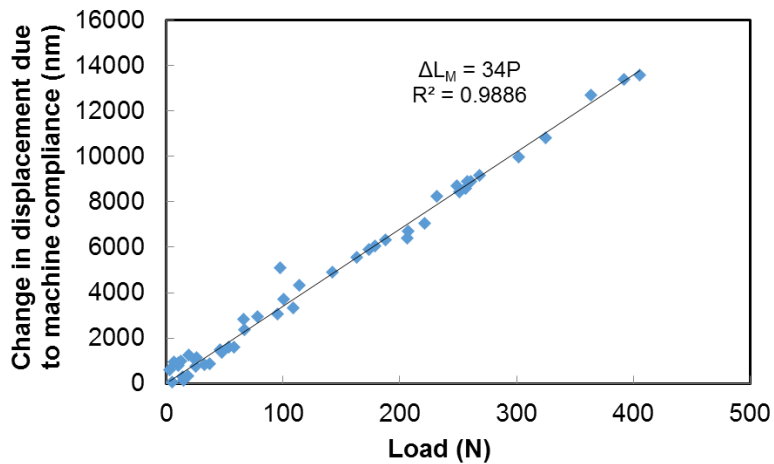
FIGURE 5-8 Machine Compliance Correction Factor Determination Plot.

FAM modulus values were calculated using the ε_{ACS} values and mastercurves were re-developed as shown in FIGURE 5-9. By using the *MCF* approach the percentage error

in the modulus calculated from actuator data is in the range of 10-32% which is still high, but substantially lower than using the actuator displacements without any correction. However, in addition to the percentage error, there were some abnormalities in the modulus data at low and high temperature which are shown as circled areas in FIGURE 5-9. At colder temperatures irregular pattern in modulus such as frequency decreases modulus of a specimen is increasing, this behavior is observed in both FAM materials. Finally, this method does not adjust the time dependency and thus cannot correct for the inconsistencies in phase angle that are shown in FIGURE 5-7.
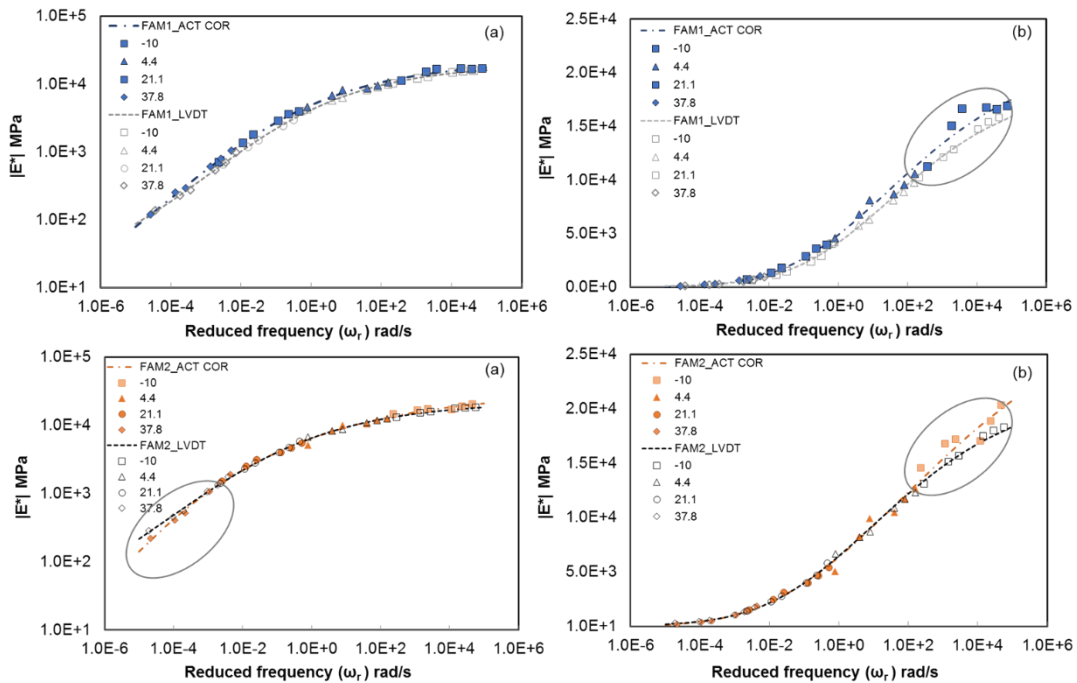
FIGURE 5-9 Master Curve Plots for FAM1 &FAM2 According to LVDT, Actuator Strain and Actuator Corrected Strain Data; Logarithmic Scale & (B) Semi-Logarithmic Scale.

5.3.2   *Uniaxial Fatigue Test Data Results*

The results from the fatigue testing are shown in the traditional strain level-failure cycle space in FIGURE 5-10. For both FAM1 and FAM2 the results are plotted using the on-specimen strain level and the actuator based strain level. Following standard convention the strain level plotted is taken at the 100th cycle. As should be expected the actuator strain is always higher than the LVDT on-specimen strain for same fatigue life. This trend is similar in both FAM cases but as test temperature increases the error in the strain value measured using the actuator is decreasing. Closer observation to theses fatigue lives plot shows that LVDT and actuator strain are much different at 10°C and then this error reduces for fatigue tests at 25°C in both FAM cases. While all of these trends could be expected based on the *MCF* function, it is of interest that the effect is one that results in the tendency of the actuator based fatigue curves from multiple temperatures to converge towards a single strain level. By contrast, the LVDT based fatigue curves remain more or less separated across all strain levels studied. The latter behavior is to be expected based on empirical fatigue models for asphalt materials like the one shown in Equation (5.9) (*10*). Behaviors like those occurring from the actuator based strains have also been observed in the literature, but these tests were based on equipment mounted transducers (*133*). Together these observations may suggest that machine compliance related phenomenon affect data that is historically cited and continually used today. This finding could be one reason why the literature on fatigue evaluation of AC mixtures is fraught with inconsistencies with respect to the impact of compositional factors and external loading conditions.
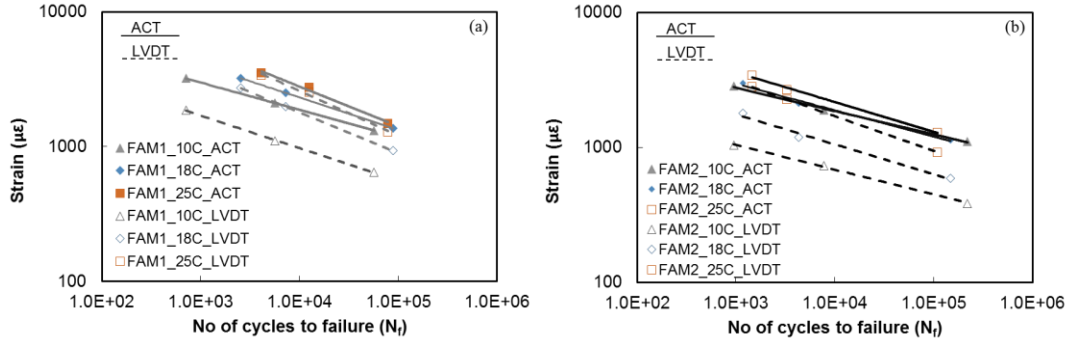
FIGURE 5-10 Fatigue Lives Plot for; (a) FAM1_1 and (b) FAM_2 at Different Temperature According to LVDT and Actuator Strain Using 100th Cycle Initial Stiffness.

$$N_f = K_1 \left(\frac{1}{\varepsilon_t} \right)^{K_2} \left(|E*| \right)^{K_3}$$
(5.9)

The uniaxial fatigue test data has also been analyzed using S-VECD modeling approach. The model derivation is described in detail in chapter 3, the S-VECD model equations were used to establish the *C* vs *S* curves based on the actuator strain, actuator corrected strain, and LVDT strain data for both FAM1 and FAM2 materials. The failure of the specimen is considered when there is a phase angle drop as proposed by Reese (*66*).

The characterization process reveals that irrespective of temperature and strain levels these curves mostly collapse together for each of FAM types and corroborates existing literature. Although this level of collapse is independent of whether the on-specimen, actuator, or actuator corrected strains are used, the resultant curve to which the collapse occurs differs, c.f. FIGURE 5-11. Damage curves developed for each FAM specimen is best fit separately for actuator, actuator corrected and LVDT data by using Equation (5.10) (*a* and *b* are model fit parameters). *C* vs *S* curves developed using actuator, actuator corrected strain and LVDT data for each FAM material are plotted together in

FIGURE 5-11. This figure shows the differences in the damage curves for both FAM1 and FAM 2 materials when actuator (labeled as FAMX_ACT), actuator corrected strain (FAMX_ACT COR), and LVDT data (FAMX_LVDT) are used. Damage curves developed for each replicate from both FAM material types are given in Appendix B (Figure B-11 to Figure B-12)

$$C = 1 - aS^b \tag{5.10}$$
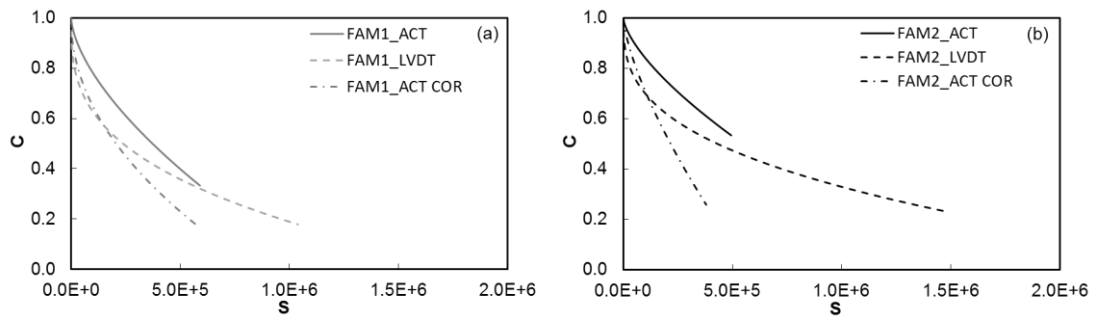
FIGURE 5-11 C-S Model Fit Plot for (a) FAM1 and (b) FAM2 According to LVDT Strain And Actuator Strain.

From these damage curves it can be observed that the actuator based plot is positioned above the LVDT damage curve in both FAM cases. Correcting the actuator strains via the *MCF* does lower the curve, but it is still positioned separately from the true, on-specimen based damage curve. In light of the fact that corrections to the actuator based modulus calculation via *MCF* generally match the on-specimen values this difference in damage curve will have tangible influences on any predictions made with the S-VECD model. This finding is particularly concerning since as shown in FIGURE 5-11 the relative difference between the actuator corrected and the true damage curves does change between

the two study materials. Thus, this effect will likely affect both absolute predictions and relative predictions.

5.4   Summary and Conclusions

The testing of FAM is rapidly gaining traction in the pavement research community due to its notable similarities with AC and the increased testing efficiency that it affords. In most of the existing studies, FAM tests are used for characterization of relative material performance in the presence of phenomenon like moisture damage and healing. However, to better understand the fundamental properties of FAM and establish the mechanistic connection between its properties and those of AC, proper fabrication and testing protocols need to be established. Testing is and will continue to be an important component in the process of designing and constructing asphalt pavements. However, the complexities of testing this material including the required time and material constraints limits the usefulness of testing for the performance based characterization and design. In this study, the authors focused on developing standard testing protocols for FAM scale materials, which afford one option to reduce the required evaluation time. In this research effort such standard testing protocols for both dynamic modulus and uniaxial fatigue testing are developed for FAM materials. In the current effort, two FAM materials are prepared with the same gradation but two different asphalt binders (PG 64-22 and PG 76-16). Pilot studies to support the development of sample fabrication protocols are explained. Both FAM materials are tested for modulus and uniaxial fatigue and during testing both on-specimen and machine actuator displacement are recorded. Material parameters were separately

calculated using these two deformation measurements and compared to uncover the errors resulting from machine based measurements of FAM.

Important conclusions from this study include,

- Miniature LVDTs with smaller span (± 0.254 mm) performed better in measuring on specimen strain compared to other sub-miniature LVDTs and extensometers.

- Equipment compliance error is an important issue to be addressed while measuring the material properties of FAM. The error due to machine compliance in measuring the modulus of FAM specimens can be as small as 5 and large as 79 % depending on the level of applied force, which in the case of FAM experiments vary by test temperature and frequency.

- Even after correcting for machine compliance the error in the modulus measurements from actuator data ranged from 10-32%. In addition the standard machine compliance correction methodology does not address time dependency issues.

- The interpretation of fatigue tests and development of the S-VECD damage curves developed using actuator data (both corrected and uncorrected) are not same as the ones developed from on specimen data for both FAM materials. This leads to errors not only in absolute predictions but also in relative predictions of fatigue life of a material.

In summary, the on specimen strain measurements should be included in FAM testing protocols for accurate measurement of material properties. The authors believe that standard fabrication and testing protocols for FAM will pave the way to characterize and

rank the mixtures based on its performance. FAM testing can also be used to study the internal mechanisms in AC for various sustainable materials like warm mix asphalt, recycled asphalt pavements and crumb rubber asphalt pavements.

CHAPTER 6 MODELING OF FINE AGGREGATE MATRIX AND ITS
RELATIONSHIP TO ASPHALT CONCRETE MIX

6.1 Introduction

This study focuses on the behaviors of FAM and its relationship with AC mix. The FAM phase is very important because it is one length scale below the AC mix and one phase closer to the location where most of the damage within the AC structure occurs (*91*). Many researchers have investigated this material to gain insight into mechanisms like moisture damage, healing, aging, fracture, and the aggregate to binder bond (*93, 95, 97, 115, 116*). In addition to these experimental and analytical studies, there are several numerical and computational studies. Some of the famous computational methods in literature are lattice models (*134*), cohesive zone models (*91*) and discrete element models (*114*, *135*) .Using these cohesive zone models Aragão et al. (*117*) simulated fracture in AC by using FAM and aggregate properties as input parameters. The literature also suggests that FAM properties form an important component in studies involving multiple scale numerical and computational simulations (*114, 117, 118*). While the aforementioned experimental studies have demonstrated the utility of FAM tests for relative material comparisons, they have not been used extensively for an accurate and quantified prediction of AC performance or even a direct comparison with AC behaviors or performance. For such so-called upscaling

analysis is based on numerical and computational simulations, which rely on experimental data gathered using torsional cycling loading (*92-99, 114-119*). This situation has resulted in the omission of an important step for assessing the engineering significance of FAM, which is the direct comparison of the mechanical properties of FAM and AC mixture under consistent loading conditions. Heretofore, such comparisons were not possible because the state of stress in the torsional loading used with most FAM experiments is more complex than what exists in the AC testing, which is generally uniaxial in nature. It is believed that a comparative assessment of the linear viscoelastic and fatigue performance of AC mix and FAM under consistent stress states will yield substantial insights.

It should be noted that the FAM within this AC mixture may be likewise subjected to complex stress states due to the heterogeneous structure of the asphalt mixture and the distribution of FAM within it (*134*). However, this state of stress is neither equivalent to that experienced in the torsion loading or that in the uniaxial conditions. Thus, stress state inconsistencies are implicitly included in any characterization and likely affect, in some complex and unknown way, upscaling analysis. However, it is a philosophical question as to whether it is best to carry out experiments under simulative stress states and use a degree of smeared mechanics or perform experiments under controlled stress states and develop comprehensive formulations. Answering this question is well beyond the scope of the current study, but it is believed that careful study following the latter approach is needed before adopting the former. So this chapter mainly focused on achieving the one of the research study objectives,

- Evaluation of the mechanical linkages between the FAM and AC mix by applying analytical upscaling methods with gross homogenization principles.

This objective has following three subtasks

➢ Report on comparisons of the mechanical properties of FAM and AC mixture in a consistent overall stress state (axial tension–compression) for both modulus and fatigue.

➢ Evaluate the mechanical linkages between the FAM and AC mix by applying analytical upscaling methods with gross homogenization principles.

➢ Evaluate the sensitivity of AC Modulus to binder oxidation with FAM phase experimental data.

6.2   Materials

The study investigated FAM and AC mix using two different Arizona binders PG 64-22 and PG 76-16. For simplicity these mixes are henceforth labeled as either AC_1 or AC_2 respectively. Likewise the corresponding FAM materials are referred to as FAM_1. The mix design for both binders was identical and given in TABLE 3-5. The data obtained from testing these AC and FAM mixtures are used for the analysis purpose in this chapter.

For the purpose of aging sensitivity, materials from the NCHRP 9-54 project were used to fabricate and test the FAM samples. Binder data obtained as a part of NCHRP 9-54 study was used to evaluate the sensitivity of AC Modulus to binder oxidation with FAM phase experimental data. The study material matrix included three binders, two aggregates and two gradations as shown in Appendix Table A-2. FAM tests were conducted at different air void contents to represent 4.5% and 7.5% air voids in the asphalt concrete

mixture. It has been estimated that between 40 and 70% of air voids that are present in an asphalt concrete are part of the FAM phase (*98*) and here it is assumed that 55% of total voids exist in the FAM phase. Table A.2 summarizes the study materials and the adopted naming convention. In this FAM material was fabricated with pre-aged asphalt binder. By pre-aging asphalt prior to mixing, the degree of oxidation in the binding medium was known and thus any changes in modulus of the composites could be quantified with respect to changes in asphalt binder aging parameter (*AP*).

6.3   Experimental Data Analysis and Results

The |*E**| data for the FAM and mix was used to develop master curves in accordance with AASHTO PP 61-09. These curves are shown for the average data in FIGURE 6-1 for FAM and AC. Although it is not shown, the repeatability of both the AC and FAM was high with an average coefficient of variation of 8%. Recall that the naming convention adopted in this particular chapter of the study is such that mixture and FAM made with PG 64-22 is AC/FAM_1 and those with PG 76-16 are AC/FAM_2. From FIGURE 6-1 it is first seen that the FAM and mixture test data similarly rank the two materials, but that the FAM experiments magnify the differences somewhat. The ratio of |*E**| from FAM_2 to FAM_1 ranges from 1.3 to 2.0, whereas this ratio in AC mix ranges from 1.1 to 1.7. The replicate modulus data of both AC and corresponding FAM materials are given in Appendix B Table B.1 to B.4.
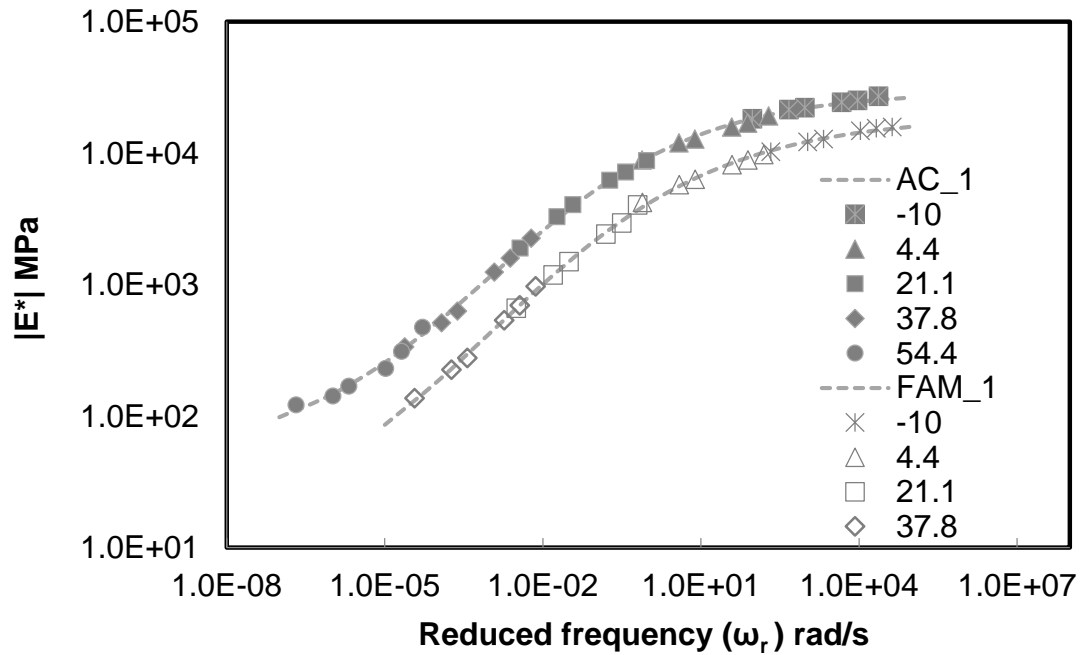
FIGURE 6-1 Dynamic Modulus Master Curves for AC_1 and FAM_1.
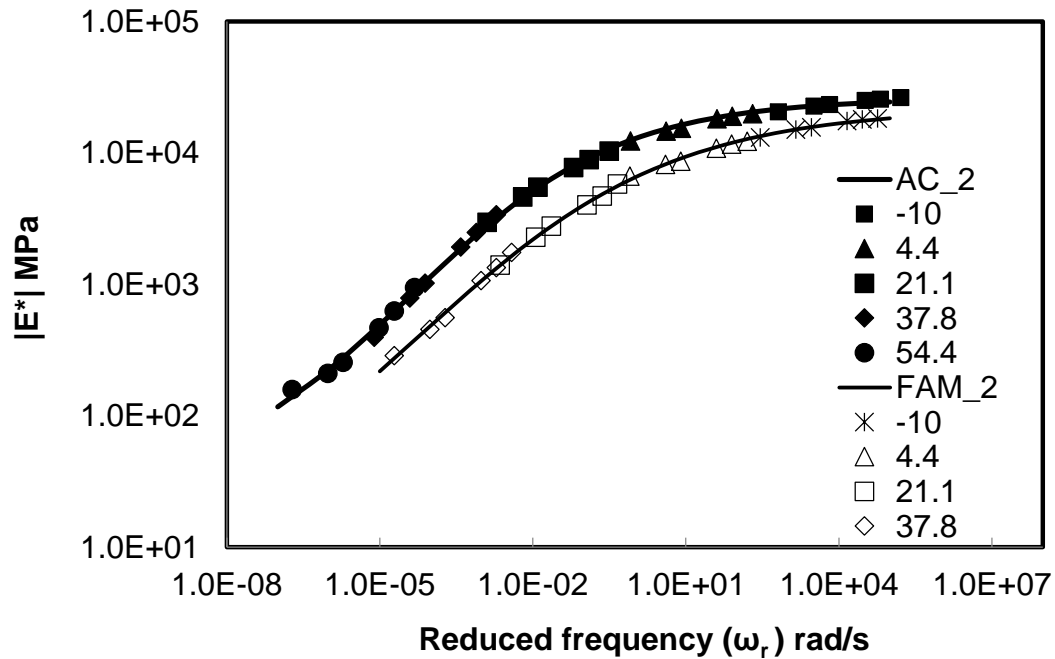
FIGURE 6-2 Dynamic Modulus Master Curves for AC_2 and FAM_2.

FIGURE 6-1 shows the AC and corresponding FAM master curves on the same plot. Note that the minimum reduced frequency is smaller for the mixture than the FAM in light of the fact that mixture tests were conducted up to 54.4°C whereas FAM tests were only tested to approximately 37.8°C. This plot shows that FAM and corresponding AC mix samples master curves exhibit a similar modulus value and that in fact the curves are almost vertically parallel to one another. FIGURE 6-1 illustrates that FAM material's dynamic modulus is very similar to AC mix, the only structural difference in these materials is the coarse aggregate particles. This vertical shift suggests that at least for the modulus, that the coarse aggregate contribution is elastic and does not considerably affect the time-dependence of the material. It also suggests a relatively simplistic relationship may exist between the FAM and mixture modulus. This issue is examined in more detail in a following section.

6.4   Fatigue Test Data Analysis and Model Fit

While comparison of the FAM and AC modulus under a consistent and uniform stress state is (apparently) new, the essential finding that FAM and AC modulus are closely related is not a particularly novel idea and has been reported on in many different locations (99, *115, 117*). However, the similarity in moduli forms a primary building block to more useful comparisons involving the fatigue and damage characteristics of these two scales. The first step in such evaluations involves direct comparison of the failure envelopes from FAM and mix testing. FIGURE 6-3 shows these failure envelope plots for the FAM and mix cases. Failure in these cases is defined by the phase angle drop criterion as proposed by Reese (*66*).

The first observation of note is that the FAM materials demonstrate qualitatively similar behaviors as is typically observed in mixture: a power law relationship between the number of cycles to failure and the strain amplitude coupled with an approximately vertical shifting of the failure envelopes according to test temperature shown in FIGURE 6-3 (a). Other observations are made by comparing the AC_1 and AC_2 performance at 19°C, FIGURE 6-3 (b), to the same curves in the FAM. It is seen that the FAM materials are able to withstand greater strain amplitudes for the same N_f. Closer comparisons show that the failure envelopes are almost parallel between the FAM and mix and that a vertical shift exists between the two results. This shift is consistent with the theory, supported by experimental and numerical studies, that during AC mix loading the FAM experiences strains greater than the overall average strains (*115*, *117*). Both types of material show this trend although the strain ratio of FAM to corresponding AC mix ratio is different in each case. From the test results the vertical distance between FAM_1 and AC_1 fatigue curves is equivalent to a strain ratio of 5.4, whereas for FAM_2 to AC_2 it is 3.4. However, these ratios cannot be interpreted as being entirely representative of the FAM to mix strain ratio since the strain value shown on the y-axis are taken from the 100th cycle, and that the N_f is based on evolving strain magnitudes during the test (recall an actuator controlled fatigue protocol has been followed).

The second observation in comparing these 19°C failure envelopes is that the FAM tests reflect the mixture ranking. As with the on the $|E^*|$ testing, the difference between the two materials is amplified in the FAM results, (FAM_1 is 3.6 times better than FAM_2, but AC_1 is only 2.7 times better than AC_2). The practical significance of this increased sensitivity is not immediately clear. What seems apparent is that the increased sensitivity

in the FAM scale experiments is providing information necessary to bridge the gap between the binder/mastic properties (which would show an even greater sensitivity) and mixture performance. Which means that FAM based experiments may detect differences in materials that do not noticeably manifest in the mixture scale. Whether then such sensitivity is particularly useful is a philosophical question beyond the scope of the current study. The authors contend that developing a mathematical understanding for the reasons of increased sensitivity will lead to improved understanding of materials and subsequently improved material design.
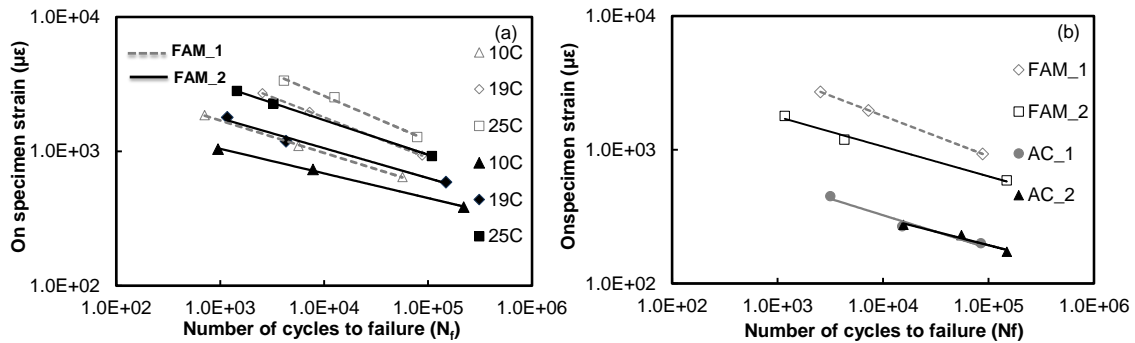
FIGURE 6-3 Fatigue Lives Plot for; (a) FAM_1 and 2 at Various Temperatures And Strain Levels (b) AC_1 and 2 at 19°C for 3 Strain Levels Using 100th Cycle Initial Stiffness.

The fundamental similarities or differences between FAM and AC mix are examined by analyzing the two sets via the simplified viscoelastic continuum damage theory (S-VECD). The model and its capabilities are described in detail in chapter 3. The C- S curves were developed for all FAM_1 and FAM_2 samples at 3 tested temperatures until failure. Irrespective of temperature and strain levels it was observed that C-S curves mostly collapse together for each of FAM types corroborating exiting literature. Some deviation of the damage curves at 25°C was observed in both materials, but similar

behaviors have been reported for mixture tests as well and can be related to the presence of some viscoplasticity or other mechanism (56, 71). Due to this observed behavior, C-S tests at 25°C were separated from those at 10 and 19°C for the purposes of characterizing the C-S model. Data for individual replicates at 19°C for the FAM and mixture cases are shown in FIGURE 6-4, where it is seen that within the variability of the C-S results that the curves from both the FAM and mixture are very similar. Differences include the fact that the terminal C value, e.g., the C value when failure occurs, is generally lower in the FAM than in the mix, which suggests that FAM can endure a greater overall reduction in material integrity before failure occurs. Similar trends are observed for the FAM_2 and AC_2 cases as well. Another difference between these curves lies is its slope near the failure point. For the mix this slope is slightly greater than in the FAM. FIGURE 6-5 more clearly demonstrates the aforementioned differences in the mix and FAM C-S relationship by showing only the best fit functions, Equation (6.1) (a and b are model fit parameters) instead of the individual replicate data. It's also noted that early on the mixture damage curve is positioned slightly higher than the FAM damage curve. Based on the analysis considering each replicate data, shown in FIGURE 6-4, it is believed that this vertical separation of the curves is likely not significant and that conceptually the damage characteristics are essentially the same until S values of approximately 3×10^5.

$$C = 1 - aS^b \qquad\qquad (6.1)$$
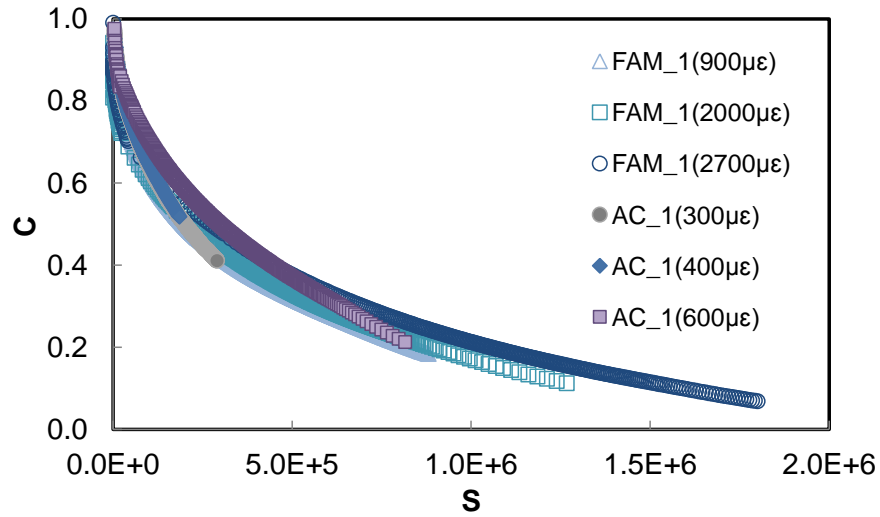
FIGURE 6-4 Collapse of C-S Curve for FAM_1 and AC_1 Mix.
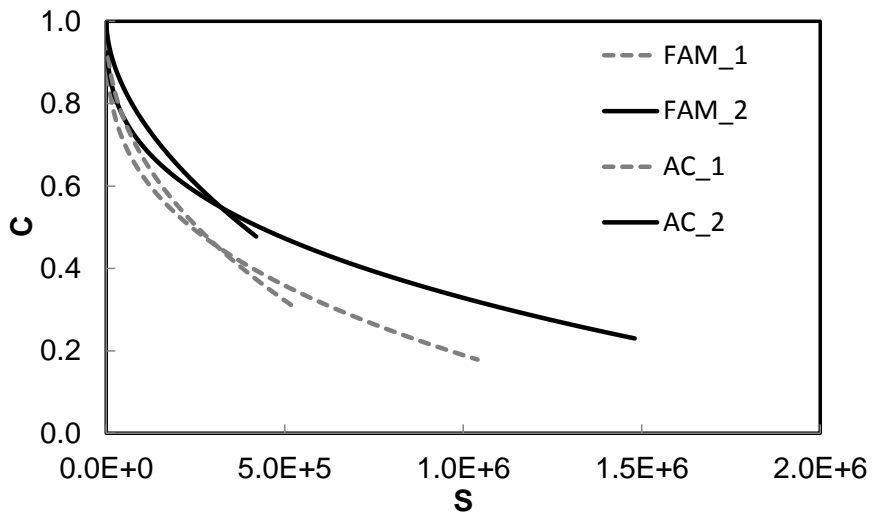
FIGURE 6-5 C-S Model Fit Plot for AC and FAM.

6.5   FAM To AC Upscaling

6.5.1   *Modulus Upscaling*

One of the objectives of this study is to understand the stiffening and fatigue differences

observed between the FAM and mixture scales. A review of the literature shows that

substantial analytical and numerical trials at multiple scale modeling have been carried out (*87*, 117*, 118, 136*). Through this review it is interesting to find that much of the work that attempts to bridge the gap between asphalt binder or mastic and asphalt mixture uses well-known micromechanical formulations such as the composite sphere model generalized self-consistent scheme, differential scheme, and others (*136-139).* Numerical models have, by and large, been used to examine the link between asphalt mixture and FAM (*114, 117, 126*). This situation is surprising because as data in FIGURE 6-1 shows, the similarities between FAM and mix may mean that many mechanisms are similar across these length scales, e.g., the bridge is relatively short. Comparatively, the difference between mixture and binder or mastic is considerably wider and there exist a broader range of mechanisms that should be considered, such as perhaps rigid aggregate contact, which can contribute to a rapid increase in stiffening with increases in particle concentration (*98*). Accounting for these behaviors in any accurate way with analytical approaches is a much greater challenge than handling them via computational means, where local stress and strain rates can be directly accounted for.

Here, in light of the relative similarities that are observed between the FAM and mixture $|E^*|$, analytical models are examined as a means to upscale the modulus and damage behaviors. The models listed above were examined along with the rule of mixtures (ROM) and inverse rule of mixtures (IROM). In the interest of brevity, only the results from the most promising model, the IROM, are shown here. IROM is based on the iso-stress assumption, and though usually applied for elastic predictions, it can be cast into the following viscoelastic form through the elastic-viscoelastic correspondence principle (*140*)

given in Equation(6.2).

$$E*_M = \left(\frac{E*_f \, E_P}{E_P V_f + \left(1 - V_f\right) E*_f} \right) \tag{6.2}$$

where;

$E*_f$ =   FAM complex modulus,

$E*_M$ =   AC mix complex modulus,

E_P =   Aggregate modulus (assumed = 51,300 MPa) and

V_f =   Volume concentration of FAM in AC mix.

The complex modulus can be separated into storage and loss components to separately calculate the mixture moduli, Equations (6.3) and (6.4), which can then combined to find the mixture $|E*|$ value via Equation (6.5).

$$E'_M = \frac{E_P \left(E_P E'_f V_f + V_P E'^2_f + V_P E''^2_f \right)}{\left(E_P V_f + V_P E'_f \right)^2 + \left(V_P E''_f \right)^2} \tag{6.3}$$

$$E''_M = \frac{E_P^{\,2} E''_f V_f}{\left(E_P V_f + V_P E'_f \right)^2 + \left(V_P E''_f \right)^2} \tag{6.4}$$

$$|E*|_M = \sqrt{E'^{\,2}_M + E''^{\,2}_M} \tag{6.5}$$

where;

E'_f =   FAM storage modulus,

E''_f =   FAM loss modulus,

E'_M =   AC mix storage modulus,

E''_M =   AC mix loss modulus, and

$|E^*|_M$ =   dynamic modulus of mix.

       The results of the upscaling analysis using the IROM are shown in FIGURE 6-6. The IROM model data predicts $|E^*|$ of AC_1 with an average of 10 % variation. The agreement is similar, but slightly greater (approximately 20% variation) for the AC_2 case. The fact that such simple model, is capable of successfully predicting the mixture data leads to some interesting suggestions regarding contributions from the coarse aggregate skeleton. First it suggests that the FAM material either fully or nearly fully captures any physico-chemical related interactions between the aggregate and binder. It also suggests that a portion of the particle contact related stiffening, which will tend to stiffen the material and push the composite modulus more towards an iso-strain condition (*139*) has also manifested itself largely in the FAM scale. The hypothesis is that, since most of the modulus is achieved at FAM scale the influence of the coarse aggregate particle contact on stiffening in AC is negligible or small.
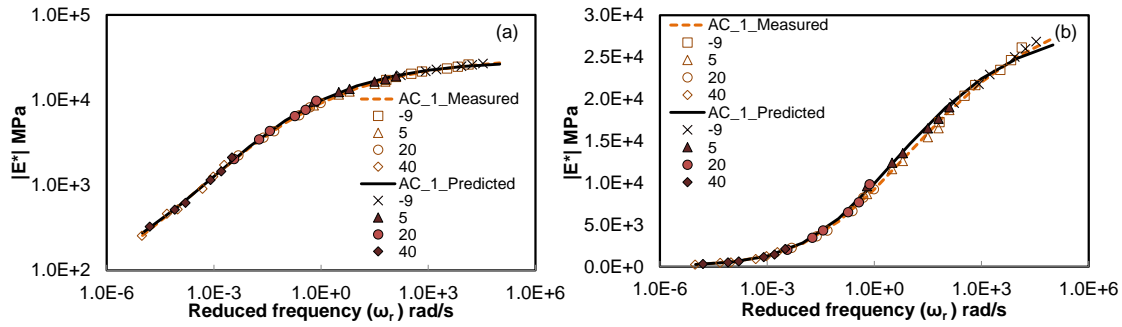
FIGURE 6-6 Master Curve Plots from Upscaling and Experimental Data for AC_1; (a) Logarithmic Scale & (b) Semi-Logarithmic Scale.

6.5.2   Damage Upscaling

Damage is a complex phenomenon because it is a result of the cumulative contribution of growing and coalescing damage at the microstructure level. In the initial stage, microstructure damage evolves by the accumulation of micro cracks and air voids which are distributed uniformly over an entire structure (*141*). These defected areas grow rapidly and interact with each other which lead to the complete failure of AC mix.

Here a relatively simplistic homogenized continua approach relying on an average strain differences and the IROM predicted modulus relationship is adopted. The motivation for embarking on such a simplistic approach is that the modulus and damage characteristic curves are so similar across the material length scales, and that this may suggest a relatively simple relationship between the fatigue processes. The goal for this upscaling method is to accurately predict the reduction in modulus in the AC mix test by using only the LVE and damage characteristics of the FAM. It is postulated that the damage occurs only in the FAM phase and that the reduction in the mixture modulus is the consequence of damage growth in the FAM. While it is true that localized regions may experience complex states of stress,

112

it is further assumed that the through continua average can be simply related to the overall mixture strains through a simple strain ratio. The ratio is expected to be slightly larger than the one predicted from the iso-stress assumption (which can be found to equal 2.2 to 2.4 depending on the precise $|E^*|$ of the FAM). The ratio is expected to be slightly larger than the average strain ratio implied by the iso-stress assumption in light of the fact that localized regions of higher strain will have a higher probability of failing than locations with the overall average. The step by step procedure for upscaling from the FAM properties to the AC response in fatigue loading is given below.

1. The mixture strain history is assumed or taken from actual mixture tests;

2. The homogenized equivalent FAM strain in each cycle is calculated from the mixture strains by multiplication with the assumed FAM to mixture strain ratio, which is taken to be equal to 1.33 times the iso-stress implied ratio.

3. The pseudo strain amplitude of FAM material in each cycle is calculated from the strain level in step 2 using the FAM LVE via Equation (4.3).

4. Calculate the damage parameter (S) and pseudo stiffness (C) in the FAM at each cycle using Equation (2.7) with the FAM based damage function coefficients in Equation (6.1).

5. The modulus, $|E^*|_{FN}$, of the FAM is calculated at each cycle from the pseudo stiffness in step 4, by multiplying C with the FAM LVE modulus. Here $|E^*|_{FN}$ is the ratio of stress to strain amplitude in the FAM at any given cycle in the test.

6. Calculate $|E^*|_N$ of the AC mix in each cycle by inputting $|E^*|_{FN}$ for each cycle into the IROM, Equation (6.5).

113

Some of the upscaling results for both AC mix types are shown in the. It can be seen that overall the process shows positive, but mixed results. FIGURE 6-7(a) and (c) show the best upscaling predictions for the AC_1 and AC_2 mixtures respectively, while parts (b) and (d) show the worst upscaling predictions for these two materials. It can be seen from these comparisons that, while the upscaling method does not yield a perfect match between the measured and predicted values, the agreement appears to be reasonable, and generally equivalent to what can be seen when performing S-VECD model predictions of AC mix behavior by starting with the mix derived LVE and damage properties.
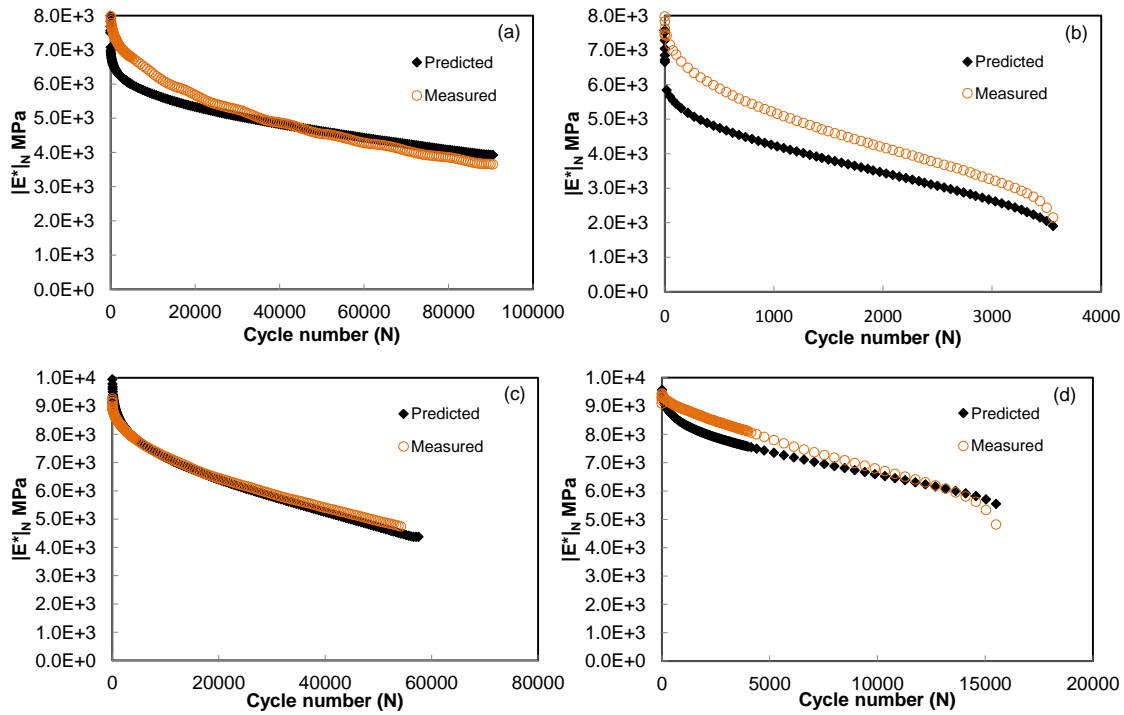
FIGURE 6-7 Modulus Reduction Plot for Experimental and IROM Upscaling; (a) AC_1_ 300με, (b) AC_1_600με, (c) AC_2_350με and (d) AC_2_450με.

6.6   FAM Material Aging Study and its Sensitivity to Binder Aging

In the present study, effort is made to evaluate the sensitivity of mechanical properties of AC mixture to asphalt binder oxidation through a multiscale evaluation approach. The study involves temperature and frequency sweep experiments on unaged and aged asphalt binder (to establish baseline properties), and fine aggregate matrix (FAM - to consider air voids and aggregate interaction effects). The multiscale approach separates effects of aggregate-binder physico-chemical interactions from those caused by air voids and physical aggregate interactions. Also, all binders were pre-aged to specific aging levels before incorporating to prepare respective aged FAM samples. The methodology adopted for assessment of sensitivity was based on the theory of crossover modulus and second order rate kinetics of asphalt binder oxidation. Mechanical properties of FAM materials prepared with softer binders are more sensitive to oxidation than those with stiffer binders. It is found that if laboratory aging procedure used in this study can match the in-service level of binder oxidation at a given accuracy, then the expected accuracy in the resulting modulus of a mixture aged with same procedure will be 1.5 to 3.6 times higher. But the question of interest for further study is that how this accuracy will be changed when the AC mix compacted samples are aged in the lab according to the standard specification (AASHTO R30). It was observed that aging of compacted samples in the oven shows the aging gradient across the diameter of the samples. The sensitivity of uneven aging will be simulated in computational framework to see impact of the aging gradient on the accuracy of in-service binder aging to the lab aging.

6.6.1   *Background on Aging Studies*

Oxidation in asphalt binders has long been recognized to affect performance of asphalt concrete pavements by causing the material to stiffen and embrittle, which leads to a high potential for cracking. Laboratory investigations of oxidation have been traditionally performed using two approaches. In the first, asphalt binders are subjected to various durations of extended heating with or without pressure and then subsequently tested to identify their mechanical properties as a function of exposure condition (*142, 143, 144*) in the other approach, asphalt mixtures are subjected to extended heating and then their corresponding mechanical properties are measured (*145, 146 ,147*). In both approaches, some parameter/metric based on mechanical properties is defined to quantify and evaluate the effect of oxidation.

Many have used the ratio of aged modulus to unaged modulus as this indicator (*142, 148, 149*). Huang et al. (*144*) likened the effect of aging time on modulus of binder to the reverse effect of temperature and instead used similarities or differences in variation of slope of modulus as evaluated by shifting isothermal modulus curves at different aging times using the Williams-Landel-Ferry (WLF) equation. Aspects of binder oxidation chemistry as reported by Petersen et al. (*150*) and Glover et al. (*151*) were also explored to quantify aging based on carbonyl area (CA) growth (*152, 153*). Aging has also been quantified based on changes in crossover modulus, G_c^* (*154*), which is simply the modulus at the point where storage modulus G' and loss modulus G'' are equal.

Overall there has been considerable interest in developing laboratory based simulation procedures for long-term oxidation process in asphalt mixtures (*156, 157, 158,*

159) and for understanding how asphalt binder and asphalt mixture properties are related. The current oxidation method given in AASHTO R30 is based largely on experiments that compared modulus values from in-service pavements with laboratory samples that had been exposed to varying conditioning time. A potential shortcoming with this approach is that changes in AC properties over time can occur as a result of other factors besides oxidation, particularly moisture and load induced damage. A more direct evaluation of oxidative impacts can be made through study of asphalt binder alone, specifically by comparing properties of field aged binder with those from binder extracted from mixtures after applying different simulative aging methods. However, because there does not currently exists a means to accurately map changes in asphalt binder to resultant changes in mechanical properties of asphalt mixtures, it cannot be determined how closely the laboratory procedure needs to replicate the field aged binder properties.

6.7 Quantifying Oxidation and Sensitivity of Study Materials

Oxidation in this study is quantified in multiple ways. The simplest metric, and one that is used regularly in literature (*142, 148, 149*) is based on the ratio of moduli values before and after aging, Equation (6.6). In this study it is referred to as aging ratio (*AR*) and it is the mathematical ratio of $|G^*|$ or $|E^*|$ after aging to the value before aging. It is calculated at multiple temperatures (T_j) and frequencies (ω_i) to gain a complete picture of the impacts of oxidation. It should be recalled that in the present study aged FAM are prepared by blending the aged binder and aggregate and not by aging FAM by themselves.

$$AR = \begin{cases} \left(\dfrac{|G^*|\left(\omega_i,T_j\right)_{after\ aging}}{|G^*|\left(\omega_i,T_j\right)_{before\ aging}} \right) & binder \\[2em] \left(\dfrac{|E^*|\left(\omega_i,T_j\right)_{after\ aging}}{|E^*|\left(\omega_i,T_j\right)_{before\ aging}} \right) & FAM \end{cases} \qquad (6.6)$$

The *AR* is a convenient parameter to quickly identify the mechanical effects of oxidation, especially when evaluated across a large range of temperature and frequency combinations. However, drawing conclusions related to sensitivity based only on *AR* might be inappropriate. Consider an example of binder and its corresponding FAM. The differences in *AR* for the two materials reflect the influence of aggregate particles in stiffening the asphalt binder composite as well as any potentially mitigating physico-chemical surface reactions occurring between asphalt binder and aggregate. As a consequence of this dual influence, care should be taken when directly comparing the differences in binder and FAM *AR* as a means to compare the relative sensitivity of the two materials to oxidative aging products.

In order to overcome this limitation, it is necessary to define a second aging quantity related to only the oxidation in asphalt binder. The parameter chosen for this purpose was based on crossover modulus, G_c^*, which is defined as the modulus when phase angle is 45° (*154*). It is related to the shape parameter in Christensen- Anderson model (*161*) or it can be identified through direct interpolation of the temperature and frequency sweep data. The latter approach was adopted here and involved first plotting the measured |G^*| versus measured ϕ, then fitting the plot in the range of ϕ between 40° and 50°, and finally

interpolating for 45° to compute G_c^*. The importance of using this quantity is that it has been shown to correlate to oxidation induced chemical changes in asphalt binder (*154*). In the same work it was also reported that the inverse of G_c^* varied with time according to a 2nd order rate law. In this rate law two relevant crossover moduli are considered; G_c^* from the un-aged case, e.g., at t=0, G_{c0}^*, and crossover modulus at different oxidation times, G_{ct}^*

The change in G_c^* over time, $G_{c0}^* \rightarrow G_{ct}^*$, is associated with some rate, r, which is mathematically described by Equation (6.7).

$$r = -\frac{d\left[G_c^*\right]}{dt} \tag{6.7}$$

Assuming that this reaction obeys a 2nd order rate law, the rate can also be written as;

$$r = k\left[G_c^*\right]^2. \tag{6.8}$$

Then setting Equation (6.7) equal to Equation (6.8) and solving for time yields;

$$\frac{1}{G_{ct}^*} - \frac{1}{G_{c0}^*} = kt \Rightarrow Aging\ Parameter\ = AP = kt. \tag{6.9}$$

Thus it follows from 2nd order aging kinetics that, difference in the inverse of these moduli over time is a direct indication of oxidation, thus as it is shown in Equation (6.9) , a second aging metric, *AP*, has been defined based on the difference in the inverse of these moduli. The primary purpose of this parameter is to establish the level of oxidation that has occurred in the asphalt binder.

Since sensitivity essentially entails identifying how strongly the mechanical properties of a composite are affected by chemical changes in asphalt binder, assessment of sensitivity involves combining *AR* and *AP* quantities. Mathematically, the aging sensitivity parameter (*ASP*) is defined to be the impact of a differential change in AP of the binder on AR of a binder, FAM, Equation (6.10). The *ASP* can be determined directly by cross-plotting *AR* of the binder or FAM with the aging parameter from the asphalt binder. Since *AR* and *AP* vary with temperature and frequency, *ASP* also varies by temperature and frequency.

$$ASP = \frac{d(AR_{mastic\ or\ binder})}{d\left(AP_{binder}\right)} \tag{6.10}$$

6.8 Dynamic Modulus Results

The experimental results from dynamic modulus tests are first examined by creating and comparing modulus mastercurves. For FAM, |*E**| mastercurves are developed by fitting test data to a sigmoidal function. The mastercurves developed for FAM B2A2G2-F-7.5 are presented in FIGURE 6-8. The replicate modulus data of each aging level are given Appendix B Table B.5 to B.12.
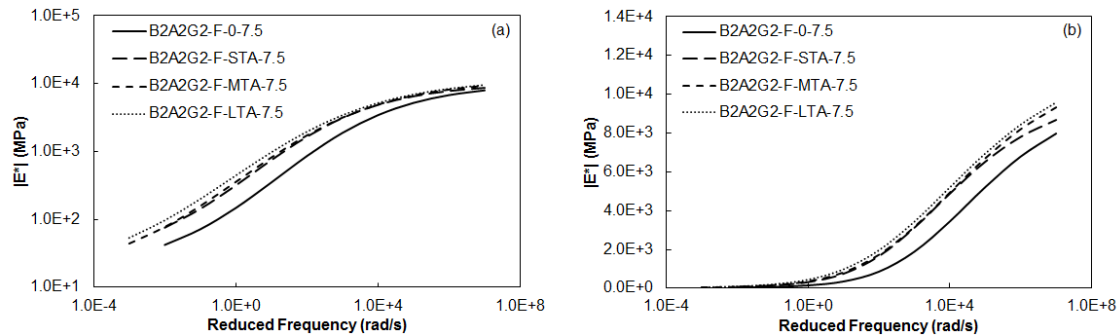
FIGURE 6-8 Modulus Mastercurves for FAM, B2A2G2-F-7.5 at Different Aging Levels and Air Void Contents in: (A) Log-Log Space and (B) Semi-Log Space.

It can be observed from FIGURE 6-8 that as aging levels become more severe, the modulus increases. Also, it is seen that from year 0 to the STA level, shift in modulus is greater when compared to that from STA to MTA and LTA. The data in these graphs was used in Equation (6.2) to calculate *AR* and typical results for B2 and its corresponding FAM are shown in FIGURE 6-9. The general trend that is observed is that binder shows a larger increase in *AR* than FAM. This is due to the dual influences that aggregate particles impart with respect to mitigation of aging effects on modulus and overall stiffening. Also, *AR* increases with increase in temperature, which can be attributed to greater binder mobility resulting in greater influences from oxidation products at higher temperatures. As indicated before, the dual influences hinder sensitivity analysis based purely on *AR*. In order to better quantify sensitivity, a procedure based on crossover modulus was applied. The description of the study materials is given in Appendix A (Table A.4).

6.9   Sensitivity Assessment

The *ASP* from Equation (6.10) is determined by cross-plotting *AR* of the binder and FAM with *AP* from asphalt binder, as shown in FIGURE 6-9. Since asphalt binder is pre-aged, *AP* of the binder in FAM is identical and equal to what was measured for the non-mixed asphalt binder. The *ASP's* for materials shown in the figure are slopes of the respective trend lines, which for B2, and B2A2G2-F-4.5 are 5.98×10^7, and 2.31×10^7 respectively. Through FIGURE 6-9 inferences on sensitivity can be made by comparing the proximity of FAM trend lines to that of binder. Although, these observations can be quantified, generalization based on the goals of the study is difficult to achieve through this approach.
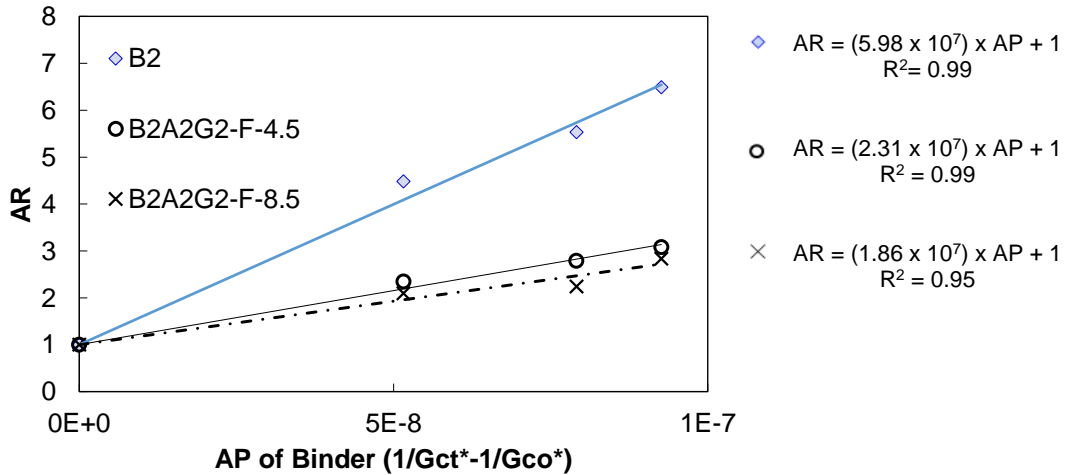
FIGURE 6-9 Relationship Between AR of binder B2, and FAM B2A2G2-F-4.5/8.5 to AP of B2 for Different Aging Conditions at 30°C and 10 rad/s.

Since the motivation for this study is to identify the accuracy with which laboratory aging processes should replicate in-service aging. In this case sensitivity can be viewed from two perspectives; 1) how accurately does *AP* need to be matched in order to achieve a chosen level of accuracy in mechanical properties and 2) what is the expected accuracy in mechanical properties given a level of accuracy in matching *AP*. Both questions have been evaluated for different levels of accuracy as detailed below.

6.9.1   *Question 1: How accurately should the laboratory process replicate binder AP in order to match asphalt mixture properties?*

To evaluate how accurately the laboratory process should replicate the binder *AP*, consider the effect of an arbitrary change in *AR* on AP. For this purpose let AR_1 be a given aging ratio of the material (binder, or FAM) and AP_1 be the *AP* at AR_1. Since the relationship between *AP* and *AR* is a linear line with an intercept of one and a slope equal to *ASP*, AP_1 can be calculated by Equation (6.11)

122

$$AP_1 = \frac{(AR_1 - 1)}{ASP} \tag{6.11}$$

Next consider a second aging ratio, AR_2, which represents aging ratio after a percentage change (denoted as x),

$$AR_2 = AR_1 \left(1 + \frac{x}{100}\right) \tag{6.12}$$

In this case AP_2 is defined as the aging parameter corresponding to AR_2, and can be calculated as,

$$AP_2 = \frac{(AR_2 - 1)}{ASP} \tag{6.13}$$

The accuracy required in AP to match AR within a predetermined level of accuracy, x, is determined by first selecting AR_1. Then, a value of x is assumed and substituted into Equation (6.12) to find AR_2. Finally Equations (6.11) and (6.13) are used to calculate AP_1 and AP_2 respectively. The percent difference between AP_1 and AP_2, Equation (6.14), represents the accuracy required to match binder AP in order to achieve the assumed accuracy in AR. These calculations are performed at each of the temperatures and frequencies evaluated, for each of STA, MTA, and LTA conditions, and at a range of AR accuracy.

$$\% Difference_{AP} = \frac{(AP_2 - AP_1)}{AP_1} \times 100 \tag{6.14}$$

The results for B2 and two of FAM are presented in FIGURE 6-10 (a) and (b). The data presented in this figure represents the accuracy required in matching the binder AP in

order to achieve a 20% accuracy in *AR*. Note that for the sake of brevity only the 20% accuracy case is shown in this study, but conclusions and observations below were developed based on analysis covering a range of accuracy from 1-20%. FIGURE 6-10(a) should be read as follows, if a laboratory procedure can estimate *AP* of binder B2 at LTA level within approximately 35% then it can be ensured that the resultant modulus of B2A2G2-F-7.5 at 22 years and 30°C will be within 20% of its true modulus. Results are shown at only 10°C and 30°C as they are lowest and highest common temperatures for which experimental data were available. They also demonstrate the lowest and highest observed sensitivities in the dataset. A frequency of 10 rad/s is used in this analysis, but similar results are obtained at other frequencies. The main observations from this data are; 1) The accuracy required in *AP* increases with increase in aging level, that is to say a more accurate *AP* must be achieved at LTA level than at MTA or STA levels to match an assumed accuracy of *AR*. 2) Higher temperatures require *AP* to be more closely matched. Although not shown here the inverse statement occurs with respect to frequency, as the frequency decreases the *AP* must be matched more closely. 3) Fine graded (G2) FAM, FIGURE 6-10 (a), require higher accuracy in *AP* than coarse graded (G1) materials, FIGURE 6-10 (b). 4) FAM materials containing 4.5% air voids require higher accuracy in *AP* than FAM materials containing 7.5% air voids.
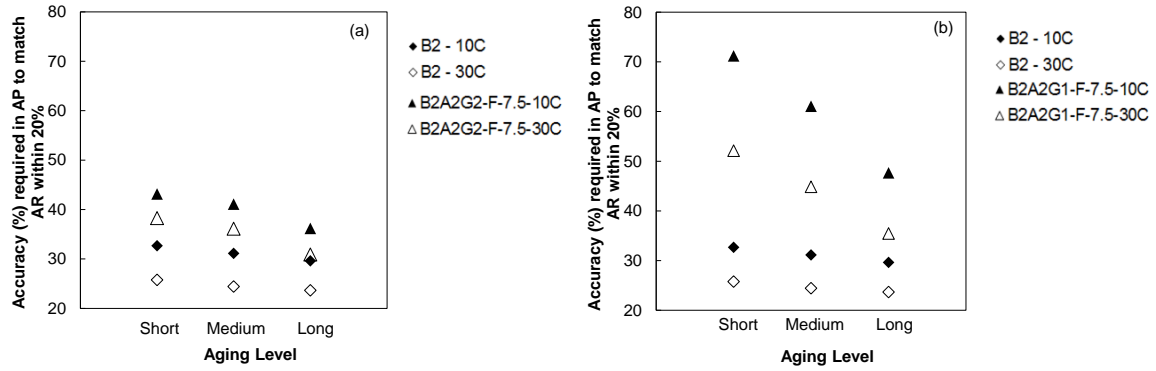
FIGURE 6-10 Accuracy (%) Required In Binder *AP*, at Three Different Aging Levels, to Match The Mechanical Property (*AR*) within 20% for (a) Binder and FAM (G2 gradation) and (b) binder and FAM (G1 gradation)

6.9.2 *Question 2: How accurately can asphalt mixture properties be matched at different levels of AP accuracy?*

To answer second sensitivity related question, consider the effect of an arbitrary error in *AP* on *AR*. Like in the derivation to answer the first question, let AR_1 be a given aging ratio of the material (binder and FAM) and AP_1 be AP at AR_1. The relationship between AP_1 and AR_1 is given by Equation (6.11). Next consider a second aging parameter, AP_2, which represents the aging parameter after a percentage error (denoted as *y*) is factored in,

$$AP_2 = AP_1\left(1 + \frac{y}{100}\right) \tag{6.15}$$

In this case AR_2 is defined as the aging ratio corresponding to AP_2, and can be calculated as;

$$AR_2 = (AP_2 \times ASP) + 1 \tag{6.16}$$

125

The percent difference between AR_1 and AR_2, Equation (6.17), represents the resulting error in AR due to the effect of the arbitrary percentage error in AP.

$$\%Error_{AR} = \frac{(AR_2 - AR_1)}{AR_1} \times 100 \qquad (6.17)$$

The results of this analysis for B2 and two of its corresponding FAM are presented in FIGURE 6-11 The data presented in this figure represents the resulting error in AR due to a given percentage error in AP, which in this case is set at 20%. The data from FIGURE 6-11 should be interpreted as follows, if error in matching AP of binder B2 at STA is 20% then the resultant error in AR at STA at 30°C for binder B2 is 15.5%, but for FAM B2A2G2-F-7.5 it is only approximately 10.5%. This shows that for a fixed accuracy in AP the error in estimated mechanical properties would be less for FAM than for binders. Since the analysis relies on the same ASP values as in question 1, other major findings with respect to impacts from temperature, gradation, and binder aggregate interactions essentially remain the same.
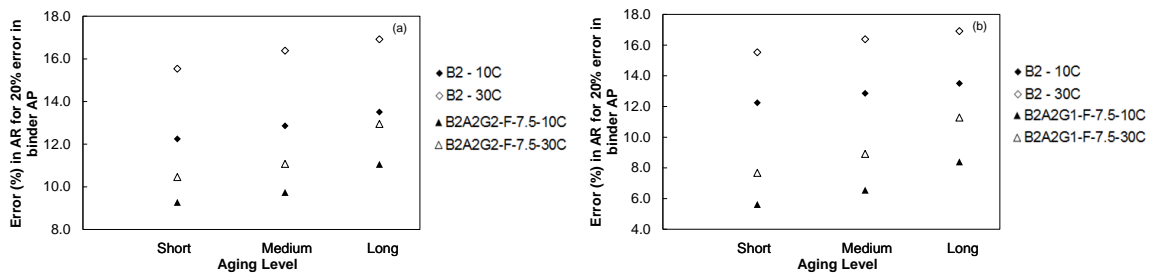
FIGURE 6-11 Error (%) in Mechanical Property (AR) due to 20% Error in Binder AP for (a) B2G2 Gradation Based Materials; and (b) B2G1 Gradation Based Materials.

6.10 Summary and Conclusions

In the current chapter FAM and AC samples were tested for two types of materials in similar test conditions. From the results, it was observed that FAM and corresponding AC $|E^*|$ master curves exhibit similar frequency dependence in both material cases. The fatigue response of AC and FAM were also measured and analyzed for their damage characteristics. From the analysis, it was observed that FAM material C-S plots mostly collapsed irrespective of temperature and strain level, which is consistent and agrees with existing literature on AC mix. Other important observations from this study include;

- The C-S curves for FAM and corresponding AC mix are collapsing together until some point of damage and deviate from that point.

- From the fatigue analysis it was observed that FAM material can resist much higher strains than the AC for the same fatigue life. The strain ratio of FAM to AC mix during the fatigue loading was found to vary in between 3 to 5.4.

- The upscaling of AC modulus and damage response using FAM properties showed promising results from a relatively simple homogenized continuum scheme.

Aging study was performed to estimate the sensitivity of the mechanical properties of AC to asphalt binder oxidation. In this regard, experimental characterization was performed at binder and FAM scales. Testing was performed on asphalt binder to establish baseline properties and FAM to consider air voids and aggregate interaction effects. Dynamic modulus experiments were run on the aforementioned materials to determine modulus and subsequently the aging ratio. The approach adopted here to evaluate sensitivity was based

on the concept of crossover modulus and the principles of second order rate kinetics of binder oxidation.

- Quantification of differences was not clearly understood through direct analysis of *AR* and binder *AP*, so more involved methodology followed. In the first application of this approach, the accuracy required in binder *AP* to match the binder, and FAM *AR* at varying levels of accuracy (1-20%) is estimated. In the second application the errors in *AR* when *AP* was matched at 1-20% were evaluated.

- The primary conclusions from these analyses were that the accuracy levels required in binder *AP* to match the FAM *AR* at 1%, 10% and 20% levels of accuracy were 1.5 – 3.6%, 14.8 – 35.6%, and 29.6 – 71.2% respectively.

- Based on the recent advances in studies comparing mechanical properties of FAM and asphalt concrete, it is expected that the sensitivity in full asphalt concrete mixture would be less than FAM, but by only a relatively small amount.

- The continuation to this study focuses on addressing the sensitivity of accuracy that need to be matched when AC samples are aged in the lab. The so called uneven aging of AC samples will be simulated in computational framework to predict aging ratio of AC mix.

To conclude, testing FAM material in an overall stress condition consistent with that in an AC mix leads to very similar comparisons between the FAM and AC. These similarities suggest that the FAM scale may be accounting for most of the physico-chemical interaction and aggregate stiffening, at least with respect to loads used to measure $|E^*|$ and in fatigue response. The similarity in material properties between the two material scales suggests

that if careful attention is given to material fabrication protocols there is a potential use of FAM testing for material characterization and ranking mixtures. In addition, experimental and mechanical studies with these materials may provide better insights into the internal mechanics of AC and potentially lead to better designed longer lasting AC mixtures.

CHAPTER 7 RELIABILITY OF FATIGUE LIFE PREDICTION USING FINE AGGREGATE MATRIX DATA

7.1 Introduction

As mentioned earlier, the reliability of prediction measurement is an important parameter to consider in the development of test methods and prediction models. In this research effort, FAM experimental data was used to predict the reliability of fatigue life prediction. FAM experimental data was also used to upscale it to AC and predict the fatigue life of material to assess whether the reliability of fatigue life prediction in AC can be improved with FAM phase experimental data.

7.2 Materials and Test Methods

Materials, mix design, sample preparation, and testing methods for AC and FAM were described in detail in Chapters 4 & 5. For the purpose of reliability study, modulus and uniaxial fatigue test data obtained from both FAM and AC materials was used. Each replicate data from both material types was analyzed under various experimental and model failure criteria to predict the deterministic fatigue life using the S-VECD model formulations. Details regarding the reliability analysis of AC for different experimental and model failure criteria were presented in the Chapter 4. Similar to AC data, reliability analysis was conducted on FAM data to predict the fatigue life of FAM material using S-VECD modeling approach. The variation observed from both experimental and model failure criteria and the corresponding deterministic fatigue life prediction of FAM material is presented in the following sections.

7.3 Reliability Study of Fatigue Life Prediction for FAM

Reliability framework developed for AC data in Chapter 4 was used for analyzing the reliability of fatigue life prediction using the FAM experimental data. Since experimental studies on FAM were conducted in similar test and loading as AC, the same S-VECD model and its formulations were used for predicting the fatigue life of FAM material. Similar to AC reliability analysis, various experimental and model failure criteria were considered to predict reliability of fatigue life for FAM. Comparisons were made for reliability of fatigue life prediction between FAM and AC.

7.3.1 Experimental Failure Criteria Variation

Some of the frequently used criteria to define failure in fatigue experiments are; phase angle (PA) drop (*66, 67*), cycle when the modulus is 50% of the initial value (*68*), and peak of the product of stiffness (C) and corresponding load cycle number (N) (*69, 70*). These three criteria were used to define failure point identification of FAM samples during the fatigue data analysis. Number of failure cycles (N_f) obtained from different experimental failure criteria approaches are shown TABLE 7-1. Similar to AC data, N_f changes from one failure criteria approach to other for the FAM. One important observation can be made from TABLE 4-1 (AC failure cycles) and TABLE 7-1 is that the variability in the failure cycles from one experimental approach to other is not very different in AC, whereas this difference is found to be quite large for the FAM fatigue analysis. The coefficient of variation observed in number of failure cycles between experimental failure criteria methods for AC ranged from 5-18% whereas this range for FAM data was observed to be 30-70% depending on the failure cycles. In both AC and FAM experiments, the 50%

reduction of modulus shows lesser number of failure cycles than other methods with FAM data having a greater variation compared to AC. As FAM material is softer than the corresponding AC, it can sustain damage much longer according to *PA* drop and *C* x *N* approaches. The 50% reduction of initial modulus approach considers failure as the point at which the materials reaches half of its initial modulus, which may not be the realistic failure point especially for softer materials.

TABLE 7-1 Variation in FAM Number of Failure Cycles for Different Experimental Failure Criteria

Strain Level ($\mu\varepsilon$)	N_f		
	PA drop	*C* x *N*	50% reduction of initial modulus
930	87,979	66,746	23,285
1962	7,622	5,823	4,124
1970	7,093	5,394	1,751
2710	2,682	1,921	410

7.3.2 *Variation in Model Failure Criteria Approaches*

Similar to the AC reliability study, both the pseudo stiffness at failure (C_f) approach (*19, 54, 56, 71*) and the pseudo energy release rate (G^R) approach (*72, 73, 74*) were used to identify failure in the S-VECD model. Since the number of failure cycles change depending on the experimental definition of failure, the corresponding C_f value in the S-VECD characterization test also changes. In the case of FAM experimental data C_f is 0.119 when using the *PA* drop method, 0.327 for 50% initial modulus method, and 0.231 for the *C* x *N* method. Number of failure cycles for each experimental failure criteria were calculated using the Equation (4.1). This equation produces an estimate of the number of cycles to failure for a given strain amplitude, damage characteristic relationship, and C_f of FAM.

Since the average C_f value is different from one failure point identification method to another, the predicted fatigue life is expected to vary as shown in shown in FIGURE 7-1.
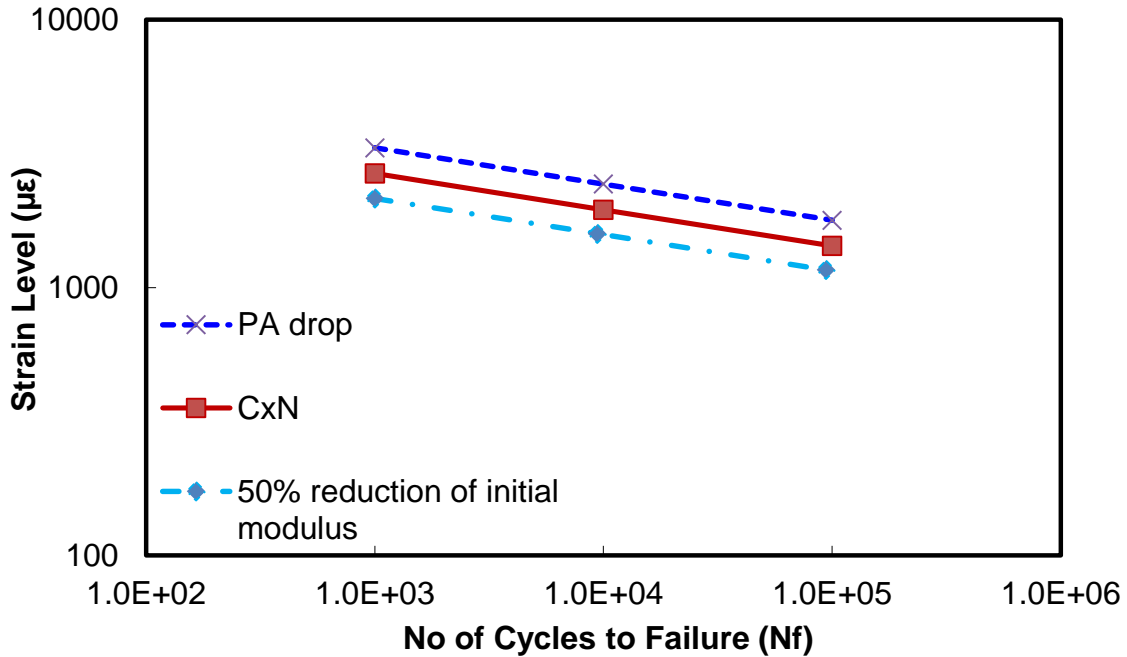
FIGURE 7-1 Simulated Fatigue Lives Plot for FAM According C_f Model Failure Criteria Using Three Different Experimental Failure Point Identification Methods.

Another model failure criteria approach considered was average pseudo strain energy release, G^R rate. For each of the experimental failure criteria G^R was calculated using Equation (2.12). The relationship between G^R and N_f follows the power law function shown in Equation (2.14). Similar to the C_f approach, since the number of cycles to failure changes from one experimental failure point identification method to another, the corresponding characteristic relationship or slope also changes which is shown in FIGURE 7-2 . Due to the differences in G^R characteristic equation slope, the number of failure cycles predicted using the S-VECD model (calculated using Equation (4.2)) for deterministic inputs are also different. The differences in the G^R characteristic equation in predicting

133

number of failure cycles for FAM_1 from one experimental failure criteria to another is

shown in FIGURE 7-3.
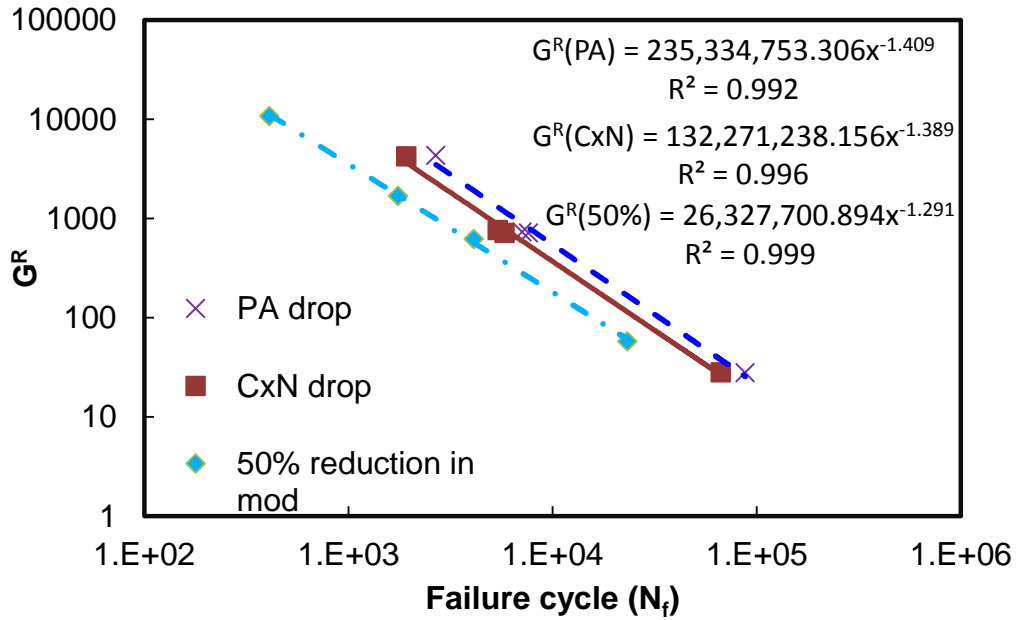
FIGURE 7-2 FAM Variation in G^R Characteristic Equation for Different Experimental
Failure Criteria.
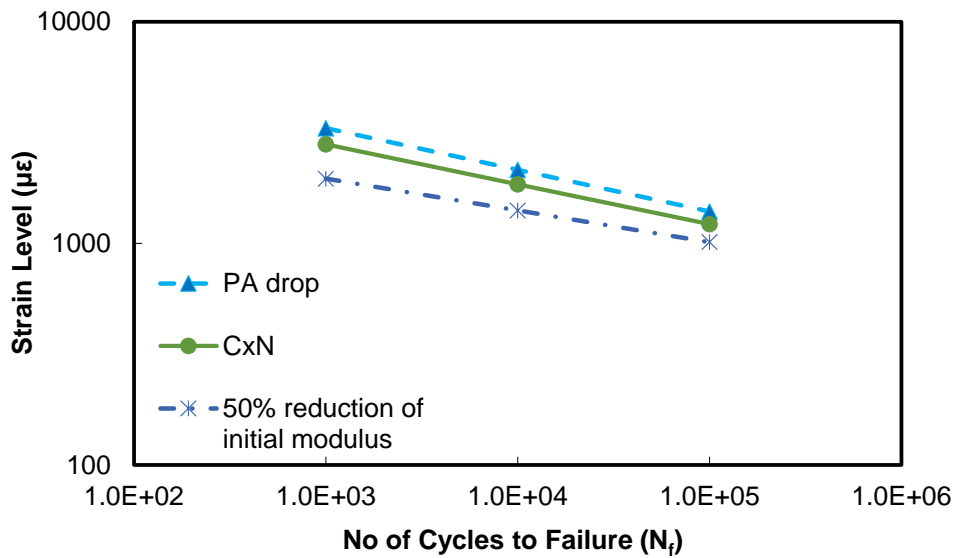
FIGURE 7-3 FAM Simulated Fatigue Lives Plot or AC Mixture According G^R Model
Failure Criteria Using Three Different Experimental Failure Point Identification Methods.

134

7.3.3 *Reliability of Fatigue Life Prediction for FAM using C_f as Model Failure Criteria*

Reliability of fatigue life prediction for FAM material using the C_f as model failure criteria in S-VECD model was performed using the Monte Carlo simulations. The variation in input variables, modulus ($|E^*|$), damage characteristic equation (C_{12}) and pseudo stiffness at failure (C_f) used for the Monte Carlo simulations are presented in TABLE 7-2. The variation in the input variables were used for developing probabilistic parameters of S-VECD model equation inputs for the Monte Carlo simulation. The remaining parameters of the S-VECD model equation were assumed to be constant in the simulation. Monte Carlo simulation was run for 100 iterations. The resultant reliability measurements from the 100 iterations are shown in FIGURE 7-4. This figure shows the reliability of fatigue life predictions for different failure criteria as a function of prediction percentage error with respect to the accurate value. As mentioned in Chapter 4 AC reliability analysis, accurate fatigue life prediction for FAM was considered as number of failure cycles predicted from the deterministic approach for a given experimental definition of failure. Similar to the AC reliability approach, the reference cycles to failure was set based on the deterministic prediction from each failure criteria for calculating the percentage error.

TABLE 7-2 FAM_1 Variation of Input Parameters for Predicting Fatigue Life Using C_f Approach

Experimental Failure Criteria	Parameter	Mean	Standard Deviation	CV
PA drop	$|E^*|$ (MPa)	3544	142	4.0
	C_{12}	0.306	0.002	0.6
	C_f	0.119	0.021	17.5
	G^R (High cycles) [1]	2422.2	307.4	12.7
	G^R (Low cycles) [2]	24.1	8.2	34.2
C x N	$|E^*|$ (MPa)	3544	142	4.0
	C_{12}	0.306	0.002	0.6
	C_f	0.231	0.013	5.7
	GR (High cycles) [1]	1571.6	114.1	9.3
	G^R (Low cycles) [2]	25.2	6.4	25.2
50% reduction of initial modulus	$|E^*|$ (MPa)	3544	142	4.0
	C_{12}	0.306	0.002	0.6
	C_f	0.327	0.024	7.3
	G^R (High cycles) [1]	3546.3	99.4	8.6
	G^R (Low cycles) [2]	62.9	5.4	2.8

[1]$high$ = 100,000 cycles, [2]Low = 1,000 cycles

The resultant reliability predictions obtained from all three different failure criteria methods are shown in FIGURE 7-4. From this figure it can be observed that the reliability measurements are not very different for low and high number of failure cycle predictions for phase angle drop and 50% modulus reduction approaches. But the C x N failure criteria method is showing rather large difference in reliability predictions compared to the other two approaches at low number of failure cycles. Despite the differences in reliability at low and high number of failure prediction cycles, the C x N approach is observed to exhibit greater reliability than the other two approaches. This trend is observed to exhibit correlation with the variation observed for the input variable pseudo stiffness at failure. Quantitatively to achieve 90% reliability, the error associated with the prediction is approximately ±40% with the FAM experimental data.
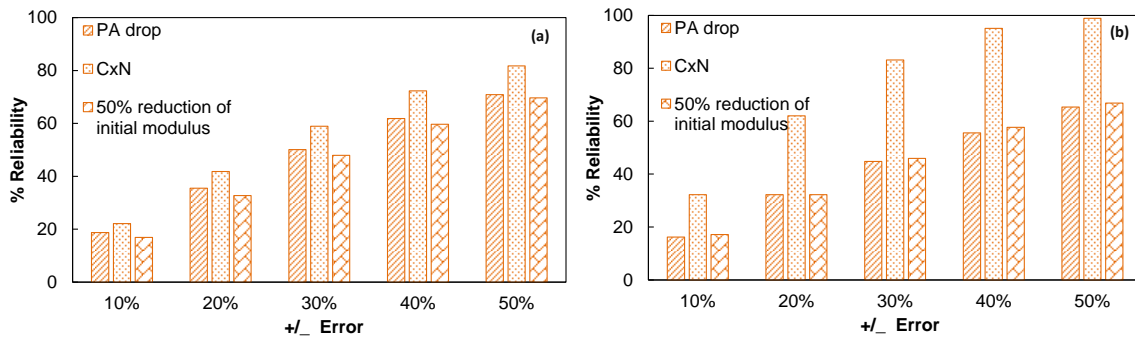
FIGURE 7-4 FAM_1 Reliability of Fatigue Life Prediction for Various Experimental Failure Point Identification Methods Using C_f Failure Criteria for; (A) High and (B) Low Number of Failure Cycles.

7.3.4 *Reliability of Fatigue Life Prediction for FAM material using* G^R *Model Failure Criteria*

The variations in input variables used for the Monte Carlo simulations for G^R as the model failure criteria are shown TABLE 7-2. Similar to the AC reliability approach, characteristic equation coefficients for FAM data were calculated for every combination of three out of the four tests conducted. The variation in G^R values were calculated using the characteristic equations developed for each of the three test combinations. The G^R value distribution was then randomly generated within the observed experimental G^R range to ensure the characteristic equation coefficients used for simulations are within the observed experimental G^R range. Randomly generated G^R coefficients were used in the Monte Carlo simulation procedure to develop the reliability measurements for both high and low number of failure cycles prediction using S-VECD formulation with G^R as model failure criteria. The reliability results obtained from this analysis are presented in FIGURE 7-5. The accurate fatigue life prediction (or reference fatigue life prediction) for the percentage error calculation was based on the experimental definition of failure. From FIGURE 7-5, it can

137

be observed that the reliability measurements for different experimental failure criteria are not substantially different at high number of failure cycles but they are showing significant differences at low number of failure cycles. The 50% modulus reduction approach shows more reliability compared to the other two failure criteria approaches for both high and low number of failure cycles. This trend is also observed to exhibit correlation with the variation observed in the G^R values shown in TABLE 7-2. From the FIGURE 7-5, it can be observed the error associated to achieve 50% reliability is approximately ±20%. However this number might vary depending on the type of failure criteria and the number of failure cycles prediction.
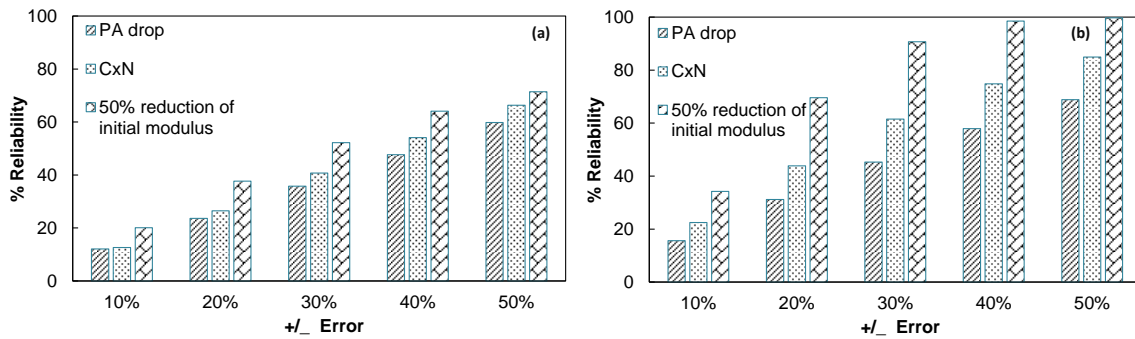
FIGURE 7-5 Reliability of Fatigue Life Prediction for FAM_1 at Various Experimental Failure Point Identification Methods Using G^R Failure Criteria for (a) High and (B) Low Number of Failure Cycles.

7.3.5   Reliability Comparisons between C_f and G^R Model Failure Criteria for FAM

To avoid any errors associated with extrapolation in fatigue life prediction with respect to model failure criteria comparison, reliability analysis for both C_f and G^R failure criteria was conducted at 10,000 cycles. FIGURE 7-6 shows the reliability measurements of different experimental failure criteria for both C_f and G^R approaches at 10,000 cycles. It can be

observed from the figure that G^R approach is showing more reliable measurements than the C_f approach in *PA* drop and 50% modulus reduction methods. In case of *C* x *N* failure method, both model failure criteria approaches are showing very similar reliability measurements. This trend is rather intriguing since the reliability analysis with AC data showed that C_f approach as more reliable than G^R approach. One reason for this trend could be the difference in fitting the G^R characteristic equation between AC and FAM. It can be observed from FIGURE 4-2 and FIGURE 7-2 that the FAM experimental data fits quite well for G^R characteristic equation than AC. From this observation it can be postulated that since the G^R characteristic equation fits the FAM experimental data well, the error associated with the reliability prediction with the G^R approach could be less compared to the C_f approach. As mentioned earlier, this statement is with respect to reliability predictions only, but not for accurate fatigue life predictions. To decipher the impact of input variables on reliability prediction of failure cycles between one model failure criteria to another, parametric sensitivity analysis is warranted.
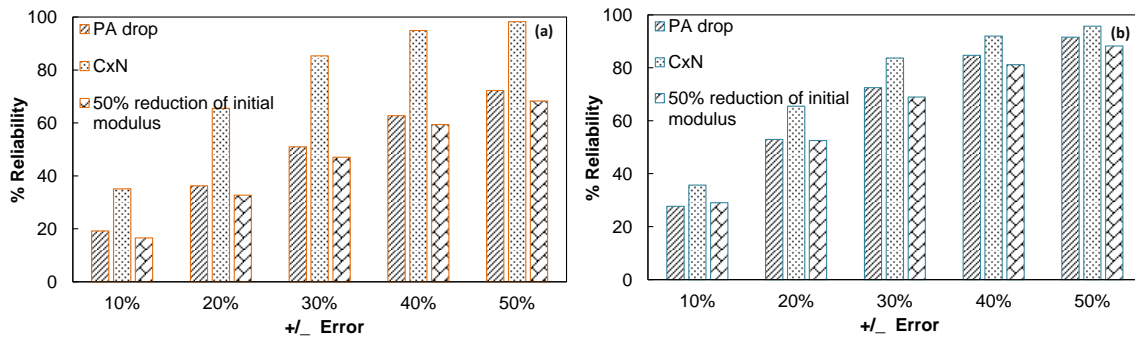
FIGURE 7-6 AC_1 Reliability of Fatigue Life Prediction for Various Experimental Failure Point Identification Methods for 10,000 Cycles (A) C_f Failure Criteria And (B) G^R Failure Criteria.

7.4 Reliability Comparisons between AC and FAM

The comparison of reliability of fatigue life prediction between AC and FAM materials was performed for both C_f and G^R approaches at different experimental failure criteria. FIGURE 7-7 depicts the comparison of reliability predictions of FAM and AC using S-VECD model formulations with C_f as model failure criteria. From this figure it can be observed that FAM phase experimental data is showing more reliability in predicting fatigue life compared to AC for *PA* drop and *C* x *N* failure criteria. However, the 50% reduction of initial modulus failure criterion is showing more reliable measurements with AC data. One reason for this reverse trend compared to other failure criteria might be due to the fact that 50% reduction of initial modulus approach simply considers failure as the point at which the material reaches half of its initial modulus, which might not be the realistic failure point especially for the softer materials such as FAM. The variation of C_f at this particular point might be more from one replicate to other. From TABLE 4-2 and TABLE 7-2 it can be observed that the variation of C_f for FAM is lesser than AC for *PA* drop and *C* x *N* experimental failure criteria approaches but this variation in case of 50% initial modulus reduction case is high. The higher variation observed in input variables of C_f for FAM phase testing might be impacting the reliability analysis. However it should be noted that this is just a hypothesis developed from the trends observed in FIGURE 7-7. Another notable observation from the FIGURE 7-7 is that FAM material is showing substantial improvement in the reliability of fatigue life prediction over AC with the *C*x*N*. This improvement can be explained in part from the variation of input parameters observed in TABLE 4-2 and TABLE 7-2. From the tables noted, it can be observed that variation of C_f parameter in FAM material is about half of the variation observed in C_f parameter for

AC material. The 50% lower variation in FAM might be getting reflected as twice the improvement in the reliability of fatigue life predictions. One caveat to be noted here is, since the variation of other input parameters also have impact on the reliability predictions, quantitative comparison of this nature should be taken with a grain of salt. For accurate comparisons, analysis should be performed by fixing the variation of other input variables in both FAM and AC materials. To establish more general conclusions and gain additional insights, parametric sensitivity analysis of the S-VECD model with C_f as the model failure is conducted, and the results are presented in the following Chapter.
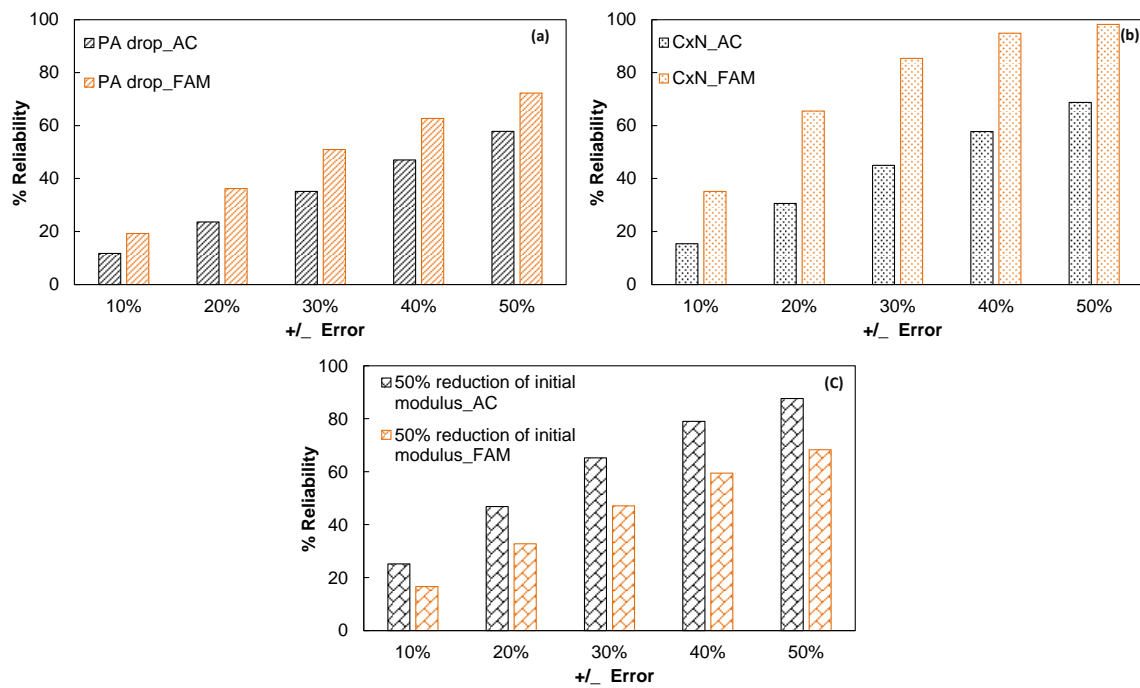
FIGURE 7-7 Comparison of Reliability of Fatigue Life Predictions Between AC and FAM using C_f Failure Model Criteria for (a) *PA* drop (b) *C* x *N* and (c) 50% Reduction of Initial Modulus.

Similar comparisons were performed between AC and FAM using G^R as the model failure criteria for reliability of fatigue life prediction. The reliability predictions for AC and FAM for each failure criteria are shown in FIGURE 7-8. From this figure, it can be observed that irrespective of experimental failure criteria, FAM phase experimental data is showing higher reliability in predicting fatigue life of the material using S-VECD model. One more observation from the FIGURE 7-8 is that the difference in the reliability measurements between FAM and AC is substantially higher in case of *PA* drop and *C* x *N* approaches whereas this difference is less in the case of 50% initial modulus reduction approach. Issues pertaining to the usage of 50% initial modulus reduction approach for failure point identification (particularly for softer materials such as FAM) might be impacting the reliability results of G^R approach, but the impact is not as significant as in case of C_f approach. The reason for this trend in C_f approach is due to the definition of 50% reduction in modulus which might have direct influence in S-VECD model formulation for C_f approach than in G^R approach.
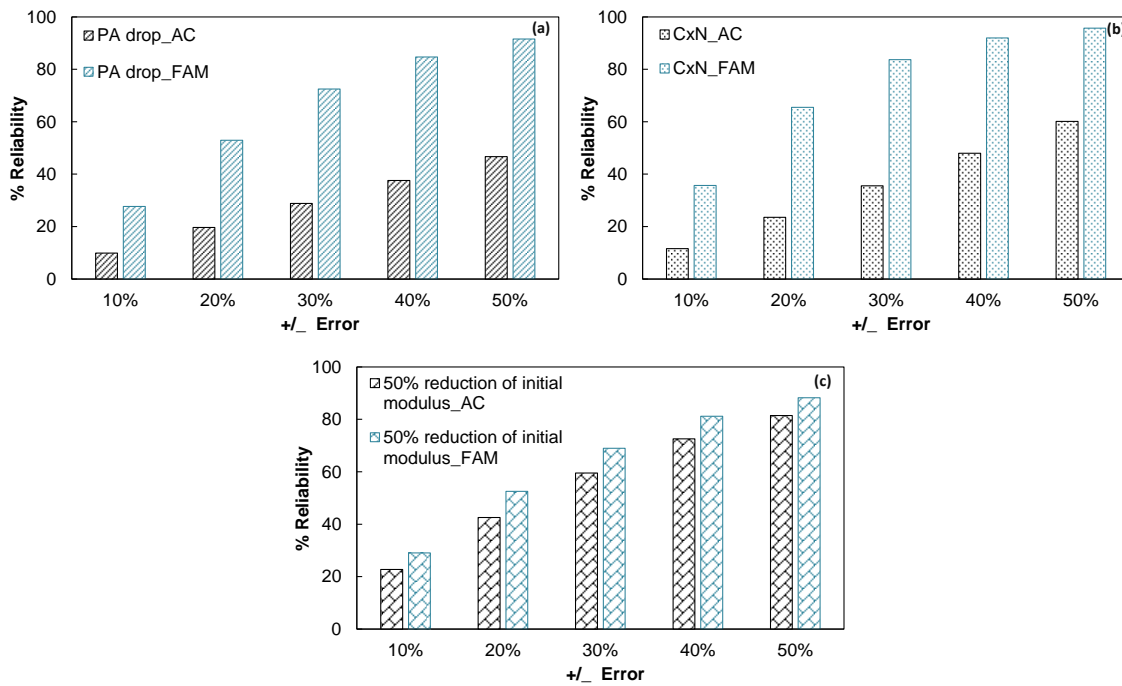
FIGURE 7-8 Comparison of Reliability of Fatigue Life Predictions Between AC and FAM using G^R Failure Model Criteria for (a) *PA* drop (b) *C* x *N* and (c) 50% Reduction of Initial Modulus.

7.5   Hypothesis Testing: Improvement in Reliability of Fatigue Life Prediction of AC with FAM Phase Testing

For the purpose of reliability study on upscaled AC data FAM experimental data was used to upscale it to AC mix properties. The reliability of fatigue life prediction trends obtained for both upscaled AC and FAM materials were used to test the hypothesis that "*reliability of fatigue modeling approach of AC can be improved with FAM phase experimental support as a surrogate measure*". The details of the Upscaling analysis was given in the sections below.

Damage upscaling analysis was performed using a similar procedure as the one described in Chapter 6 for predicting the damage characteristic curve (C-S curve) of AC using FAM experimental data. In this analysis, instead of using the increasing on specimen strain level, constant on specimen strain level was used to predict the damage characteristic curves for AC using the FAM properties. To check the strain level dependency of the upscaling procedure, analysis was performed at multiple strain levels. The resultant upscaling predictions of AC damage curves are shown in FIGURE 7-9. From the figure, it can be observed that irrespective of strain level used in the upscaling analysis, all the predicted C-S curves are collapsing together for constant damage curve parameters (a, b) of FAM.
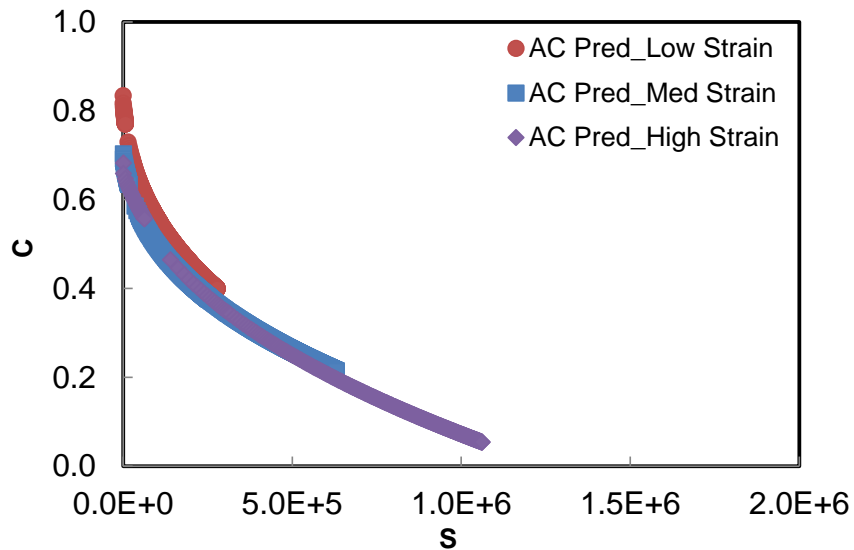
FIGURE 7-9 Predicted AC Damage Curves Developed from FAM Damage Properties.

7.5.1 Upscaling of FAM to AC properties for Fatigue Life Prediction Using C_f as Model Failure Criteria

Input variables required for calculating the reference fatigue life of AC material (using FAM experimental data) were predicted using the procedure outlined below.

1. The average modulus values of AC material at each temperature and frequency were predicted using the IROM Equation (6.3) to (6.5)

2. Modulus and phase angle data obtained from step 1 was used for developing the master curve and to predict the shift factor coefficients, α, and the Prony terms.

3. The average damage characteristic curve parameters (a, b) of FAM were used to develop damage curves of AC using the procedure detailed in Chapter 6 of the damage upscaling analysis.

4. Pseudo stiffness value at failure was considered same as the value observed from the actual AC experimental data. An accurate procedure to predict this input variable from the FAM experimental data was not developed as a part of this research study. However, from experimental data it was observed that C_f at failure of AC is 60 % more than the value that was observed for FAM.

5. The input variables obtained from steps 1-4 were used for calculating the reference fatigue life prediction for AC material at different strain levels. Percentage errors in the reliability analysis were calculated with respect to reference fatigue life.

The deterministic fatigue life of AC material predicted using the Equation(4.1) with experimental data and upscaling data and is shown in FIGURE 7-10. From the figure, it can be observed that the percentage error between experimental and predicted fatigue life of AC material is 5%. It is showing very good prediction with the FAM experimental data.

145

In general the variation of the fatigue life from one replicate to other also more than what is observed here from the predicted data. However one limitation of this study is not having a definitive procedure on the prediction of AC material C_f.
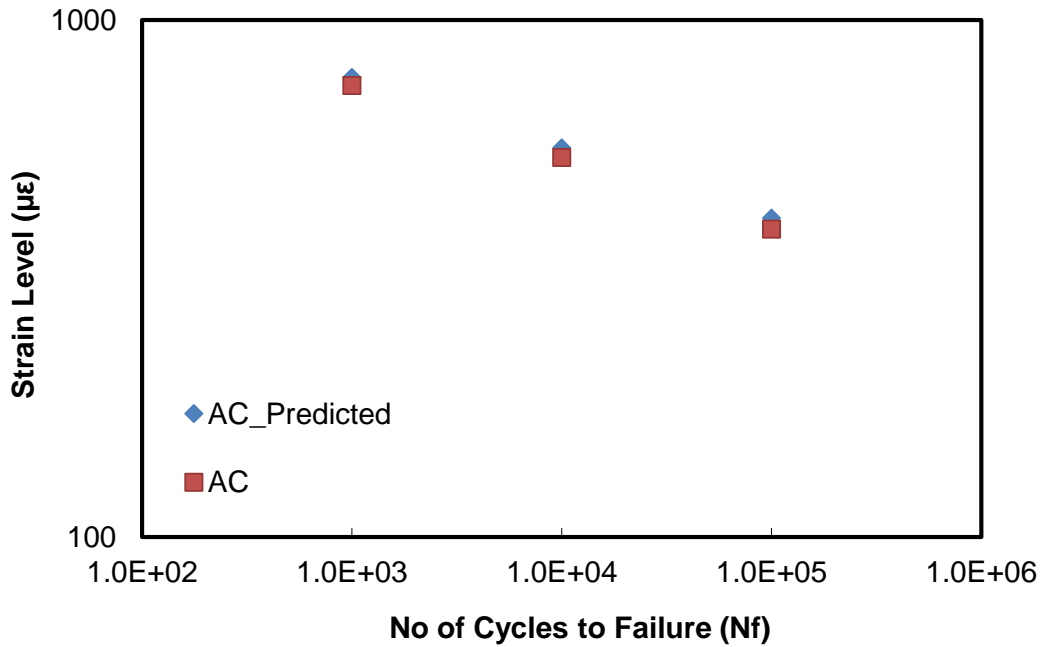
FIGURE 7-10 Fatigue Life Plot for Experimental And Predicted AC

7.5.2   *Reliability Analysis of Upscaling Prediction*

Variation of input variables for the reliability analysis was obtained from FAM replicate experimental data using the upscaling procedure detailed in section 7.4.1. The variation thus obtained was used to generate the probabilistic distributions of input variables for Monte Carlo simulation. One deviation was that the probabilistic distribution for input variable C_f was developed using average C_f value from the AC experimental data and variation observed in the FAM experimental data. The parameters variations were provided as input to the reliability framework described in Chapter 4 to predict the reliability of

fatigue life predictions for the upscaled AC data. FIGURE 7-11 presents the fatigue life reliability values at 10,000 cycles for the upscaled AC data (AC_predicted), together with reliability measurements for AC and FAM experimental data. From the figure, it can be observed that the fatigue life predicted using the AC experimental data is showing least reliability followed by upscaled AC data, and FAM experimental data. Though the upscaled AC reliability results are not as good as the FAM data they definitely shows an improvement over the reliability obtained from experimental AC data. A possible reason for lesser reliability with upscaled data in comparison to FAM experimental data could be due to the numerical error in the starting stage (transient stage) of damage calculation from one replicate to other. This error might be getting manifested as more variation to the fit parameters and eventually impacting the reliability prediction calculation. Irrespective of the observed discrepancies, upscaled AC data is showing more reliable fatigue prediction than the experimental AC data. With the help of upscaling reliability prediction the postulated hypothesis "*reliability of fatigue modeling approach of AC can be improved with FAM phase experimental support*" was vetted using a comparative assessment between the reliability prediction of FAM, upscaled AC and AC experimental data.
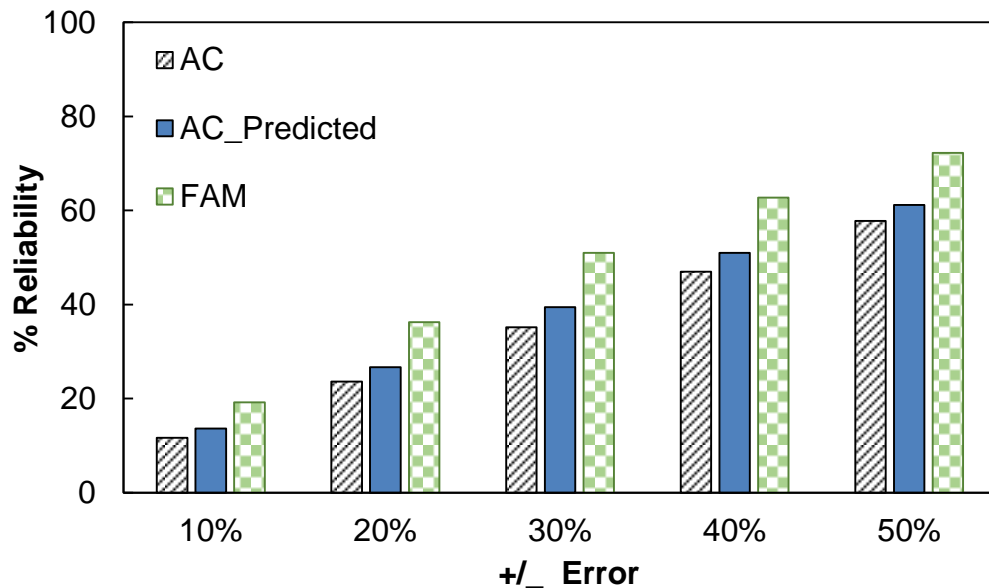
FIGURE 7-11 Comparison of Reliability of Fatigue Life Predictions from AC
Experimental Data, Predicted AC Data and FAM Experimental Data

7.6   Summary and Conclusions

Data obtained from FAM experiments was used to develop reliability analysis for fatigue

life prediction using S-VECD model formulations. The newly established protocols

facilitated the testing of FAM as well as AC materials in similar loading conditions. Fatigue

life predictions were performed using S-VECD model formulations. Comparison of

reliability of fatigue life prediction was made between AC, predicted AC and FAM

experimental data. Using the comparative assessment, the hypothesis "*reliability of fatigue*

modeling approach of AC can be improved with FAM phase experimental support as a

surrogate measure" was tested. Key findings from this study are:

- FAM phase experimental data showed more reliable fatigue life predictions using the C x N experimental failure criteria for C_f model formulations whereas for the G^R model failure criteria 50% reduction in modulus approach showed higher reliability. This trend was observed to be in correlation with the variation observed in the input parameters of the respective models.

- In was found that the G^R approach is showing higher prediction reliability than the C_f approach with FAM phase experimental data. This trend was observed to be the opposite of what was observed with AC experimental data.

- Upscaling analysis was performed with the FAM experimental data to predict the input variation and then to predict the reliability of predicted AC fatigue life.

- The established hypothesis (*reliability of fatigue modeling approach of AC can be improved with FAM phase experimental support as a surrogate measure*) was vetted using a comparative assessment between the reliability prediction of FAM predicted AC and AC. From this study it was observed that predicted AC with the help of FAM phase experimental support showed greater reliability than AC data in predicting the fatigue life of a material.

CHAPTER 8 PARAMETRIC SENSITIVE STUDY OF S-VECD MODEL FOR RELIABILITY OF FATIGUE LIFE PREDICTION

8.1 Introduction

Any mathematical model that involves experimental/statistical data as an input inherently involves uncertainty. The parametric sensitivity study is a common approach used in the risk assessment analysis to predict the impact of uncertainty associated with input data. Simulation of most of the mathematical models involves uncertainties at various scales. Sensitivity analysis of these models is often conducted to predict the error associated with the uncertainty of specific input variables. Though many of the input variables in the models are associated with the uncertainty, the impact of these parameters on the output might not be the same. When the variation of all input variables is used together in simulation, the error associated with the output variable is oftentimes masked. To prevent this masking effect, necessary measures should be taken while carrying out this type of analysis. One such measure is to generate random numbers based on the probabilistic distribution of input variables. As mentioned in Chapter 7 (section 7.3.6), parametric sensitivity analysis is necessary to comprehend the impact of uncertainty (or variation) in input on fatigue life prediction using the S-VECD model. Terms uncertainty and variation are used interchangeably in this study.

The parametric sensitivity study not only assesses the impact of uncertainty of input variables on the model output, but also serves as a guide for practitioners regarding which input variable(s) of a material should be measured (for example, mechanical properties) and which variables can be reasonably assumed or predicted in light of time and resource

constraints. This chapter presents the assessment of parametric sensitivity of input variables in predicting the reliability of fatigue life for both C_f and G^R model failure criteria. Monte Carlo simulation method was used to conduct parametric sensitivity assessment.

8.2   Parametric Sensitivity Study Methodology

Parametric sensitivity analysis was performed on input variables of the S-VECD model with an intent to analyze the reliability of fatigue life predictions using C_f and G^R model failure criteria. The input parameters considered for the parametric sensitivity study were $|E^*|$, damage characteristic equation (C vs S) fit, C_f, and G^R. The methodology followed in the parametric sensitivity study of $|E^*|$ variable is described below. The same methodology is adopted for the sensitivity analysis of all other selected input variables as well.

1. Mean of the $|E^*|$ parameter at the test temperature and frequency was obtained from the experimental data. This analysis was conducted for a given parameter variation of 1, 2, 5, 10, and 20%. From the experimental data, it was observed that most of the input parameters vary within the selected range of analysis.

2. Standard deviation (*Stdev*) of the analysis parameter ($|E^*|$) was calculated using the Equation (8.1) at a given variation.

$$Variation\ (Uncertainity) = \frac{Stdev(x_1, x_2, \dots x_n)}{Mean(x_1, x_2, \dots x_n)} \tag{8.1}$$

3. Using the mean and standard deviation as point estimator's probabilistic distribution was developed at a given variation level for the analysis parameter.

4. Monte Carlo simulation approach was used to predict the reliability of fatigue life prediction for a given uncertainty level of the $|E^*|$ variable. All other input variables were kept constant in each simulation step.

5. Average values of all the input variables were used to predict the deterministic (or reference) fatigue life. This reference fatigue life was used to calculate the percentage error of the prediction using Equation (4.5).

6. Steps 2-5 were repeated to predict the reliability of fatigue life at different variations of the input parameter ($|E^*|$).

8.3 Parametric Sensitivity Study on Reliability of Fatigue Life Prediction with C_f as a Model Failure Criteria

Parametric sensitivity analysis was performed on S-VECD model for the reliability of fatigue life prediction using C_f as model failure criteria. The parameters considered in the S-VECD model formulation for the sensitivity study were $|E^*|$, damage characteristic equation (C vs S), and C_f. Parametric sensitivity procedure described in previous section was used to predict the reliability of fatigue life prediction at a given variations of selected input variables in this model formulation. Details of the sensitivity studies conducted on each of the input variables of fatigue life prediction using the S-VECD model are presented in the following sections.

8.3.1 Sensitivity study on |E*| parameter for fatigue life prediction with C_f as model failure criteria

Sensitivity study on $|E^*|$ parameter was performed with C_f as the model failure criteria in the S-VECD model. Average values of all the input variables were used to predict the

deterministic (or reference) fatigue life. Sensitivity analysis was performed at several uncertainty levels (1-20% variation from the mean) of $|E^*|$ parameter using Monte Carlo simulation. Since the parametric sensitivity study was performed to understand the impact of uncertainty in a specific variable, all other input parameters in the S-VECD model formulations were kept constant. For a given uncertainty range of the $|E^*|$ parameter, the percentage error in fatigue life prediction from the reference was calculated. Results of the analysis are shown in the FIGURE 8-1.

From the figure, it can be observed that the uncertainty in $|E^*|$ parameter had a substantial impact on the reliability of fatigue life prediction. If the variation of $|E^*|$ parameter is within 10%, then the reliability of fatigue life prediction to be within ± 20% error is 22%. With decrease in the range of error prediction, the reliability of fatigue life prediction decreases drastically. This indicates that reliability of fatigue life prediction is very sensitive to variation in the $|E^*|$ parameter.

FIGURE 8-1 Sensitivity of $|E^*|$ Parameter on The Reliability of Fatigue Life Prediction Using The C_f As Model Failure Criteria.

8.3.2 *Sensitivity study on damage characteristic curve for fatigue life prediction with*

$\mathbf{C_f}$ *as model failure criteria*

Sensitivity analysis of damage characteristic equation slope (C vs S) on prediction reliability of fatigue life was challenging, as the C vs S curve fit coefficients (C_{11}, C_{12}) that serve as input to the model formulations are correlated. It was not practically feasible to incorporate simultaneous variation in both the parameters (C_{11}, C_{12}) in Monte Carlo simulation. In addition, it is necessary that the damage curve developed with the variation of C_{11}, C_{12} parameters should be within the range of given uncertainty of damage characteristic curve. To overcome these issues parameter C_{11} was kept constant and the variation of the slope parameter C_{12} was predicted by fitting the C vs S characteristic equation at different locations of the damage. For example, for 20% variation in the C vs S curve from the fitted data, the variation of C values were measured at different stages from the final damage parameter (S_f). The stages considered for measuring the variation of the parameter C were S_f, 3/4 S_f, 1/2 S_f, 1/4 S_f, and 1/8 S_f. The percentage variation in C value was measured with respect to the average fitted C value at different stages of the damage for a given uncertainty range. The variation in C value is presented in TABLE 8-1. The C vs S values obtained from the uncertainty analysis were fit using Equation (6.1). The fitted curves are shown in FIGURE 8-2. The fitted range for parameter b obtained for a given uncertainty of 20% was used in the Monte Carlo simulation to predict fatigue life.

TABLE 8-1 FAM_1 Percentage Variation of C vs S Curve at Different Stage of Damage for a Given Uncertainty

+/- Range	C (1%)	C (2%)	C (5%)	C (10%)	C (20%)
1/8Sf	0.2	0.9	2.3	2.0	4.0
1/4Sf	0.4	1.2	3.0	4.0	7.9
1/2Sf	0.8	1.6	4.1	7.6	15.2
3/4Sf	1.3	2.2	5.5	13.1	26.3
Sf	2.4	3.2	8.1	23.6	47.3
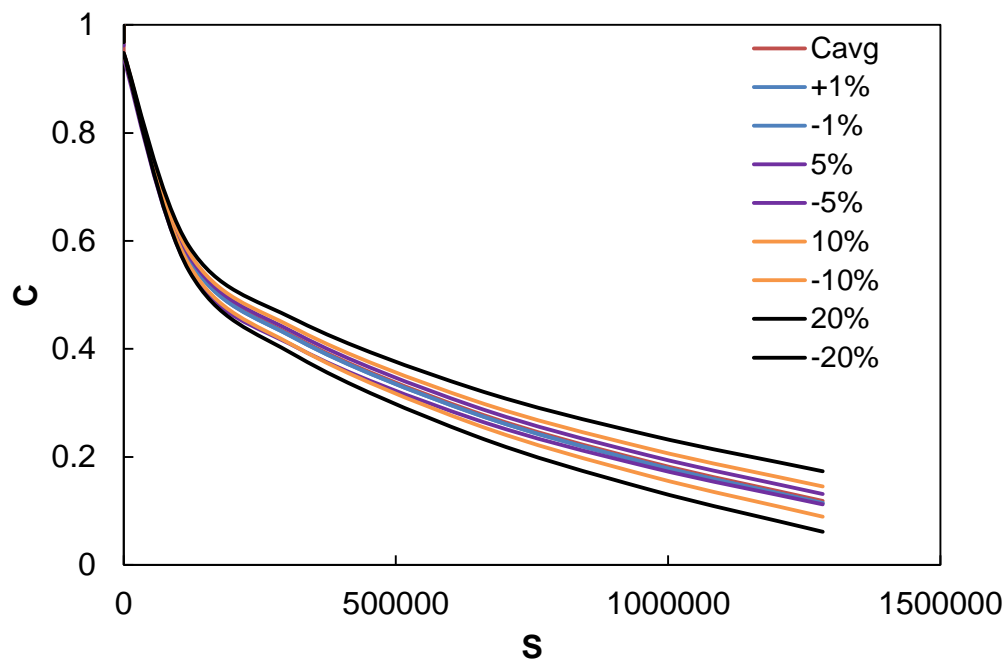
FIGURE 8-2 Variation of Damage Characteristic Curves Fit for A Given Variation In the C_f

To asses the impact of variation in the fit of damage characteristic eqaution on the relibility of fatigue life predcition, Monte Carlo simulation was performed for a given

155

uncertainty of the slope of fitted equation paramer C_{12}. The reliability of fatigue life predcition for a given variation at target range of percentage error is shown in FIGURE 8-3. If the observed variation in damage characteristic curve fit is within 10%, then the reliability of fatigue life prection to be within ±20% of error (to the reference fatigue life) is 55%. It can also be observed from the figure that unlike for the variation in $|E^*|$, the decrease in reliability of fatigue life prediction is rather gradual in this case.
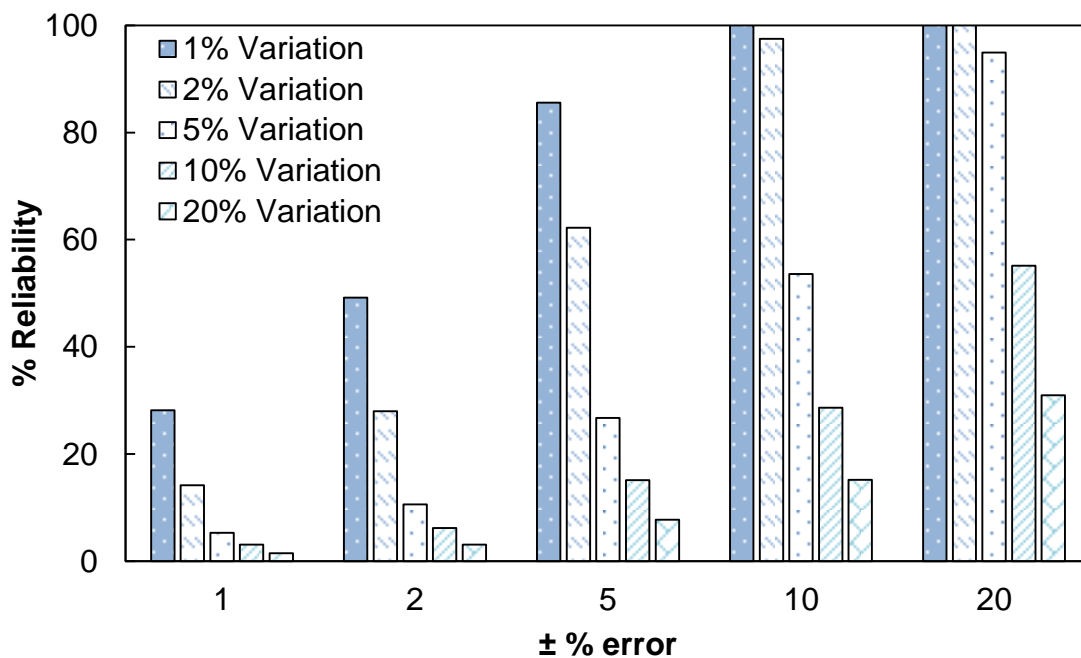
FIGURE 8-3 Sensitivity of Damage Characteristic Curve Fit on The Reliability of Fatigue Life Prediction Using The C_f as Model Failure Criteria.

8.3.3 *Sensitivity study on C_f parameter for fatigue life prediction with C_f as model failure criteria*

Pseudo stiffness at failure (C_f) is also an important parameter which influences the fatigue life prediction of a material (when C_f is used as the model failure criteria to identify the failure point in the S-VECD model). To assess the impact of this parameter on reliability

of fatigue life prediction, Monte Carlo simulation was performed for a given variation of the C at failure (C_f). The reliability of fatigue life prediction for a given uncertainty of C_f parameter at different percentage errors is shown in FIGURE 8-4. From the figure it can be observed that the reliability to predict fatigue life within 10% error for a given 20% variation of C_f value is 74%.
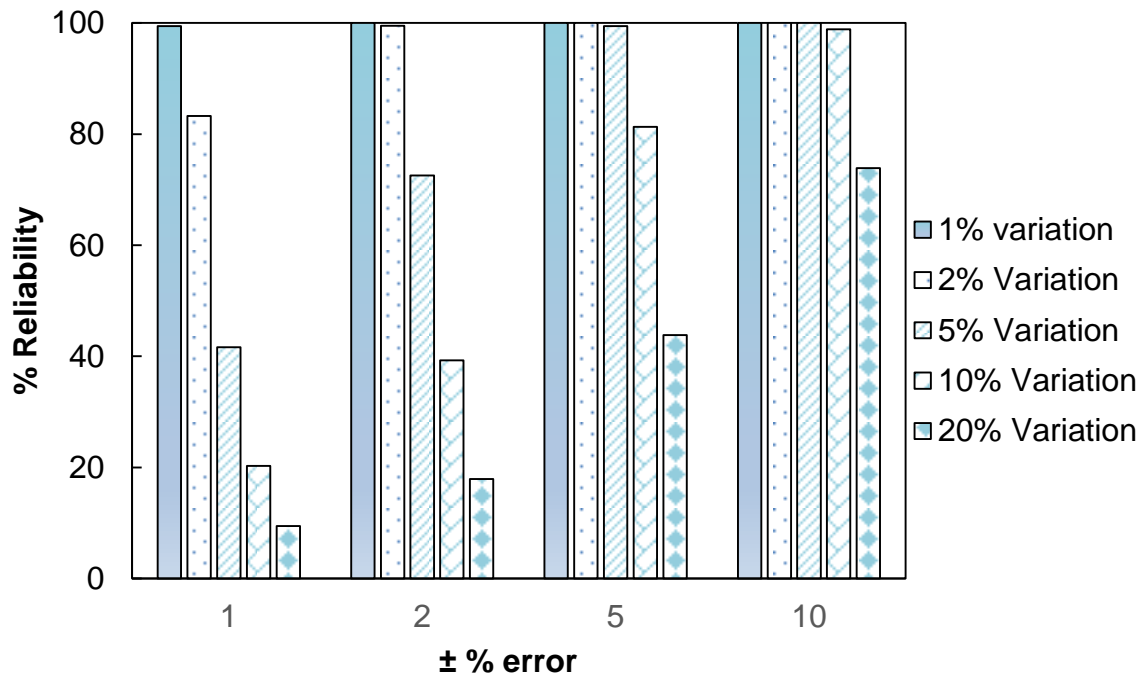
FIGURE 8-4 Sensitivity of C_f Parameter on The Reliability of Fatigue Life Prediction Using The C_f as Model Failure Criteria.

8.3.4 *Parametric sensitivity comparison on the reliability of fatigue life prediction using the C_f as model failure criteria*

Sensitivity analysis was performed to assess the impact of uncertainty in input parameters on the reliability of fatigue life prediction using the S-VECD model formulation. Comparison of fatigue prediction reliability measurements for 10% variation of each of the

input variables is presented in FIGURE 8-5. From the figure, it can be observed that $|E*|$

parameter has the greatest impact on the reliability of fatigue life prediction followed by C

vs S curve fit and C_f parameters. It should be noted that the assessment is based on the

probabilistic distribution assumptions from the experimental variation observed in this

research effort.
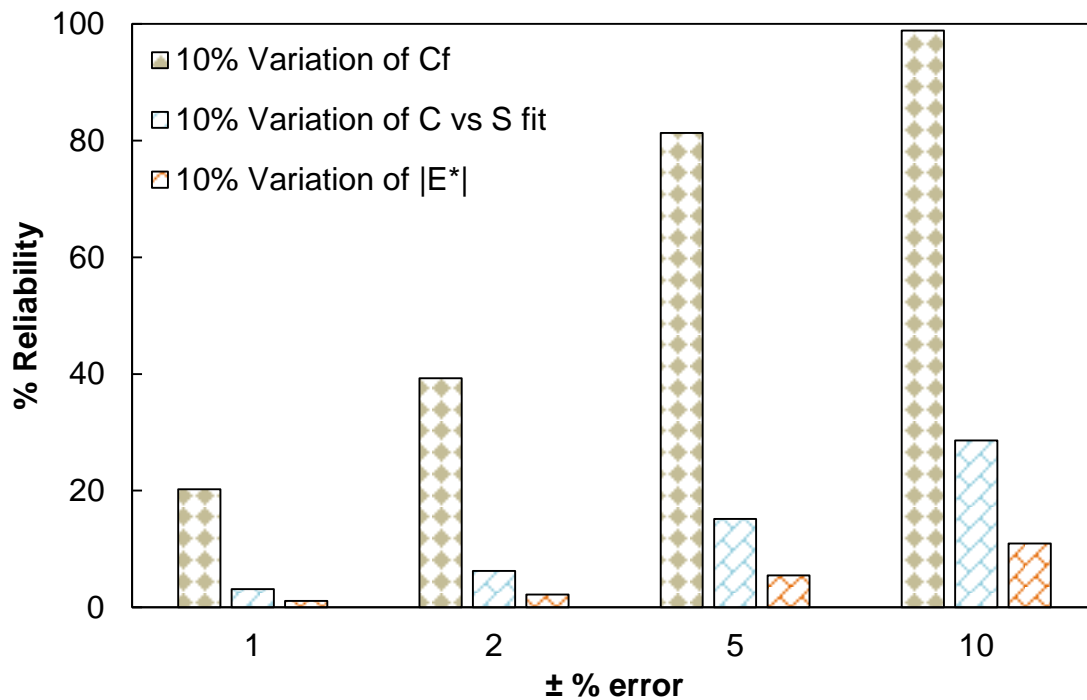
FIGURE 8-5 Parametric Sensitivity Comparison on The Reliability of Fatigue Life
Prediction Using The C_f as Model Failure Criteria.

8.4 Parametric Sensitivity Study on Reliability of Fatigue Life Prediction with G^R as Model Failure Criteria

Parametric sensitivity study was performed on S-VECD model for assessing the reliability

of fatigue life prediction using G^R as the model failure criteria. The parameters considered

in the S-VECD model formulation for the sensitivity study were $|E*|$, damage characteristic

equation (C vs S) and G^R. The probabilistic distribution of input variables developed in C_f approach were used in this analysis as well, except for the G^R parameter. Similar to C_f approach, Monte Carlo simulation was performed to predict the impact of uncertainty of specific input variables on the reliability of fatigue life prediction. The fatigue life of each simulation for a given set of input parameters was calculated using Equation (4.2). The sensitivity studies conducted on each of the input variables considered for fatigue life prediction reliability using the S-VECD model are described in the following sections.

8.4.1 *Sensitivity study on |E*| parameter for fatigue life prediction with G^R as model failure criteria*

Sensitivity study on $|E*|$ parameter was performed with G^R as the failure criteria in the S-VECD model for predicting the fatigue life. Similar to the C_f approach, average input variables were used to compute reference fatigue life using Equation (4.2). Probabilistic distribution of the $|E*|$ parameter developed in the C_f approach was used for parametric sensitivity analysis using the S-VECD formulations with G^R as the model failure criteria. For a given uncertainty in the $|E*|$ parameter, the reliability at target percentage error in fatigue life prediction was calculated. The reliability values obtained for various percentage errors are presented in FIGURE 8-6. If observed variation of $|E*|$ parameter is within 10%, then the reliability of fatigue life prediction to achieve ± 20% error is found to be 30%.
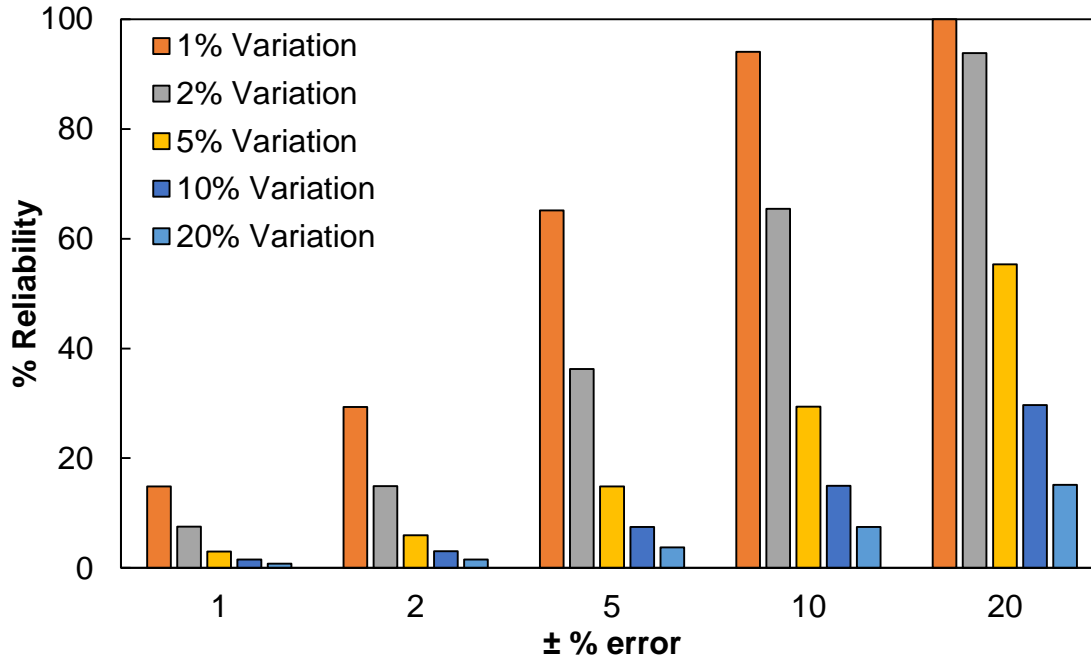
FIGURE 8-6 Sensitivity of |E^*| Parameter on the Reliability of Fatigue Life Prediction Using the G^R as Model Failure Criteria.

8.4.2 Sensitivity study on damage characteristic curve fit for fatigue life prediction with G^R as model failure criteria

To asses the impact of variation in the fit of damage characteristic eqaution on the reliability of fatigue life predcition, a sensitivity study was performed using the Monte Carlo simulation for given uncertainty of the slope of fitted equation paramer C_{12}. The methodology developed for C vs S curve fit in C_f approach was used in this study as well. The reliability of fatigue life predcition for a given variation in the fit of damage characteristic eqaution is shown in FIGURE 8-7. If the observed variation in damage characteristic curve fit is within 10%, then the reliability of fatigue life prediction to be within ±10% of error (to the reference fatigue life) is close to 100%. From this analysis, it

can be stated that variation in the slope of the characteristic equation is less sensitive in fatigue life predcition when G^R approach is used as the model failure criteria.
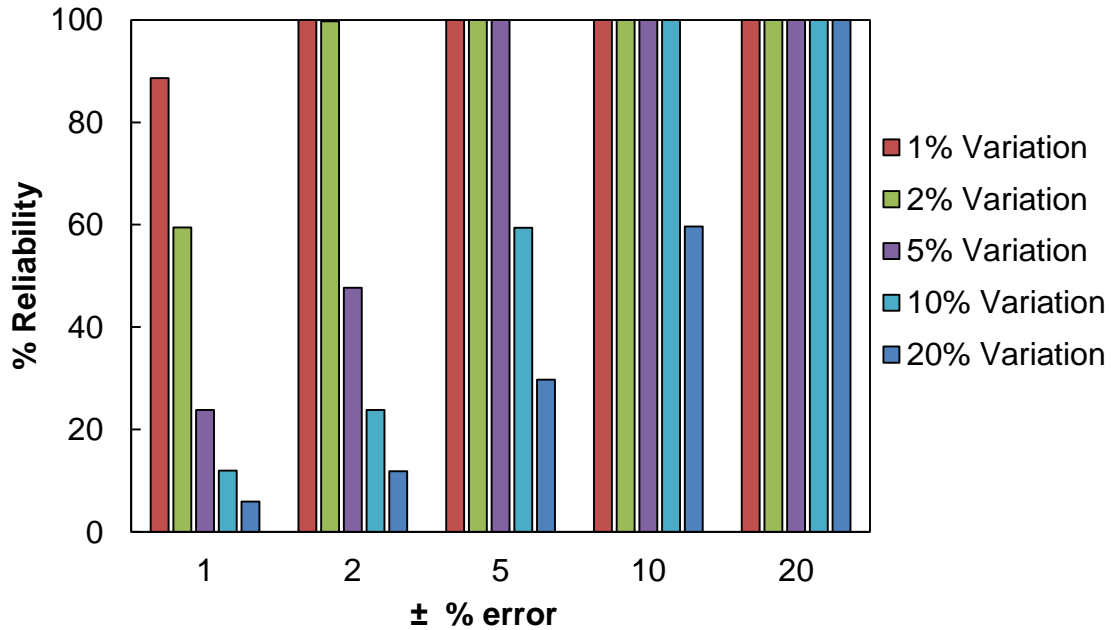
FIGURE 8-7 Sensitivity of Damage Characteristic Curve Fit on The Reliability of Fatigue Life Prediction Using The C_f as Model Failure Criteria

8.4.3 *Sensitivity study on G^R parameter for G^R model failure criteria*

Sensitivity analysis was performed on the variation in the average pseudo strain energy release rate (G^R) for predicting the fatigue life. The relation between G^R and N_f was fit to a power function. The equation coefficients (a, b) goes as some of the input parameters into the S-VECD model formulations for predicting the fatigue life. To avoid any errors associated with the correlation of G_R vs N_f equation coefficients (a, b), the slope of G_R vs N_f equation was calculated for a given variation of G^R parameter at low as well as high number of cycles for each simulation step. The variation of slope parameters obtained

161

(outside the simulation step) was used in the Monte Carlo simulation. The reliability of fatigue life prediction for a given uncertainty of G^R parameter are shown in FIGURE 8-8. From the figure, it can be observed that the reliability to predict fatigue life within 10% of reference fatigue life for a 20% variation in G^R is 20%.
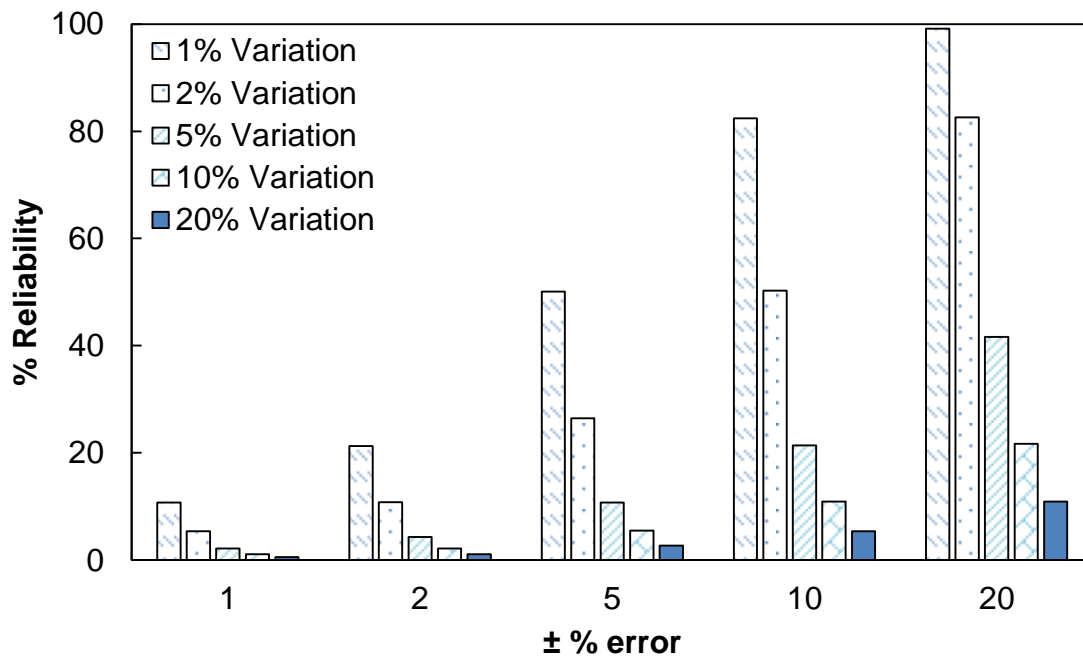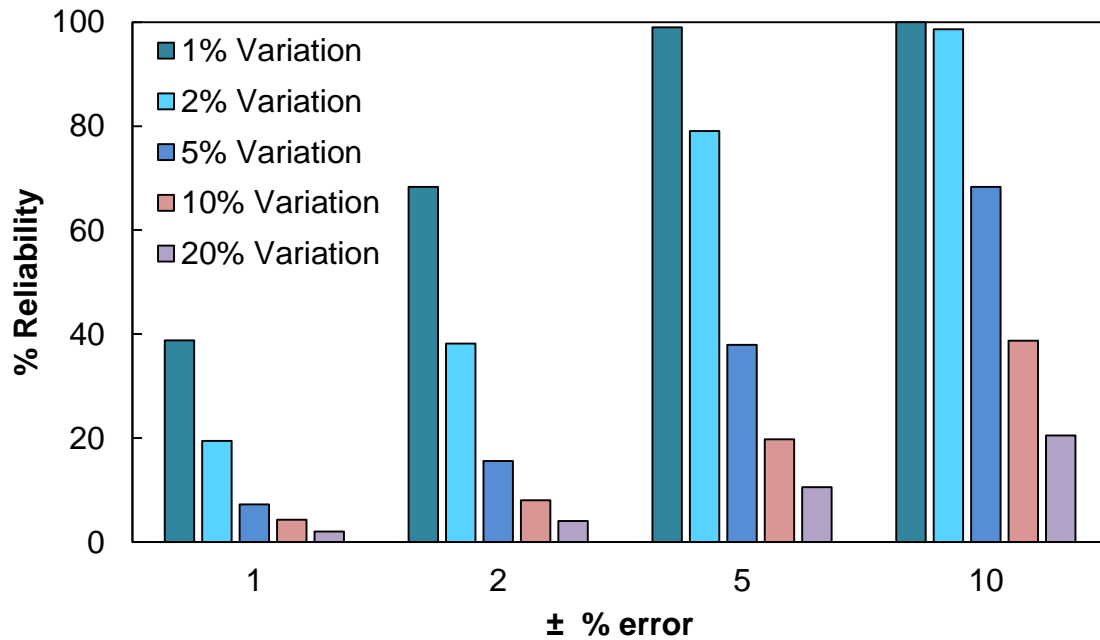

FIGURE 8-8 Sensitivity of G^R Parameter on The Reliability of Fatigue Life Prediction Using the G^R as Model Failure Criteria.

8.4.4 Parametric sensitivity comparison on the reliability of fatigue life prediction using the G^R as model failure criteria

Three input variables were chosen to perform sensitivity analyses and assess the impact of uncertainty in input parameters on the fatigue life prediction using S-VECD model with G^R as the model failure criteria. Similar to the C_f approach, comparative assessment was performed for 10% variation of each input variables. The comparisons are shown in

FIGURE 8-9. From the figure, it can be observed that the $|E^*|$ parameter has greater impact on the reliability of fatigue life prediction compared to the other two parameters.
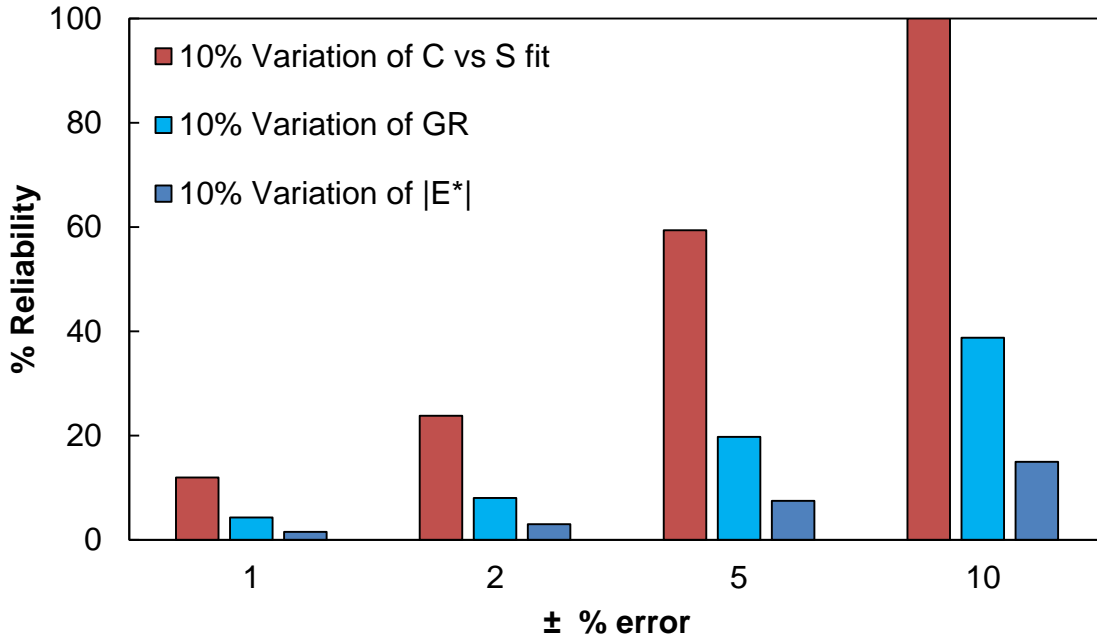
FIGURE 8-9 Parametric Sensitivity Comparison on The Reliability of Fatigue Life Prediction Using the G^R as Model Failure Criteria.

8.5 Comparison of Parametric Sensitivity Study between C_f and G^R Model Failure Criteria Approaches

Parametric sensitivity was performed for both C_f and G^R model failure criteria in the S-VECD model to predict the reliability of fatigue life. Comparative assessment was performed between the input parameters within each model failure criteria to assess the sensitivity of uncertainty in input variables on reliability of fatigue life prediction. To assess the impact of model failure criteria for the variation of the input variables on fatigue life prediction reliability, a comparative assessment was performed between the two model

failure criteria. FIGURE 8-10 shows the comparison between the C_f and G^R model failure criteria prediction results for a 10% variation in each of the input variables. From the figure it can be observed that G^R approach is showing more reliable measurements for the same variation in the input parameters $|E^*|$ and C vs S fit. However this trend is observed to be reverse in the case of C_f and G^R input parameter variation comparison (FIGURE 8-10 (c)). This clearly depicts the sensitivity of G^R slope parameter over C_f parameter on the reliability of fatigue life prediction using the S-VECD model. From these observations it can be inferred that G^R model failure criteria might deliver greater reliability in predicting the fatigue life provided a good G^R characteristic equation fit can be achieved using the experimental data.
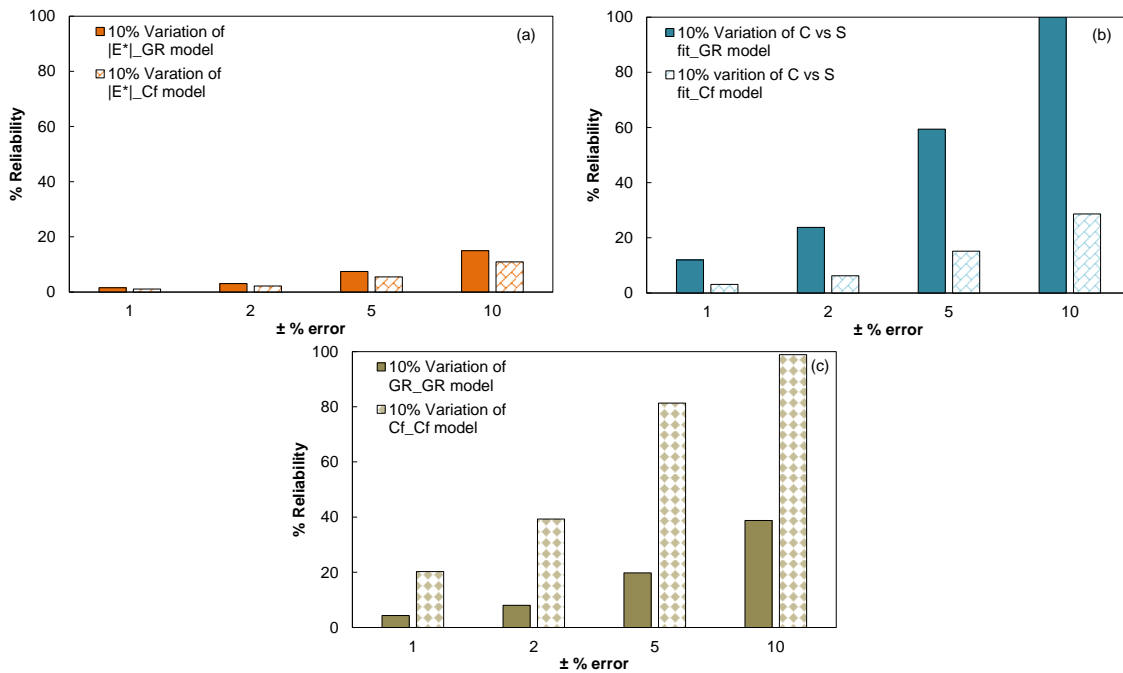
FIGURE 8-10 Parametric Sensitivity Comparison On The Reliability Of Fatigue Life Prediction In Between C_f and G^R as Model Failure Criteria (a) Variation of $|E^*|$ (b) Variation of C vs S fit and (c) Variation of C_f and G^R.

8.6 Summary and Conclusion

Parametric sensitivity assessment was performed to better understand the impact of uncertainty (or variation) in input parameters on the reliability of fatigue life prediction of the S-VECD model. This sensitivity analysis was performed for both C_f and G^R model failure criteria. The reliability predictions were used to perform a comparative assessment for input parameters within each failure criteria as well as between the model failure criteria. Sensitivity analysis was performed between the input parameters within each model failure criteria approach to assess which parameter has a greater impact on the fatigue life prediction. The comparative assessment was performed between the model criteria for a given variation of input parameters to gain insights as to which failure criteria provides more reliable fatigue life prediction. The parametric sensitivity presented in this chapter is a useful tool for qualitative assessment of test data, when limited amount of resources are available. Important observations made from the parametric sensitivity assessment are:

- Among the input parameters considered for analysis, $|E^*|$ parameter is showing the greatest impact on the reliability of fatigue life prediction irrespective of the model failure criteria chosen.

- G^R model failure criteria is showing higher reliability for a given variation of input parameters of $|E^*|$ and C vs S fit than the C_f model failure criteria. But for a given variation of C_f vs G^R slope parameters, the C_f model failure criteria is showing higher reliability in fatigue life prediction.

- The comparative assessment between C_f vs G^R slope parameters shows that G^R slope parameter has greater impact than the C_f parameter on fatigue life prediction. This finding indicates that a good fit of the experimental data to the G^R characteristic equation is very important when of G^R is adopted as the model failure criteria.

One caveat to be noted here is that the conclusions drawn from the parametric sensitivity assessment are based on the probabilistic distributions assumed for the input parameters from the observed variation of the current research effort experimental data. More experimental studies of this nature are required to corroborate the findings from this research effort.

CHAPTER 9 SUMMARY, CONCLUSIONS AND FUTURE SCOPE OF WORK

9.1 Summary and Conclusions

Since its inception, there has been considerable improvement in the characterization of AC materials for various traffic and climatic conditions. However, due to the complex nature of AC, most of the studies were based on the experimental and/or anecdotal observations. The scope for improvement was limited owing to the lack of understanding of AC material at its fundamental level. Despite this historical limitation there have been considerable advances in mechanical models used for AC mixtures over the last 5-10 years. Most of these models are purported to deliver better performance predictions of AC mixtures than their earlier, simpler counterparts. However, they still lack in adequately addressing the changes in the composition of various materials in AC. In addition, these methods involve experimental variation at different levels, which induces additional sources of uncertainty. An important component that needs attention in the evaluation and further improvement of these models is the assessment of their reliability. To address these issues, this dissertation research focuses on development of a reliability framework for the fatigue life prediction of AC materials and improvements of fatigue life reliability prediction using FAM phase experimental data. Summary and conclusions drawn from this research effort are summarized below.

9.1.1 *Reliability of fatigue life prediction*

- A reliability frame work was developed using the Monte Carlo simulation for fatigue life prediction of AC materials using the S-VECD modeling approach.

- Fatigue life prediction reliability analysis was performed for a combination of three distinct experimental failure identification approaches and two model failure criteria identification methods for both AC and FAM materials.

- For the AC mix experimental data, fatigue life prediction using the C_f model failure criterion was observed to be more reliable than the G^R based model failure criterion approach irrespective of the experimental failure criterion considered.

- Fatigue life prediction analysis performed using the FAM experimental data concluded G^R approach as more reliable than the C_f approach. The likely reason for the reverse trend observed in FAM results compared to the AC results could be due to higher variation in the fit of G^R for AC experimental data than FAM.

- From the parametric sensitivity study of S-VECD model on fatigue prediction, it was observed that the slope parameter variation, G^R had a greater impact than C_f variation.

- For a given variation in the input variables, the $|E^*|$ parameter was observed to have a greater impact on the fatigue life prediction of AC using the S-VECD model irrespective of the model failure criteria used.

- The reliability trends were in line with the variation observed from all the five different AC mixtures analyzed in this study. This observation corroborates the robustness of the reliability framework developed in this study.

- The fatigue life predictions using the FAM phase experimental data showed more reliable results than AC experimental data.

- From the fatigue life prediction reliability study, it was observed that the error percentage to achieve 50% reliability with AC experimental data was

approximately 50% whereas this error reduces to 30% with FAM based experimental data.

- Fatigue life prediction analysis performed using the FAM phase modulus and damage upscaling to AC was also showing more reliable fatigue life prediction than the fatigue life predicted using the AC experimental data.

- All of the reliability prediction results and conclusions drawn from the parametric sensitivity study were based on the probabilistic distributions assumed for the input parameters. More experimental data of the replicates would help corroborate the findings from this study.

9.1.2 *FAM testing protocols and upscaling of FAM to AC*

- FAM samples were compacted to a geometry of 150 mm diameter and 100 mm height using a Superpave gyratory compactor to achieve uniform air voids of FAM test samples.

- The final FAM specimens used for testing (geometry of 20 mm diameter and 50 mm height) were cored and cut from the compacted FAM samples.

- FAM testing protocols for modulus and uniaxial fatigue test were developed in similar loading conditions (uniaxial) as AC samples.

- During the testing phase, on specimen strain of FAM samples was measured using two sets of miniature LVDTs (± 0.254 mm span) mounted on the FAM samples 180° apart.

- From experimental studies conducted on FAM material, it was learnt that equipment compliance is a vital issue for FAM testing as well. It produced

169

erroneous results even after correcting for the machine compliance error which was in the range of 10 to 32 %.

- Interpretation of fatigue tests and development of the S-VECD damage curves using actuator corrected strain data were not the same as the ones developed from on specimen data for FAM materials. This finding highlights the importance of measurement of on specimen strain in FAM experiments.

- Comparisons were performed between FAM and AC modulus and damage properties. From the results, it was observed that $|E^*|$ master curves exhibit similar frequency dependence in both FAM and AC materials. With respect to damage characterization, FAM material C-S plots collapsed irrespective of temperature and strain level, similar to the AC C-S plots.

- It was observed that the C-S curves for FAM and corresponding AC mix mostly collapsed together until some point of damage and deviated from that point.

- On specimen FAM strain data was used to upscale the FAM modulus and damage properties to AC. The upscaling of AC modulus and damage characterization from FAM properties using a relatively simple homogenized continuum approach showed promising results.

- The upscaled AC modulus from FAM experimental data exhibited an average variation of 10-20 % from the experimentally measured modulus of AC.

- From the fatigue analysis, it was observed that FAM material can resist much higher strains than the AC for the same fatigue life. The strain ratio of FAM to AC mix during the fatigue loading was found to vary in between 3 to 5.4.

In summary, this research effort contributes to the existing literature in AC studies by developing a generalized reliability framework for the prediction of AC fatigue life. Further this framework uses upscaled AC material properties using the FAM phase experimental data to improve the reliability of fatigue life prediction.

9.2 Future Scope of Work

Conclusions drawn from this research effort recommend the continuation of the work in the following areas.

- Development of permanent deformation testing protocols for FAM materials in similar loading condition as AC material.

- Development of a more accurate approach (either an experimental or imaging technique) is to predict the amount of air voids present in the FAM material in the overall AC samples.

- Tests should be carried out on different FAM materials and the corresponding AC mix at different gradations using the protocols developed in this study. Such studies would help immensely to postulate more general conclusions with respect to the linkage between FAM and corresponding AC.

- A computational framework coupled with the experimental studies on FAM should be developed to better understand the damage behavior of AC material. Such a framework would be useful to assess the location of higher stress and strain levels which lead to the formation of micro cracks and eventually formation of macro cracks in the FAM phase of AC material. Further research on this modeling approach may also helpful in assessing the stress level that lead to the failure of the

sample whether in the FAM phase or interface between the FAM and aggregate in the overall AC mix.

- FAM material testing should be extended to different modified AC mixtures such as fiber reinforced, rubber modified and warm mix AC mixtures.

- A definitive procedure should be developed for predicting the pseudo stiffness at failure (C_f) with FAM experimental data.

- In this research effort, reliability framework was analyzed using a Macro code written in the Microsoft Excel. A user friendly reliability analysis tool can be developed as an executable file using the Excel code generated for this research effort.

REFERENCES

1. Mangum, M. [2006] Asphalt Paving Sector Presentation. Health Effects of Occupational Exposure to Emissions from Asphalt/ Bitumen Symposium. Dresden, Germany.

2. The Year is 2045 U.S Department of Transportation https://www.transportation.gov/sites/dot.gov/files/docs/TheBluePaper.pdf Accessed July. 19, 2015.

3. American Geosciences Institute. Aggregate and the Environment http://www.americangeosciences.org/sites/default/files/aggregate.pdf Accessed July. 29, 2014.

4. Beyond Traffic Trends and choices 2045 https://www.transportation.gov/sites/dot.gov/files/docs/Draft_Beyond_Traffic_Framework.pdf Accessed December. 27, 2015.

5. FHWA Forecasts of Vehicle Miles Traveled (VMT): May 2015 Office of Highway Policy Information Federal Highway Administration June 5, 2015

6. Hveem, F.N. (1955), "Pavement Deflections and Fatigue Failures," Bulletin 114 HRB, National Research Council, Washington, D.C., pp. 43-87.

7. Monismith, C.L., J.A. Epps, D.A. Kasianchuk, and D.B. McLean (1971), *Asphalt Mixture Behavior in Repeated Flexure*, Reprot TE 70-5, University of California, Berkeley, p.303.

8. Pell, P.S. (1973), Characterization of Fatigue Behavior, Special Report 140: *Structural Design of Asphalt Concrete Pavement Systems to Pavement Fatigue Cracking*, HRB, National Research Council, Washington, D.C.

9. Monismith, C.L., J.A. Epps, and F.N. Finn (1985), Improved Asphalt Mix Design. Proceedings, Association of Asphalt Paving Technologists, Vol. 54, February.

10. Bonnaure, F., Gravois, A., and Udron, J. (1980), A New Method of Predicting the Fatigue Life of Bituminous Mixes. Journal of the Association of Asphalt Paving Technologists, Vol. 49, pp. 499-529.

11. Asphalt Institute. Thickness Design Manual (MS-1), 9th ed. The Asphalt Institute, College Park, MD, 1981.

12. Tayebali, A.A., Deacon, J.A., Coplantz, J.S., Harvey, J.T., and Monismith, C.L., Fatigue Response of Asphalt Aggregate Mixes. SHRP-A-404, Strategic Highway Research Program, National Research Council, Washington, D.C., 1994.

13. NCHRP, Guide for Mechanistic-Empirical Design of New and Rehabilitation Pavement Structures, Transportation Research Board of the National Academics, Washington, D.C., 2004.

14. Van Dijk, W. (1975). "Practical Fatigue Characterization of Bituminous Mixes." Proceedings of the Association of Asphalt Paving Technologists (AAPT), Vol. 44, pp. 38.

15. Rowe, G.M., (1993). "Performance of Asphalt Mixtures in the Trapezoidal Fatigue Test." Proceedings of Associations of Asphalt Paving Technologists, Vol. 62, pp. 344-384.

16. Baburamani, P.S., and Porter, D.W., (1996). "Dissipated Energy Approach to Fatigue Characterisation of Asphalt Mixes." Proceedings of Combined 18th ARRB TR Conference Transit New Zealand Symposium, Part 2, pp. 327-347.

17. Ghuzlan, K., (2001). "Fatigue Damage Analysis in Asphalt Concrete Mixtures Based Upon Dissipated Energy Concepts." Ph.D. Thesis, University of Illinois at Urbana-Champaign, Urbana, IL.

18. Shen, S., and Carpenter, S.H., (2005). "Application of Dissipated Energy Concept in Fatigue Endurance Limit Testing." Journal of Transportation Research Record: Transportation Research Board, No. 1929, pp. 165-173.

19. Daniel, J.S., and Y. R. Kim. Development of a Simplified Fatigue Test and Analysis Procedure Using a Viscoelastic Continuum Damage Model. Journal of the Association of Asphalt Paving Technologists. Vol. 71, 2002, pp. 619-650.

20. Majidzadeh, K., Kaufmann, E.M., and Ramsamooj, D.V., Application of Fracture Mechanics in the Analysis of Pavement Fatigue, Proceedings of Association of Asphalt Pavement Technologists, Vol. 40, 1970, pp. 227-246.

21. Broek, D. *Elementary Engineering Fracture Mechanics*. 4th ed. Netherlands: Springer, Netherlands, 1986.

22. Dugdale, D. S., Yielding in Steel Sheets Containing Slits, Journal of the Mechanics and Physics of Solids, Vol. 8, pp. 100-108, 1960.

23. Barenblatt, G.I., The Mathematical Theory of Equilibrium Cracks in Brittle Fracture, *Advances in Applied Mechanics*, Academic Press, Vol. VII, pp. 55-129, 1962.

24. Uzan, J., and Levenberg, E., Strain Measurements in Asphalt Concrete Specimens towards the Development of a Fracture Model, *International Journal of Pavement Engineering*, Vol. 2, No. 4, pp. 243-258, 2001.

25. Molenaar, A.A.A., *Structural Performance and Design of Flexible Road Constructions and Asphalt Concrete Overlays*, Ph.D. Dissertation, Delft University of Technology, The Netherlands, 1983.

26. Molenaar, A.A.A., Fatigue and Reflection Cracking due to Traffic Loads, Proceedings of the *Association of Asphalt Paving Technologists*, Vol. 53, pp. 440-474, 1984.

27. Majidzadeh, K., Dat, M., and Makdisi-Ilyas, F., Application of Fracture Mechanics for Improved Design of Bituminous Concrete, Vol. 2 *Evaluation of Improved Mixture Formulations, and the Effect of Temperature Conditions on Fatigue Models*, Report No. FHWA-RD-76-92, Final Report, June 1976.

28. Elmitiny, M.R.N., *Material Characterization for Studying Flexible Pavement Behavior in Fatigue and Permanent Deformation*, Ph.D. Dissertation, The Ohio State University, 1980.

29. Jacobs, M.M.J., *Crack Growth in Asphaltic Mixes*, Ph.D. Dissertation, Delft University of Technology, the Netherlands, 1995.

30. Jacobs, M.M.J., Hopman, P.C., and Molenaar, A.A.A., Application of Fracture Mechanics in Principles to Analyze Cracking in Asphalt Concrete, *Journal of the Association of Asphalt Paving Technologists*, Vol. 65, pp 1-39, 1996.

31. Wagnoner, M. P., Buttlar, W. G., & Paulino, G. H. Disk-shaped compact tension test for asphalt concrete fracture. Experimental Mechanics, Vol 45 (3), pp. 270-277, 2005.

32. Huang, B., Shu, X. & Tang, Y., Comparison of semi-circular bending and indirect tensile strength tests for HMA mixtures. Proceedings of the Sessions of the ASCE Geo-Frontiers - Advances in Pavement Engineering, GSP 130, pp. 155-169, 2005.

33. Kim, Y.R. and Wen, H., Fracture Energy from Indirect Tension Testing. *Journal of the Association of Asphalt Paving Technologists, 71*, 2002: 779-793.

34. Roque, R., Zhang, Z. and Sankar, B., Determination of Crack Growth Rate Parameters of Asphalt Mixtures Using the Superpave IDT. *Journal of the Association of Asphalt Paving Technologists*, Vol. 68, pp. 404-433, 1999.

35. Lee, N.K., Morrison, G.R. and Hesp, S.A.M, Low Temperature Fracture Toughness of Polyethylene-Modified Asphalt Binders and Asphalt Concrete Mixes. *Journal of the Association of Asphalt Paving Technologists, 64*, 1995: 534-574

36. Lee, N.K. and Hesp, S.A.M., Low Temperature Fracture Toughness of Polyethylene- Modified Asphalt Binders, Transportation Research Record 1436, pp. 54-59, 1994.

37. Mobasher, B., Mamlouk, M and Lin, H-M. Evaluation of Crack Propagation Properties of Asphalt Mixtures." ASCE Journal of Transportation Engineering, Vol. 123(5) pp. 405-413, 1997.

38. Wagoner, M.P., Buttlar, W., Paulino, G. & Blankenship, P., Development of a Single- Edge Notched Beam Test for Asphalt Concrete Mixtures. *ASTM Journal of Testing and Evaluation*, Vol. 33(6), pp. 1-9, 2005.

39. Krans, R.L., Tolman, F. & Van de Ven, M.F.C., Semi-Circular Bending Test: A Practical Crack Growth Test using Asphalt Concrete Cores. Reflective Cracking in Pavements, RILEM, London, pp. 123-132, 1996.

40. Aragao, Francisco. Computational microstructure modeling of asphalt mixtures subjected to rate-dependent fracture. Civil Engineering. Lincoln, University of Nebraska. PhD dissertation, 2011.

41. Im, Soohyok. Characterization of viscoelastic and fracture properties of asphaltic materials in multiple length scales. Civil Engineering. Lincoln, University of Nebraska. PhD dissertation, 2012..

42. Nsengiyumva, G. Development of Semi-Circular Bending (SCB) Fracture Test for Bituminous Mixtures. Civil Engineering. Lincoln, University of Nebraska. Master's thesis, 2015.

43. Zhou, F., Hu, S., Scullion, T., Chen, D., Qi, X., and Claros, G., Development and Verification of an Overlay Tester Based Fatigue Crack Prediction Approach, Journal of Association of Asphalt Paving Technologist, March 2007, San Antonio, TX.

44. Anderson, T.L. Fracture Mechanics 3rd Edition, Fundamentals and Applications. Boca Raton, FL: Taylor and Francis, 2005.

45. Stempihar, Jeffrey. *Development of the C* Fracture Test for Asphalt Concrete Mixtures*. Arizona State University, 2013.

46. Hiltunen, D.R., and Roque, R., "A Mechanics-Based Prediction Model for Thermal Cracking of Asphaltic Concrete Pavements", *Journal of the Association of Asphalt Paving Technologists*, Vol. 63, 1994, pp. 81-117.

47. Schapery, R.A., "Correspondence Principles and a Generalized J-Integral for Large Deformation and Fracture Analysis of Viscoelastic Media." *International Journal of Fracture*, Vol. 25, 1984, pp. 195-223.

48. Di Benedetto, H., A. Ashayer Soltani, and P. Chaverot. "Fatigue damage for bituminous mixtures: a pertinent approach." *Journal of the Association of Asphalt Paving Technologists*, Vol. 65, 1996.

49. Di Benedetto, H., C. De La Roche, H. Baaj, A. Pronk, and Robert Lundström. "Fatigue of bituminous mixtures." *Materials and structures,* Vol.37 (3), pp. 202-216, 2004.

50. Lemaitre, Jean. *A course on damage mechanics*. Springer Science & Business Media, 2012.

51. Kutay, M. Emin, Nelson Gibson, and Jack Youtcheff. "Conventional and viscoelastic continuum damage (VECD)-based fatigue analysis of polymer modified asphalt pavements (with discussion)." *Journal of the Association of Asphalt Paving Technologists,* Vol.77, PP. 2008.

52. Kim, Y. R., and D. N. Little (1990). One-Dimensional Constitutive Modeling of Asphalt Concrete. *ASCE Journal of Engineering Mechanics*, Vol. 116, No. 4, pp. 751-772.

53. Kim, Y. R., D. N. Little, and R. L. Lytton (2003). Fatigue and Healing Characterization of Asphalt Mixtures. *Journal of Materials in Civil Engineering*, Vol. 15, No. 1, pp. 75-83.

54. Lee, H. J., and Y. R. Kim. A Uniaxial Viscoelastic Constitutive Model for Asphalt Concrete under Cyclic Loading. *ASCE Journal of Engineering Mechanics*, Vol. 124, No. 1, 1998a, pp. 32-40.

55. Castelo Branco, V.T.F., E. Masad, A. Bhasin, and D.N. Little (2008). ―Fatigue Analysis of Asphalt Mixtures Independent of Mode of Loading,‖ *Transportation Research Record*, 2057, National Research Council, Washington, D.C., 149-156.

56. Chehab, G. R., Y. R. Kim., R. A. Schapery., M. Witczack., and R. Bonaquist. Characterization of Asphalt Concrete in Uniaxial Tension Using a Viscoelastoplastic Model. *Journal of the Association of Asphalt Paving Technology*, Vol. 72, 2003, pp. 315-355.

57. Underwood, B. S., Y. R. Kim., and M. N. Guddati. Characterization and Performance Prediction of ALF Mixtures Using a Viscoelastoplastic Continuum Damage Model. *Journal of the Association of Asphalt Paving Technologists*, Vol. 75, 2006, pp. 577-636.

58. Shakiba, M., R. K. Abu Al-Rub, M. K. Darabi, T. You, E. A. Masad, and D. N. Little. Continuum Coupled Moisture–Mechanical Damage Model for Asphalt Concrete. In Transportation Research Record: *Journal of the Transportation Research Board,* No. 2372, Washington, D.C., 2013, pp. 72–82

59. Darabi, M. K., R. K. Abu Al-Rub, E. A. Masad, C. W. Huang, and D. N. Little. A Thermoviscoelastic Viscoplastic-Viscodamage Constitutive Model for Asphaltic Materials. *International Journal of Solids and Structures*, Vol. 48, 2011, pp. 191–207

60. Aurangzeb, Q., Al-Qadi, I. L., & Ozer, H. (2012). Effect of testing method on the fatigue behavior of asphalt mixtures with high reclaimed asphalt pavement (RAP) content. In *5th Euroasphalt and Eurobitume Congress, Istanbul, Turkey*.

61. Norouzi, A., M. Sabouri, and Y. R. Kim (2014). Evaluation of the Fatigue Performance of High RAP Asphalt Mixtures. Asphalt Pavements, CRC Press, *Journal of Taylor and Francis Group*, pp. 1069-1077.

62. Lancaster, I.M., and H.A.Khalid. Viscoelastic continuum damage analysis of polymer modified asphalt in the cyclic semicircular bending test. 6th International Conference on Bituminous Mixtures and Pavements", June 2015, Liverpool, UK.

63. Underwood, B. S., Y. R. Kim, and M. N. Guddati. Improved Calculation Method of Damage Parameter in Viscoelastic Continuum Damage Model. *International Journal of Pavement Engineering*, Vol. 11, No. 6, 2010, pp. 459-476.

64. Underwood, B.S., Y. R. Kim, S. Savadatti, S. Thirunavukkarasu, and M. N. Guddati (2009). ―Response and Fatigue Performance Modeling of ALF Pavements Using 3-D Finite Element Analysis and a Simplified Viscoelastic Continuum Damage Model,‖ *Journal of the Association of Asphalt Paving Technologists*, 78, 829-868.

65. Underwood, B.S., M. Eslaminia, S. Thirunavukkarasu, M.N. Guddati, and Y.R. Kim (2010a). ―Asphalt Concrete Pavement Response and Fatigue Performance Modeling using Advanced Techniques,‖ Proceedings of the *11th International Conference on Asphalt Pavements*, ISAP, Nagoya, Japan, August.

66. Reese, R. Properties of Aged Asphalt Binder Related to Asphalt Concrete Fatigue Life. *Journal of the Association of Asphalt Paving Technologists*, Vol. 66, 1997, pp. 604-632.

67. Kim, Y. R., D. N. Little., and R. L. Lytton. Fatigue and Healing Characterization of Asphalt Mixtures. *Journal of Materials in Civil Engineering*, Vol. *15*(1), 2003, pp. 75-83.

68. Pronk, A. C., and P. C. Hopman. Energy Dissipation: The Leading Factor of Fatigue. In *Highway Research: Sharing the Benefits: Proceedings of a Conference of the United States Strategic Highway Research Program*, London, 1990, pp. 255-267.

69. Rowe, G. M., and M. G. Bouldin. Improved Techniques to Evaluate the Fatigue Resistance of Asphalt Mixtures. Proceeding of 2nd Euroasphalt & Eurobitumen Congress, Barcelona, Spain, 2000, pp. 754–763.

70. Safaei, F., J. Lee, L. A. H. Nascimento., C. Hintz., and Y. R. Kim. Implications of Warm-Mix Asphalt on Long Term Oxidative Aging and Fatigue Performance of Asphalt Binders and Mixtures. *Road Materials and Pavement Design,* Vol. 15(sup1), 2014, pp. 45-61.

71. Hou, T., B. S. Underwood., and Y. R. Kim. Fatigue Performance Prediction of North Carolina Mixtures Using the Simplified Viscoelastic Continuum Damage Model. *Journal of the Association of Asphalt Paving Technologists*, Vol. 79, 2010, pp. 35-80.

72. Sabouri, M., and Y. Kim. Development of A Failure Criteria for Asphalt Mixtures Under Different Modes of Fatigue Loading. In *Transportation Research Record: Journal of the Transportation Research Board, No. 2447*, Transportation Research Board of the National Academies, Washington, D.C., 2014, pp. 117-125.

73. Zhang, J., M. Sabouri., Y. R. Kim., and M. N. Guddati (2013). Development of a Failure Criteria for Asphalt Mixtures under Fatigue Loading. *Road Materials and Pavement Design*, Vol. 14, Supplement 2, 2013, pp. 1-15.

74. Shen, S., and S.H. Carpenter. Application of Dissipated Energy Concept in Fatigue Endurance Limit Testing. In *Transportation Research Record: Journal of Transportation Research Board, No. 1929,* Transportation Research Board of the National Academies, Washington, D.C., 2005, pp. 165-173.

75. Van Dijk, W., H. Moreaud, A. Quedeville, and P. Uge (1972). The Fatigue of Bitumen and Bituminous Mixes. Proceedings, 3rd International Conference on the Structural Design of Asphalt Pavements, Vol. 1, 1972, London, pp. 354-366.

76. Kim, H. B., and S. H. Lee. Reliability-Based Design Model Applied to Mechanistic Empirical Pavement Design. *KSCE Journal of Civil Engineering,* Vol. 6, No. 3, 2002, pp. 263–272.

77. Masad, E., V. T. F. Castelo Branco, D. N. Little, and R. L. Lytton (2008). A Unified Method for Analysis of Controlled-Strain and Controlled-Stress Fatigue Testing. *International Journal of Pavement Engineering*, Vol. 9, No. 4, pp. 233-246.

78. Applied Research Associates. 2002 Design Guide: Design of New and Rehabilitated Pavement Structures. NCHRP 1-37A Project, National Cooperative Highway Research Program. National Research Council. Washington, D.C., 2004.

79. Xie, J, and Michael P. "Reliability prediction modeling of semiconductor light emitting device." *Device and Materials Reliability, IEEE Transactions on* 3.4, pp. 218-222, 2003.

80. Goel, A., & Graves, R. J. Electronic system reliability: collating prediction models. *Device and Materials Reliability, IEEE Transactions on*, Vol *6*(2), pp. 258-265, 2006.

81. Pecht, M., Dasgupta, A., Barker, D., & Leonard, C. T. The reliability physics approach to failure prediction modelling. *Quality and Reliability Engineering International*, Vol *6*(4), pp. 267-273, 1990.

82. Leahy, R. B., G. A. Huber., J. S. Moulthrop., and T. Ferragut. NCHRP Web Document 186: *The Superpave Mix Design System: Anatomy of A Research Program*. Transportation Research Board of the National Academies. Washington, D.C., 2011.

83. American Association of State Highway, Transportation Officials, Arizona State University, Fugro Consultants (Firm). NCHRP Web Document 704: *A Performance-related Specification for Hot-mixed Asphalt*. Transportation Research Board of the National Academies. Washington, D.C., 2011.

84. American Association of State Highway, Transportation Officials. AASHTO Guide: *Design of Pavement Structures 1986.* Washington, D.C., 1986.

85. Marasteanu, M., A. Zofka., M. Turos., X. Li., R.Velasquez., W.G. Buttlar., G.Paulino., A.Braham., E. Dave., J. Ojo., H. Bahia., C. Williams., J. Bausano., A. Gallistel., and J. McGraw. *Investigation of Low Temperature Cracking In Asphalt Pavements National Pooled Fund Study 776*. Rep. No. MN/RC 2007-43, Dept. of Civil Engineering, Univ. of Minnesota, Minneapolis, 2007.

86. Dave, E.V., W.G. Buttlar., S.E. Leon., B. Behnia., and G.H. Paulino. IlliTC – Low Temperature Cracking Model for Asphalt Pavements. *Road Materials and Pavement Design*, Vol. 14(Sup. 2), 2013, pp. 57-78.

87. Kahil, N. S., Najjar, S. S., & Chehab, G. Probabilistic Modeling of Dynamic Modulus Master Curves for Hot-Mix Asphalt Mixtures. *Transportation Research Record: Journal of the Transportation Research Board*, 2507, pp. 90-99, 2015.

88. Zhao, Y-X., Qing Gao, and J-N. Wang. "An approach for determining an appropriate assumed distribution of fatigue life under limited data." *Reliability Engineering & System Safety* Vol. 67(1), pp. 1-7, 2000.

89. Janežič, M., J. Klemenc, and M. Fajdiga. "A neural-network approach to describe the scatter of cyclic stress–strain curves." *Materials & Design* vol (31)1 pp. 438-448, 2010.

90. Christensen Jr, D. W., T. Pellinen, and R. F. Bonaquist., "Hirsch Model for Estimating the Modulus of Asphalt Concrete," *Journal of Association of Asphalt Paving Technologists*, Vol. 72, 2003, pp. 97-121.

91. Kim, Y.R. *Mechanistic Fatigue Characterization and Damage Modeling of Asphalt Mixtures*. Ph.D. Dissertation, Texas A&M University, College Station, TX, 2003.

92. Kim, Y. R., & Little, D. N. (2005). *Development of specification-type tests to assess the impact of fine aggregate and mineral filler on fatigue damage* (No. FHWA/TX-05/0-1707-10).

93. Izadi, A., A. Bhasin, and A. Motamed. *Designing Fine Aggregate Mixtures to Evaluate Fatigue Crack Growth in Asphalt Mixtures*. No. SWUTC/11/161022-1, Southwest Region University Transportation Center, Center for Transportation Research, University of Texas at Austin, 2011.

94. Sousa, P. K., E. A. Masad, and D. N. Little. New Design Method of Fine Aggregates Mixtures and Automated Method for Analysis of Dynamic Mechanical Characterization Data. *Construction and Building Materials*, Vol. 41, 2013, pp. 216-223.

95. Palvadi S., A. Bhasin and D. N. Little. A Method to Quantify Healing in Asphalt Composites Using Continuum Damage Approach. In *Transportation Research Record: Journal of the Transportation Research Board, No. 999*, Transportation Research Board of the National Academies, Washington, D.C.,2011, pp. 86-96.

96. Kim Y.R, D. N. Little and R. L. Lytton., Use of Dynamic Mechanical Analysis (DMA) to Evaluate the Fatigue and Healing Potential of Asphalt Binders in Sand Asphalt Mixtures, *Journal of Association of Asphalt Paving Technologists*, Vol. 71, 2002, pp. 176-206.

97. Zollinger, C. J. *Application of Surface Energy Measurements to Evaluate Moisture Susceptibility of Asphalt and Aggregates.* Master Thesis, Texas A&M University, College Station, 2005.

98. Underwood, B. S. and Y. R. Kim., Microstructural Investigation of Asphalt Concrete for Performing Multiscale Experimental Studies, *International Journal of Pavement Engineering*, Vol. 14, No. 5, 2013, pp. 498-516.

99. Underwood, B. S. and Y. R. Kim., Effect of Volumetric Factors on the Mechanical Behavior of Asphalt Fine Aggregate Matrix and the Relationship to Asphalt Mixture Properties, *Construction and Building Materials*, Vol. 49, 2013, pp. 672-681.

100. Radovskiy, B. (2003). Analytical Formulas for Film Thickness in Compacted Asphalt Mixture, Transportation Research Record, 1829, National Research Council, Washington, D.C., pp.26-32.

101. Stanton, T.E. and F.N. Hveem (1933). Role of the Laboratory in the Preliminary Investigation and Control of Materials for Low Cost Bituminous Pavements, Proceedings of the Fourteenth Annual Meeting of the Highway Research Board, 14-54.

102. Underwood, B. S. (2011). Multiscale Constitutive Modeling of Asphalt Concrete. Ph.D. Dissertation, North Carolina State University, Raleigh.

103. Witzcak, Matthew W. Simple performance test for superpave mix design. Vol. 465. Transportation Research Board, 2002.

104. Arizona Department of Transportation, Standard Specifications for Road and Bridge Construction, Arizona, 2008.

105. Zeiada, W. A. Endurance Limit for HMA Based on Healing Phenomenon Using Viscoelastic Continuum Damage Analysis. PhD dissertation. Arizona State University, Tempe, 2012

106. AASHTO T 342-11, Standard Method of Test for Determining Dynamic Modulus of Hot-Mix Asphalt (HMA), Standard Specifications for Transportation Materials and Methods of Sampling and Testing, American Association of State Highway Transportation Officials, Washington, DC, 2011.

107. Zhao, Y., and Y. R. Kim. The Time-Temperature Superposition for Asphalt Mixtures with Growing Damage and Permanent Deformation in Compression. CD-ROM. Transportation Research Board of the National Academies, Washington, D.C., 2003.

108. AASHTO TP107-14, Proposed Standard Method of Test for Determining the Damage Characteristic Curve of Asphalt Concrete from Direct Tension Cyclic Fatigue Tests, American Association of State Highway and Transportation Officials, Washington, DC, 2014.

109. Xiao, F., S. Amirkhanian., and C. H. Juang. Prediction of Fatigue Life of Rubberized Asphalt Concrete Mixtures Containing Reclaimed Asphalt Pavement Using Artificial Neural Networks. Journal of Materials in Civil Engineering, Vol. 21(6), 2009, pp. 253-261.

110. Roque, R., D. R. Hiltunen., and W. G. Buttlar. Thermal Cracking Performance and Design of Mixtures Using Superpave (With Discussion). Journal of the Association of Asphalt Paving Technologists, Vol. 64, 1995, pp. 718-752

111. Roque, R., J. Zou., Y. R. Kim., C. Baek., S. Thirunavukkarasu., B. S. Underwood., and M. N. Guddati. NCHRP Web Document 162: Top-down Cracking of Hot-Mix Asphalt Layers: Models for Initiation and Propagation. Transportation Research Board of the National Academies, 2010.

112. Birgisson, B., J. Wang., and R. Roque. Implementation of the Florida cracking model into the mechanistic-empirical pavement design. No. UF# 0003932, 2006.

113. Nowak, A. S., and Collins, K. (2000) "Reliability of Structures". McGraw-Hill Publisher.

114. You, Z., Q. Dai, and B. Gurung., "Development and Implementation of a Finite Element Model for Asphalt Mixture to Predict Compressive Complex Moduli at Low and Intermediate Temperatures," Geotechnical Special Publication (GSP): Asphalt Concrete: Simulation, Modeling, and Experimental Characterization. American Society of Civil Engineers, 2006, pp. 21-28.

115. Masad, E. A., C. Zollinger, D. N. Little, and R. L. Lytton., "Characterization of HMA Moisture Damage Using Surface Energy and Fracture Properties (With Discussion)," Journal of the Association of Asphalt Paving Technologists, Vol. 25, 2006, pp. 713-754.

116. Miller, C., K. L. Vasconcelos., D. N. Little and A. Bhasin., "Investigating Aspects of Aggregate Properties that Influence Asphalt Mixtures Performance," Research Report for DTFH61-06-C-00021, Texas A & M University at College Station and University of Texas at Austin, Texas, 2011

117. Aragão, F. T. S. and Y. R. Kim., "Characterization of Fracture Properties of Asphalt Mixtures Based On Cohesive Zone Modeling and Digital Image Correlation Technique," 90th Annual Meeting of the Transportation Research Board. Washington D.C., 2011.

118. Im S., H. Ban and Y. R. Kim., "Characterization of Mode-I and Mode-II Fracture Properties of Fine Aggregate Matrix Using a Semicircular Specimen Geometry," Construction and Building Materials, Vol. 52, 2014, pp. 413-421.

119. Mo, L. T., "Damage Development in the Adhesive Zone and Mortar of Porous Asphalt Concrete," TU Delft, Delft University of Technology, 2010.

120. Wu, J., M. Yusoff, N. Izzi, F. Mohd Jakarni and M. R. Hainin., "Correction of Compliance Errors in the Dynamic Shear Modulus of Bituminous Binders Data." Sains Malaysiana 42, Vol. 6, 2013, pp. 783-792.

121. Petersen, J. C., "Binder Characterization and Evaluation Volume 4: Test Methods SHRP-A-370." Washington, DC: Transportation Research Board, Strategic Highway Research Program, 1994.

122. Carswell, J., M. J. Claxton and P. J. Green., "Dynamic Shear Rheometers: Making Accurate Measurements on Bitumens," THE ASPHALT YEARBOOK 1997, 1997.

123. Zeiada, W. A., B. S. Underwood, T. Pourshams, J. Stempihar and K. E. Kaloush., Comparison of Conventional, Polymer, and Rubber Asphalt Mixtures Using Viscoelastic Continuum Damage Model, Road Materials and Pavement Design 15, no. 3, 2014, pp. 588-605.

124. Cross, S. A., Y. Jakatimath and K.C, Sumesh., Determination of Dynamic Modulus Master Curves for Oklahoma HMA Mixtures, No. FHWA-OK-07-05. 2007.

125. Kim, Y. R., M. King and M. Momen., Typical Dynamic Moduli for North Carolina Asphalt Concrete Mixes, No. FHWA/NC/2005-03. 2005.

126. Woldekidan, M. F., M. Huurman and L. T. Mo., Testing and Modeling of Bituminous Mortar Response, Journal of Wuhan University of Technology-Mater. Sci. Ed. 25, no. 4, 2010, pp. 637-640.

127. ASTM D2726M-14, Standard Test Method for Bulk Specific Gravity and Density of Non-Absorptive Compacted Bituminous Mixtures, Annual Book of ASTM Standards, ASTM International, West Conshohocken, PA, 2014.

128. ASTM D2041M-11, Standard Test Method for Theoretical Maximum Specific Gravity and Density of Bituminous Paving Mixtures, Annual Book of ASTM Standards, ASTM International, West Conshohocken, PA, 2011.

129. Zhao, Y. and Y. R. Kim., The Time-Temperature Superposition for Asphalt Mixtures With Growing Damage and Permanent Deformation in Compression, In TRB Annual Meeting CD-ROM. 2003.

130. Witczak, M. W. and Javed Bari, Development of a Master curve (E*) Database for Lime Modified Asphaltic Mixtures, Arizona *State University Research Report, Tempe (Arizona, USA): Arizona State University*, 2004.

131. Costa, A. L., D. J. Shuman, R. R. Machado and M. S. Andrade., Determination of the Compliance of an Instrumented Indentation Testing Machine, *Proc. of HARDMEKO*, 2004.

132. Mike, F., C. Sui, S. Salmans and Q. Qian., *Determining the Low-Temperature Rheological Properties of Asphalt Binder Using a Dynamic Shear Rheometer (DSR)*, Western Research institute, FHWY No. DTFH61-07-D-00005, 2015

133. Monismith, C. C. and D. B. McLean. "Structural Design Considerations," *Road, Journal of the Road Engineering Association* 1. Analytic, 1976.

134. Guddati, M. N., Z. Feng, and Y.R. Kim. Towards a Micromechanics-Based Procedure to Characterize Fatigue Performance of Asphalt Concrete. In *Transportation Research Record: Journal of the Transportation Research Board, No. 1789*, Transportation Research Board of the National Academies, Washington, D.C.,2002,pp121-128.

135. Abbas, A., E. Masad, T. Papagiannakis, and A. Shenoy. Modeling Asphalt Mastic Stiffness Using Discrete Element Analysis and Micromechanics-Based Models, *International Journal of Pavement Engineering*, Vol.6, No.2, 2005, pp.137-146.

136. Shu, X., and B. Huang. Predicting Dynamic Modulus of Asphalt Mixtures with Differential Method. *Road Materials and Pavement Design*, Vol. 10, No. 2, 2009, pp337-359.

137. Hashin, Z. The Elastic Moduli of Heterogeneous Materials. *Journal of Applied Mechanics*, Vol.29, No. 1, 1962, pp.143-150.

138. Herve, E., and A. Zaoui. N-layered Inclusion-Based Micromechanical Modelling. *International Journal of Engineering Science*, Vol. 31, No. 1, 1993, pp.1-10.

139. Christensen, R. M., and K. H. Lo. Solutions for Effective Shear Properties in Three phase Sphere and Cylinder Models. *Journal of the Mechanics and Physics of Solids*, Vol. 27, No. 4, 1979, pp. 315-330.

140. Tschoegl, N. *The Phenomenological Theory of Linear Viscoelastic Behavior: An Introduction.* Berlin: Springer-Verlag, 1989.

141. Coenen, E. W. C., V. G. Kouznetsova, and M. G. D. Geers. Enabling Microstructure-Based Damage and Localization Analyses and Upscaling: Modelling And Simulation. *Materials Science and Engineering*, Vol. 19, No. 7, 2011, 074008

142. Anderson, D.A., D.W. Christensen, H.U. Bahia, R. Dongre, M.G. Sharma, C.E. Antle, and J. Button. *Binder Characterization and Evaluation Volume 3: Physical Characterization*. Project Document SHRP-A-369, Strategic Highway Research Program, National Research Council, Washington D.C., 1994.

143. Glaser, R. R., J.F. Schabron, T.F Turner, J.P. Planche, S.L. Salmans, and J.L. Loveridge. Low Temperature Oxidation Kinetics of Asphalt Binders. In *Transportation Research Record: Journal of the Transportation Research Board*, No. 2370, Transportation Research Board of the National Academies, Washington, D.C., 2013, pp. 63-68.

144. Huang, S.C., and M. Zeng. Characterization of Aging Effect on Rheological Properties of Asphalt-Filler Systems, *International Journal of Pavement Engineering*, Vol. 8(3), 2007, pp. 213-223.

145. Bell, C. A., and D. Sosnovske. SHRP-A-384: Aging: Binder Validation. TRB, National Research Council, Washington, D.C., 1994

146. Daniel, J.S., Y.R. Kim, and H.J. Lee. Effects of Aging on Viscoelastic Properties of Asphalt-Aggregate Mixtures. In *Transportation Research Record: Journal of the Transportation Research Board*, No. 1630, Transportation Research Board of the National Academies, Washington, D.C., 1998, pp. 21-27.

147. Baek, C., B.S. Underwood, and Y.R. Kim. Effects of Oxidative Aging on Asphalt Mixture Properties. In *Transportation Research Record: Journal of the Transportation Research Board*, No. 2296, Transportation Research Board of the National Academies, Washington, D.C., 2012, pp. 77-85

148. Plancher, H., E.L. Green, J.C. Petersen. Reduction of Oxidative Hardening of Asphalts by Treatment with Hydrated Lime- A Mechanistic Study. *Journal of the Association of Asphalt Paving Technologists*, Vol. 45, 1976, pp. 1-19.

149. Delaporte, B., H. Di Benedetto, P. Chaverot, and G. Gauthier. Linear Viscoelastic Properties of Bituminous Materials: from Binders to Mastics. *Journal of the Association of Asphalt Paving Technologists*, Vol. 76, 2007, pp. 455-494.

150. Petersen, J. C. A Review of the Fundamentals of Asphalt Oxidation: Chemical, Physicochemical, Physical Property, and Durability Relationships. TRB Transportation Research Circular E-C140, Transportation Research Board of the National Academies, 2009.

151. Glover, C. J., A. E. Martin, A. Chowdhury, R. Han, N. Prapaitrakul, X. Jin, and J. Lawrence. Evaluation of Binder Aging and its Influence in Aging of Hot Mix Asphalt Concrete: Literature Review and Experimental Design. *Report 0-6009-1. Texas Transportation Institute*, College Station, Texas, 2008.

152. Liu, M., K. M. Lunsford, R. R. Davison, C.J. Glover, and J. A. Bullin. The Kinetics of Carbonyl Formation in Asphalt. *AlChE Journal*, 42(4), 1996, pp. 1069-1076.

153. Morian, N., E.Y. Hajj, C.J. Glover, and P.E. Sebaaly. Oxidative Aging of Asphalt Binders in Hot-Mix Asphalt Mixtures. In *Transportation Research Record: Journal of the Transportation Research Board*, No. 2207, Transportation Research Board of the National Academies, Washington, D.C., 2011, pp. 107-116

154. Farrar, M.J., T.F. Turner, J.P. Planche, J.F. Schabron, and P.M. Harnsberger. Evolution of the Crossover Modulus with Oxidative Aging: A Method to Estimate the Change in Viscoelastic Properties of an Asphalt Binder with Time and Depth on the Road. In *Transportation Research Record, Journal of the Transportation Research Board*, Washington, D.C., 2013, pp. 76-83.

155. Morian, N.E. Influence of Mixture Characteristics on the Oxidative Aging of Asphalt Binders. Ph.D. Dissertation, University of Nevada, Reno, NV, 2014.

156. Bell, C. A., M. J. Fellin, and A. Wieder. Field Validation of Laboratory Aging Procedures for Asphalt Aggregate Mixtures. *Journal of the Association of Asphalt Paving Technologists*, Vol. 63, 1994, pp. 45-80.

157. Houston, W. M., M. W. Mirza, C. E. Zapata, and S. Raghavendra. NCHRP Web Document 113: *Environmental Effects in Pavement Mix and Structural Design Systems*. Transportation Research Board of the National Academies, Washington, D.C., 2005.

158. Reed, J. Evaluation of the Effects of Aging on Asphalt Rubber Pavements, M.S. Thesis, Arizona State University, Tempe, AZ, 2010.

159. Airey, G., Y. K. Choi, A. Collop, A. J. V. Moore, and R. C. Elliott. Combined Laboratory Aging /Moisture Sensitivity Assessment of High Modulus Base Asphalt Mixtures, *Journal of the Association of Asphalt Paving Technologists*, 2005, Vol. 74, pp. 307-345.

160. Gudipudi, P., and B.S. Underwood. Testing and Modeling of Fine Aggregate Matrix and Its Relationship to Asphalt Concrete Mix. In *Transportation Research Record: Journal of the Transportation Research Board*, In Press, Transportation Research Board of the National Academies, Washington, D.C., 2015.

161. Christensen, D.W. and D.A. Anderson. Interpretation of mechanical test data for paving grade asphalt cements. *Journal of the Association of Asphalt Paving Technologists*, Vol. 61, 1992, pp. 67-116.

APPENDIX A

AC AND FAM MATERIAL VOLUMETRIC PROPERTIES

TABLE A.1 AC and Corresponding FAM Mixdesign

Aggregate size (mm)	AC Gradation	FAM Gradation
	(% Passing)	(% Passing)
25	100	100
19	91	100
12.5	83	100
9.5	76	100
4.75	60	100
2.36	46	100
1.18	32	100
0.6	22	67
0.3	13	38
0.15	8	21
0.075	4.9	11
Pan	0	0
Volumetric Concentration of Filler		27.20%
Binder Content of FAM		12.90%
Binder Content of AC		6%
Thickness of Mastic Film		25.14 (μm)

TABLE A.2 Percentage Air voids of FAM Samples for Both Mixtures

FAM	Sample Id	% Air voids	Sample Id	% Air voids
PG 64-22	F16-1	5.3	F16-1	5.3
	F16-2	5.8	F16-2	5.8
	F16-3	5.3	F16-3	5.3
	F16-4	5.5	F16-4	5.5
	F16-5	5.5	F16-5	5.5
	F16-6	5.4	F16-6	5.4
	F16-7	5.3	F16-7	5.3
	F16-8	5.4	F16-8	5.4
	F16-9	5.8	F16-9	5.8
	F16-10	5.6	F16-10	5.6
	F16-11	5.9	F16-11	5.9
	F16-12	5.7	F16-12	5.7
PG 76-16	F17-1	5.8	F27-1	5.4
	F17-2	5.6	F27-2	5.4
	F17-3	6.3	F27-3	5.6
	F17-4	5.8	F27-4	5.6
	F17-5	5.9	F27-5	5.6
	F17-6	6.3	F27-6	5.4
	F17-7	5.9	F27-7	5.4
	F17-8	6.1	F27-8	5.5
	F17-9	6.2	F27-9	5.6
	F17-10	6.3	F27-10	5.3
	F17-11	6.0	F27-11	5.6
	F17-12	5.8	F27-12	5.4

TABLE A.3 Percentage Air voids of AC Samples for Both Mixtures

AC Mix	Sample Id	% Air voids
PG 64-22	PM61	3.7
	PM62	4.1
	PM63	3.9
	PM64	3.7
	PM65	4.1
	PM66	4.3
	PM67	4.2
	PM68	3.9
PG 76-16	PM71	4.5
	PM72	4.9
	PM73	4.4
	PM74	4.5
	PM75	4.7
	PM76	4.8
	PM77	4.2
	PM 78	4.5
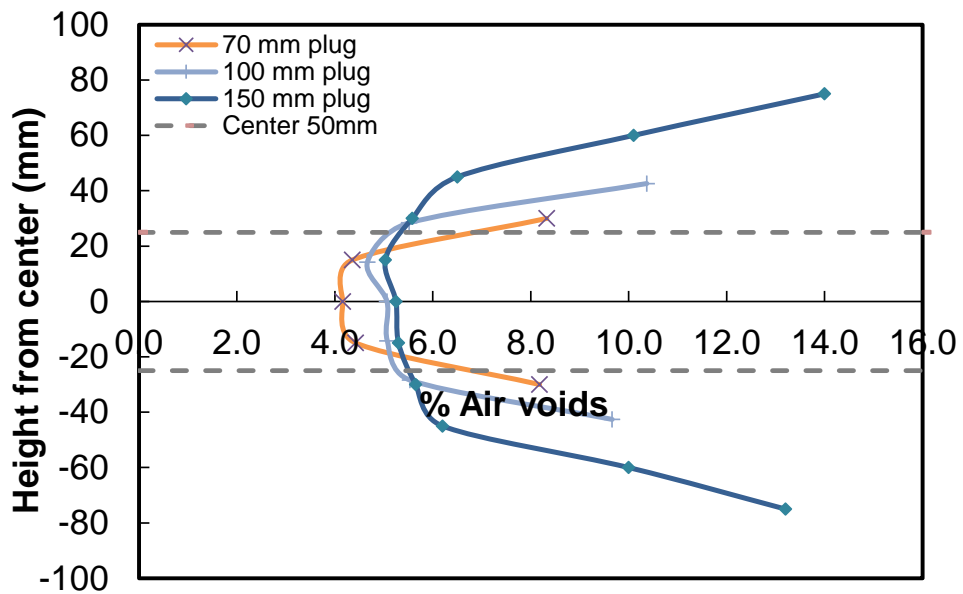
FIGURE A-1 Air voids of three different compaction height FAM samples.

Aging Study Material Description and Mixdesign

TABLE A.4 Aging Study Materials and their Description

Notation	Notation Description	Binder			Aggregate		Gradation		Air Voids (%)	
		B1	B2	B3	A1	A2	G1	G2	4.5	7.5
B1	PG 58-28 (Unmodified)	X								
B2	PG 64-22 (Unmodified)		X							
B3	PG 70-28 (SBS)			X						
A1	Limestone				X					
A2	Granite					X				
G1	Coarse Gradation						X			
G2	Fine Gradation							X		
B2A2G1-F-7.5	FAM : AC = 15.4%		X			X	X			X
B2A2G2-F-7.5	FAM : AC = 15.4%		X			X		X		X
B2A2G2-F-4.5	FAM : AC = 15.4%		X			X		X	X	
B1A2G2-F-4.5	FAM : AC = 11.2%	X				X		X	X	
[c] V_c = Volume content of filler in mastic. [d] AC = Percentage asphalt content in FAM.										

TABLE A.5 Aging Study AC and Corresponding FAM (B2A2G2) Mixdesign

Aggregate size (mm)	AC Gradation	FAM Gradation
	(% Passing)	(% Passing)
25	100	100
19	100	100
12.5	100	100
9.5	97	100
4.75	73	100
2.36	52	100
1.18	40	100
0.6	29	100
0.3	19	64.1
0.15	10	34.0
0.075	6	19.1
Pan	0	0.0
Volumetric Concentration of Filler		24.10%
Binder Content of FAM		15.40%
Binder Content of AC		6.6%
Thickness of Mastic Film		23.8 (mm)

APPENDIX B

AC AND FAM MATERIAL REPLICATE MODULUS AND DAMAGE PROPERTIES

AC Replicate Modulus Data Tested In This Study

TABLE B.1 AC_64-22 Replicate Modulus Data

AC_64-22									
Temp.	Freq.	Dynamic Modulus, |E*| (MPa)				Phase Angle (PA, degree)			
	Hz	Rep1	Rep2	Rep3	Avg. |E*|	Rep1	Rep2	Rep3	Avg. PA
-10	25	26988	27126	26193	26769	3.8	3.9	3.0	3.6
	10	23956	26377	24358	24897	5.5	6.2	5.1	5.6
	5	22966	25601	23443	24003	6.5	7.1	6.4	6.7
	1	20925	23303	20906	21711	7.6	8.6	7.9	8.0
	0.5	20291	22443	20255	20996	8.3	9.2	8.4	8.6
	0.1	20336	20124	18033	19498	12.0	10.2	9.4	10.5
5.4	25	17702	18396	18345	18148	8.9	8.4	8.8	8.7
	10	15475	16979	16156	16204	11.0	10.8	9.8	10.5
	5	14409	15909	15086	15135	12.5	12.3	11.7	12.1
	1	11774	13069	12248	12364	15.4	15.0	15.1	15.2
	0.5	10737	11941	11318	11332	16.2	15.8	15.8	15.9
	0.1	8281	9378	8388	8683	19.5	18.7	18.4	18.9
21	25	8622	8984	9123	8910	18.8	17.7	17.8	18.1
	10	7012	7443	7978	7478	22.4	21.6	19.5	21.2
	5	6100	6389	6485	6324	25.7	24.4	23.8	24.6
	1	4025	4159	4199	4128	32.1	30.1	30.3	30.8
	0.5	3243	3388	3526	3386	34.4	32.6	32.4	33.2
	0.1	1852	1964	2108	1974	40.1	38.1	38.1	38.8
38	25	2128	2210	1718	2019	39.1	37.7	40.2	39.0
	10	1492	1512	1200	1401	44.1	42.7	44.5	43.7
	5	1185	1138	872	1065	45.8	44.9	45.7	45.5
	1	624	571	488	561	48.1	48.1	46.7	47.6
	0.5	526	448	445	473	47.6	48.2	47.1	47.6
	0.1	371	252	238	287	39.7	50.5	44.9	45.0
54.4	25	465	489	454	469	48.5	49.0	47.0	48.2
	10	309	309	317	312	48.8	49.6	46.7	48.3
	5	229	230	234	231	47.4	48.8	46.5	47.6
	1	154	179	164	166	38.4	40.5	36.6	38.5
	0.5	138	132	142	138	38.4	39.0	35.5	37.6
	0.1	128	117	122	122	30.1	33.4	31.6	31.7

TABLE B.2 AC_76-16 Replicate Modulus Data

AC_76-16									
Temp.	Freq.	Dynamic Modulus, |E*| (MPa)				Phase Angle(PA, degree)			
	Hz	Rep1	Rep2	Rep3	Avg. |E*|	Rep1	Rep2	Rep3	Avg. PA
-10	25	26690	27030	27074	26931	0.7	1.3	1.9	1.3
	10	24838	26487	24701	25342	2.7	3.2	3.7	3.2
	5	24176	25934	23987	24699	3.7	4.9	6.2	5.0
	1	22585	24016	21672	22758	4.5	5.1	17.0	8.8
	0.5	22013	23275	21190	22159	3.9	4.7	24.4	11.0
	0.1	20012	21424	18958	20132	6.0	6.5	8.7	7.1
5.4	25	18970	20531	19572	19691	6.6	6.0	5.5	6.0
	10	17611	19321	18034	18322	8.9	7.8	7.5	8.1
	5	16691	18355	17026	17357	10.1	9.8	10.5	10.1
	1	14326	15622	13650	14533	10.9	16.5	22.6	16.7
	0.5	13776	14493	13068	13779	10.5	14.0	24.0	16.2
	0.1	12077	11944	11279	11767	15.8	14.9	11.1	13.9
21	25	10352	10853	11664	10957	14.5	14.8	12.8	14.0
	10	8835	9461	9831	9376	17.8	15.8	15.0	16.2
	5	7817	8373	8774	8322	20.4	18.1	18.1	18.9
	1	5521	5879	6148	5850	24.5	23.8	24.2	24.2
	0.5	4720	4990	5399	5036	26.9	25.4	24.8	25.7
	0.1	3022	3230	3417	3223	31.6	30.1	26.7	29.5
38	25	3274	3529	3155	3319	30.4	31.5	26.1	29.3
	10	2385	2606	2438	2476	35.1	34.7	30.6	33.5
	5	1853	2026	1772	1884	37.8	38.0	33.7	36.5
	1	1008	1050	1087	1049	41.3	41.5	38.6	40.5
	0.5	769	814	833	805	43.1	41.3	41.0	41.8
	0.1	390	407	436	411	45.2	40.8	48.9	44.9
54.4	25	847	1048	1086	994	41.8	40.9	38.6	40.4
	10	580	681	755	672	42.8	41.7	40.7	41.8
	5	431	504	567	501	43.4	44.7	40.8	43.0
	1	246	266	322	278	39.2	39.1	38.7	39.0
	0.5	206	216	276	233	37.8	36.7	35.0	36.5
	0.1	128	132	213	158	30.1	35.4	33.0	32.8

FAM Replicate Modulus Data Tested In This Study

TABLE B.3 FAM_64-22 Replicate Modulus Data

Temp.	Freq.	Dynamic Modulus, |E*| (MPa)				Phase Angle(PA, degree)			
	Hz	Rep1	Rep2	Rep3	Avg. |E*|	Rep1	Rep2	Rep3	Avg. PA
-9.5	25	15500	16630	15382	15837	8.9	6.8	7.8	7.9
	10	14873	16042	14745	15220	9.3	7.4	8.2	8.3
	5	14185	15346	14055	14529	10.1	8.1	8.5	8.9
	1	12314	13404	12314	12677	11.6	9.3	9.8	10.2
	0.5	11442	12694	11580	11905	11.9	9.8	10.3	10.7
	0.1	9614	10830	9860	10101	12.0	10.0	10.5	10.8
5.3	25	8988	10024	9073	9361	16.1	13.3	12.9	14.1
	10	8182	9258	8317	8586	16.4	14.0	13.6	14.7
	5	7485	8512	7600	7866	17.5	14.8	14.6	15.6
	1	5794	6643	5993	6143	19.5	16.7	16.7	17.7
	0.5	5148	5981	5355	5495	20.7	17.7	17.9	18.8
	0.1	3836	4434	3987	4085	21.4	19.7	19.6	20.2
20.5	25	3380	4031	3528	3646	24.2	23.6	22.4	23.4
	10	2827	3401	2967	3065	25.9	25.4	23.9	25.1
	5	2345	2818	2469	2544	27.8	27.1	25.8	26.9
	1	1431	1699	1511	1547	32.0	30.8	30.3	31.0
	0.5	1135	1345	1208	1229	33.3	32.4	31.6	32.4
	0.1	649	748	704	700	35.0	35.3	34.2	34.8
30.5	25	1608	1883	1687	1726	30.1	30.7	30.3	30.3
	10	1256	1487	1322	1355	32.5	32.9	32.7	32.7
	5	976	1170	1034	1060	33.9	34.9	33.8	34.2
	1	508	599	571	560	36.8	39.5	36.1	37.5
	0.5	402	484	441	443	36.3	38.7	37.0	37.4
	0.1	211	267	241	240	36.2	39.1	34.4	36.5
40.5	25	725	822	750	766	37.0	37.3	36.1	36.8
	10	528	618	550	565	36.8	39.5	38.6	38.3
	5	423	482	433	446	37.6	38.2	36.5	37.4
	1	225	246	232	234	35.5	38.0	36.7	36.8
	0.5	191	202	188	194	33.8	37.9	33.0	34.9
	0.1	126	132	110	123	27.5	30.4	23.4	27.1

TABLE B.4 FAM_76-16 Replicate Modulus Data

		Dynamic Modulus, |E*| (MPa)				Phase Angle(PA, degree)			
Temp.	Freq.								
	Hz	Rep1	Rep2	Rep3	Avg. |E*|	Rep1	Rep2	Rep3	Avg. PA
-9.5	25	18561	17163	18873	18199	6.2	7.1	7.3	6.9
	10	18385	16587	18357	17776	6.5	8.8	7.3	7.5
	5	17851	16056	17844	17250	7.1	9.2	7.4	7.9
	1	15937	14395	15932	15421	8.0	10.2	8.3	8.8
	0.5	15288	13687	15186	14720	8.5	10.7	9.0	9.4
	0.1	13370	12070	13121	12854	8.2	10.7	8.3	9.0
5.3	25	12241	11272	12080	11865	11.1	14.6	9.9	11.9
	10	11470	10476	11245	11064	11.8	15.9	10.3	12.7
	5	10634	9651	10377	10221	12.7	16.6	11.2	13.5
	1	8565	7667	8370	8201	14.3	17.7	13.0	15.0
	0.5	8010	7066	8185	7754	14.9	19.1	13.3	15.8
	0.1	6532	5547	6809	6296	15.3	20.8	14.9	17.0
20.5	25	5740	5136	5268	5381	18.9	21.6	21.3	20.6
	10	4983	4332	4529	4615	20.9	23.7	22.8	22.5
	5	4360	3682	3901	3981	22.4	25.2	23.5	23.7
	1	2988	2376	2592	2652	25.9	27.4	26.8	26.7
	0.5	2495	1935	2126	2185	27.4	28.9	28.6	28.3
	0.1	1560	1146	1306	1338	30.1	31.6	30.5	30.7
30.5	25	2996	2451	2664	2704	25.0	25.3	28.0	26.1
	10	2458	1958	2168	2194	26.9	27.2	29.8	28.0
	5	2009	1552	1733	1765	28.8	29.2	31.5	29.8
	1	1191	854	978	1008	32.4	33.5	35.8	33.9
	0.5	938	659	754	783	34.4	34.4	37.9	35.6
	0.1	527	373	442	447	34.0	34.1	38.9	35.7
40.5	25	1487	1140	1266	1298	32.1	31.5	33.6	32.4
	10	1148	879	939	989	33.6	33.8	36.2	34.5
	5	875	675	708	753	36.2	33.7	37.9	35.9
	1	487	353	368	403	36.7	37.6	41.5	38.6
	0.5	374	291	309	325	36.6	34.0	39.9	36.8
	0.1	192	181	176	183	37.8	30.5	37.7	35.4

Aging Study FAM Material Replicate Modulus Data

TABLE B.5 B2A2G2F-0-4.5 FAM Replicate Modulus Data

B2A2G2F-0-4.5									
Temp.	Freq.	Dynamic Modulus, |E*| (MPa)				Phase Angle(PA, degree)			
	Hz	Rep1	Rep2	Rep3	Avg. |E*|	Rep1	Rep2	Rep3	Avg. PA
-11.5	25	11099	11131	9934	10721	15.8	12.3	12.1	13.4
	10	10372	10481	9443	10099	14.1	11.1	10.9	12.0
	5	9600	9911	8869	9460	14.5	10.9	11.5	12.3
	1	7962	8137	7249	7783	15.0	12.6	12.7	13.4
	0.5	7209	7418	6501	7043	15.8	13.6	13.5	14.3
	0.1	5597	5836	5162	5532	17.6	15.3	14.9	15.9
4.4	25	4939	5199	4597	4912	24.6	22.5	21.6	22.9
	10	4257	4536	4005	4266	24.5	22.3	21.6	22.8
	5	3654	3891	3444	3663	25.8	23.2	22.8	23.9
	1	2390	2580	2224	2398	28.8	27.0	26.1	27.3
	0.5	1963	2128	1817	1969	30.7	28.9	27.5	29.0
	0.1	1197	1276	1036	1170	33.3	31.5	30.9	31.9
20.4	25	1210	1334	1178	1241	39.3	38.5	39.1	39.0
	10	915	1008	890	937	39.9	38.9	39.2	39.3
	5	672	765	665	701	40.4	39.5	40.6	40.2
	1	344	371	328	347	39.5	41.3	41.6	40.8
	0.5	261	281	246	263	38.6	42.0	41.1	40.6
	0.1	129	136	132	132	31.7	37.6	36.6	35.3
30.5	25	480	499	454	478	51.3	46.6	46.2	48.0
	10	324	362	340	342	45.2	45.2	44.3	44.9
	5	236	271	242	250	45.1	42.0	41.4	42.8
	1	118	143	136	132	39.2	39.0	36.4	38.2
	0.5	92	110	101	101	36.8	37.7	33.5	36.0
	0.1	59	74	72	68	27.4	23.3	24.1	24.9

TABLE B.6 B2A2G2F-7-4.5 FAM Replicate Modulus Data

Temp.	Freq.	Dynamic Modulus, |E*| (MPa)				Phase Angle(PA, degree)			
	Hz	Rep1	Rep2	Rep3	Avg. |E*|	Rep1	Rep2	Rep3	Avg. PA
-11.5	25	11770	12153	12476	12133	9.2	10.6	9.7	9.9
	10	11232	11623	11870	11575	7.4	9.2	8.7	8.4
	5	10709	11168	11391	11089	7.7	9.1	8.2	8.3
	1	9248	9525	9757	9510	7.9	10.1	8.7	8.9
	0.5	8618	8723	8950	8764	8.5	10.9	9.6	9.7
	0.1	7121	7016	6920	7019	9.1	10.6	9.6	9.8
4.4	25	6402	6573	6775	6584	16.5	18.1	17.2	17.3
	10	5756	5930	6125	5937	15.3	17.5	16.7	16.5
	5	5187	5265	5456	5303	15.3	17.9	17.0	16.7
	1	3766	3898	4033	3899	17.5	19.8	18.6	18.6
	0.5	3318	3394	3488	3400	18.8	21.0	19.8	19.9
	0.1	2286	2358	2446	2363	21.0	23.2	22.1	22.1
20.4	25	2231	2144	2313	2229	29.6	30.5	29.9	30.0
	10	1800	1729	1878	1803	29.5	30.5	29.9	30.0
	5	1455	1398	1502	1452	30.7	31.5	31.3	31.1
	1	806	778	834	806	34.2	34.9	34.7	34.6
	0.5	608	591	665	622	36.1	36.4	35.4	36.0
	0.1	344	317	340	334	36.4	37.3	35.8	36.5
30.5	25	945	897	1001	948	37.1	38.0	38.1	37.7
	10	720	688	763	723	35.7	37.4	37.7	36.9
	5	557	539	565	554	35.6	36.4	37.6	36.6
	1	301	286	295	294	34.1	36.4	38.5	36.3
	0.5	228	233	222	228	34.2	34.0	37.5	35.2
	0.1	142	130	127	133	30.8	33.1	33.8	32.6
38.5	25	461	455	469	462	40.1	40.9	42.3	41.1
	10	362	327	350	346	36.7	40.1	40.1	38.9
	5	281	264	274	273	34.9	36.2	38.1	36.4
	1	164	155	156	158	30.3	31.9	34.6	32.3
	0.5	140	130	129	133	26.7	29.2	31.1	29.0
	0.1	102	98	94	98	14.0	19.3	24.8	19.4

TABLE B.7 B2A2G2F-15-4.5 FAM Replicate Modulus Data

Temp.	Freq.	Dynamic Modulus, |E*| (MPa)				Phase Angle(PA, degree)			
	Hz	Rep1	Rep2	Rep3	Avg. |E*|	Rep1	Rep2	Rep3	Avg. PA
-11.5	25	12111	12277	12194	12194	11.1	10.3	10.3	10.5
	10	11634	11795	11570	11666	9.7	8.6	8.7	9.0
	5	11086	11271	11014	11124	9.4	8.2	8.4	8.7
	1	9749	9697	9536	9661	10.0	8.8	8.4	9.1
	0.5	9147	9044	8913	9035	10.4	9.4	8.9	9.5
	0.1	7677	7530	7221	7476	10.9	9.9	9.0	9.9
4.4	25	6909	6887	6767	6854	18.2	17.0	16.9	17.4
	10	6316	6228	6119	6221	17.2	16.0	16.2	16.5
	5	5692	5630	5507	5610	17.7	16.3	16.6	16.8
	1	4323	4198	4155	4225	19.8	18.1	17.9	18.6
	0.5	3774	3634	3635	3681	20.8	19.2	19.1	19.7
	0.1	2634	2540	2560	2578	22.3	20.6	21.4	21.5
20.4	25	2537	2509	2397	2481	28.5	29.3	29.3	29.0
	10	2087	2059	1846	1997	28.6	29.0	30.0	29.2
	5	1687	1671	1501	1620	29.7	29.8	30.2	29.9
	1	980	977	913	957	32.5	33.9	32.3	32.9
	0.5	767	759	755	760	32.0	34.6	33.1	33.2
	0.1	400	413	433	415	33.6	35.6	33.1	34.1
30.5	25	1105	1082	1079	1089	36.3	36.6	36.1	36.3
	10	860	835	833	843	35.9	36.1	35.8	35.9
	5	664	639	638	647	36.1	36.3	35.9	36.1
	1	360	346	336	347	36.0	34.9	36.5	35.8
	0.5	278	268	273	273	35.0	33.9	35.3	34.7
	0.1	156	160	155	157	32.8	30.5	31.8	31.7
38.5	25	567	531	544	547	39.8	41.6	39.0	40.1
	10	426	403	409	413	38.2	40.0	36.6	38.3
	5	333	314	327	325	36.3	38.0	34.8	36.4
	1	198	180	191	190	32.3	34.3	31.1	32.6
	0.5	160	153	160	158	30.5	32.1	27.7	30.1
	0.1	115	99	114	109	27.6	26.7	23.6	26.0

TABLE B.8 B2A2G2F-22-4.5 FAM Replicate Modulus Data

Temp.	Freq.	Dynamic Modulus, |E*| (MPa)				Phase Angle(PA, degree)			
	Hz	Rep1	Rep2	Rep3	Avg. |E*|	Rep1	Rep2	Rep3	Avg. PA
-11.5	25	12743	12084	12838	12555	10.0	9.9	12.5	10.8
	10	12127	11606	12429	12054	8.1	8.7	11.2	9.3
	5	11609	10969	11746	11441	7.6	7.8	11.3	8.9
	1	10065	9605	10351	10007	8.4	8.4	11.4	9.4
	0.5	9416	8986	9708	9370	9.0	8.8	12.4	10.1
	0.1	7731	7208	8152	7697	9.3	8.9	12.4	10.2
4.4	25	7518	6882	7494	7298	16.7	16.6	19.7	17.7
	10	6862	6246	7081	6730	15.9	16.0	18.7	16.9
	5	6299	5709	6443	6151	15.9	15.9	18.2	16.6
	1	4777	4362	4930	4690	17.4	17.3	19.9	18.2
	0.5	4210	3855	4428	4164	18.2	18.4	20.9	19.2
	0.1	3222	2360	3391	2991	19.7	23.4	22.8	21.9
20.4	25	2696	2634	2641	2657	27.3	27.9	30.0	28.4
	10	2242	2191	2191	2208	27.0	27.9	29.9	28.3
	5	1817	1795	1803	1805	27.9	27.9	30.7	28.8
	1	1074	1078	1072	1075	31.8	31.5	32.9	32.1
	0.5	843	847	841	844	33.3	33.4	34.0	33.6
	0.1	461	473	482	472	36.1	34.2	34.9	35.1
30.5	25	1225	1234	1163	1207	35.9	35.6	36.2	35.9
	10	951	968	900	940	35.4	35.4	36.1	35.6
	5	738	772	689	733	35.4	35.1	36.6	35.7
	1	394	422	361	392	36.7	35.6	37.9	36.7
	0.5	307	334	271	304	37.3	34.6	38.1	36.7
	0.1	161	189	143	164	35.1	35.8	37.9	36.3
38.5	25	614	623	568	602	41.6	41.5	40.3	41.1
	10	467	469	424	453	39.8	40.5	38.6	39.6
	5	357	364	319	347	39.2	39.9	38.7	39.2
	1	191	197	181	190	36.6	39.8	34.4	36.9
	0.5	158	160	149	156	34.8	38.2	31.9	35.0
	0.1	113	112	89	105	23.5	35.4	20.8	26.6

TABLE B.9 B2A2G2F-0-7.5 FAM Replicate Modulus Data

Temp.	Freq.	Dynamic Modulus, |E*| (MPa)				Phase Angle(PA, degree)			
	Hz	Rep1	Rep2	Rep3	Avg. |E*|	Rep1	Rep2	Rep3	Avg. PA
-11.5	25	8290	8153	8432	8292	10.5	11.2	12.4	11.4
	10	7866	7692	7934	7831	9.7	10.3	11.8	10.6
	5	7417	7120	7487	7341	9.2	10.1	11.4	10.2
	1	6145	5832	6203	6060	11.0	11.9	13.0	12.0
	0.5	5607	5305	5626	5513	11.9	12.9	14.0	12.9
	0.1	4402	4110	4400	4304	14.1	14.7	16.1	14.9
4.4	25	3826	3679	3661	3722	21.8	22.5	22.7	22.3
	10	3319	3170	3134	3208	21.6	22.3	22.6	22.1
	5	2829	2715	2667	2737	23.2	23.5	23.4	23.3
	1	1823	1703	1733	1753	27.0	27.8	27.5	27.5
	0.5	1479	1371	1407	1419	28.7	30.2	30.0	29.6
	0.1	847	767	781	799	31.8	34.4	33.3	33.2
20.4	25	985	938	898	940	40.0	40.5	39.9	40.1
	10	743	696	675	705	40.1	41.0	40.1	40.4
	5	565	530	509	535	39.6	41.2	40.6	40.5
	1	283	261	260	268	41.5	40.1	40.7	40.8
	0.5	223	198	204	208	39.7	39.0	38.4	39.0
	0.1	122	109	114	115	34.7	39.1	34.7	36.2
30.5	25	385	332	348	355	48.6	47.8	48.2	48.2
	10	287	250	260	266	47.5	46.4	46.2	46.7
	5	216	183	197	199	45.6	43.9	44.3	44.6
	1	119	90	110	106	42.9	38.6	39.4	40.3
	0.5	89	70	95	85	40.3	37.7	35.7	37.9
	0.1	60	42	64	55	30.4	31.9	38.0	33.4

TABLE B.10 B2A2G2F-7-7.5 FAM Replicate Modulus Data

		Dynamic Modulus, |E*| (MPa)				Phase Angle(PA, degree)			
Temp.	Freq.								
	Hz	Rep1	Rep2	Rep3	Avg. |E*|	Rep1	Rep2	Rep3	Avg. PA
-11.5	25	9741	8856	9193	9263	9.2	9.0	9.9	9.4
	10	9312	8456	8734	8834	7.7	7.7	8.5	8.0
	5	8750	8048	8359	8385	7.3	7.2	8.7	7.7
	1	7512	6965	7168	7215	8.4	9.0	9.1	8.8
	0.5	6949	6414	6666	6676	9.1	9.6	9.7	9.5
	0.1	5769	5103	5587	5486	9.6	9.0	10.7	9.8
4.4	25	5302	4829	4950	5027	16.8	17.1	18.2	17.4
	10	4752	4374	4466	4531	15.7	16.1	17.7	16.5
	5	4218	3931	3943	4031	16.6	16.8	17.4	16.9
	1	3101	2856	2917	2958	17.7	18.9	19.6	18.7
	0.5	2678	2430	2516	2541	19.0	19.6	20.9	19.8
	0.1	1830	1689	1705	1741	21.3	21.3	23.3	22.0
20.4	25	1762	1677	1663	1700	30.4	30.4	30.4	30.4
	10	1422	1358	1336	1372	30.3	30.1	30.1	30.2
	5	1130	1069	1055	1085	30.9	31.3	31.7	31.3
	1	624	591	589	601	33.7	34.8	34.7	34.4
	0.5	485	441	451	459	34.6	35.2	35.5	35.1
	0.1	271	233	239	248	31.7	36.9	34.4	34.3
30.5	25	766	729	718	738	37.4	38.7	38.2	38.1
	10	590	552	545	562	37.1	37.9	37.3	37.4
	5	450	417	411	426	36.7	37.8	37.3	37.3
	1	235	214	213	221	36.6	36.3	37.3	36.7
	0.5	191	166	159	172	33.5	35.7	36.5	35.2
	0.1	112	87	89	96	25.9	30.8	34.9	30.5
38.5	25	390	348	347	361	41.2	41.3	42.0	41.5
	10	293	261	264	273	38.3	39.2	38.1	38.5
	5	238	207	195	213	38.2	35.4	38.8	37.5
	1	131	119	120	123	32.0	32.0	32.8	32.2
	0.5	120	100	98	106	25.9	27.6	29.7	27.7
	0.1	82	73	73	76	24.2	32.7	21.5	26.2

The heading spans: B2A2G2F-7-7.5

TABLE B.11 B2A2G2F-15-7.5 FAM Replicate Modulus Data

Temp.	Freq.	Dynamic Modulus, |E*| (MPa)				Phase Angle(PA, degree)			
	Hz	Rep1	Rep2	Rep3	Avg. |E*|	Rep1	Rep2	Rep3	Avg. PA
-11.5	25	9800	9794	9485	9693	10.5	9.8	9.3	9.9
	10	9334	9363	9093	9264	9.3	8.1	8.3	8.5
	5	8840	8923	8542	8768	8.6	8.6	7.2	8.1
	1	7552	7666	7437	7552	10.1	9.3	7.8	9.0
	0.5	6962	7086	6983	7010	10.7	9.8	8.7	9.7
	0.1	5408	5688	5779	5625	11.0	10.0	9.4	10.2
4.4	25	5214	5295	5080	5196	18.2	17.7	17.0	17.6
	10	4685	4767	4618	4690	17.7	17.3	15.6	16.8
	5	4174	4300	4063	4179	17.9	16.7	15.7	16.8
	1	3009	3121	3016	3048	19.5	19.2	17.7	18.8
	0.5	2581	2684	2623	2629	20.3	20.7	18.9	20.0
	0.1	1728	1845	1788	1787	22.2	22.7	21.3	22.1
20.4	25	1711	1838	1754	1767	30.8	29.6	29.5	29.9
	10	1374	1486	1419	1426	31.0	29.5	29.8	30.1
	5	1114	1195	1137	1149	31.7	30.8	30.3	30.9
	1	610	681	652	648	34.7	34.0	33.0	33.9
	0.5	471	528	504	501	36.1	34.4	34.1	34.9
	0.1	282	253	266	267	34.4	35.2	35.7	35.1
30.5	25	738	775	750	754	38.8	38.2	39.0	38.7
	10	561	594	568	574	38.9	38.1	39.4	38.8
	5	437	457	425	440	37.2	37.1	39.6	38.0
	1	297	244	216	252	37.9	35.5	41.6	38.3
	0.5	181	176	159	172	35.8	36.6	42.4	38.3
	0.1	82	83	76	80	37.6	38.2	40.0	38.6
38.5	25	369	380	350	366	41.5	42.8	47.3	43.9
	10	265	279	253	266	41.4	41.0	46.1	42.9
	5	215	219	176	203	40.8	38.8	50.3	43.3
	1	118	122	80	107	36.2	36.5	50.1	40.9
	0.5	90	94	95	93	36.1	33.4	42.2	37.2
	0.1	65	70	68	68	35.9	34.3	38.2	36.1

TABLE B.12 B2A2G2F-22-7.5 FAM Replicate Modulus Data

B2A2G2F-22-7.5									
Temp.	Freq.	Dynamic Modulus, |E*| (MPa)				Phase Angle(PA, degree)			
	Hz	Rep1	Rep2	Rep3	Avg. |E*|	Rep1	Rep2	Rep3	Avg. PA
-11.5	25	11407	9756	9571	10244	10.3	14.8	8.9	11.3
	10	10919	9304	9172	9798	8.7	13.9	7.5	10.0
	5	10325	8930	8630	9295	8.6	12.7	7.0	9.4
	1	9027	7664	7524	8072	9.3	13.9	8.2	10.5
	0.5	8528	7135	6928	7531	9.9	14.8	8.7	11.1
	0.1	7488	5912	5790	6397	10.2	16.3	8.2	11.6
4.4	25	6241	5345	5272	5619	17.2	21.4	16.1	18.2
	10	5619	4829	4781	5076	16.1	21.0	15.0	17.4
	5	5109	4355	4298	4587	16.7	21.8	14.9	17.8
	1	3799	3246	3207	3417	17.7	23.1	16.7	19.2
	0.5	3299	2822	2792	2971	18.6	23.9	17.7	20.1
	0.1	2313	2065	1983	2121	20.4	25.0	19.0	21.5
20.4	25	2266	1968	1906	2047	27.7	30.6	27.6	28.6
	10	1866	1626	1571	1688	27.4	30.5	27.4	28.4
	5	1539	1337	1265	1381	27.6	30.7	28.8	29.0
	1	895	787	741	808	30.3	33.6	31.7	31.9
	0.5	713	627	591	643	30.8	34.5	32.2	32.5
	0.1	404	361	329	365	31.1	36.1	31.8	33.0
30.5	25	948	899	834	894	35.5	37.0	36.0	36.2
	10	733	708	640	694	35.2	36.5	36.0	35.9
	5	568	559	503	543	34.3	36.6	36.0	35.7
	1	304	313	259	292	33.0	37.6	38.0	36.2
	0.5	239	250	199	229	33.3	37.3	38.0	36.2
	0.1	130	149	107	129	28.4	31.6	35.0	31.7
38.5	25	488	502	454	481	37.6	41.8	39.0	39.5
	10	367	397	343	369	35.7	40.9	37.0	37.9
	5	283	301	278	287	35.3	39.6	34.0	36.3
	1	148	193	160	167	30.7	38.3	31.0	33.3
	0.5	121	166	135	141	30.4	35.5	29.0	31.6
	0.1	74	110	87	90	22.3	30.8	30.0	27.7

Oklahoma Department of Transportation Project AC Material Replicate Modulus data

TABLE B.13 S3 64-22 Replicate Modulus Data

Temp.	Freq.	Dynamic Modulus, |E*| (MPa)				Phase Angle(PA, degree)			
	Hz	Rep1	Rep2	Rep3	Avg. |E*|	Rep1	Rep2	Rep3	Avg. PA
4	25	16895	17715	18393	17668	7.4	7.4	7.8	7.5
	10	15622	16122	16991	16245	8.8	9.0	8.8	8.8
	5	14645	15076	15970	15230	9.4	9.6	9.3	9.4
	1	12347	12722	13556	12875	11.1	11.4	11.1	11.2
	0.5	11370	11730	12527	11876	12.0	12.2	11.8	12.0
	0.1	9177	9508	10157	9614	14.4	14.7	14.4	14.5
20	25	9239	9562	10083	9628	15.7	15.7	15.7	15.7
	10	8030	8228	8660	8306	16.8	17.2	17.2	17.1
	5	7164	7311	7704	7393	17.6	18.2	18.2	18.0
	1	5265	5369	5660	5431	20.2	21.1	21.1	20.8
	0.5	4570	4664	4928	4721	21.1	22.2	22.1	21.8
	0.1	3143	3234	3412	3263	23.8	25.1	25.0	24.6
40	25	3371	3511	3849	3577	26.7	27.7	26.6	27.0
	10	2650	2725	3017	2797	27.0	28.8	27.8	27.9
	5	2177	2257	2496	2310	27.1	29.2	28.3	28.2
	1	1254	1372	1510	1379	28.4	30.5	29.7	29.5
	0.5	1001	1124	1217	1114	27.8	29.8	29.3	29.0
	0.1	562	664	711	646	27.5	29.2	29.0	28.6
	0.01	262.4	322.1	340.5	308	25.54	26.54	26.61	26.2

TABLE B.14 S4 64-22 Replicate Modulus Data

S4 64-22									
Temp.	Freq.	Dynamic Modulus, |E*| (MPa)				Phase Angle(PA, degree)			
	Hz	Rep1	Rep2	Rep3	Avg. |E*|	Rep1	Rep2	Rep3	Avg. PA
4	25	16964	16800	17339	17034	8.3	9.5	7.1	8.3
	10	15486	15149	14936	15190	9.5	10.2	9.7	9.8
	5	14379	14009	13644	14011	10.2	11.1	10.8	10.7
	1	11923	11526	11183	11544	12.1	13.1	13.0	12.7
	0.5	10884	10520	10159	10521	13.0	14.1	14.0	13.7
	0.1	8624	8337	7972	8311	15.7	16.6	16.9	16.4
20	25	9018	9511	9113	9214	16.0	16.4	16.4	16.3
	10	7585	7966	7640	7730	18.1	18.1	18.4	18.2
	5	6633	6982	6668	6761	19.4	19.4	19.8	19.5
	1	4698	4983	4705	4795	22.8	22.7	23.3	22.9
	0.5	4020	4291	4022	4111	24.0	23.8	24.6	24.1
	0.1	2685	2904	2671	2753	27.1	26.8	27.8	27.2
40	25	2666	3115	2724	2835	29.9	29.2	30.1	29.7
	10	2007	2373	2054	2145	31.3	30.5	31.3	31.0
	5	1623	1942	1667	1744	31.8	30.9	31.7	31.4
	1	922	1137	954	1004	33.2	32.3	32.9	32.8
	0.5	740	924	772	812	32.5	31.5	32.2	32.1
	0.1	408	527	434	456	32.0	30.9	31.4	31.4
	0.01	180.9	241.3	199.8	207	29.02	28.06	28.26	28.4

TABLE B.15 S4 70-28 Replicate Modulus Data

		Dynamic Modulus, |E*| (MPa)				Phase Angle(PA, degree)			
					S4 70-28				
Temp.	Freq.	Dynamic Modulus, |E*| (MPa)				Phase Angle(PA, degree)			
	Hz	Rep1	Rep2	Rep3	Avg. |E*|	Rep1	Rep2	Rep3	Avg. PA
4	25	11078	11091	10362	10844	13.6	13.4	13.1	13.4
	10	9691	9671	9118	9493	14.8	14.6	14.2	14.6
	5	8689	8693	8225	8536	15.8	15.6	15.1	15.5
	1	6595	6636	6344	6525	18.3	18.0	17.4	17.9
	0.5	5814	5857	5635	5769	19.2	19.0	18.3	18.9
	0.1	4277	4315	4195	4262	21.7	21.5	20.8	21.3
20	25	4583	4540	4517	4547	24.3	23.7	23.2	23.7
	10	3653	3658	3625	3645	25.6	25.0	24.6	25.1
	5	3084	3109	3075	3089	26.3	25.6	25.5	25.8
	1	1977	2025	1998	2000	28.2	27.4	27.7	27.8
	0.5	1673	1706	1697	1692	28.2	27.4	27.8	27.8
	0.1	1051	1069	1078	1066	29.1	28.6	29.0	28.9
40	25	1249	1169	1233	1217	32.5	32.6	32.1	32.4
	10	858	824	875	852	32.9	33.1	32.5	32.8
	5	670	644	683	666	32.6	32.7	32.3	32.5
	1	350	333	348	344	32.2	32.8	32.7	32.6
	0.5	284	270	288	280	30.7	31.3	30.9	31.0
	0.1	163	158	168	163	29.4	29.4	29.3	29.4
	0.01	95.1	92	96.5	95	24.69	25.27	25.26	25.1

TABLE B.16 S4 76-28 Replicate Modulus Data

S4 76-28									
Temp.	Freq.	Dynamic Modulus, |E*| (MPa)				Phase Angle(PA, degree)			
	Hz	Rep1	Rep2	Rep3	Avg. |E*|	Rep1	Rep2	Rep3	Avg. PA
4	25	12092	13231	11934	12419	11.9	12.9	12.6	12.5
	10	10679	11389	10548	10872	12.9	13.8	14.0	13.6
	5	9699	10217	9536	9817	13.8	14.7	15.0	14.5
	1	7599	7879	7321	7600	16.0	17.2	17.7	17.0
	0.5	6779	6962	6460	6734	17.0	18.2	18.9	18.0
	0.1	5097	5136	4685	4973	19.4	20.8	21.8	20.6
20	25	5105	5254	4978	5112	22.6	23.4	24.3	23.4
	10	4109	4202	3955	4089	24.0	24.9	25.8	24.9
	5	3490	3549	3315	3451	24.8	25.7	26.6	25.7
	1	2280	2292	2075	2216	26.9	27.6	28.7	27.7
	0.5	1935	1926	1730	1864	26.9	27.5	28.6	27.7
	0.1	1231	1202	1048	1160	28.0	28.4	29.2	28.5
40	25	1388	1383	1274	1348	30.9	31.0	31.5	31.1
	10	990	978	885	951	31.3	31.2	31.6	31.4
	5	778	764	682	741	31.0	30.7	31.2	31.0
	1	401	401	343	382	31.8	30.5	31.1	31.1
	0.5	338	337	285	320	30.0	28.7	29.1	29.3
	0.1	201	207	173	194	28.7	27.1	27.3	27.7
	0.01	119.8	129.6	104.9	118	25.03	23.23	23.77	24.0

TABLE B.17 S5 76-28 Replicate Modulus Data

S5 76-28									
Temp.	Freq.	Dynamic Modulus, |E*| (MPa)				Phase Angle(PA, degree)			
	Hz	Rep1	Rep2	Rep3	Avg. |E*|	Rep1	Rep2	Rep3	Avg. PA
4	25	13759	13880	13137	13592	11.7	12.0	11.4	11.7
	10	12155	12186	11673	12005	12.8	13.0	12.4	12.7
	5	10975	11072	10626	10891	13.6	13.9	13.3	13.6
	1	8586	8672	8375	8544	15.8	16.1	15.4	15.7
	0.5	7633	7740	7474	7616	16.7	17.0	16.4	16.7
	0.1	5784	5806	5663	5751	19.0	19.3	18.7	19.0
20	25	6184	5993	5764	5980	21.3	22.3	21.7	21.7
	10	5039	4859	4686	4861	22.7	23.7	23.2	23.2
	5	4296	4127	3988	4137	23.6	24.5	24.1	24.1
	1	2883	2704	2637	2741	25.9	26.7	26.3	26.3
	0.5	2442	2278	2228	2316	26.2	26.8	26.6	26.5
	0.1	1581	1442	1425	1483	27.6	27.9	27.7	27.7
40	25	1621	1579	1426	1542	30.1	31.0	32.3	31.1
	10	1179	1138	1035	1117	30.3	31.2	32.3	31.3
	5	938	900	823	887	29.9	30.6	31.7	30.8
	1	536	489	466	497	29.2	30.4	30.8	30.1
	0.5	437	411	384	410	28.0	28.6	29.4	28.7
	0.1	267	258	235	253	26.6	26.8	27.7	27.0
	0.01	151.8	161.7	143.9	152	24.36	23.36	24.22	24.0
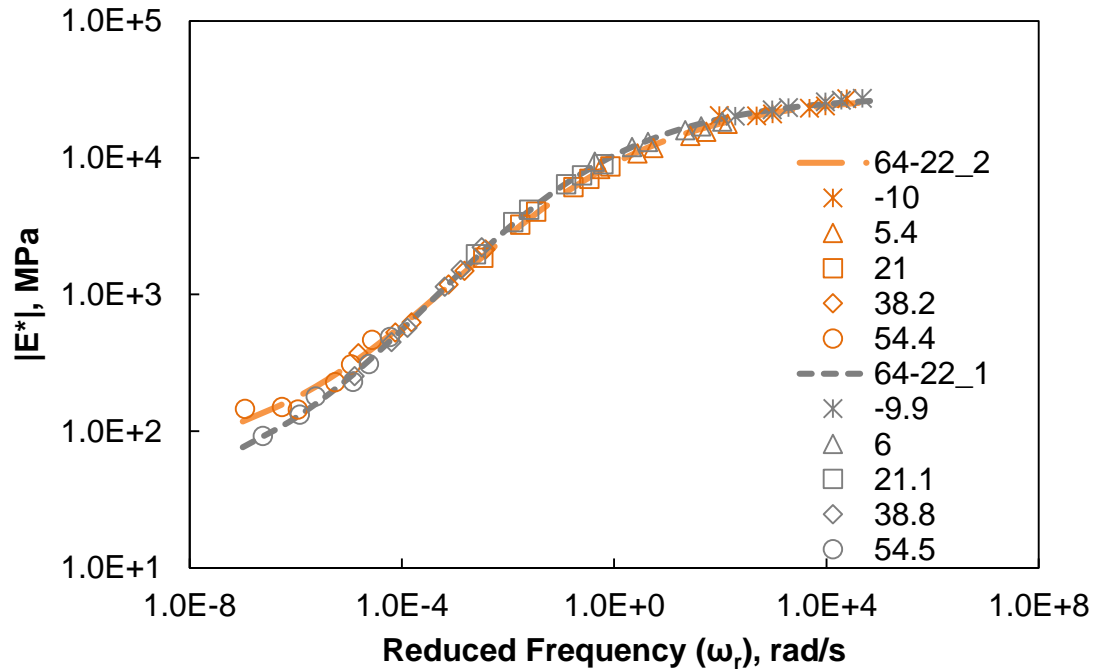
FIGURE B-1 Master Curve plots for AC_1 replicates
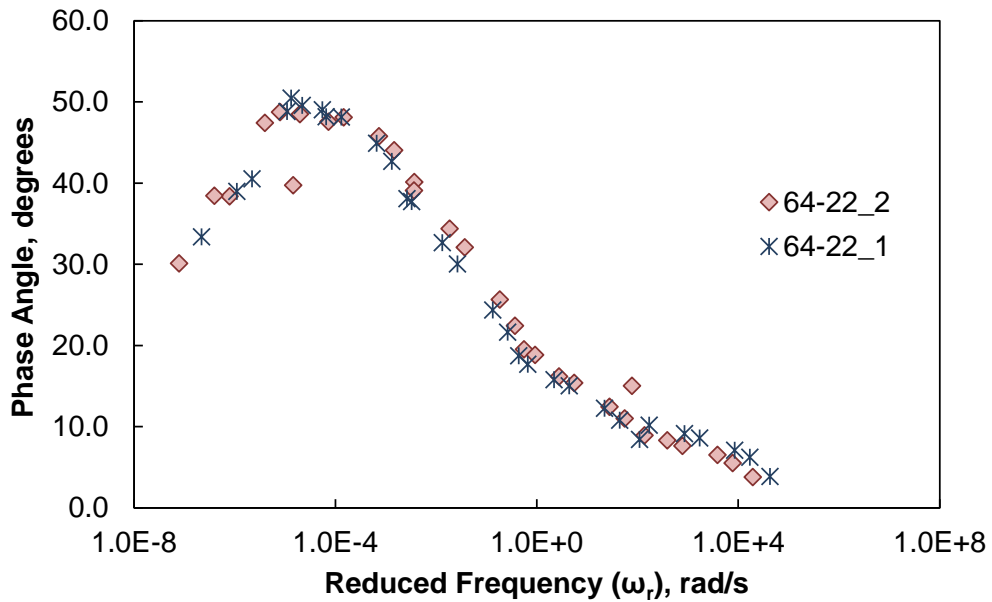
FIGURE B-2 Phase angle plots for AC_1 replicates
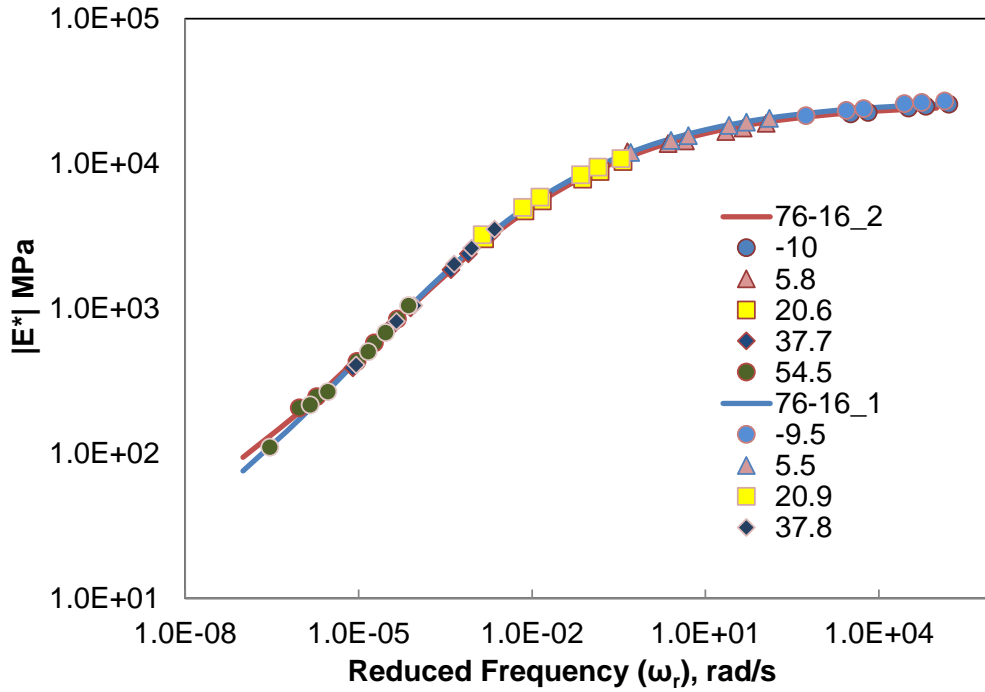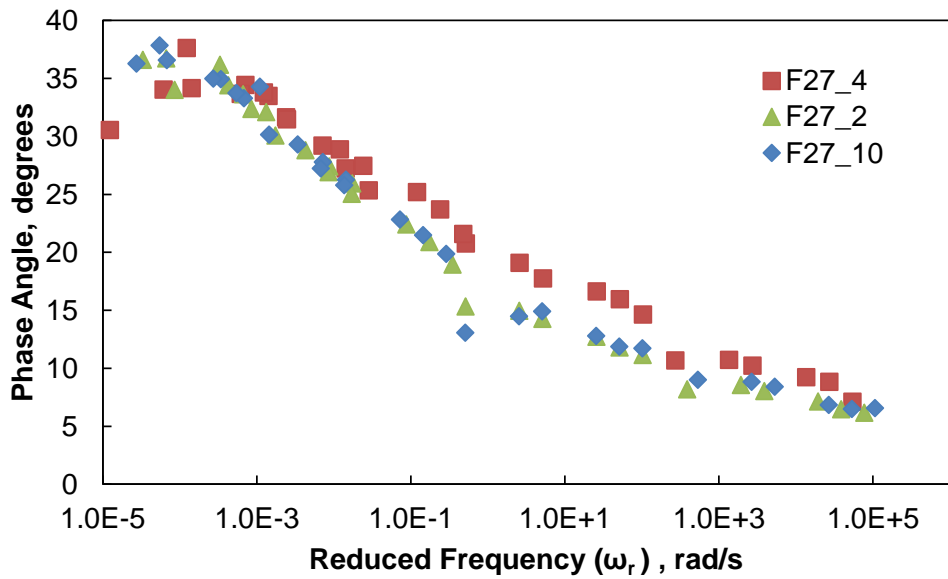
FIGURE B-3 Master Curve plots for AC_2 replicates
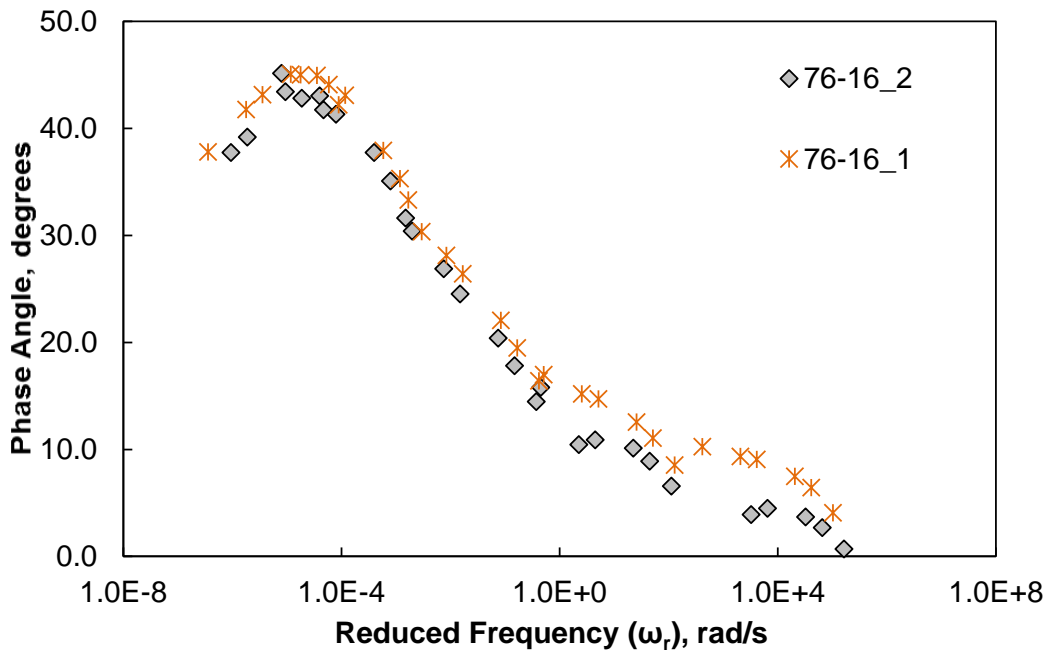
FIGURE B-4 Phase angle plots for AC_2 replicates

216
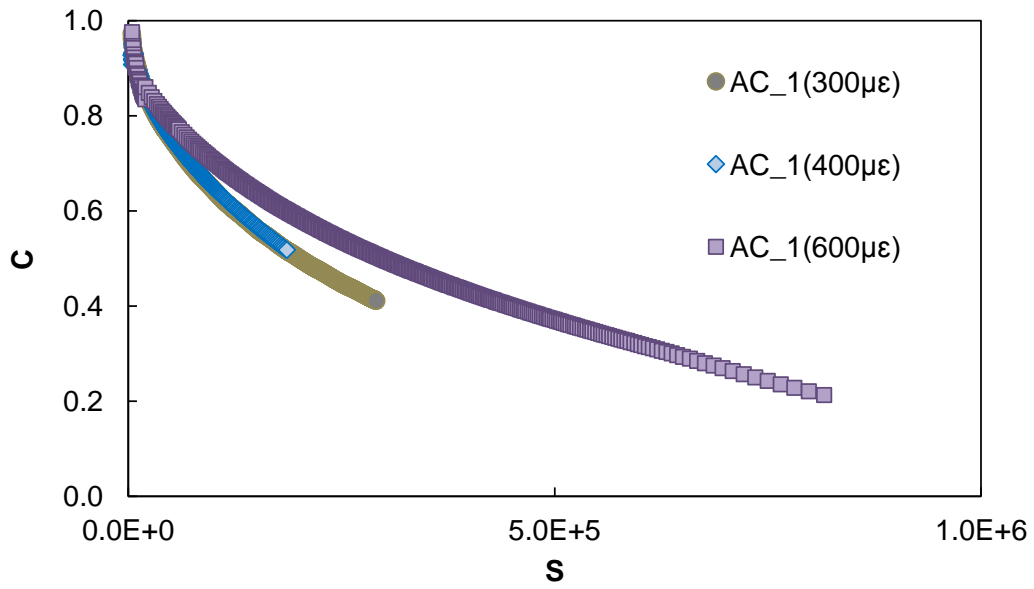
FIGURE B-5 C-S plots for replicates of AC_1
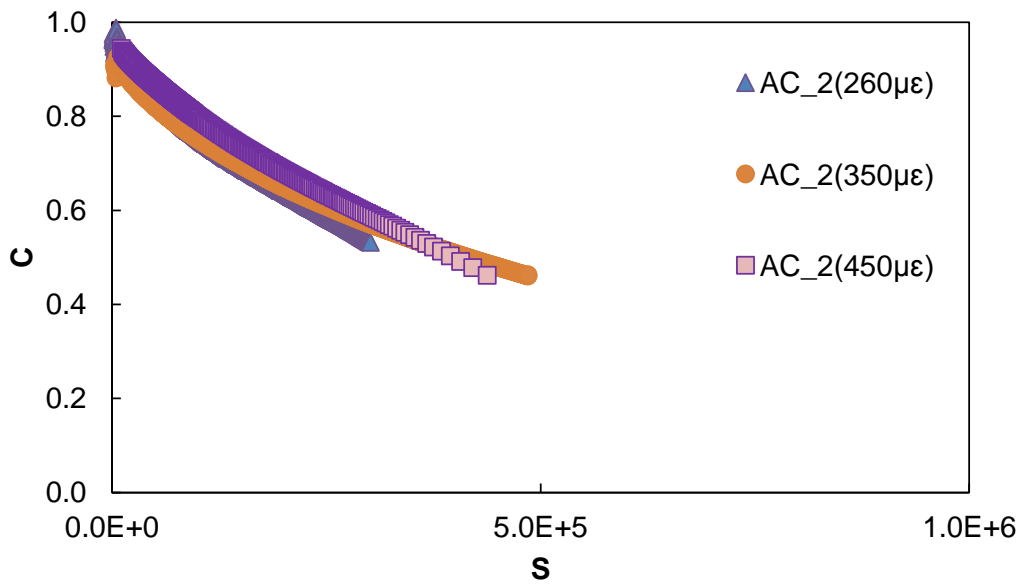
FIGURE B-6 C-S plots for replicates of AC_2
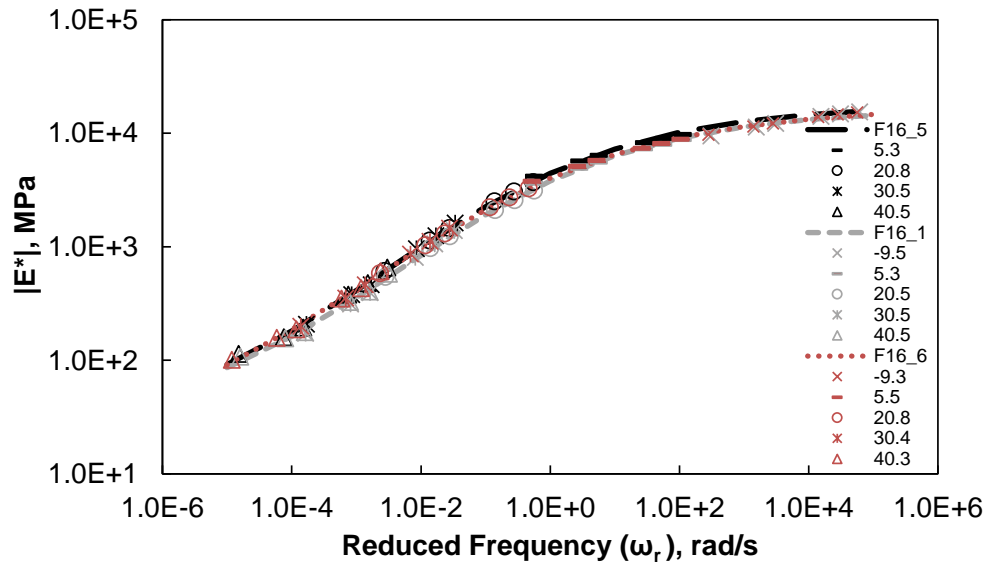
FIGURE B-7 Master Curve plots for FAM_1 replicates
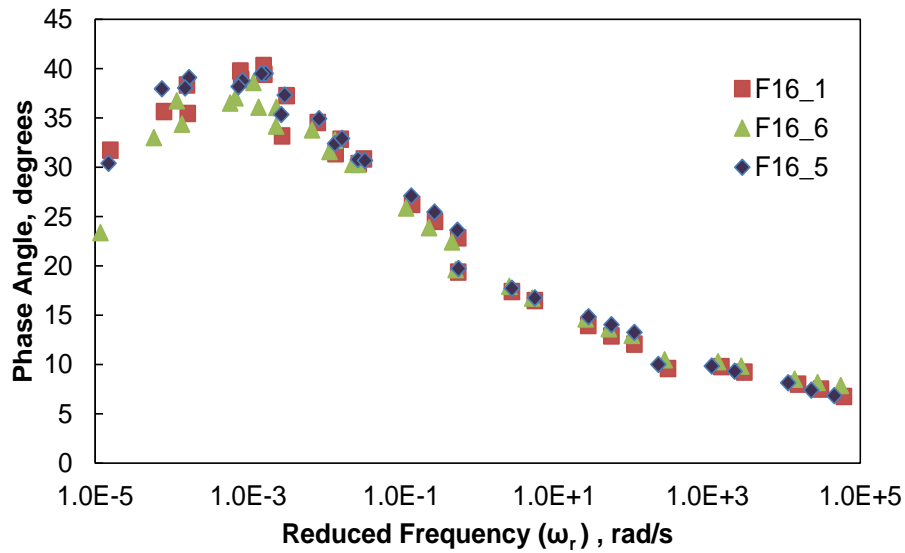
FIGURE B-8 Phase angle plots for FAM_1 replicates
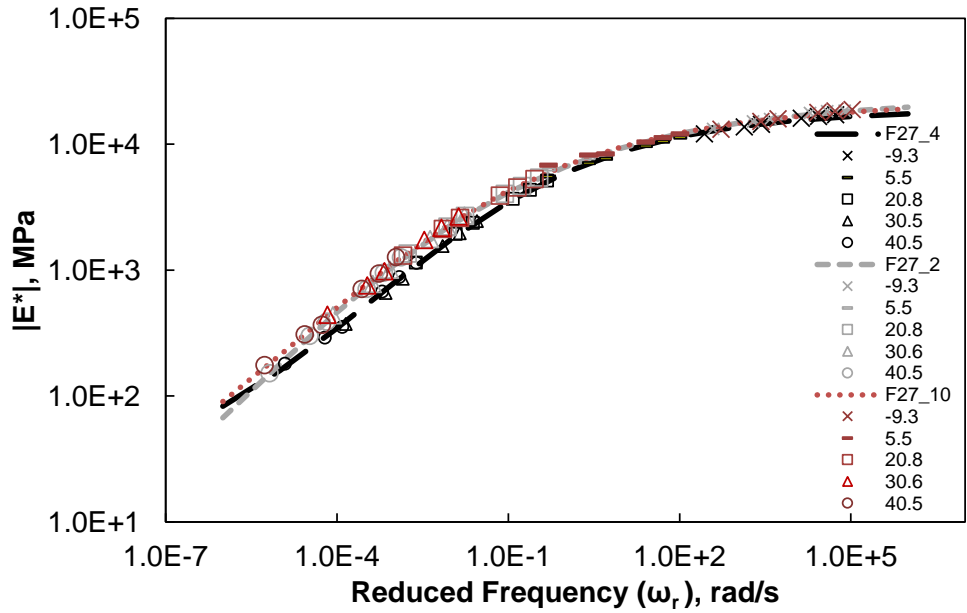
FIGURE B-9 Master Curve plots for FAM_2 replicates

FIGURE B-10 Phase angle plots for FAM_2 replicates

219
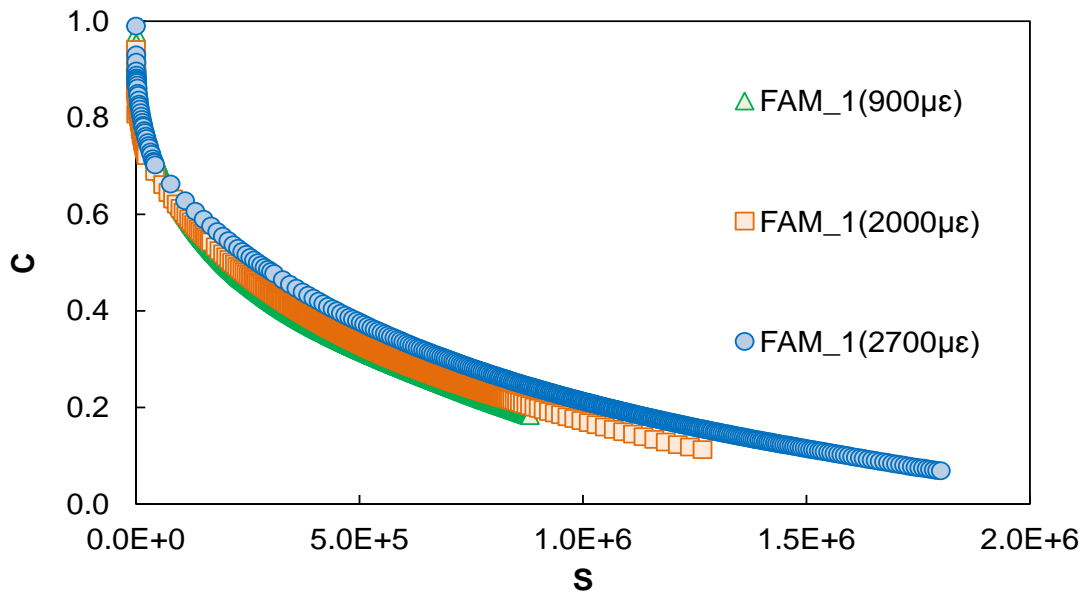
FIGURE B-11 C-S plots for replicates of FAM_1
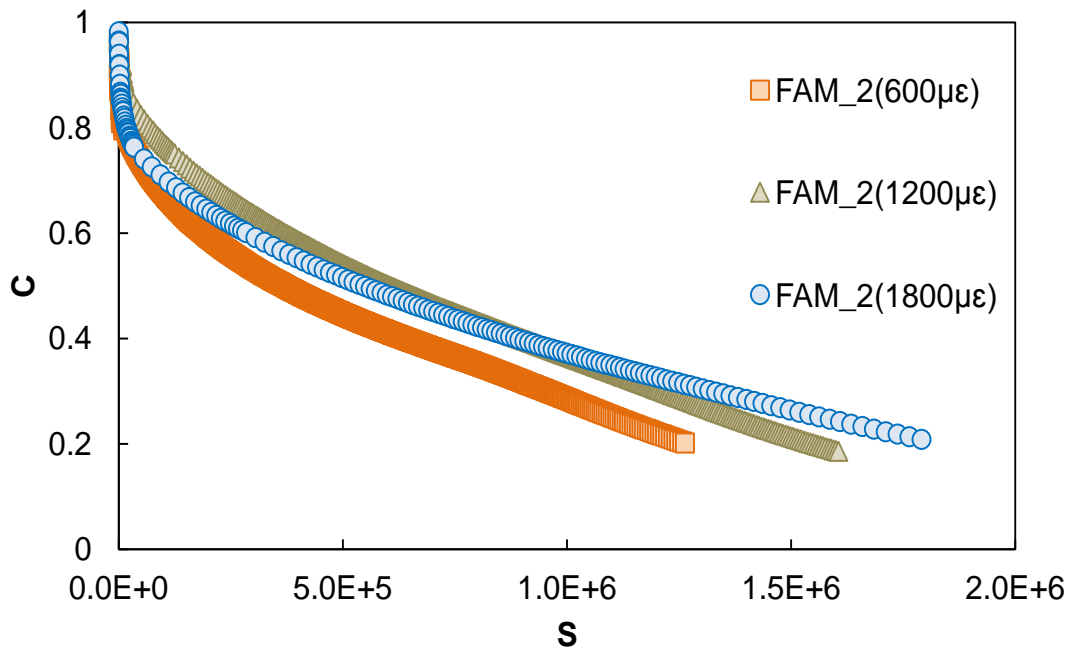
FIGURE B-12 C-S plots for replicates of FAM_2
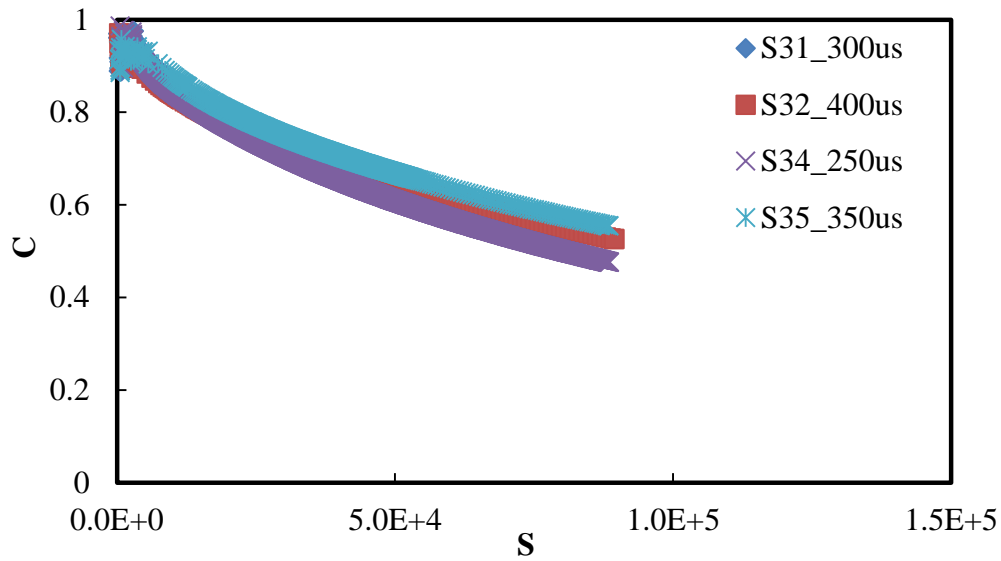
FIGURE B-13 C-S plots for replicates of S3 64-22 AC mix
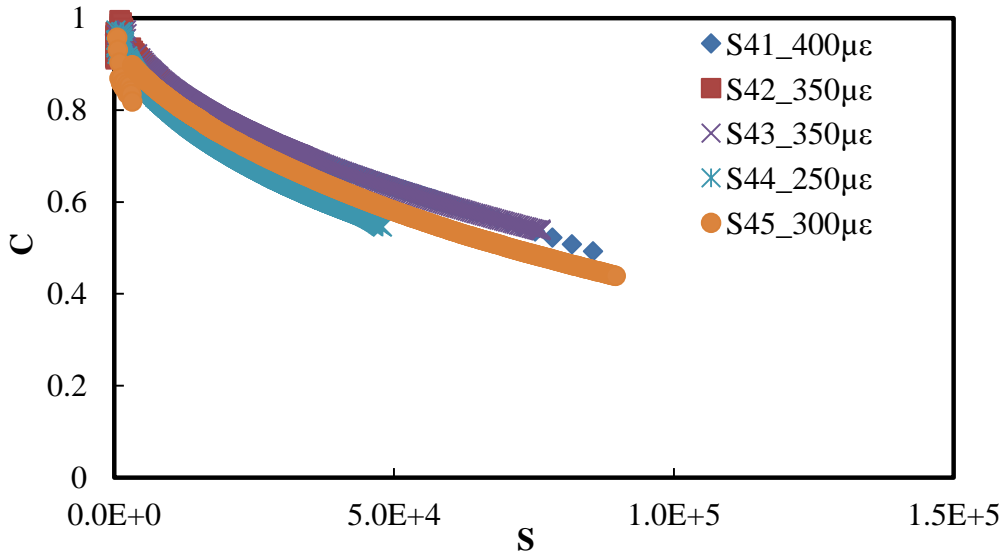
FIGURE B-14 C-S plots for replicates of S4 64-22 AC mix
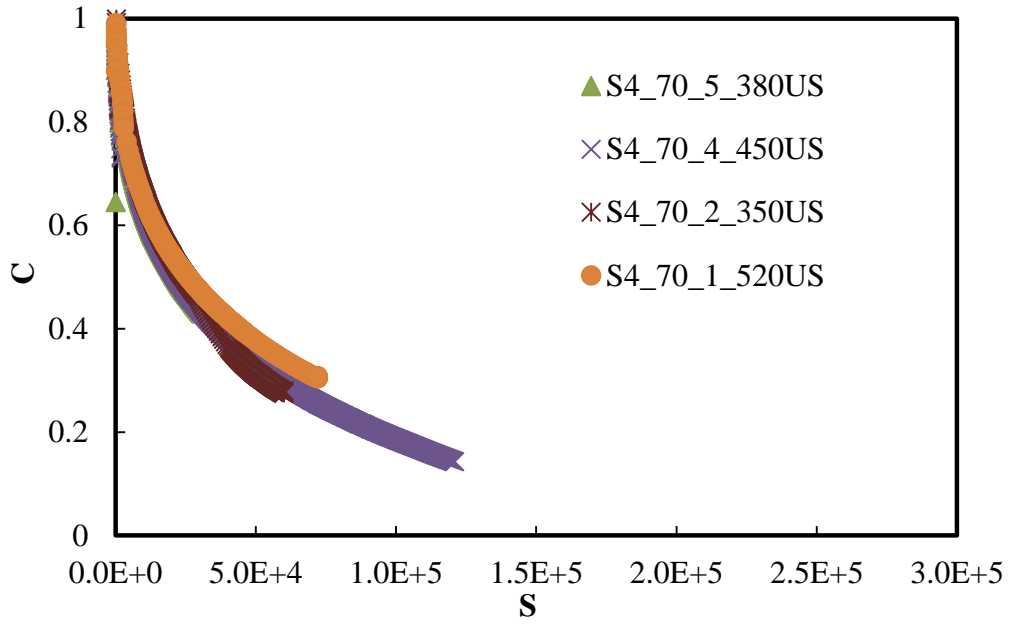
FIGURE B-15 C-S plots for replicates of S4 70-28 AC mix
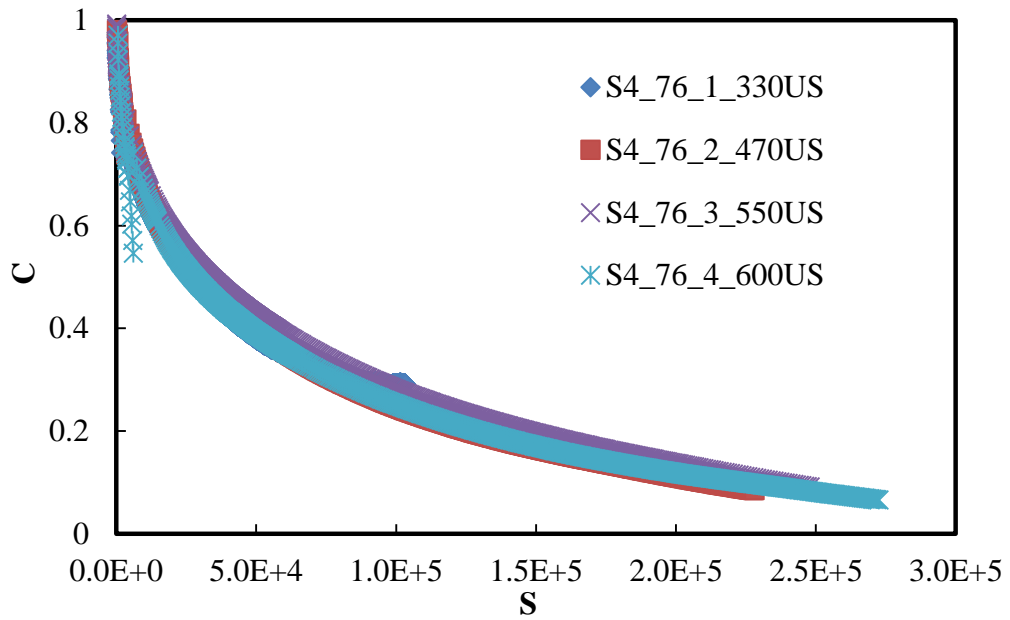
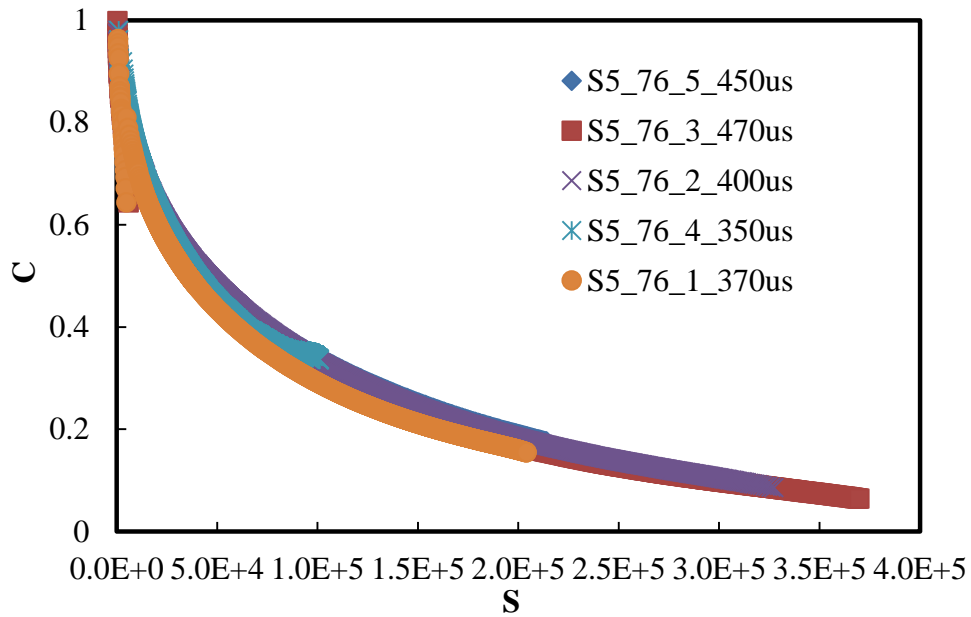FIGURE B-16 C-S plots for replicates of S4 76-28 AC mix

FIGURE B-17 C-S plots for replicates of S5 76-28 AC mix

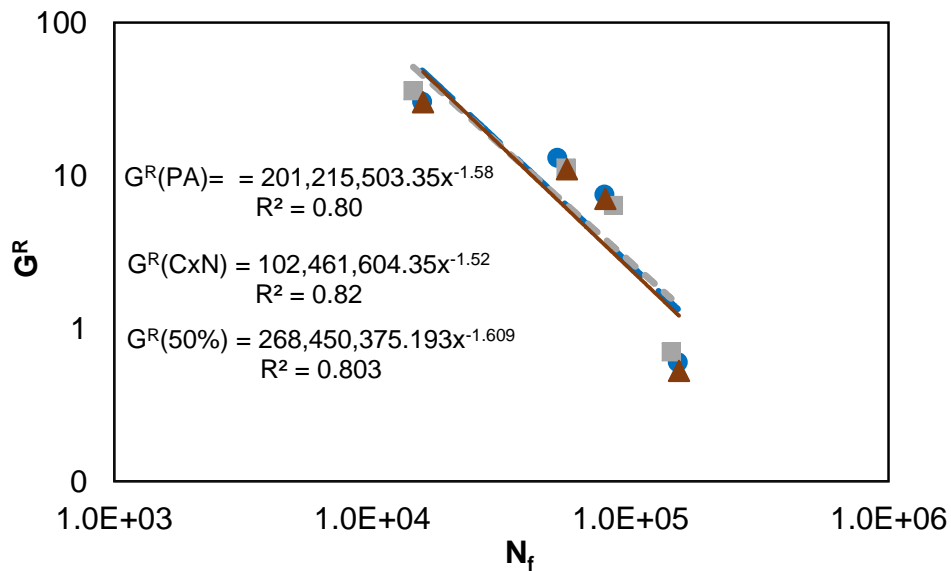*AC_2 Variation with respect to different failure criteria approaches*

$G^R(PA)= = 201,215,503.35x^{-1.58}$
$R^2 = 0.80$

$G^R(CxN) = 102,461,604.35x^{-1.52}$
$R^2 = 0.82$

$G^R(50\%) = 268,450,375.193x^{-1.609}$
$R^2 = 0.803$

FIGURE B-18 AC_2 Variation in G^R characteristic equation for different experimental failure criteria.
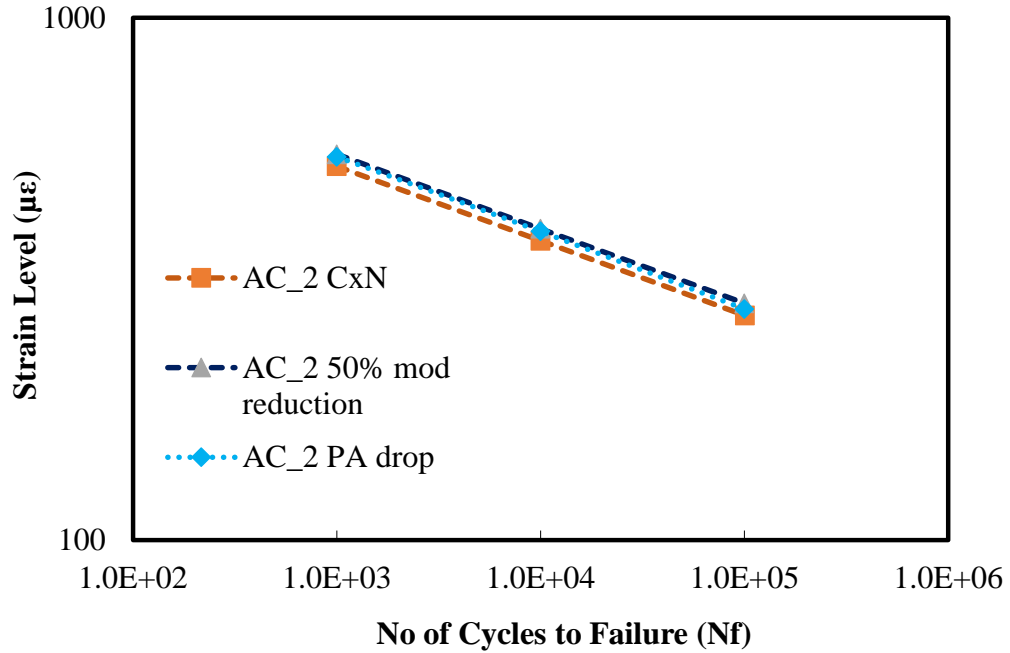
FIGURE B-19 AC_2 Simulated fatigue lives plot or AC mixture according C_f model failure criteria using three different experimental failure point identification methods.
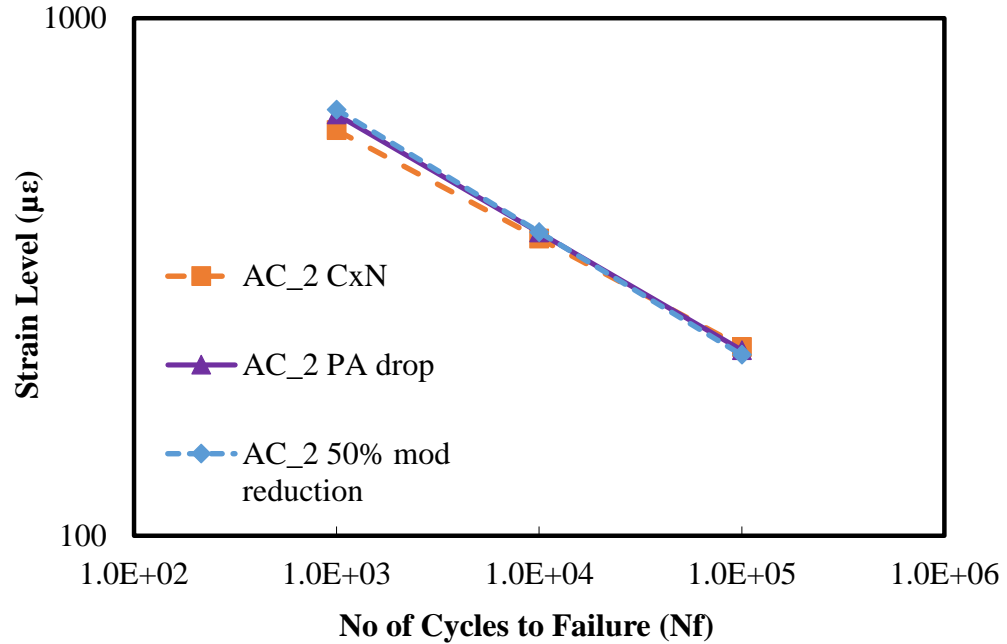

FIGURE B-20 AC_2 Simulated fatigue lives plot or AC mixture according G^R model failure criteria using three different experimental failure point identification methods.